東海大學生命科學系 博士論文

Department of Life Science, Tunghai University

Ph.D. Thesis

指導教授：劉薏雯 教授

Advisor: Dr. Yi-Wen Liu

內皮細胞訊號在斑馬魚腎間腺器官發育中所扮演的多重角色

The multiple roles of the endothelium for the interrenal gland organogenesis in the zebrafish

研究生：周志薇

Chih-Wei Chou

中華民國 **105** 年 **7** 月

東海大學生命科學系 博士論文

Department of Life Science, Tunghai University

Ph.D. Thesis

內皮細胞訊號在斑馬魚腎間腺器官發育中所扮演的多重角色

The multiple roles of the endothelium for the interrenal gland organogenesis in the zebrafish

研究生：周志薇

Chih-Wei Chou

指導教授：劉慧雯 教授

Dr. Yi-Wen Liu

中華民國 **105** 年 **7** 月

東海大學生命科學系
博士論文學位考試審定書

生命科學系博士班研究生 周志薇 君所撰寫之論文

（中文）

內皮細胞訊號在斑馬魚腎間腺器官發育中所扮演的多重角色

（英文）

The multiple roles of the endothelium for the interrenal gland organogenesis in the zebrafish

經本委員會審定通過，特此證明。

學位考試委員會　召集人 鍾邦柱 （簽名）

委　員 江運金

黃聲華

劉惠雯

鄭色塗

中華民國 105 年 7 月 14 日

誌謝

在東海大學多年的日子裡，特別感謝劉蕙雯老師在各方面細心耐心的教導，讓我從大學轉系生到如今能順利完成博士學位。劉老師總是能夠看到學生的好的一面並且給予正向的指導，並且在實驗困境中找出解決之道；我也要感謝系上的蔡玉真老師和胡承波老師讓我在課堂上獲益良多；另外我要感謝國衛院游美淑老師幫忙進行細胞移植實驗，以及中研院鍾邦柱老師、中研院黃聲蘋老師、國衛院江運金老師、和長庚大學鄭邑荃老師在口試以及研討會中提供許多寶貴的意見，還有台灣斑馬魚中心數度的支援，讓這本論文能夠順利完成。

我也要謝謝一路走來陪伴我的朋友們，謝謝研究所的學長姐以及同學們在我遭遇困難時給予精神上的鼓勵，並在學術上提供良好的典範；也謝謝學弟妹們在實驗以及生活上的協助。另外我要特別感謝我的家人，因為有我先生和兩個可愛女兒的陪伴及包容，還有我的媽媽和婆婆的幫忙，讓我能夠兼顧家庭及學業；最後我要感謝上帝無時無刻的看顧保守，讓我平安順利的度過生命中每個時刻。

Contents

摘要

腎上腺皮質是哺乳動物“下視丘-腦下垂體-腎上腺軸”中的一員，當生物體感受到壓力時會合成及分泌固醇類荷爾蒙。作為一個內分泌器官，腎上腺皮質內部佈滿許多的血管；過去由體外實驗發現腎上腺的血管內皮細胞會影響腎上腺皮質細胞的功能，然而在活體中，血管內皮細胞是否及如何調控腎上腺皮質的發育和功能目前仍不清楚。斑馬魚是一個很適合用來研究血管內皮細胞與器官發育的模式動物，斑馬魚的腎間腺器官相等於哺乳動物的腎上腺，本研究藉由探索斑馬魚的腎間腺器官發育，發現靜脈內皮細胞、腎臟和腎間腺組織在早期發育過程中的協同移行需要內胚層及 VegfC/Flt4 訊號傳遞，本研究也發現動脈和靜脈軸血管的形成會影響腎間腺組織在中軸融合後的不對稱再移行，此外本研究也證實血流動力所調控的血管微環境會促使腎間腺組織往中軸再延伸以及促使嗜鉻細胞的移行，藉此來調控腎間腺器官的組合。總結以上發現，本研究顯示血管內皮細胞經由不同類型的訊號來調控腎間腺器官在不同時期的發育過程，包括 (1) 早期胚胎發育時期腎臟及腎間腺組織往中軸的聚合；(2) 腎間腺組織在中軸融合後的不對稱再移行；(3) 在腎間腺器官功能性組合時，腎間腺組織往中軸再延伸的過程以及同時間嗜鉻細胞的移行。

Abstract

The adrenal cortex is a component of the hypothalamic-pituitary-adrenal (HPA) axis, and functions in synthesis and secretion of steroid hormones in response to stress. As an endocrine organ, the adrenal cortex is highly vascularized. *In vitro* studies have shown that interactions between the endothelium and the adrenocortical cells could modulate the function of the adrenal cortex. However, whether and how the endothelial signaling regulates the adrenal gland development is not clear. Zebrafish interrenal organ is the teleostean counterpart of mammalian adrenal gland, and is an excellent model for studying how the endothelial signaling guides organogenesis. In the zebrafish, we found that coordinated morphogenetic movements of the axial veins, the kidney, and the interrenal tissue were modulated by the endoderm and required Vascular endothelial growth factor receptor C (VegfC)/Fms-related tyrosine kinase 4 (Flt4) signaling pathway. This study has also discovered that arterial and venous vessels are required for modulating developmental relocalization and laterality of the interrenal tissue. Furthermore, this study has found that the hemodynamically-regulated vascular microenvironment promotes migration of the steroidogenic tissue during its interaction with chromaffin cells in the zebrafish embryo. Taken together, this study has demonstrated that the endothelium, through various modes of signaling, modulate (1) midline convergence of the kidney and the interrenal tissue during early embryogenesis, (2) lateral relocalization of the steroidogenic interrenal tissue after the interrenal central fusion, and (3) medial extension of the steroidogenic interrenal tissue as well as migration of chromaffin cells during the functional interrenal organ assembly.

Introduction

1. The kidney and the adrenal gland in the mammalian system

1.1. The structure and function of the kidney

The mammalian kidneys are bilateral organs and contain the outer renal cortex and the inner renal medulla. The main functions of the kidney are filtration of the waste from metabolism in the blood, maintaining the homeostasis of pH, blood pressure and electrolytes, and reabsorption of water, amino acids, and glucose. In human, there are around one million nephrons in each of the kidney and about 20% of the cardiac output pass through the kidney capillaries every day (reviewed in Fox, 2009). The nephron is the basic filtration unit and is composed of a glomerulus, the proximal convoluted tubule (PCT), the loop of Henle and the distal convoluted tubule. The glomerulus is a tuft of capillaries enveloped by the Bowman's capsule which is composed of a specialized epithelial cell, the podocyte, and the long foot process of the podocyte forms the filtration slits. Between the podocyte and the capillary is a specialized basal lamina named glomerular basement membrane (GBM). The filtration slits in podocyte, GBM, and the fenestrated endothelium together make up the filtration membrane of the glomerulus (reviewed in Quaggin and Kreidberg, 2008; McKinley and O'Loughlin, 2008; Fox, 2009).

1.2. The structure and function of the adrenal gland

The mammalian adrenal glands are located superior to the bilateral kidneys, and is made up of two different tissues: the outer adrenal cortex and the inner adrenal medulla (Fig. 1). As one component of the HPA axis, the adrenal cortex synthesizes and secrets steroid hormones in response to long-term stress (Fig. 2). When the body faces the stress, it stimulates the

paraventricular nucleus of the hypothalamus to release the corticotropin-releasing factor (CRF) into the blood vessel, and the anterior pituitary gland receives this signal and releases the adrenocorticotropic hormone (ACTH). ACTH travels via blood vessels and stimulates the adrenal cortex to release the corticosteroid, and by the bloodstream the corticosteroid travels to the target organs. There are three zones in the adrenal cortex which secrete different steroid hormones: the zona glomerulosa secretes mineralocorticoids which targets to the kidney and regulates the balance of salt and water; the zona fasciculate secretes glucocorticoids such as cortisol which targets to the liver and the muscle and promotes the glucose synthesis, and the zona reticularis secretes sex hormone targeting to the gonads. The cortisol also plays as the negative feedback regulator: the cortisol can reach the hypothalamus and inhibits CRF releasing so that restores the level of ACTH and the level of cortisol turns to normal (reviewed in McKinley and O'Loughlin, 2008; Lightman and Conway-Campbell, 2010; Fox, 2009).

While the adrenal cortex responds to the long-term stress, the adrenal medullary is innervated by the sympathetic preganglionic neurons which responds to the short-term stress. The main hormone-producing cells in the adrenal medulla is the chromaffin cell which produces and releases the catecholamines including epinephrine, norepinephrine, and dopamine. Functions of epinephrine and norepinephrine are closely related to the “fight-or-flight response” including acceleration of the heartbeat, increase of the blood pressure and the cardiac output, constriction of the blood vessel in the muscle, skin, and gastrointestinal tract but dilatation of the coronary artery, and increase of the metabolism. These physical responses to the catecholamines help the body raise the energy supply for the emergent situation (reviewed in McKinley and O'Loughlin, 2008; Fox, 2009).

1.3. Development of the mammalian kidney

During gastrulation, three developmental germ layers are formed: the ectoderm, the mesoderm and the endoderm. The ectoderm develops to the epidermis, the neural tube and the derivatives of neural crest cells such as peripheral nervous system, chromaffin cells, cartilage and pigment cells. The mesoderm is divided into four regions: (1) the chordamesoderm which forms the notochord, (2) the paraxial mesoderm which develops to the somite and the head, (3) the intermediate mesoderm which develops to the urogenital system which is composed of the kidney, the adrenal cortex and the gonads, and (4) the lateral plate mesoderm which develops to the cardiovascular system. The endoderm generates the pharynx and the digestive system such as the liver, the pancreas, and the intestine (reviewed in Gilbert, 2013). The kidneys, the adrenal cortex, the gonads and their respective duct systems arise from the urogenital ridge in the intermediate mesoderm (Mesiano and Jaffe, 1997). During gastrulation, the dorsal-ventral signaling such as the Bone Morphogenetic Proteins (BMPs) patterns specification and formation of the intermediate mesoderm. Research in the chick embryo has shown that signals from the paraxial mesoderm also contribute to the initiation of the intermediate mesoderm (Mauch et al., 2000).

Development of the mammalian kidney goes through three different phases: the pronephros, the mesonephros, and the metanephros. Approximately at 22th day of human gestation and mice embryonic day (E) 8.0, cells in the bilateral cranial intermediate mesoderm express *Paired-box transcription factor (Pax)2* and *Pax8* and go through a mesenchymal-to-epithelial transition (MET) to form the bilateral pronephric duct (also known as the nephric or Wolffian duct). *Gata3* acts downstream of the *Pax2* and *Pax8*, and the expression of *Gata3* in the pronephric duct controls growth and elongation of the pronephric duct. *LIM homeobox*

1 is also expressed in the nephric duct to maintain the survival of nephric duct from necrosis. The adjacent mesenchymal cells are stimulated by the pronephric duct and express *Eyes-absent1* which promotes aggregation and condensation of mesenchymal cells to form the pronephric nephron precursors. As the pronephric duct grows caudally, the adjacent mesenchymal cells aggregate and condense to form the pronephric nephron precursors. The cranial pronephric nephron does not connect to the pronephric duct and degenerates quickly by apoptosis, so the pronephros in mammals is considered to have no function (reviewed in Davidson et al., 2009; Gilbert, 2013).

During the continuous growing of the nephric duct, cells adjacent to the middle position of the nephric duct are induced to form the mesonephric tubule through MET at day 25 of human gestation and mice E9.0. Studies in the mouse have shown that the rostral mesonephros develop to rudimentary glomeruli with branched tubules which connect to the nephric duct. However, the nephric duct and the mesonephric tubules begin to degenerate by apoptosis from E14.5, only some of the anterior mesonephric tubules remain and contribute to epididymal ducts of testis. Despite the unclear role in blood filtration, the mesonephros is important for blood cell development because it is the main sources of hematopoietic stem cells (reviewed in Davidson et al., 2009, Gilbert, 2013).

The permanent kidney in mammals is the metanephros. At mouse E10.5, the caudal nephric duct is budding to form the ureteric bud, and the adjacent mesenchymal cells are specialized to be the metanephric mesenchyme. Interactions between the ureteric bud and the metanephric mesenchyme give rise the metanephros. At mouse E11.5, the ureteric bud invades into the metanephric mesenchyme and promotes aggregation and condensation of the mesenchyme around the tip of the ureteric bud. The condensed mesenchyme (also known as

"induced mesenchyme" or "cap mesenchyme") then forms the renal vesicle through MET, and the renal vesicle stimulates more branching of the ureteric bud. Meanwhile, there is more condensation of the mesenchyme, and more renal vesicles are formed. The branching ureteric bud eventually develops to the collecting system of the kidney, while the rest of the ureteric bud eventually develops to the ureter. Each of the renal vesicles develops into the S-shaped body where the cells are subdivided into podocyte progenitors and the precursors of distal and PCTs (Dressler, 2006). Therefore, each of the S-shaped body grows to a functional nephron through three events: the podocyte express VEGF to attract angioblasts forming the glomerular capillary (Eremina et al., 2003), the proximal and distal tubule become convoluted and link with the loops of Henle, and the distal convoluted tubule fuses with the collecting duct (reviewed in Davidson et al., 2009, Gilbert, 2013).

1.4. Development of the mammalian adrenal gland

The adrenal cortex and medulla arise from two different embryonic sources. The adrenal cortex develops from the urogenital ridge of the intermediate mesoderm, while the adrenal medullary cell develops from the neural crest cells (NCCs), which are a transient embryonic cell population from the dorsal aspect of the neural tube (reviewed in Gilbert, 2013).

Function of the fetal adrenal cortex is critical for fetal survival during pregnancy. Development of the adrenal gland is as early as 4th week of gestation in humans and E9.0 in mice, and goes through several histological phases (reviewed in Else and Hammer, 2005; Wood and Hammer, 2011). In the beginning, the adrenogonadal primordium (AGP) expresses *Steroidogenic factor 1* (*Sf1*) and is specified from the bilateral urogenital ridge. *Sf1* knockout mice lack the adrenal cortex and gonads due to severe apoptosis of the AGP, and die after

birth due to the adrenocortical insufficiency (Luo et al., 1994). The AGP differentiates into the adrenocortical and gonadal primordium at 8th week gestation in humans and E10.5 in mice. The *Sf1* expressions are maintained in the two primordia but are regulated by different factors. The transcription factors, Wilm's tumor suppressor 1 (Wt1) and Lim homeobox protein, Sox9, (Lhx9, also known as Gata4), regulate *Sf1* expression in the developing gonad, while Wt1 and the transcriptional co-factor Cbp/p300-interacting transactivator, with Glu/Asp-rich carboxy-terminal domain, 2 (Cited2) together modulate the expression of *Sf1* in the developing adrenal cortex (Val et al., 2007; and reviewed in Hoivik et al., 2010). The adrenocortical primordium contains two distinct layers, the outer definitive zone (DZ) and the inner fetal zone (FZ). Mechanism of DZ and FZ formation is not clear. The two layers might come from the same precursor but differ by distinct migrations, or the adrenocortical primordium differentiates into two populations of different precursors which then give rise to the DZ and the FZ. Around 8-9th week of gestation in humans and E11.5-E12.5 in mice, the precursors of the adrenal medullary cells, the sympatho-adrenal (SA) cells, migrate and invade into the fetal cortex and embedded within the adrenocortical precursor cells until birth. During the migration of adrenal medullary cells, the fetal cortex is encapsulated by mesenchymal cells and the capsule might modulate differentiation of the outer zona glomerulosa and the inner zona fasciculata form the DZ. The zona glomerulosa produces mineralocorticoids; the zona fasciculata produces glucocorticoids; and the FZ produces the dehydroepiandrosterone for estrogen formation in placental during pregnancy. However, the human FZ degenerates after birth and the mouse fetal zone regresses during the first pregnancy in females or at the age of sexual organ development in males (Kim et al., 2009). As the FZ regresses, the zona fasciculate expands and replaces the FZ, and the inner layer of

the adrenal cortex develops to the zona reticularis at age 6-8 years (reviewed in Else and Hammer, 2005; Wood and Hammer, 2011).

1.5. The morphogenetic movement of adrenal medullary cells

The NCCs give rise to variant cell lineages such as craniofacial cartilage, melanocytes, smooth muscle, glia of the peripheral nervous system, and adrenal chromaffin cells through different paracrine factors from the microenvironment. The SA cell is one of the sympathetic division of the autonomic nervous system (reviewed in Gilbert, 2013).

Studies in the chick embryo have revealed that morphogenesis of adrenal medullary cells undergoes three steps: (1) Common precursors of SA cells migrate ventrally form the neural tube toward the dorsal aorta (DA) and accumulate at the para-aorta region; (2) The SA cells differentiate into sympathetic ganglionic precursors and adrenomedullary precursors; and (3) The adrenomedullary precursors translocate ventrally to invade the adrenal cortex. During SA migration, the DA serves as a signaling center for the proper migration, specification, and differentiation of the SA cells (reviewed in Huber, 2006; Saito and Takahashi, 2015). In step (1), the DA-expressed BMP4 and 7 pattern the distribution of the chemoattractant factors Neuregulin 1 (NRG1) and the stromal derived factor 1 (SDF1; also known as Chemokine (C-X-C motif) ligand 12 (CXCL12)) in the para-DA mesenchyme. Inhibition of either the erb-b2 receptor tyrosine kinases (ErbBs; the receptor of NRG1) or the CXCR4 (the receptor of SDF1) in the NCCs reduces the migration of SA precursors. In addition, simultaneous knockdown of *NRG*1 and *SDF1* results in more severe defects in the SA migration, suggesting that NRG1 and SDF1 synergistically attract the migration and accumulation of the SA precursors near the DA. In step (2), the BMP signaling promotes the specification of

adrenomedullary precursors; while the BMP downstream factor, phosphorylated SMAD family member (pSmad), is specifically expressed in the adrenomedullary precursors but not in the sympathetic ganglionic precursors. Inhibition of the BMP signaling abolishes the adrenomedullary cells, but the sympathetic ganglionic cells are not affected. In step (3), the NRG1 expressed by both the para-aortic mesenchyme and the adrenal cortex, and these NRG1 expressions might be involved in the regulation of adrenomedullary cells dismissing form the DA and invading the adrenal cortex (Saito et al., 2012; and reviewed in Saito and Takahashi, 2015).

1.6. The endothelium in the adrenal gland

As an endocrine organ, the adrenal cortex is highly vascularized. There are three arteries: the superior, middle and inferior suprarenal arteries; and one suprarenal vein, that supply each of the adrenal gland. The adrenal vasculature displays centripetal distribution; the blood flow from the suprarenal arteries first reaches the outer surface (the capsular artery), pass by the cortical arteriole or the medullary arteriole, and then flows into the medullary vein and joins the suprarenal veins (reviewed in Koeppen and Stanton, 2008).

Interactions between the adrenal cell and the endothelial cell (EC) have been found in the cell line studies. Adrenal EC-derived nitric oxide (NO) binds to the cytochrome P450 enzymes and inhibits aldosterone release by zona glomerulosa cells (Hanke and Campbell, 2000). The adrenocortical cell also modulates proliferation, migration, and fenestration of the adjacent ECs by releasing the endocrine gland EGF, such as Endocrine gland derived-VEGF (EG-VEGF) (LeCouter et al., 2001). Moreover, the adrenal-medulla derived cell line adrenal pheochromocytoma (PC12) could be induced by co-culture with the adrenal medulla ECs to

acquire the chromaffin-like characteristics, such as increasing synthesis of the Met-enkephalin and being less sensitive to nerve growth factor (Mizrachi et al., 1990). It suggests that tissue-specific ECs modulate adrenal cell functions. However, whether and how these interactions occur *in vivo* remains unknown. Furthermore, the fetal adrenal in mammals develops in early embryonic stage, making it difficult to study the specification and differentiation of the adrenal cell as well as the coordinated interactions among adrenocortical cells, adrenal medullary cells, ECs, and pronephric cells.

2. The head kidney and the vasculature in the zebrafish

Despite some differences in organ morphology, the zebrafish has been established as an excellent vertebrate model for studying the developmental process of multiple organs, such as vasculogenesis (reviewed in Gore et al., 2012), segmentation of nephric tubes, renal development and kidney regeneration (Drummond, 2003; Wingert and Davidson, 2008; Diep et al., 2011). In addition to the advantages of external fertilization, rapid development, and transparency of embryos, the molecular regulatory mechanisms of organogenesis in the zebrafish are highly conserved. By the well-established techniques for imaging and gene manipulation, the zebrafish is applicable to investigate orchestrated developmental processes of the kidney, interrenal gland, and the endothelium (reviewed in Liu, 2007).

2.1. Organogenesis of the zebrafish kidney and interrenal gland

Despite exerting no function in mammals, the pronephros begins simple filtration in zebrafish as early as 2 days post-fertilization (dpf) and the glomerular function reaches complete maturation after 4 dpf (Drummond et al., 1998; Kramer-Zucker et al., 2005). The

structure of zebrafish pronephros is relatively simple; composed of one fused glomerulus and bilateral segmental pronephric tubules. The zebrafish pronephric tubules, connecting the glomerulus to the cloaca, can be divided into several segments, namely the neck, the PCT, the proximal straight tubule, the distal early tubule, the corpuscle of Stannius, the distal late tubule, the pronephric duct, and the cloaca. These segments are similar to that in the mammals (Wingert and Davidson, 2008). The permanent kidney in zebrafish is the mesonephros which contains hundreds of nephrons, each nephron locates on the top of each mesonephric branches (Zhou et al., 2010).

The teleostean counterpart of the mammalian adrenal gland, the interrenal gland, is firstly identified by Grassi Milano et al. (1997). In zebrafish, the interrenal gland is composed of the interrenal tissue and chromaffin cells, which equals to the adrenal cortex and the adrenal medulla, respectively. The early functional interrenal gland is situated caudal to the pronephric glomerulus during 2- to 3- somite stages and displays a “V-shape” at 3 dpf (Hsu et al., 2003; To et al., 2007; and reviewed in Liu, 2007).

Recently Diep et al (2015) demonstrate that the pronephros serve as a scaffold for the development of the mesonephros. Form 10 dpf, new nephrons and their tubules are formed at the rostral (pronephric glomerular/interrenal region), middle, and caudal region of the pronephros, so that shapes the head, trunk, and tail region of the adult kidney. The pronephros, the new-formed nephrons, and their tubules together form the mesonephros (Diep et al., 2015; Zhou et al., 2010), and the interrenal gland is at the head kidney of the adult zebrafish (Hsu et al., 2003). The interrenal tissue is specified from the pronephros, and these two tissues are tightly associated during their development (Hsu et al., 2003; and reviewed in Liu, 2007).

At around 14 hours post-fertilization (hpf), the *WT1* ortholog, the *wt1a*, can be detected in the bilateral intermediate mesoderm with a broad expression domain. Later at 17 hpf, the *wt1*a paralog, the *wt1b*, is expressed in the caudal region of the *wt1a* expression domain (Bollig et al., 2006). Knockdown of *wt1a* results in severe inhibition of head kidney development, while knockdown of *wt1b* affects the pronephric function and leads to cyst formation in the pronephric glomerulus after 2 dpf (Perner et al., 2007; Hsu et al., 2003). At around 22 hpf, the interrenal precursors are specified from the bilateral pronephric glomerular region and expressed the *SF1* ortholog, the *ff1b* (*nr5a1a*). Ff1b positively regulates the steroid synthesis enzymes such as *cyp11a1* and *3β-Hydroxysteroid dehydrogenase/Δ5-Δ4-isomerase* (*3βHsd*) (Hsu et al., 2003; Chai and Chan, 2000; Chai et al., 2003; Quek and Chen, 2009), knockdown of *ff1b* by anti-sense morpholino (MO) injection disrupts the development of embryonic interrenal tissue (Chai et al., 2003). After specification, interrenal precursors converge on the caudal region of the pronephros and migrate toward the midline at around 24 hpf. Around 28 hpf, the fused interrenal tissue is differentiated, and the enzymatic activity of 3βHsd can be detected. The bilateral pronephric glomeruli coalesce at 36-40 hpf and fuse at the central midline at around 48 hpf. Before the glomerular fusion, the ECs invade the glomerular epithelium, and become surrounded by podocytes which is the specialized epithelial cell in the glomerular tufts (Drummond et al., 1998). After lateral relocalization of the fused interrenal tissue, the caudal region of the interrenal tissue extends across the midline. In the meantime, chromaffin cells migrate to the interrenal area, and integrate with the interrenal tissue to form the functional interrenal organ at 3 dpf (Fig. 3) (Hsu et al., 2003; Liu and Guo, 2006; To et al., 2007; and reviewed in Liu, 2007).

2.2. Vasculogenesis in the zebrafish

The structure of axial vasculature in the zebrafish is relatively simple, as the PCV is immediately ventral to the DA. At the midtrunk, the DA joins to the lateral dorsal aortae (LDA) which connects to the ventricle of the heart, while the anterior branches of the PCV connects to the common cardinal vein (CCV) which links to the atrium of the heart (Isogai et al., 2001; Lawson and Weinstein, 2002, Fig. 4A).

The primitive hematopoietic cells and the endothelium arise from a common precursor, the hemangioblast, which is suggested by the characterization of zebrafish *cloche* (*clo*) mutant which lacks nearly all of the blood and the ECs (Stainier et al. 1995). It is thought that the E26 transformation-specific sequence (ETS) family gene, *ets variant 2* (*etv2*), and *T-cell acute lymphocytic leukemia 1* (*tal1*; also known as *stem cell leukemia* (*scl*)) functions downstream of the *clo* (Patterson and Patient, 2006; Liao et al., 1998). ETS transcription factors regulate expression of the endothelial specific genes such as *fetal liver kinase-1* (*flk1*; also known as *vegf receptor 2* (*vegfr2*) or *kinase insert domain receptor* (*kdr*)) and *vascular endothelial cadherin* (also known as *cadherin 5* (*cdh5*)) (Wakiya et al. 1996; Lelievre et al. 2000), and a loss of *etv2* results in vascular deletion (Sumanas and Lin 2006). *tal1* translates the basic helix-loop-helix transcription factor and is responsible for the formation of both hematopoietic stem cells and angioblasts (Liao et al., 1998). The ETS family proteins also synergistically work with other transcriptional regulatory factors, such as Forkhead (FOX) family and Krüppel-like transcription factor (KLF) genes family to regulate the formation of the angioblast (reviewed in Gore et al., 2012).

At around 7 somite stage in the zebrafish, the first angioblasts which express ETS family transcription factors arise from the bilateral lateral plate mesoderm. The angioblast migrates

toward the midline during 10 to15 somite stage, and the endoderm is required for the initiation of angioblast migration (Alexander et al., 1999; Jin et al., 2005). Meanwhile, the angioblast obtains the arterial cell fate by activation of *hes-related family bHLH transcription factor with YRPW motif 2* (*hey2*; also known as *gridlock*) which is the direct target of the Notch signaling pathway, or differentiates into the venous angioblast by the silencing of the *hey2* (Zhong et al., 2001).

Studies in the lower trunk axial vessel formation have shown that the arterial and venous angioblasts assemble into a cord-like structure during 17 to 20 hpf, and then the venous EC sprouts ventrally to form the axial vein during 22 to 25 hpf (Parker et al., 2004; Jin et al., 2005; Herbert et al., 2009). During this process, the endothelium-secreted extracellular matrix (ECM) protein, EGF-like domain 7 (Egfl7), might create a proper microenvironment for the sprouting of venous ECs, and the expression of EGFL7 is downregulated in mature vessels (Parker et al., 2004). However, detail developmental processes of assembly of the anterior DA and formation of the branched PCV near the head kidney region remain unidentified.

2.3. The role of the endothelial signaling for morphogenetic movements of the head kidney

Both of the pronephros and the steroidogenic interrenal tissue are tightly associated with the axial vessels and undergo angiogenesis during their development. The fused pronephric glomerulus is immediately ventral to the DA. The podocyte-released angiogenic molecules such as Vegfs and Angiopoietin2 attract angiogenesis from the DA to form the pronephric glomerular capillaries (Carmeliet et al., 1996; Majumdar and Drummond, 1999). The steroidogenic interrenal tissue is located between the DA and the right branch of the posterior cardinal vein (PCV) from the dorsal view of around 30 hpf, and the interrenal vessel (IRV) is

sprouted from the DA, and invades the interrenal region during 2 to 3 dpf (Liu and Guo, 2006; Chiu, Master thesis, 2012; Chiu et al., 2012).

During early embryogenesis, the midline convergence of the head kidney is correlated with the migration of mid-trunk angioblasts temporally and spectrally (Fig. 4). Morphogenetic movements of both the pronephros and the interrenal tissue are regulated by the adjacent ECs through different endothelial signals. During the pronephric central fusion, the hemodynamic force in the DA near the pronephric glomerulus stimulates Matrix metalloproteinase-2 (MMP2) release from the EC. MMP2 digests the ECM and promotes the migration and fusion of bilateral pronephric glomeruli. Inhibition of the blood flow by 2,3-Butanedione monoxime (2,3-BDM) or blockage of the MMP2 activity by tissue inhibitor of metalloproteinase-2 results in disrupted fusion of the pronephric glomeruli (Serluca et al., 2002). Angiogenesis of the pronephric glomerular tufts is independent of the blood flow, as indicated by the normal angiogenesis of the bilateral glomeruli in the blood flow-inhibited embryo (Liu and Guo, 2006). Central fusion of the interrenal tissue is regulated by the angioblast adjacent to the interrenal tissue. The *clo* mutant manifests a reduced mRNA expression of the ECM, *fibronectin1* (*fn1*) in the midtrunk (Trinh and Stainier, 2004), and displays the unfused interrenal phenotype which can be rescued by the compensation of ECs loss (Liu and Guo, 2006). However, whether the angioblast mediates central fusion of the interrenal tissue through Fn is not clear. It is also unclear whether the arterial or venous angioblast regulates interrenal central fusion, and whether either the DA or the PCV plays a role for the morphogenetic movements of the interrenal tissue after central fusion remains unknown.

2.4. Vascular microenvironment in the adrenal cortex/interrenal tissue

The microenvironment established by ECM proteins modulates functions of cultured human fetal adrenal cells. Collagen IV enhances cortisol secretion for ACTH-stimulated fetal adrenal cells, while Fibronectin and Laminin together tend to increase the ACTH-stimulated androgen secretion (Chamoux et al., 2001).

Previously in our laboratory, we have investigated the vascular microenvironment in the interrenal region during the interrenal medial extension in the zebrafish. We have found that Fn deposits at the ventral side of the DA and the tip of the IRV, and that the deposition is required for the IRV growth and the medial extension of the steroidogenic interrenal tissue. In the *fn1* mutant, morphogenetic movements of the steroidogenic interrenal tissue and formation of the IRV are inhibited. Accumulation of Fn is regulated by the blood flow, an inhibition of the blood flow disrupts the pattern of Fn deposition and affects the direction of IRV growth. Moreover, the Fn-Integrinα5 interaction activates focal adhesion kinase (FAK) as well as the upregulation of the phosphorylated FAK (pFAK) expression, suggesting that the Integrin-Fak signaling pathway is involved in the process of IRV growth and interrenal medial extension (Chiu, Master thesis, 2012; Chiu et al., 2012). Other studies in the zebrafish have suggested that the blood flow promotes pronephric glomerular fusion through EC-released MMP2 (Serluca et al., 2002), regulates HSC development through Klf2a-NO signaling cascades (Wang et al., 2011), and facilitates heart valve formation through Klf2a but NO-independent signaling pathway (Vermot et al., 2009). However, how the blood flow regulates Fn deposition, and whether Fn is involved in IRV growth and interrenal medial extension are not clear. In the blood flow-defecient embryo, the effect of the defective interrenal medial extension on chromaffin cell migration, as well as the functional assembly of the interrenal organ, remains unknown.

2.5. The role of endoderm for the midline convergence of the mesodermal tissues

The *casanova* (*cas*) mutant lacks the endoderm and exhibits the phenotype of bilateral heart tubes, an abnormal vasculature, and defective convergence of blood and pronephric precursors. It suggests that the endoderm may provide signal(s) or serve as a substrate in midline convergence of these mesodermal organs (Alexander et al., 1999). Although a loss of endoderm does not affect angioblast differentiation, the midline convergence of bilateral angioblasts is perturbed. Although the migrating angioblasts eventually reach the midline at 22 hpf and form the lumen of the axial vessels in the *cas* mutant, the PCV is more dilated compared to its wildtype sibling (Jin et al., 2005).

We have been characterizing the phenotype of the steroidogenic interrenal tissue in the *cas* mutant. Knockdown of the mutated gene in *cas* mutant, *SRY (sex determining region Y)-box 32* (*sox32*) (Kikuchi et al., 2001; Dickmeis et al., 2001), results in severe inhibition of the interrenal midline convergence, malformed vasculature, and defective angiogenesis of the pronephric glomeruli (Hsu, Master thesis, 2010). Previous study has shown that *odd-skipped related transcription factor 1* (*osr1*) restricts early endodermal differentiation from the mesendoderm which is the common precursor of the mesoderm and the endoderm, and knockdown of *osr1* results in expansion of the endoderm (Mudumana et al., 2008). Therefore, we have performed additional knockdown of *osr1* in the endodermless embryo to rescue the endoderm loss, and we have found that the severe interrenal convergence phenotype can be rescued, suggesting a role of endoderm for the interrenal midline convergence. To our surprise, the severe defects in the interrenal midline convergence can also be rescued by a loss of vasculature. The distance between bilateral interrenal tissues is decreased in the *sox32*MO-

injected *clo* mutant, as compared to that in the *sox32*MO-injected wildtype sibling (Hsu, Master thesis, 2010).

Taken together, roles of endothelial signaling for the interrenal morphogenesis have been found by our previous studies: (1) the endoderm interacts with the endothelium that regulates the process of interrenal midline convergence (Hsu, Master thesis, 2010); (2) the endothelium patterns interrenal central fusion and lateral relocalization (Liu and Guo, 2006); (3) the blood flow-regulated Fn deposition mediates interrenal medial extension and IRV growth (Chu, Master thesis, 2012). However, the orchestrated interactions among the ECs, the pronephros, the interrenal tissue, and the chromaffin cell during interrenal development remains unclear. Therefore, in this thesis, we want to further investigate the multiple roles of the endothelium during interrenal organogenesis, including (1) the role of the migrating angioblast for midline convergence of the head kidney during early embryogenesis by studying in the endodermless embryo; (2) the effects of either the DA or the PCV formation on interrenal morphogenetic movement; and (3) the roles of blood flow and Fn for the process of interrenal organ functional assembly, namely the integration of interrenal tissue and chromaffin cells.

Materials and methods

Fish stocks

The zebrafish (*Danio rerio*) was raised by standard method (Westerfield, 2000). Embryos for staining experiment were cultured in egg water and treated by phenylthiourea (PTU, 0.03%; Sigma) to inhibit pigment formation. *Tg(kdrl:mCherry)*^{ci5} was obtained from Taiwan Zebrafish Core Facility; *Tg(fli1:EGFP)*^{Y1} and *Tg(sox17:EGFP)*^{s870} were obtained from Zebrafish International Resource Center (Eugene, OR); *Tg(kdrl:GFP)*^{s843} was gifted from Prof. Didier Stainier (Max Planck Institute, Germany); *Tg(wt1b:GFP)*^{li1} was gifted from Dr. Christoph Englert (Fritz-Lipmann Institute, Germany); *Tg(ff1bEx2:GFP)* was gifted from Dr. Woon-Khiong Chan (National University of Singapore, Singapore).

Two-color whole-mount *in situ* hybridization (ISH)

Embryos for ISH analyses were fixed by 4% paraformaldehyde containing 0.1% Tween 20 (4%PFAT) (Sigma) at 18~20°C for overnight, stepwise dehydrated by methanol and stepwise rehydrated by PBS containing 0.1% Tween 20 (PBST). After rehydration, embryos were digested by proteinase K (Amibion), post-fixed by 4%PFAT, washed by PBST, equilibrated in Hyb- (50%formamide/5xSSC/0.1% Tween 20), and then equilibrated in Hyb+ (Hyb- solution containing heparin and tRNA) solution. For hybridization, the embryos were incubated in Hyb+ solution containing digoxigenin (DIG)-labelled and fluorescein (Flu)-labelled antisense riboprobes at 66°C for around 1 day. The information of plasmids for making anti-sense riboprobes was listed in Table 2. The DIG-labelled riboprobe was detected by anti-DIG antibody conjugated with alkaline phosphatase (Roche) and visualized by 5-Bromo-4-chloro-3-indolyl phosphate (BCIP) and 4-nitroblue tetrazolium (NBT) (Promega).

The Flu-labelled riboprobe was detected by anti-Flu antibody conjugated with alkaline phosphatase (Roche) and visualized by Fast Red (Roche). After ISH, the yolk-sac of the stained embryo was removed for flat-mount analysis and mounted in 50% glycerol for imaging.

Microinjections

Microinjection was performed by Nanoject injector (Drummond Scientific Company) with Borosilicate glass capillaries (Sutter Instrument) at one- to two-cell stage. For injections of MOs, the MOs were synthesized by Gene tools LLC, dissolved by ddH2O at 2 mM for storage and diluted by 1x Danieau solution before injections. The dosage and sequence of the MOs were listed in Table 1. For mRNA injections, the *hey2* mRNA and the *sox32* mRNA were synthesized by SP6 RNA polymerase mMESSAGE mMACHINE kit (Ambion).

3βHsd enzymatic activity assay and immunohistochemistry (IHC)

The method of 3βHsd enzymatic activity staining was modified from Grassi Milano et al. (1997). Embryos were fixed by 2% paraformaldehyde containing 0.1% Tween 20 (2%PFAT) (Sigma) at 4°C for overnight, washed by PBST for 10 minutes four times. Then the washed embryos were incubated in fresh-made staining solution until the clear signal was shown. The staining solution was mixed by two mixtures: mixI containing 0.1 mg/ml dehydroandrosterone (Sigma) and 0.2 mg/ml β-nicotinamide adenine dinucleotide hydrate (Sigma) in dimethyl sulfoxide (DMSO); mixII containing 0.1 mg/ml nicotinamide (Vitamin B3; Sigma), and 0.1mg/ml NBT (Promega) in PBST. For IHC, the 2%PFAT-fixed embryo or the 3βHsd stained-embryo was embedded by 4% NuSieve GTG low-melting agarose (Lonza)

and sectioned by Leica VT1000M vibratome. Then the slide was permeabilized with PBS containing 0.5% Triton X-100 (PBSTx) 15 minutes six times and washed with 1% BSA/1% DMSO/0.1% Triton X-100 in PBS (PBDTx) 10 minutes four times at room temperature. After blocking with PBDTx containing 2% fetal calf serum (FCS) (as the blocking solution) at room temperature for 1 hour, the slide was incubated in PBDTx containing primary antibody at 4°C for 1.5 day and washed by PBDTx 10 minutes six times. After blocking at room temperature for 1 hour, the slide was incubated in PBDTx containing 1/200 Dylight^{TM594}-conjugated goat anti-rabbit IgG (Abcam) or PBDTx containing 1/200 Dylight^{TM650}-conjugated goat anti-mouse IgG (Abcam) at 4°C for 1.5 day. Before confocal imaging, the slide was washed with PBDTx 10 minutes six times and PBST 10 minutes four times then mounted in 50% glycerol. The concentration of antibodies was listed in Table 3. For staining α-1 subunit of Na/K ATPase (α6F), the embryo was fixed by Dent's solution (80% methanol and 20% DMSO), and rehydrated stepwise by PDBTx. After blocking at room temperature for 2 hours, the embryo was incubated in the PDBTx containing 1% FCS and 4% α6F antibody (Developmental Studies Hybridoma Bank) at 4°C for 1.5 day. After washing the embryo with PBDTx containing 1% FCS, the embryo was blocked by PBDTx containing 10% FCS. Then the embryo was incubated in PBDTx containing 1% FCS and 1/200 Dylight^{TM594}-conjugated goat anti-rabbit IgG (Abcam) at 4°C for 1.5 day. Before imaging, the embryo was washed with PBDTx containing 1% FCS for 30 minutes five times, PBSTx for 10 minutes four times, and cleared by 50% glycerol.

Pharmacological treatments

Dechorionated embryos were incubated with egg water supernatant with 0.03% PTU to inhibit pigmentation during pharmacological treatment. For inhibition of the blood flow, the 2,3-BDM (Sigma) was dissolved in ddH_2O at 40 mM for storage and diluted by egg water before being applied on the embryos. Treatments were started from 1.5 dpf. The embryos were shocked by 20 mM 2,3-BDM for 5 mins to stop the heartbeat and then incubated in egg water, or egg water containing 2 or 6 mM 2,3-BDM until fixation. For the recovery of blood flow, 6 mM 2,3-BDM was replaced with egg water at 2.5 dpf for further incubation until fixation. For acceleration of the blood flow, norepinephrine (Sigma) was freshly prepared by egg water at 0.01, 0.1 or 1 mM, and the treatment period was from 33 hpf to 2 dpf. For camptothecin (Sigma) treatment, the 48 hpf embryos were incubated with camptothecin at 60 mM containing 0.1% DMSO (Sigma) and were harvested at 57 hpf for the 3βHsd activity assay. For L-arginyl-L-glycyl-L-aspartic acid (RGD; Sigma) treatment, the peptide was dissolved by filter-sterilized egg water at 1 mM and applied to the embryo at a final concentration of 100 mM. RGD treatment was performed from 26 hpf to 2.5 dpf.

Transplantation

Methods for transplantation were similar to that used by Chung and Stainier (2008) and the schematic diagram of the transplantation experiment was shown in figure 9A. The donors (AB strain) were labelled by injection with a fluorescein dextran mixture (5% Alexa Fluor fixable 568 in 0.2 M KCl, 10,000 MW; Invitrogen) and the *sox32* mRNA (20 ng/ul) at 2- to 4-cell stage, while the recipients (*Tg(fli1:EGFP)*^{Y1}) were injected with *sox32*MO (5 ng/ul) at the one-cell stage. At midblastula stag (approximately 1,000-2,000 cells) of the donor embryo, about 20-40 cells were taken off from the animal pole and carefully transplanted into the 4

hpf recipients along the blastoderm margin without damaging the yolk. The recipients were allowed to develop and fixed at 34 hpf for 3βHsd enzymatic activity assay and confocal imaging.

Imaging and quantification

Whole mount samples, deyolked samples, and sections were cleared by 50% glycerol in PBS and captured either as single confocal section or as projection of a Z-stack by the LSM microscope (Carl Zeiss Ltd., Germany) equipped with Fluar 10x/0.5 objective lens and Fluar 20x/0.75 objective lens. The GFP, mCherry/dylight 594, dylight 650, and 3βHsd staining (bright field) were recorded by Argon 488-nm (with bandpass filter 505-530 nm), Helium-Neon 543-nm (with bandpass filter 560-615 nm), Helium-Neon 633 (longpass filter 650 nm), and Helium-Neon 543-nm (with transmitted light channel), respectively. For time-lapse imaging, the *Tg(ff1bEx2:GFP)* embryo was embedded in 3% methylcellulose with the dorsal side up and the GFP was recorded as a z stack (6-μm slices) in an interval of 1 minutes. The z stack was assembled as a 3D projection and the projected image was merged with the bright field by the LSM510 version 3.5 software (Carl Zeiss). The deyolked whole-mount ISH sample was photographed under Nomaski optics on an Olympus (Center Valley, PA) BX51 microscope system. Distance measurement and quantification of 3βHsd activity staining were performed by AxioVision 3.0 software (Carl Zeiss) and Image Gauge version 4.0 (Fuji Photo Film), respectively. IRV length and fluorescence intensities of the region of interest (ROI) were quantified by LSM 510 version 3.5 software (Carl Zeiss).

Statistical analysis

All quantitative results are presented as the mean and the standard error of the mean (SEM). Data was evaluated by either analysis of variance (ANOVA), followed by Duncan's new multiple range test or Student's t test. A P value less than 0.05 was considered statistically significant.

Results

Part 1. The role of the migrating angioblast in midline convergence of the head kidney

1.1. Midline convergence of the head kidney and the angioblast are disrupted in the endodermless embryo

In order to verify the pronephric and interrenal phenotype in the endodermless embryo, we performed two color ISH of either *wt1a* plus *ff1b* or *wt1a* plus *ff1b* in the *cas* mutant and its wildtype sibling at 34 hpf (Fig. 5). The pronephric glomerulus was marked by either the *wt1a*- or the *wt1b*-expression, and the interrenal tissue was marked by the *ff1b*-expression. We found that the wildtype sibling displayed a fused interrenal tissue associated with a closely connected-pronephric glomeruli, but the *cas* mutant exhibited a widely bilateral interrenal tissues connected to a widely bilateral pronephric glomeruli. It suggested that loss of endoderm resulted in a severely defective midline convergence of the head kidney.

In order to understand the effects of the endoderm on the differentiated steroidogenic interrenal tissue and the pronephros, we injected *sox32*MO into the *Tg(wt1b:GFP)*^{li1} embryo and performed 3βHsd enzymatic activity assay. In agreement with Bollig et. al. (2009), the *wt1b*-driven green fluorescent protein (GFP) was expressed in the pronephric glomeruli, which was consistent with the *wt1b* mRNA expression domain, and was also ectopically expressed in the pronephric tubules (neck and PCTs) and partial endodermal tissues (gut and pancreas) (Fig. 6A,B). The 3βHsd-detected steroidogenic interrenal tissue was segregated form the pronephric region and located caudal to the right pronephric glomerulus from the dorsal view in the control embryo (Fig. 6A,B). In the *sox32* morphant, midline convergence of the steroidogenic interrenal tissue and the pronephric glomerulus was severely inhibited (Fig. 6B), which was consistent with the result of ISH on the *cas* mutant (Fig. 5). Distance

between the bilateral interrenal tissues and distance between the bilateral pronephric glomeruli were largely increased in the *sox32* morphant than that in the control embryo (Fig. 6C,D). In addition, the steroidogenic interrenal tissue still resided in the pronephric region in the *sox32* morphant, suggesting a role of endoderm for segregation but not differentiation of the head kidney (Fig. 6B).

In order to verify the phenotype of axial vasculature as well as the pronephric angiogenesis in the endodermless embryo, the *sox32*MO was injected into the *Tg(wt1b:GFP)*^{li1} x*Tg(kdrl:mCherry)*^{ci5} embryo in which the pronephros was labelled by GFP and the EC was labelled by red fluorescence. In the control embryo, the bilateral pronephric convoluted tubules were adjacent to the PCV and the angiogenesis of the pronephric glomeruli could be detected. But in the *sox32* morphant, glomerular angiogenesis was defective and the two branches of the PCV were more dilated (Fig. 6E) which was consistent with the observation in Alexander et al. (1999) and our previous finding (Hsu, Master thesis, 2010). Moreover, the steroidogenic interrenal tissue was located between the DA and the right branch of the PCV in the control embryo, but the bilateral interrenal tissues were disassociated with the DA and still tightly associated with the two branches of the PCV in the *sox32* morphant (Fig. 6F). The glomerular capillary is sprouted form the DA (Drummond et al., 1998), and the defective glomerular angiogenesis in the endodermless embryo also suggested that the bilateral pronephric glomeruli were associated with the PCV but not the DA. These results indicated that, loss of endoderm inhibited the midline convergence of the head kidney as well as the migration of venous angioblast, and the bilateral head kidneys were still closely associated with the malformed PCV.

1.2 The phenotype of the head kidney in the *sox32* morphant is not due to a perturbed laterality

The Kupffer's vesicle is a developmental cilia organ and is responsible for determination of the left-right asymmetry. Knockdown of *sox32* resulted in a defective Kupffer's vesicle, so that left-right asymmetry was perturbed in the *sox32* morphant (Alexander et al., 1999). In order to figure out whether the phenotype of the head kidney in the *sox32* morphant was due to a disruption of general laterality instead of a loss of endoderm, we analyzed the effect of *polycystic kidney disease 2* (*pkd2*) knockdown on the interrenal tissue. *pkd2* functions downstream of *sox32* and is essential for cilia function and therefore determination of left-right asymmetry, but not required for endoderm formation (Bisgrove et al., 2005). The *pkd2* morphant displayed a curly tail phenotype (Fig. 7A) which phenocopied the *pkd2* mutant (*curly up*) (Schottenfeld et al., 2007), and a randomized laterality (Fig. 7B-E) but no severe convergence defect of the interrenal tissue. Furthermore, the glomerular angiogenesis was unperturbed and the morphology of the PCV was nearly normal in the *pkd2* morphant (Fig. 7B'-E'). It suggested that the convergence phenotype of the head kidney and the EC in the *sox32* morphant was specifically due to a loss of endoderm rather than a disrupted left-right asymmetry.

1.3. Defective midline convergence of the interrenal tissue and the pronephros in the endodermless embryo is rescued by the knockdown of *osr1*

Previously we have compensated the endoderm loss in the *sox32* morphant by simultaneous knockdown of *osr1*, and found that the severe convergence defect of the steroidogenic interrenal tissue and the malformed PCV were both rescued (Hsu, Master thesis, 2010). In order to further address whether the severe convergence phenotype of the

pronephros in the endodermless embryo could be rescued by a simultaneous knockdown of *osr1*, we co-injected the *osr1*MO plus *sox32*MO into the *Tg(wt1b:GFP)*^{li1} embryo. The expanded endoderm in the *osr1* morphant alteres the balance between the renal and the vascular development, and resulted in a loss of anterior pronephric tubules and an expanded population of angioblasts. Moreover, the loss of anterior pronephric tubules can be rescued by a simultaneous knockdown of *sox32* (Mudumana et al., 2008). Consistently, we found that the anterior pronephric tubules labelled by *wt1b*-GFP were missing in the *osr1* morphant (Fig. 8C), and that could be rescued in the *sox32*MO/*osr1*MO double morphant (Fig. 8D). In addition, we also performed IHC of α6F to mark the epithelial cells in whole pronephric tubules (Drummond et al., 1998; Fig. 8K). The absent anterior pronephric tubules in the *osr1* morphant and the rescued anterior pronephric tubules in *sox32*MO/*osr1*MO double morphant (Fig. 8K) suggested that the phenotype that caused by *osr1*MO could be rescued by simultaneous injection of *sox32*MO. It also suggested that the endodermless phenotype caused by *sox32*MO could be rescued by a simultaneous injection of *osr1*MO. Furthermore, the *sox32*MO/*osr1*MO double morphant also exhibited nearly normal midline convergence of the head kidney (Fig. 8D). Distance between the bilateral interrenal tissues and distance between the bilateral PCTs in the *sox32*MO/*osr1*MO double morphant were shorter than that in the *sox32* morphant (Fig. 8B,D,I,J). These results suggested that double knockdown of *sox32* and *osr1* rescued the effects of either *sox32*MO or *osr1*MO. So the compensation of the endoderm loss in the *sox32* morphant rescued the severely defective midline convergence of the head kidney.

In order to confirm whether the endodermal loss in the *sox32* morphant was actually rescued by a simultaneous knockdown of *osr1*, we co-injected the *osr1*MO plus *sox32*MO

into the *Tg(sox17:EGFP)*^{s870}embryo. *Tg(sox17:EGFP)*^{s870} is the endoderm-specific reporter line, in agreement with Sakaguchi et al. (2006), the *sox17*-driven GFP is expressed in the endodermal organs such as the gut and the pancreas (Fig. 8E). Those endodermal tissues were absent in the *sox32* morphant, but expanded in the *osr1* morphant (Fig. 8F,G). Interestingly, the endodermal phenotype in both of the *sox32* morphant and *osr1* morphant could be rescued by a double knockdown of *sox32* and *osr1* (Fig. 8H), indicating that the endodermal loss caused by the *sox32*MO could be compensated by the *osr1*MO. Besides, the steroidogenic interrenal tissue was still tightly associated with the pronephric glomerulus in all of the treatments, suggesting that the genetic interaction between *sox32* and *osr1* did not affect the head kidney differentiation and association.

1.4. Transplantation of *sox32*-overexpressing cells rescues severe convergence defects of the head kidney in endodermless embryos

In order to further understand the effect of the endoderm on midline convergence of the head kidney, we transplanted the dextran-labelled *sox32*-overexpressing cells into the *sox32* morphant along the blastoderm margin of the recipients at around 4 hpf (Fig. 9A) and analyzed the interrenal phenotype at 34 hpf. We found that the severe convergence of the steroidogenic interrenal tissue and the malformed PCV in the *sox32* morphant could be rescued by transplantation of the *sox32*-overexpressed cells (Fig. 9D). Distance between the bilateral interrenal tissues and distance between the two branches of the PCV in the recipient were similar to that in the control embryo and was much shorter than that in the *sox32* morphant (Fig. 9F,G), suggesting that compensation of the endodermal cell in the *sox32* morphant rescued the severe midline convergence phenotype of the interrenal tissue.

Moreover, we found that the dextran-labelled transplanted cells were tightly associated with the host venous vasculature in all of the recipients (n=12; Fig. 9E), indicating a strong interaction between the endodermal cell and the venous cell.

Taken together, a lack of endoderm resulted in the bilateral head kidneys and the malformed PCV, while compensation of the endodermal loss by either knockdown of *osr1* or transplantation of *sox23*-overecpressing cells could rescue the head kidney and PCV phenotypes.

1.5. A loss of endothelium suppresses the severe convergence defect of the head kidney in endodermless embryos

Previously we have identified the role of ECs in endoderm-regulated midline convergence of the steroidogenic interrenal tissue by injection of the *sox32*MO into the *clo* mutant and its wildtype sibling (Hsu, Master thesis, 2010). In order to further analyze the effects of the malformed vasculature in the *sox32* morphant on midline convergence of the pronephros, we inhibited the *clo*-regulated genes in the endodermless embryo by co-injection of the *sox32*MO plus *etv2*MO or *sox32*MO plus *tal1*MO into the *Tg(wt1b:GFP)*^{li1} embryo. The control embryo displayed a fused interrenal tissue on the right side of the midline, but the *etv2* morphant or the *tal1* morphant displayed a fused the interrenal tissue at central midline (Fig. 10A,C; 11A,C). It suggested that knockdown of either *etv2* or *tal1* did not affect midline convergence or fusion of the interrenal tissue, but instead inhibited asymmetric movement of the fused interrenal tissue. In the *sox32*MO/*etv2*MO- and the *sox32*MO/*tal1*MO- double morphants, the segregation between interrenal tissue and pronephros was not affected, but there was a big cyst in the pronephric glomerulus which phenocopied the *sox32* morphant

(Fig. 10B’,D’,E’; 11B’,D’,E’). Besides, compared to the *sox32* morphant, the inter-distance between bilateral interrenal tissues and the distance between bilateral pronephric glomeruli were decreased in both of the *sox32*MO/*etv2*MO double morphant and the *sox32*MO/*tal1*MO double morphant (Fig. 10F,G; 11F,G), indicating that the severe midline convergence phenotype of the head kidney in the endodermless embryo was rescued by removing the malformed vasculature.

In order to confirm the effects of the MO injections on the midtrunk vasculature, we repeated the double knockdown experiments on *Tg(kdrl:GFP)*^{s843} embryos. Consistent with the previous findings, knockdown of either *etv2* or *tal1* led to a severe reduction of ECs at the midtrunk (Liao et al., 1998; Sumanas and Lin, 2006; Fig. 12C-F), and the severe defects in midline convergence of interrenal tissues was rescued by a loss of endothelium (Fig. 12E,F). We also noticed that some ECs were present at the midtrunk in both of the *etv2* morphant and *tal1* morphant, and we speculated that the residual ECs might promote the central fusion of interrenal tissues (Fig. 12B,C), so the closely bilateral interrenal tissues in the *clo* mutant was due to the complete loss of the angioblast (Liu and Guo, 2006).

Taken together, loss of the endoderm inhibited midline convergence of the venous EC and led to a more dilated branches of the PCV. The endoderm was not necessary for midline convergence of the head kidney, since a simultaneous inhibition of endoderm and endothelium did not generate a severe midline convergence phenotype of the head kidney (Fig. 10D-G; Fig. 11D-G; Fig. 12D,F). However, in the endodermless embryo, the malformed PCV restricted the midline convergence of the head kidney by the tight association between the head kidney and the venous EC, resulting in a widely bilateral head kidney phenotype.

1.6. VegfC/Flt4 is required for the interaction between venous vasculature and the head kidney

During vasculogenesis, angiogenesis, and lymphangiogenesis, the VegfC receptor, Flt4 (also known as Vegfr3), is expressed in the venous structures such as the PCV, the CCV, the caudal vein, and the intersegmental vein (Hogan et al., 2009; Kuchler et al., 2006; Ober et al., 2004). On the other hand, *vegfC* is abundantly expressed in the developing anterior hindbrain, the boundary of the midbrain and hindbrain, and is weakly expressed in the DA and the pronephros; and these expression domains are adjacent to the *flt4*-expressing cells (Ober et al., 2004). The interaction between Flt4 and VegfC modulates the PCV development, the ensheathment of the CCV lumen, the lymph formation, and the spouting of intersegmental arteries (Hogan et al., 2009; Kuchler et al., 2006; Ober et al., 2004). However, whether the VegfC/Flt4 signaling was involved in the head kidney development is unknown.

In order to further confirm whether *vegfC* was expressed in the pronephros and interrenal tissue, we analyzed the expression of either *vegfC* plus *wt1b,* or *vegfC* plus *ff1b,* by two color ISH. Although the expression of *vegfC* was weak, it was readily detected in both the pronephric glomerulus and the interrenal tissue (Fig. 13A). Next we would like to verify whether the VegfC protein was expressed in the pronephros, we performed vibratome cryosection on *Tg(wt1b:GFP)*^{li1} embryos, and IHC staining of VegfC on the section of the pronephric glomerulus (Fig. 13B). We found that the VegfC protein could be detected in the neural tube, gut, and enriched in the pronephric glomerulus (Fig. 13C), suggesting a role of VegfC/Flt4 signaling in the head kidney-venous EC interaction.

In order to examine whether the VegfC/Flt4 signaling is involved in the interaction between the venous angioblast and the head kidney during midline convergence of the head

kidney, we downregulated either *vegfC* or *flt4* in the control embryo by injection of *vegfC*MO or *flt4*MO, or downregulated either *vegfC* or *flt4* in the endodermless embryo by co-injection of *sox32*MO/*vegfC*MO or *sox32*MO/*flt4*MO into the *Tg(kdrl:GFP)*^{s843} embryo. We found that the structure of CCV was malformed in either the *vegfC* morphant or the *flt4* morphant (Fig. 14C',D'), which was consistent with the finding in the *vegfC* mutant (Helker et al., 2013). In addition, knockdown of either *vegfC* or *flt4* did not inhibit midline convergence of the steroidogenic interrenal tissue, however, the lateral relocalization of the fused interrenal tissue was inhibited (Fig. 14C,D). Moreover, we found that the steroidogenic interrenal tissue was associated with the DA instead of the PCV (Fig. 15B), implying that the *vegfC*/*flt4* signaling was required for the interaction between the interrenal tissue and the venous angioblast.

We found that 85% of the *sox32*MO/*vegfC*MO double morphant population and 41% of the *sox32*MO/*flt4*MO double morphant population displayed a single interrenal cluster at the midline (Fig. 14E,G). The inter-distance of the bilateral interrenal tissue and the distance between the two branches of the PCV were both decreased in either the *sox32*MO/*vegfC*MO or the *sox32*MO/*flt4*MO double morphant, compared to that in the *sox32* morphant (Fig. 15A). It suggested that the severe midline convergence phenotype of the interrenal tissue in the endodermless embryo could be rescued by knockdown of either *vegfC* or *flt4*. Therefore, the VegfC/Flt4 signaling was required for the interaction between the head kidney and the venous angioblast.

1.7. Conclusion

Taken together, the head kidney was tightly associated with the venous angioblasts through VegfC/Flt4 signaling during early embryogenesis. The midline signal was

independent of the endoderm and it attracted the migration of the bilateral mesodermal tissues toward the midline (Fig. 16A). The endoderm is required for the venous angioblast migration, loss of endoderm inhibited migration of the venous angioblast and resulted in a malformed PCV. Midline convergence of the head kidney was also inhibited in the endodermless embryo because it was tightly associated with the malformed PCV (Fig. 16B). Severe midline convergence defects of the head kidney in the endodermless embryo could be rescued by either elimination of the ECs (Fig. 16C) or breakage the interaction between the head kidney and the venous ECs (Fig. 16D). Therefore, we speculated that the widely bilateral head kidney phenotype in the endodermless embryo was secondary to the malformed PCV. In conclusion, in this part of study we found that the endoderm indirectly regulated the midline convergence of the head kidney through venous ECs and VegfC/Flt4 signaling.

Part 2. The role of axial vessel formation for the interrenal morphogenetic movement

2.1. The interrenal tissue undergoes lateral relocalization after central fusion

In order to further identify the process of interrenal fusion and repositioning in the developing embryo, we recorded the process of interrenal morphogenetic movement by a time-lapse confocal analysis on one *Tg(ff1bEx2:GFP)* embryo where the GFP is driven by the *ff1b* promoter (Quek, Ph.D. thesis, 2009). The *ff1b*-driven GFP is expressed in the ventral medial hypothalamuses with their neuronal projections and the interrenal tissue which recapitulates the *ff1b* mRNA expression. The GFP is also ectopically expressed in slow muscle precursors (Chai, Ph.D. thesis, 2002; Fig. 17B). We confirmed the GFP-expressing cluster in the third somite was the interrenal tissue, evidence by the colocalization with the 3βHsd enzymatic activity staining at 32 hpf. We also found that the GFP-expression domain

was more expanded than the NBT/BCIP-deposited 3βHsd activated region, suggesting the *ff1b*-driven GFP was expressed in both differentiated and undifferentiated interrenal tissue (Fig. 17A).

The GFP-marked bilateral interrenal tissues could be detected as early as 21-somite stage, and the time-lapse confocal analysis starts from this stage. From the dorsal view, after the two cluster of interrenal cells fused at central midline, the fused interrenal tissue migrated locally to right of the midline (Fig. 17B). So this data excluded the possibility of asymmetric migration and fusion of the bilateral interrenal tissues, and it also rule out the possibility that one of the bilateral interrenal tissues degenerated during early interrenal organogenesis. The size of *ff1b*-driven GFP was increased during interrenal development, suggested that the interrenal cells as migration as proliferation (Fig. 17C) and also supported that no asymmetric apoptosis happened in the bilateral interrenal tissues. Due to the temperature of the confocal imaging was low (~23°C), the time for the bilateral interrenal fusion and lateral relocalization (around 4 hours) was much longer than that in the standard situation. Therefore, we performed ISH of *ff1b* during interrenal fusion and lateral relocalization, the bilateral interrenal tissues fused at central midline around 22 somite stage and started to relocate away from the midline around 24 somite stage. At 26 somite stage, the interrenal tissue became to be a leaf-shape cluster at left side of the midline by the ventral flat-mount view (Fig. 17D).

2.2. The EC is required for central fusion and lateral relocalization of the interrenal tissue

Morphogenetic movement of the interrenal tissue was closely related to the adjacent ECs. In the part 1 study of this thesis, we revealed that the head kidney was tightly associated with the migrating venous angioblast and this association patterned head kidney midline

convergence during early embryogenesis. Study in the the *clo* mutant indicates that the angioblast regulates the process of interrenal tissue central fusion (Liu and Guo, 2006). In the *etv2* morphant and the *tal1* morphant, the fused interrenal tissue remained at central midline rather than at right of the midline compared with the control embryo (Fig. 10C;11C). Moreover, simultaneous inhibition of the endoderm and the endothelium could rescue the severe midline convergence phenotype of the interrenal tissue in the endodermless embryo, but could not rescue the defective lateral relocalization of the interrenal tissue. Therefore, the endothelium must be involved in the process of interrenal central fusion and lateral relocalization.

In order to further verify the role of the EC in interrenal central fusion and lateral relocalization, we performed *etv2*MO injection on the *Tg(fli1:EGFP)*^{Y1} embryo, in which the EC was labelled by the GFP, and increased the sample number. We found most of the control embryo exhibited a single interrenal cluster at the right of the midline with a normal vasculature (symbol as “normal”) (n=112, 96.6%; Fig. 18A) and the others exhibited a closely bilateral interrenal tissues with a normal vasculature (n=4, 3.4%). The *etv2* morphant displayed three different degrees of interrenal phenotypes (Fig. 18B-D): normal, n=12, 11.3%; class(I) phenotype, single cluster from the midline fusion of bilateral ones (n=36, 34.0%); class (II) phenotype, closely bilateral elongated clusters with caudal ends fusing at the midline (n=31, 29.2%); class (III) phenotype, closely bilateral clusters across the midline (n=27, 25.5%) (Table. 4). Consistent with previous findings, development of the ECs was severely inhibited (Liao et al., 1998; Sumanas and Lin, 2006; Fig. 12C,D), and the steroidogenic interrenal tissue was associated with the residual ECs in all of the *etv2* morphants (Fig. 18B-D). We found that the degree of the interrenal central fusion phenotype was correlated to the

different amount of the residual ECs, further confirming that the ECs was required for interrenal tissue central fusion (Liu and Guo, 2006). Furthermore, the class (I) phenotype in the *etv2* morphant showed a fused interrenal tissue at the central midline but fail to migrate laterally, suggesting that the lateral relocalization of the interrenal tissue was inhibited by the loss of endothelium as well as the malformed vasculature.

Lack of the axial vessels also inhibits the blood flow. The time point we analyzed the interrenal phenotype of the *etv2* morphant was 34 hpf, while the blood flow started form 26 hpf. In order to understand the effect of blood flow on interrenal lateral relocalization, we analyzed the interrenal phenotype in the *cardiac troponin T2* (*tnnt2a*) morphant at 34 hpf. Tnnt2a is one component of the cardiac myocyte; mutation of the *tnnt2a* (*silent heart*) results in an absent of blood flow (Sehnert et al., 2002). We found that the *tnnt2a* morphant displayed a fused interrenal tissue at right of the midline (Fig. 18E) and the gross development of the vasculature such as the DA, the PCV, the intersegmental vessel (ISV), the glomerular capillaries, and the subintestinal vessel (SIV) were unperturbed (Fig. 18E,F), indicating that the interrenal lateral relocalization required the ECs but not the blood flow.

2.3. The artery is required for lateral relocalization of the interrenal tissue

The fused interrenal tissue moved away from the central to the right of the midline at around 24-26 somite stage (Fig. 17D). In the meantime, the cord-like angioblast aggregates formed the DA and PCV at around 21-25 hpf (Parker et al., 2004; Jin et al., 2005; Herbert et al., 2009). The DA is implicated to be a regulator for lateral relocalization of the interrenal tissue due to a defective lateral repositioning of the interrenal tissue in the *hey2* morphant (Liu and Guo, 2006). The transcription factor, Hey2, is expressed in the arterial EC and is

responsible for the arterial cell fate determination (Zhong et al., 2001). In order to further investigate whether the formation of DA regulates interrenal lateral relocalization, we performed *hey2*MO injection and analyzed the phenotype of arterial and venous EC differentiation as well as the morphogenesis of interrenal tissue by two color ISH of either *eph receptor B2a* (*ephb2a*) plus *ff1b* or *flt4* plus *ff1b*. Consistent with Zhong et al. (2001), the arterial marker *ephb2a* was strongly expressed in the pronephric glomerulus and the DA in the control embryo, while the expression of *ephb2a* was completely absent in the *hey*2 morphant (Fig. 19A-a,b), suggesting that the arterial cell was abolished by *hey2*MO. On the other hand, differentiation of the venous EC was unaffected by the knockdown of *hey2*. The venous marker *flt4* was expressed in the PCV in both of the control embryo and the *hey2* morphant (Fig. 19A-c,d). In addition, the *ff1b*-expressing interrenal tissue was located at the central midline in the *hey2* morphant (Fig. 19A-b,d), but was located at the left of the midline in the control embryo from the ventral flat-mount view (Fig. 19A-a,c), suggesting that the interrenal lateral relocalization was inhibited by a loss of DA.

In order to further visualize the structure of the vasculature and verify whether the absence of DA affected steroidogenic interrenal morphogenesis, we injected the *hey2*MO into the *Tg(kdrl:GFP)*^{s843} embryo and performed 3βHsd enzymatic activity assay at 54 hpf. Consistent with the ISH results, the steroidogenic interrenal tissue was located at the central midline rather than at the right of the midline in most of the *hey2* morphants (n=60, 95.2%). Moreover, formation of the DA, as well as angiogenesis of the glomerular and the ISV, were absent in the *hey2* morphant, further confirming that the development of arterial EC was inhibited by *hey2*MO (Fig. 19B-c,d). This result suggested that interrenal lateral relocalization was inhibited in the embryo lacking arterial ECs. Therefore, formation of the DA was

necessary for interrenal lateral relocalization.

2.4. Relocalization and laterality of the interrenal tissue are guided by the processes of both arterial and venous assembly

Overexpression of *hey2* disrupts the venous cell fate determination (Zhong et al., 2001). Therefore, we inhibited venous EC formation by injection of *hey2* mRNA and repeated the analysis to figure out whether the PCV patterned interrenal morphogenesis. In agreement with Zhong et al. (2001), the venous marker, *flt4*, was absent in the *hey2*-overexpressed embryo (Fig. 20A-b-f), indicating that injection of *hey2* mRNA inhibited venous EC differentiation. However, formation of the DA, labelled by either *ephb2* or *kdrl*-driven GFP, was defective, and laterality of the interrenal tissue was also disrupted in the *hey2* overexpressed embryo (Fig. 20A-h-l,B-b-f). The interrenal tissue displayed five phenotypes in the *hey2* overexpressed embryo (Table 5; the ratio of each class based on the result of 3βHsd enzymatic activity assay (Fig. 20B-b-f)): class (I), bilateral clusters widely across the midline (n=76, 30.1%); class (II), bilateral clusters immediately across the midline (n=45, 17.9%); class (III), single cluster at the central midline (n=74, 29.4%); class (IV), single cluster to the left of the midline (n=38, 15.1%); and class (V), single cluster to the right of the midline (n=19, 7.5%). We also found that the steroidogenic interrenal tissue was still closely associated with the malformed DA in all of the embryos, and the severity of the interrenal tissue was closely related to the different degree of the malformed DA (Fig. 20B,C). This results suggested that formation of the PCV and the DA was important for lateral relocalization and laterality of the interrenal tissue.

2.5. Conclusion

Morphogenetic movements of the interrenal tissue are correlated with the development of blood vessels temporally and spatially. Midline convergence of the head kidney was not only parallel with, but also affected by the migrating venous angioblast through VegfC/Flt4 signling. After migrating near the midline, central fusion of the bilateral interrenal tissue required the presence of the angioblast (Fig. 18; Liu and Guo, 2006). Moreover, formation of both the DA and the PCV was necessary for lateral relocalization and laterality of the interrenal tissue.

Part 3. The role of the blood flow during the integration between the steroidogenic interrenal tissue and the chromaffin cells

3.1. Morphogenesis of both pronephric glomerulus and interrenal tissue requires the blood flow

In order to further understand the morphogenesis of the head kidney after midline convergence, we performed 3βHsd enzymatic activity assay in the *Tg(wt1b:GFP)*^{li1} embryo at 34, 54, and 77 hpf. The result showed that, after interrenal lateral relocalization (34 hpf), there was a protrusion of the steroidogenic interrenal tissue at 54 hpf and the medial-caudal region of the interrenal tissue extended across the midline at 77 hpf. And the 54- and 77- hpf embryos displayed fused pronephric glomeruli which was consistent with Serluca et al. (2002) that the glimeruli fused after 2 dpf (Fig. 21A). The blood flow regulates fusion of bilateral pronephric glomeruli (Serluca et al., 2002). As development of the pronephros and the interrenal tissue is parallel (Hsu et al., 2003), we would like to verfiy whether the blood flow also regualtes interrenal tissue morphogenesis. Therefore, we analyzed the morphology of the

interrenal tissue in the *tnnt2a* morphant at 34, 54, and 77 hpf. We found that, consistent with the finding of Serluca et al. (2002), fusion of the pronephric glomeruli was inhibited in the no-blood-flow embryo. The medial extension of the steroidogenic interrenal tissue was also inhibited in the *tnnt2a* morphant, and the interrenal tissue dispalyed an oval-shape without forming a protrusion at 54 and 77 hpf (Fig. 21B).

In order to quantify the medial extension of the interrenal tissue, we measured the distance between the tip of the interrenal tissue and the midline. If the interrenal tissue extended across the midline, the value was designed as negative, and if the interrenal tissue did not across the midline, the value designed as positive (Fig. 21C). We found that the distance between the tip of the interrenal tissue and the midline did not show a significant difference between the control embryo and the *tnnt2a* morphant at 34 and 54 hpf, but exhibited an evident difference at 77 hpf. It suggested that the blood flow was not required for interrenal lateral relocalization, but played a role in the interrenal morphogenesis at a later stage. The distance between the tip of the interrenal tissue and the midline was negative in the control embryo and was positive in the *tnnt2a* morphant (Fig. 21D), suggesting that the interrenal medial extension in the control embryo was successful but defective in the *tnnt2a* morphant. In addition, we found that the growth of the steroidogenic interrenal tissue was not affected by *tnnt2a*MO injection (Fig. 21E), implicating that blood flow specifically regulated medial extension but not growth of the steroidogenic interrenal tissue.

3.2. Inhibition of the blood flow represses interrenal medial extension and IRV growth

Assembly of the functional interrenal organ requires the integration of the steroidogenic interrenal tissue and the differentiated chromaffin cell. The blood flow begins (~26 hpf)

before functional assembly of the interrenal organ (2-3 dpf). Therefore, we would like to inhibit the blood flow specifically during interrenal organ assembly by pharmacological treatment. The skeletal muscle myosin-II inhibitor, 2,3-BDM, specifically inhibits the function of the cardiac muscle, and so inhibits the blood flow. We analyzed the interrenal phenotype in the *Tg(kdrl:GFP)*^{s843} embryo under 2,3-BDM treatment from 1.5 dpf to 2.5 dpf. We found that the heart rate was decreased in the 2,3-BDM-treated embryo (Fig. 22A), and the blood flow was completely inhibited by 6 mM 2,3-BDM and slowed down by 2 mM 2,3-BDM. The general morphology of the axial vessels was not affected in 2,3-BDM-treated embryos, but the extension of the steroidogenic interrenal tissue was inhibited (Fig. 22B-D). The value of interrenal medial extension was positive in both 2 and 6 mM 2,3-BDM-treated embryos, suggesting that the interrenal midline extension was inhibited by either slowing down or stopping the blood flow (Fig. 22E). In addition, compared to the control embryo, the length of the IRV was shorter in the 2,3-BDM-treated embryo (Fig. 22F-I), indicating that angiogenesis of the IRV was positively regulated by the blood flow.

3.3. The defects of interrenal medial extension and IRV growth in the 2,3-BDM-treated embryo are rescued by recovery of the blood flow

In order to further confirm that the blood flow regulated interrenal medial extension and IRV growth, we tested whether the phenotypes of interrenal tissue and IRV in the blood flow-deficient embryo could be rescued by recovery of the blood flow. We inhibited the the blood flow by 6 mM 2,3-BDM in the *Tg(kdrl:GFP)*^{s843} embryo from 1.5 dpf, and then removed the 2,3-BDM at 2.5 dpf, before analyzing the interrenal phenotype as well as the IRV length at 3 dpf. Firstly, we confirmed that the heartbeat could be recovered after removing the 2,3-BDM,

which was evidenced by that the 2,3-BDM-recovered embryo displayed a higher rate of the heartbeat than that in the 2,3-BDM-treated embryo at either 2.5 or 3 dpf (Fig. 23A). Next, we found in the control embryo, the interrenal tissue extended across the midline and displayed a bilobed-like morphology at the central midline at 3 dpf (Fig. 23D). In the embryo under 2,3-BDM treatment from 1.5 to 3 dpf, medial extension of the interrenal tissue was inhibited, and the interrenal tissue displayed an oval-shaped at the right of the midline (Fig. 23E). However, after removing the 2,3-BDM at 2.5 dpf, the interrenal tissue elongated and developed a protrusion in the medial-caudal region at 3 dpf (Fig. 23F). The distance between the tip of the interrenal tissue and the midline in the 2,3-BDM-recovered embryo was much lower than that in the 3 dpf 2,3-BDM-treated embryo at 3 dpf, and was similar to that in the 2.5 dpf control embryo (Fig. 23G). Moreover, angiogenesis of the IRV was also rescued by the recovery of the blood flow. Although the length of the IRV in the 2,3-BDM-recovered embryo at 3 dpf was shorter than that in the 3 dpf control embryo, it was longer than that in the 3 dpf 2,3-BDM-treated embryo (Fig. 24). This result suggested that recovery of the blood flow could rescue both the inhibition of the interrenal medial extension and the reduction of the IRV angiogenesis.

3.4. Increase of the blood flow promotes interrenal medial extension and IRV growth

In order to further verify the effects of the accelerated blood flow on the interrenal medial extension and the IRV growth, we performed norepinephrine treatment on the *Tg(kdrl:GFP)*^{s843} embryo from 33 hpf to 2 dpf before the interrenal medial extension, and assayed for 3βHsd enzymatic activity. The heartbeat and the blood flow was increased by 1 and 0.1 mM norepinephrine, and exhibited a dose-dependent manner (Fig. 25D). Consistent

with the 2,3-BDM treatment, we found that the general morphology of the DA and the PCV was not affected by manipulation of the blood flow, but the medial extension of the interrenal tissue was affected. In the control embryo, the steroidogenic interrenal tissue displayed an oval-shaped at 2 dpf, however, there was a protrusion on the caudal region of the interrenal tissue in the norepinephrine-treated embryos (Fig. 25A-C). Moreover, the distance from the tip of the interrenal tissue to the midline was decreased in norepinephrine-treated embryos compared to that in the control embryo (Fig. 25H). It suggested that the process of interrenal medial extension was promoted by the increased blood flow. Besides, the length of the IRV in the norepinephrine-treated embryos was longer than that in the control embryo (Fig. 25E-G,I), suggesting that the blood flow also promoted angiogenesis of the IRV. Taken together, the blood positively regulated the process of interrenal medial extension as well as IRV angiogenesis, and both inhibition and acceleration of the blood altered the interrenal tissue and IRV development.

3.5. The Fn-rich peri-interrenal microenvironment is contributed by the ECs

Our previous study has suggested that the blood flow-patterned Fn-rich vascular microenvironment could be required for process of the interrenal tissue medial extension and the IRV growth. Knockdown of *tnnt2a* results in disrupted Fn deposition, misregualted IRV growth, and inhibited interrenal medial extension (Chiu, Master thesis, 2012; Chiu et al., 2012). In order to verify the origin of the Fn-deposition at the peri-interrenal region, we performed two color ISH of the *fn1* and *ff1b* in a wildtype embryo at 2 dpf. We found that the *fn1* was expressed in the DA as well as the ventral side of the DA near the *ff1b*-labelled interrenal tissue (Fig. 26A). In addition, Fn protein was accumulated around the *kdrl*-driven

GFP-expressing DA and in the peri-interrenal region in the control embryo, but the expression of the Fn in the peri-interrenal region was dramatically reduced in the *ets1b* morphant (Fig. 26B,C), suggesting that the accumulation of Fn in the peri-interrenal region was produced by the ECs.

3.6. Fn is not only required for the interrenal morphogenetic movements but also involved in the interrenal differentiation

Previously we have analyzed the *fn1* mutant (*natter*) at 3 dpf and found that the interrenal tissue exhibits two different phenotypes, one is the inhibition of interrenal medial extension, and another one is the defect of interrenal midline convergence (Chiu, Master thesis, 2012; Chiu et al., 2012).

In order to further verify the role of *fn1* in the interrenal development, we carefully analyzed the interrenal phenotype in the *fn1* mutant at different embryonic stages. Consistent with our previous finding, the *fn1* mutant displayed two interrenal phenotypes: class (I), single interrenal cluster at the right of the midline with the medial extension being defective (~70%); and class (II), bilateral interrenal clusters with the midline convergence being inhibited (~30%) (Fig. 27A). We also noticed that the ratio of class (II) phenotype was still maintained at about one-third at 74 hpf, suggesting that the class (II) phenotype was not due to a delayed migration of the interrenal tissue. In addition, compared to the wildtype sibling, development of the steroidogenic interrenal tissue (labelled by 3βHsd enzymatic activity assay) in the *fn1* mutant was reduced at all the stage assayed, especially at 33 hpf (Fig. 27B). However, at 24 hpf, development of the *ff1b*-expressing interrenal precursors was not affected by the loss of *fn1* (Fig. 27C). Moreover, there was no difference between the *fn1* mutant and its wildtype sibling

in either the interrenal *ff1b* expression level or *ff1b*-expressing cell number at 33 hpf (Fig. 26D-F), suggesting that the specification of the interrenal precursor was not perturbed. Therefore, the *fn1* specifically regulated steroidogenic interrenal tissue differentiation, and also played a role in the processes of both the interrenal midline convergence and the interrenal medial extension.

3.7. Loss of Fn disrupts functional assembly of the interrenal organ

Functional assembly of the interrenal organ requires the successful medial extension of the steroidogenic interrenal tissue and proper migration of the differentiated chromaffin cells. In order to verify localizations of the interrenal tissue and chromaffin cells, we performed two-color ISH of the *ff1b* plus *dopamine beta-hydroxylase* (*dβh*), the differentiated chromaffin cell marker, during functional assembly of the interrenal organ. We found that some *dβh*-labelled migrating chromaffin cells invaded the *ff1b*-labelled interrenal tissue at 54 hpf in the wildtype sibling but not in the *fn1* mutant (Fig. 28A-C). Later at 77 hpf, the chromaffin cell was intermingled with the interrenal tissue at the central midline in the wildtype sibling (Fig. 28D,E). There were some chromaffin cells located out of the interrenal region in both the class (I) and the class (II) *fn1* mutant (Fig. 28F-J). This means that in addition to the defective medial extension and the inhibited midline convergence of the interrenal tissue, the migration of the chromaffin cell was also misregulated in the *fn1* mutant.

3.8. The blood flow patterns Fn deposition and pFAK activation in the interrenal region

Fn is required for myocardial assembly, and the heart formation as was as the blood flow is inhibited in the *fn1* mutant (Trinh and Stainier, 2004). The interrenal class (I) phenotype of

the *fn1* mutant displayed an inhibition of the medial extension (Fig. 27A) which phenocopied the interrenal phenotype in the blood flow-deficient embryo (Fig. 22A), suggesting that the class (I) phenotype in the *fn1* mutant was due to a loss of blood flow. In order to further confirm the relationship between the blood flow and the Fn during interrenal medial extension, we analyzed the deposition of the Fn and the expression of the activated Fn/Integrin downstream factor, phosphorylated FAK (pFAK), in the blood flow-deficient embryo. We found that there was misregulated Fn deposition in the peri-interrenal region under the inhibition of blood flow (Fig. 29A-C), and the expression level of Fn in the peri-interrenal region did not show a significant difference among the control embryo, the *tnnt2a* morphant, and the 6 mM 2,3-BDM treated embryo (Fig. 29D). In addition, pFAK expression could be found in the *ff1b*-driven GFP-labelled interrenal tissue in the control embryo, but not in either the *tnnt2a* morphant or the 6 mM 2,3-BDM treated embryo (Fig. 29A”-C”,E). This result suggested that the blood flow patterned Fn deposition in the interrenal microenvironment and modulated the activation of FAK at the interrenal tissue, and so regulated medial extension of the interrenal tissue.

3.9. The blood flow regulates Fn-pFAK signaling and the interrenal medial extension through Klf2a and MMP2

In the zebrafish, the blood flow modulates the different developmental processes through different factors such as MMP2 (Serluca et al., 2002) and Klf2a-NO signaling pathway (Vermot et al., 2009; Wang et al., 2011). Both Klf2a and MMP2 are expressed by the EC and are mechanosensitive proteins in response to the blood flow.

In order to verify the molecular mechanism of how blood flow regulates interrenal medial extension, we analyzed the effects of *klf2a*MO and *mmp2*MO respectively on the

interrenal tissue. We found that the steroidogenic interrenal tissue in both the *klf2a* morphant and the *mmp2* morphant displayed an oval-like shape with a short protrusion on the medial-caudal region (Fig. 30A-C). Moreover, values of the distance from the tip of the interrenal tissue to the midline were higher in either the *mmp2* or the *klf2a* morphant than that in the control embryo (Fig. 30D), suggesting that medial extension of the interrenal tissue was inhibited by either the *klf2a*MO or *mmp2*MO injection.

Next we analyzed the Fn accumulation, the pFAK expression, and the IRV growth in either the *klf2a* morphant or the *mmp2* morphant. We found that both of the length of the IRV and the interrenal-pFAK expression were reduced by the knockdown of either *klf2a* or *mmp2* (Fig. 31). These phenotypes in the *klf2a* morphant and the *mmp2* morphant were consistent with that in the blood flow-deficient embryo, suggesting that the blood flow regulated processes of the Fn deposition, the FAK activation, the IRV angiogenesis, and the interrenal medial extension through the mechanosensitive proteins Klf2a and MMP2.

3.10. Medial extension of the interrenal tissue involves an EMT-like change in steroidogenic cell morphology that is hemodynamically regulated and pFAK-dependent

In order to delineate the changes in interrenal cell morphology during interrenal medial extension, we analyzed the interrenal morphology by 3βHsd enzymatic activity staining at different stages. We found that before interrenal medial extension (28-48 hpf), the steroidogenic cells aggregated together and formed a cluster at the left of the midline from the ventral flat-mount view. During the interrenal medial extension (60-72 hpf), the interrenal cell lost cell-cell contact and developed a protrusion on the cell surface, and this mesenchymal-like cell morphology was more evident at 84 and 97 hpf (Fig. 32A). In addition,

we inhibited DNA synthesis by camptothecin which is an inhibitor of type I topoisomerase to explore whether the medial extension of the interrenal tissue was dependent of cell proliferation. Interestingly, in spite of the reduced cell number in the interrenal tissue after camptothecin treatment, some mesenchymal-like steroidogenic interrenal cells still migrated across the midline (Fig. 32B). This result suggested that change of cell morphology is more important than cell proliferation during interrenal medial extension.

In order to further identify the change of interrenal cell morphology during development, we detected the expression of epithelial marker, β-Catenin (Savagner, 2001), in the control embryo at 2 and 2.5 dpf. We found that the *ff1b*-driven GFP-expressing interrenal cells formed a cluster, and the expression of β-Catenin was enriched at the cell-cell junction of the *ff1b*-driven GFP-expressing interrenal cluster at 2 dpf (Fig. 33A). At 2.5 dpf, some interrenal cells dissociated from the cluster, and the junctional β-Catenin expression of the interrenal tissue was decreased (Fig. 33B). Furthermore, the junctional β-Catenin distribution was apparent in the medial extension-deficient interrenal tissue, including the interrenal tissue of the *tnnt2a* morphant, the 2,3-BDM-treated embryo, the *klf2a* morphant, and the *mmp2* morphant (Fig. 33C,D,F,G). Besides, the embryos subject to the Fn antagonist RGD treatment also displayed a defective medial extension of the interrenal tissue with abundant β-Catenin in the cell junction (Fig. 33E). These results suggested that the interrenal cells underwent an epithelial-to-mesenchymal transition (EMT)-like change during interrenal medial extension, and that was regulated by the hemodynamic force and the pFAK signaling.

3.11. Migration of differentiated chromaffin cells requires blood flow but is independent of either mechanotransduction or Fn-mediated signaling

In order to verify the effect of disrupted blood flow as well as the Fn/pFAk signaling on interrenal organ functional assembly, we performed two-color ISH of the *ff1b* plus *dβh* at 3 dpf. We found that the *ff1b*-expressing interrenal cells intermingled with the *dβh*-expressing chromaffin cells and displayed a V-shape at the central midline in the control embryo. Although medial extension of the interrenal tissue was inhibited in the RGD treated embryo, the *klf2a* morphant, and the *mmp2* morphant, the migration of chromaffin cell was not affected (Fig. 34B,C,E). However, in the *tnnt2a* morphant, both migration of the chromaffin cells and medial extension of the interrenal tissue were inhibited (Fig. 34D). This result suggested that migration of differentiated chromaffin cells was dependent of the blood flow yet independent of either the mechanotransduction or the Fn-mediated signaling. In addition, disruptions in either medial extension of the steroidogenic interrenal tissue or migration of the chromaffin cell resulted in an incomplete assembly of the interrenal organ.

3.12. Conclusion

In this part of study, we found that during functional assembly of the interrenal organ, both of medial extension of the steroidogenic interrenal tissue and migration of the chromaffin cells were regulated by the blood flow. The hemodynamic force upregulated the expression of *mmp2* and *klf2a*, patterned Fn deposition in the peri-interrenal reion, and activated FAK in the interrenal tissue, and so led to an EMT-like change in the interrenal tissue, and promoted medial extension of the interrenal tissue. However, neither the mechanotransducer nor the Fn-pFAK signaling was required for the blood flow-regulated chromaffin cell migration.

Taken together, in this thesis we identified the multiple roles of the endothelium for interrenal gland organogenesis. We found (1) the midline convergence of the head kidney

was restricted by the venous angioblast through VegfC/Flt4 signaling; (2) formation of the axial vessels patterned lateral relocalization and laterality of the interrenal tissue; and (3) the blood flow, through distinct mechanisms, regulates medial extension of the interrenal and migration of the chromaffin cell, while both processes are required for functional assembly of the interrenal gland. Furthermore, we demonstrated that the zebrafish is a good model for studying coordinated interactions among the pronephros, the interrenal tissue, the chromaffin cells, the endothelial cells, and the endoderm during the organ development.

Discussion

The midline signaling in the zebrafish

The successful midline convergence of the head kidney (Fig. 10A; 11A) in both the *sox32*/*etv2* double morphant and the *sox32*/*tal1* double morphant indicated that the midline convergence of the head kidney was directly guided by the midline signaling and the midline signaling was dependent on neither the endoderm nor the endothelium. During gastrulation, the noncanonical-Wnt signaling pathway regulates the convergence and extension movements in the *Xenopus* and the zebrafish (Kühl 2002; Tada et al., 2002). Studies in the zebrafish have shown that the noncanonical-Wnt ligands, *wnt4a*, *silberblick/wnt11*, and *wnt11-related*, are expressed in the mesoendoderm as well as the notochord, and regulates midline convergence of the foregut and the heart tube through the noncanonical-Wnt/Dishevelled/RhoA signaling pathway (Matsui et al., 2005). Moreover, Rho A acts downstream of *wnt5* and *wnt11* and is expressed in pharyngeal arches, notochord, heart, liver and pronephric duct during early embryonic development (Zhu et al., 2006). Inhibition of either the RhoA or its effector, Rho kinase 2, disrupts the convergence and extension movements and results in an expanded expression domain of *pax2.1* as well as a broader notochord and somite formation (Zhu et al., 2006; Marlow et al., 2002). In addition, LIM domain containing preferred translocation partner in lipoma acts downstream of the Wnt11/Rho kinase 2 signaling pathway and interacts with the planar cell polarity protein Scrib to mediate the convergence and extension movements (Vervenne et al., 2008). These reports above suggest that the noncanonical-Wnt/Dishevelled/RhoA signaling pathway is required for anterior-posterior extension and mediolateral narrowing during gastrulation, shapes the organ morphology but not alters the cell fate. However, whether the nc-Wnt signaling

pathway is dependent on the endoderm and whether it is required for midline convergence of the head kidney remain unclear.

The role of the endoderm for the formation of axial vessels

Distinct guidance cues in different regions pattern the various processes of angioblast morphogenesis (Siekmann et al., 2009; and reviewed in Ellertsdóttir et al., 2010). At the lower trunk, a loss of the endoderm delays the migration of angioblasts, but eventually the formation of the DA is unaffected while the lumen of the PCV appears dilated (Jin et al., 2005). In the anterior region, migration of the *cxcr4a*-expressing LDA precursor is specifically regulated by the *cxcl12b*-expressing endoderm next to the developing LDA. The *sox32* morphant displays an absence of LDA while the trunk DA is unaffected (Siekmann et al., 2009). In agreement with these findings, we found that a knockdown of *sox32* severely inhibited the formation of LDA, and slightly affected the formation of the DA in the anterior region while the DA in the posterior region was nearly unaffected (Fig. 6E,F). Therefore, the endoderm is required for the morphogenesis of the arterial angioblast in the anterior region, but is dispensable for that at the lower trunk. However, formation of the primordial hindbrain channel by the venous angioblast in a more anterior region is independent of the endoderm, and is regulated by other tissues through VegfC/Flt4 signaling (Covassin et al. 2006). Moreover, this study demonstrated that midline convergence of the arterial angioblast was not as severely inhibited as the venous angioblast in the *sox32* morphant (Fig. 6F), suggesting that the endoderm selectively regulates the formation of the vein but not the artery in the head kidney region.

The endothelium and the interrenal laterality

The *cas* mutant exhibits a defective Kupffer's vesicle which is the left-right asymmetry organ in the zebrafish (Alexander et al., 1999). However, the *sox32* morphant displayed a severe convergence phenotype of the interrenal tissue rather than a randomized laterality of the interrenal tissue (Fig. 6B), suggesting that morphogenesis of the interrenal tissue was particularly associated with and regulated by the endothelium. Although a disruption of the general laterality by the *pkd2*MO resulted in randomization of the interrenal morphogenesis (Fig. 7), the possibility still cannot be ruled out that the randomization of the interrenal tissue in the *pkd2* morphant was secondary to defects of axial vessels; due to the tight association between the interrenal tissue and the vessels. The mechanism of arterial- and venous-regulated interrenal lateral relocalization is not clear. Formation of the DA might generate a space or secret some factors for interrenal local relocation. It is also unknown that why the fused interrenal tissue translocates to the right of the midline rather than the left. One explanation is that the axial vessels might display an asymmetric structure to influence the lateral relocalization of the interrenal tissue, however, it stills need a higher resolution of microscopy to confirm that.

Multiple roles of Fn in the interrenal development

Fn is required for the the midline convergence of other mesodermal tissues such as cardiomyocyte precursors (Matsui et al., 2007; Trinh and Stainier, 2004), and also plays a role in initiation of the angioblast migration (Jin et al., 2005). Expression of *fn1* in the midtrunk is reduced in the *clo* mutant at 15 somite stage (Trinh and Stainier, 2004). Interestingly, the *clo* mutant displays a closely bilateral interrenal tissue at the midline and

the penetrance is about 90%, suggesting that midline convergence is unaffected but central fusion of the interrenal tissue is inhibited (Liu and Guo, 2006). In addition, the *fn1* mutant displays a more severe unfused interrenal phenotype (widely bilateral interrenal tissue) with a lower penetrance (about 30%; class(II) phenotype; Fig. 27A), suggesting that the midline convergence of the interrenal tissue was severely inhibited. It suggested that Fn might be contributed by other tissues such as the endoderm and extra-embryonic yolk syncytial layer (YSL) at a later stage so that the midline convergence of the interrenal tissue is unaffected in the *clo* mutant but is severely inhibited in the *fn1* mutant. Indeed, studies on the myocardial migration have shown that the YSL patterns Fn deposition through regulation of Fn transcripts (Sakaguchi et al., 2006) or patterning the assembly of Fn (Arrington and Yost, 2009). On the other hand, there is a paralog of the *fn1*, the *fn1b*, in the zebrafish (Sun et al., 2005). *fn1* and *fn1b* synergistically regulate somitogenesis through activation of Integrinα5 (Jülich et al., 2005). Moreover, the *integrinα5* morphant displays a severe midline convergence phenotype of the interrenal tissue and the penetrance is around 44% (Chiu, Master thesis, 2012; Chiu et al., 2012), which is slightly higher than that in the *fn1* mutant. It hints that the *fn1* might cooperate with the *fn1b* or other ECM genes in the regulation of midline convergence of the interrenal tissue, yet it still needs to be confirmed by simultaneous knockdown of the *fn1* and *fn1b*.

About 70% of the *fn1* population displayed inhibition of interrenal medial extension (class (I) phenotype; Fig. 27A). Previously in out laboratory, we found that a knockdown of *fn1b* neither inhibits the accumulation of Fn at peri-interrenal region nor affects development of the interrenal tissue and the IRV. In contrast, the deposition of Fn in the peri-interrenal region is almost completely absent in the *fn1* mutant (Chiu, Master thesis, 2012; Chiu et al.,

2012). Therefore, the blood flow-regulated Fn-deposition at the peri-interrenal region should be contributed by the *fn1* only, in other words, the *fn1* but not *fn1b* patterned the medial extension of the interrenal tissue and the growth of the IRV.

Recently, Cheng et al., (2013) have shown that the endodermal cells promote mesodermal cell specification through the short-range signaling by Fn1, Fn1 then activates Integrin-β1 signaling which in terms activates the Wnt/β-catenin signaling. They have also found that inhibition of both *fn1* and *fn1b* reduces the cardiac lineage cell fate determination and promotes the endodermal cell fate determination in the zebrafish. Here we found that the *fn1* mutant displayed a normal expression of *ff1b* but a reduced 3βHsd enzymatic activity, suggesting that *fn1* did not affect interrenal specification but regulated differentiation of the steroidogenic interrenal tissue (Fig. 27). However, an opposite observation has been found in the cell line study. Human fetal adrenal cells co-cultured with Fn results in a reduction of ACTH-stimulated *3βHSD* expression. Other ECM proteins are also required for fetal adrenal cell function. Laminin enhances human fetal adrenal cells response to ACTH and results in an increase of DHEA secretion. Collagen IV increases the cortisol releasing by human fetal adrenal cell after ACTH stimulation (Chamoux et al., 2002). Nevertheless, the ECM is also required for adrenal/interrenal development, and here we have found that Fn is participated in midline convergence, medial extension, and differentiation of the interrenal tissue in the zebrafish.

Roles of the hemodynamic force in the zebrafish organogenesis and angiogenesis

The hemodynamic force might promote medial extension of the interrenal tissue through the following steps: (1) uregulation of *klf2a* in the EC; (2) patterning the Fn deposition at peri-

interrenal region through *mmp2*; (3) activation of pFAK signaling in the interrenal cell; and (4) induction of an EMT-like change in the steroidogenic interrenal cell. Interestingly, similar cellular behavior of the ECs has been found in the zebrafish valvulogenesis. The ECs in the atrioventricular canal undergo an endothelial-to-mesenchymal transition (EnMT), characterized by a loss of junctional Cdh5 expression, developing a protrusion on the cell surface, and dismissed form the lumen toward the cardiac jelly to form the valve (Kovacic et al., 2012; Steed et al., 2016). Moreover, this process is regulated by the reversing flow through upregulation of *klf2a* and *fn1b* in the ECs and accumulation of Fn at the atrioventricular canal (Vermot et al., 2009; Steed et al., 2016). Here we speculate that the flow inside the DA at interrenal region might be the pulsatile flow due to the heartbeat. It suggests that the different types of hemodynamic force could regulate organogenesis by similar molecular regulatory mechanisms.

In addition to promote the IRV growth, the blood flow also patterns angiogenesis in other tissues through different molecules. The blood flow-induced *klf2a* in the ECs upregulates the expression of the endothelial-specific microRNA, *miR126*, which in turn enhances the Vegf signaling, and so promotes angiogenesis of aortic arch vessels (Nicoli et al., 2010). During the formation of hindbrain capillaries, blood flow represses the antigenic sprouting behavior of the EC in the newborn vessels and ensures the connection between the artery and vein through inhibition of the chemokine cx*cl12b* and its receptor *cxcr4a* (Bussmann et al., 2011). In addition, the hemodynamic force promotes lumen formation of the ISV, and F-actin as well as myosin II are involved in this process (Gebala et al., 2106). Therefore, the hemodynamic force can also regulate different developmental processes through various molecular mechanisms (Freund et al., 2012).

Regulation of the chromaffin cell migration

Unlike the regulation of interrenal medial extension, the blood flow-regulated chromaffin cell migration did not go through the Integrin/pFAK signaling (Fig 34). Inhibition of the Integrin/pFAK signaling by RGD treatment from the onset of the blood flow did not affect the migration of the chromaffin cells (Fig. 34); however, the *fn1* mutant exhibited a more separated clusters of the chromaffin cell (Fig. 28) than that in the *tnnt2a* morphant (Fig. 34). It suggested that the blood flow and the *fn1* synergistically regulate the migration of chromaffin cell, and *fn1* might function earlier than the onset of the blood flow.

In the chick study, the DA-released BMPs signals mediate the migration of SA cells (Reissmann et al., 1996) through the chemokine SDF1/CXCL12 and the epidermal growth factor family protein NRG1 (Saito et al., 2012). However, mesenchymal-expressed BMPs cannot ectopic induce the expression of SDF1 and NRG, suggesting that there is/are other factor(s) that produced by the DA for patterning the SA cell migration. The DA-mediated migration of the SA cells does not seem to require the blood flow, due to the fact that the transplanted piece of DA can ectopiclly induce the expression of SDF1 and NRG and attract the migration of SA cells (Saito et al., 2012; and reviewed in Saito and Takahashi, 2015). However, it remains unclear whether the adrenomedullary cells successfully integrate with the adrenal cortex in the absent of the blood flow.

It is a long-time question that whether the adrenal cortex contributes to the migration and differentiation of the adrenomedullary cells. In the *SF1* knockout mice, despite the reduced cell number, the adrenomedullary cells still differentiate and migrate to the region of the absent adrenal cortex (Gut et al., 2005). Recently, Saito et al. (2012) demonstrate that both the para-DA mesenchyme and the adrenal cortex express NRG1 after the segregation of the

adrenomedullary cells form the SA cells. In the SF1 knockout mice, the mesenchyme-expressed NRG1 is unperturbed, so that explains why the adrenomedullary cells still migrate near the absent adrenal cortex (Saito et al., 2012). However, it remains unknown why the adrenomedullary cells only integrate with the adrenocortical cells but not the mesenchyme. Here we have found that some differentiated chromaffin cells migrated ventrally but not reached to the interrenal tissue in the blood flow-deficient embryo. Besides the attracting signals, the repulsive signals are also important for controlling NCC migration. Semaphorin3A/Neuropilin1 is expressed in the mesenchyme of the hindbrain to prevents the ectopic migration of the NCCs (Osborne et al., 2005). Furthermore, the Robo-Slit signaling can selectively inhibit trunk NCC migration into the gut (De Bellard et al., 2003). So the blood flow might initiate the repulsive signals that inhibit the invasion of the chromaffin cell into the para-DA mesenchyme. Alternatively, the blood flow might also generate an interrenal microenvironment which is independent of either the Integrin/pFAK signaling or the mechanotransducer, that attracts the migration of the chromaffin cell.

Endothelial signaling in the kidney and in the adrenal cortex

Communications between the ECs and the tissue regulate organ development and function. Podocyte-produced VEGFs plays critical role for renal angiogenesis, maturation, maintenance, and pathogenesis (Bailey et al., 1999; Eremina et al., 2003; Coultas et al., 2005; Bartlett et al., 2016). Expression of Vegf-A in the kidney begins from E14 in mice; 30 hpf in the zebrafish at the time point of renal angiogenesis, and the expression is maintained till adulthood (Tufro et al., 1999; Liang et al., 2001). Studies from human primary culture cell have shown that VEGF-A facilitates the proliferation, survival, and fenestration of the

glomerular EC (Roberts and Palade, 1995; Bates et al., 2002; Satchell et al., 2006). Moreover, the roles of VEGF-A for stimulating the formation of renal capillaries and tubules have also been found *ex vivo* (Tufro et al., 1999). Functions of podocyte-expressed VEGF-C on glomerular ECs are similar to, but much lower than that of VEGF-A (Foster et al., 2006; Joukov et al., 1998), and effects of VEGF-A neutralization can be compensated by exogenous VEGF-C (Müller-Deile et al., 2009). On the other hand, VEGF-A and VEGF-C also serve as the autocrine factors that promote the survival of the human cultured podocyte through elevation of the phosphorylated Akt and phosphorylated Mitogen-activated protein kinases (pMAPK) (Foster et al., 2005; Foster et al., 2006; Müller-Deile et al., 2009). The podocyte-specific VEGF-A homozygous knockout mice die after birth due to the renal failure with immature glomerular ECs, while the heterozygous displays the syndrome of end-stage renal disease such as loss of endothelial fenestrations, defective podocyte foot processes, and proteinuria. Specific overexpression of the VEGF-A_{164} isoform in the mouse podocyte also disrupts the renal function through a collapse of glomerular capillary with podocyte hyperplasia (Eremina et al., 2003). Other endothelium-secreted factors are also important for renal development and maintenance. Platelet-derived growth factor-B (PDGFB) is expressed by the ECs while the PDGF-Rβ, the receptor of PDGFB, is expressed by the mesangial cells in the developing and mature glomeruli (Lindahl et al., 1998). Knockout of endothelium-specific PDGFB results in an absence of the mesangial cell and a dilation of the glomerular capillarity tuft at the embryonic stage, however, this glomerular phenotype of the endothelium-specific PDGFB knockout mice is recovered after 3 weeks of age (Bjarnegard et al., 2004). Furthermore, loss of podocyte-specific VEGF-A also affects the development of

the mesangial cell (Eremina et al., 2003). These findings suggest that coordination of the endothelial signals modulates the formation and function of the glomerulus.

In mammals, the tissue-specific angiogenic factor endocrine gland-derived VEGF (EG-VEGF) is expressed in the steroidogenic tissues such as adrenal cortex, ovary, and placenta (LeCouter et al., 2001). EG-VEGF activates MAPK signaling pathway and stimulates endothelial NO synthase through activation of the Akt pathway that modulates the survival, migration, and proliferation of the adrenal cortex-derived endothelial cells (Lin et al., 2002). Moreorver, EG-VEGF also plays a role in the adrenal pathogenesis, and a higher expression of the nuclear EG-VEGF in the adrenocortical carcinomas is corelated to the lower survival rate of the patients (Heck et al., 2015). However, expression of the zebrafish homolog of EG-VEGF, Prokineticin 2, is in the brain and is elevated in the injury-induced proliferating telencephalic cells (Ayari et al., 2010). The VEGF and its receptors such as VEGFRs and Angiopoietins are expressed in the normal and cancerous adrenal cortex (Kool et al., 2014). In human fetal adrenal cortex, expression of VEGF is higher in the inner FZ and is lower in the outer DZ, and this centripetal expression is correlated with both the vasculogenesis (Shifren et al., 1998) and the Fn expression (Chamoux et al., 2001) in the fetal adrenal cortex. In the adult bovine adrenal cortex, VEGF-A is expressed in both of the glomerulosa and the fasciculata cells (Vittet et al., 2000). In addition to regulating hormone secretions, ACTH also increase the expression and secretion of the VEGF in primary culture of either human fetal adrenal cortical cells or adult bovine adrenocortical cells (Shifren et al., 1998; Vittet et al., 2000) through protein kinase A signaling pathway (Heikkila et al., 2000). Inhibition of the HPA axias by dexamethasone in the mouse inhibits the adrenal size, reduces the corticosterone levels, and decreases the expression of VEGF and its receptor Flk-1/KDR (Mallet et al., 2003).

Moreover, the effect of ACTH on adrenocortical cells can be modulated by the ECMs (Chamoux et al., 2005). It is shown in this study that the Fn deposition in the interrenal microenvironment was contributed by the ECs and regulated by the blood flow. Thus, it is possible that the adrenocortical cell might interact with the ECs in response to ACTH stimulation. In addition, downergualtion of *vegf* reduces the size of zebrafish steroidogenic interrenal tissue and is evident at 80 hpf (Liu and Guo, 2006). The earliest stage of zebrafish larvae to react to the stress is at 3 dpf, and the controlling of the pituitary on the interrenal tissue starts as early as 5 dpf (To et al., 2007). This study shows that the interaction between the endothelium and the head kidney regulates the morphogenesis of the head kidney, and demonstrates a role of the endothelial signaling for organogenesis before either vessel formation or organ function.

References

Alexander, J., Rothenberg, M., Henry, G.L., and Stainier, D.Y. (1999). *casanova* plays an early and essential role in endoderm formation in zebrafish. Dev Biol *215*, 343-357.

Arrington, B.C., and Yost, J.H., (2009). Extra-embryonic *syndecan 2* regulates organ primordia migration and fibrillogenesis throughout the zebrafish embryo. Development *136*, 3143-3152.

Ayari, B., El Hachimi, K.H., Yanicostas, C., Landoulsi, A., and Soussi-Yanicostas, N. (2010). Prokineticin 2 expression is associated with neural repair of injured adult zebrafish telencephalon. J Neurotrauma *27*, 959-972.

Bailey, E., Bottomley, M.J., Westwell, S., Pringle, J.H., Furness, P.N., Feehally, J., Brenchley, P.E., and Harpe,r S.J. (1999). Vascular endothelial growth factor mRNA expression in minimal change, membranous, and diabetic nephropathy demonstrated by nonisotopic in situ hybridisation. J Clin Pathol *52*, 735-738.

Bartlett, C.S., Jeansson, M., and Quaggin, S.E. (2016). Vascular growth factors and glomerular disease. Annu Rev Physiol *78*, 437-61.

Barwick, T.D., Malhotra, A., Webb, J.A., Savage, M.O., and Reznek, R.H. (2005). Embryology of the adrenal glands and its relevance to diagnostic imaging Clin Radiol *60*, 953-959.

Bates, D.O., Hillman, N.J., Williams, B., Neal, C.R., and Pocock, T.M. (2002). Regulation of microvascular permeability by vascular endothelial growth factors. J Anat *200*, 581-597.

Bisgrove, B.W., Snarr, B.S., Emrazian, A., and Yost, H.J. (2005). Polaris and Polycystin-2 in dorsal forerunner cells and Kupffer's vesicle are required for specification of the zebrafish left-right axis. Dev Biol *287*, 274-288.

Bjarnegard, M., Enge, M., Norlin, J., Gustafsdottir, S., Fredriksson, S., Abramsson, A., Takemoto, M., Gustafsson, E., Fässler, R., and Betsholtz, C. (2004). Endothelium-specific ablation of PDGFB leads to pericyte loss and glomerular, cardiac and placental abnormalities. Development *131*, 1847-1857.

Bollig, F., Mehringer, R., Perner, B., Hartung, C., Schäfer, M., Schartl, M., Volff, J.N., Winkler, C., and Englert, C. (2006). Identification and comparative expression analysis of a second *wt1* gene in zebrafish. Dev Dyn *235*, 554-561.

Bollig, F., Perner, B., Besenbeck, B., Kothe, S., Ebert, C., Taudien, S., and Englert, C. (2009). A highly conserved retinoic acid responsive element controls wt1a expression in the zebrafish pronephros. Development *136*, 2883-2892.

Bussmann, J., Wolfe, S.A., and Siekmann, A.F. (2011). Arterial-venous network formation during brain vascularization involves hemodynamic regulation of chemokine signaling. Development *138*, 1717-1726.

Carmeliet, P., Ferreira, V., Breier, G., Pollefeyt, S., Kieckens, L., Gertsenstein, M., Fahrig, M., Vandenhoeck, A., Harpal, K., Eberhardt, C., Declercq, C., Pawling, J., et al. (1996). Abnormal blood vessel development and lethality in embryos lacking a single VEGF allele. Nature *380*, 435-439.

Chai, C. (2002). Characterization and developmental analysis of a zebrafish *Ftz-F1* gene, *ff1b* (*nr5a4*). Ph.D Thesis. National University of Singapore.

Chai, C., and Chan, W.K. (2000). Developmental expression of a novel *Ftz-F1* homologue, *ff1b* (*NR5A4*), in the zebrafish *Danio rerio*. Mech Dev *91*, 421-426.

Chai, C., Liu, Y.W., and Chan, W.K. (2003). Ff1b is required for the development of steroidogenic component of the zebrafish interrenal organ. Dev Biol *260*, 226-244.

Chamoux, E., Bolduc, L., Lehoux, J.G., and Gallo-Payet, N. (2001). Identification of extracellular matrix components and their integrin receptors in the human fetal adrenal gland. J Clin Endocrinol Metab *86*, 2090-2098.

Chamoux, E., Narcy, A., Lehoux, J.G., and Gallo-Payet, N. (2002). Fibronectin, laminin, and collagen IV interact with ACTH and angiotensin II to dictate specific cell behavior and secretion in human fetal adrenal cells in culture. Endocr Res *28*, 637-640.

Chamoux, E., Otis, M., and Gallo-Payet, N. (2005). A connection between extracellular matrix and hormonal signals during the development of the human fetal adrenal gland. Braz J Med Biol Res *38*, 1495-503.

Cheng, P., Andersen, P., Hassel, D., Kaynak, B.L., Limphong, P., Juergensen, L., Kwon, C., and Srivastava, D. (2013). Fibronectin mediates mesendodermal cell fate decisions. Development *140*, 2587-2596.

Chiu, C.H. (2012). Studying the role of Fibronectin for the interrnal morphogenesis of the zebrafish. Master Thesis. Tunghai University.

Chiu, C.H., Chou, C.W., Takada, S., and Liu, Y.W. (2012). Development and fibronectin signaling requirements of the zebrafish interrenal vessel. PLoS One *7*, e43040.

Chou, C.W., Chiu, C.H., and Liu, Y.W. (2013). Fibronectin mediates correct positioning of the interrenal organ in zebrafish. Dev Dyn *242*, 432-443.

Chou, C.W., Hsu, H.C., Quek, S.I., Chan, W.K., and Liu, Y.W. (2010). Arterial and venous vessels are required for modulating developmental relocalization and laterality of the interrenal tissue in zebrafish. Dev Dyn *239*, 1995-2004.

Chou, C.W., Zhuo, Y.L., Jiang, Z.Y., and Liu, Y.W. (2014). The hemodynamically-regulated vascular microenvironment promotes migration of the steroidogenic tissue during its interaction with chromaffin cells in the zebrafish embryo. PLoS One *9*, e107997.

Coultas, L., Chawengsaksophak, K., and Rossant, J. (2005). Endothelial cells and VEGF in vascular development. Nature *438*, 937-945.

Covassin, L.D., Villefranc, J.A,, Kacergis, M.C., Weinstein, B.M., and Lawson, N.D. (2006). Distinct genetic interactions between multiple Vegf receptors are required for development of different blood vessel types in zebrafish. Proc Natl Acad Sci *103*, 6554-6559.

Davidson, A.J. (2009). Mouse kidney development. StemBook [Internet].

De Bellard, M.E., Rao, Y., and Bronner-Fraser, M., (2003). Dual function of Slit2 in repulsion and enhanced migration of trunk, but not vagal, neural crest cells. J Cell Biol *162*, 269-279.

Dickmeis, T., Mourrain, P., Saint-Etienne, L., Fischer, N., Aanstad, P., Clark, M., Strahle, U., and Rosa, F. (2001). A crucial component of the endoderm formation pathway, CASANOVA, is encoded by a novel *sox*-related gene. Genes Dev *15*, 1487-1492.

Diep, C.Q., Ma, D., Deo, R.C., Holm, T.M., Naylor, R.W., Arora, N., Wingert, R.A., Bollig, F., Djordjevic, G., Lichman, B., et. al. (2011). Identification of adult nephron progenitors capable of kidney regeneration in zebrafish. Nature *470*, 95-100.

Diep, C.Q., Peng, Z., Ukah, T.K., Kelly, P.M., Daigle, R.V., and Davidson, A.J. (2015). Development of the zebrafish mesonephros. Genesis *53*, 257-269.

Drummond, I. (2003). Making a zebrafish kidney: a tale of two tubes. Trends Cell Biol *13*, 357-365.

Drummond, I.A., Majumdar, A., Hentschel, H., Elger, M., Solnica-Krezel, L., Schier, A.F., Neuhauss, S.C., Stemple, D.L., Zwartkruis, F., Rangini, Z., Driever, W., and Fishman, M.C. (1998). Early development of the zebrafish pronephros and analysis of mutations affecting pronephric function. Development *125*, 4655-4667.

Ellertsdóttir, E., Lenard, A., Blum, Y., Krudewig, A., Herwig, L., Affolter, M., and Belting, H.G. (2010). Vascular morphogenesis in the zebrafish embryo. Dev Biol *341*, 56-65.

Else, T., and Hammer, G.D. (2005). Genetic analysis of adrenal absence: Agenesis and aplasia. Trends Endocrinol Metab *16*, 458-468.

Eremina, V., Eremina, V., Sood, M., Haigh, J., Nagy, A., Lajoie, G., Ferrara, N., Gerber, H.P., Kikkawa, Y., Miner, J.H., and Quaggin, S.E. (2003). Glomerular-specific alterations of VEGF-A expression lead to distinct congenital and acquired renal diseases. J Clin Invest *111*, 707-716.

Foster, R.R., Saleem, M.A., Mathieson, P.W., Bates, D.O., and Harper, S.J. (2005). Vascular endothelial growth factor and nephrin interact and reduce apoptosis in human podocytes. Am J Physiol Renal Physiol *288*, F48-57,

Foster, R.R., Satchell, S.C., Seckley, J., Emmett, M.S., Joory, K., Xing, C.Y., Saleem, M.A., Mathieson, P.W., Bates, D.O., and Harper, S.J. (2006). VEGF-C promotes survival in podocytes. Am J Physiol Renal Physiol *291*, F196-207.

Foster, R.R., Slater, S.C., Seckley, J., Kerjaschki, D., Bates, D.O, Mathieson, P.W., and Satchell, S.C. (2008). Vascular endothelial growth factor-C, a potential paracrine regulator of glomerular permeability, increases glomerular endothelial cell monolayer integrity and intracellular calcium. Am J Pathol *173*, 938-948.

Fox, S.I. (2009). Human Physiology. McGraw-Hill, Tenth Edition, pp.528-540.

Freund, J.B., Goetz, J.G., Hill, K.L., and Vermot, J. (2012). Fluid flows and forces in development: functions, features and biophysical principles. Development *139*, 1229-1245.

Gebala, V., Collins, R., Geudens, I., Phng, L.K., and Gerhardt, H. (2016). Blood flow drives lumen formation by inverse membrane blebbing during angiogenesis *in vivo*. Nat Cell Biol *18*, 443-450.

Gilbert, S.F. (2013). Developmental Biology. Sinauer, Eight Edition, pp.416-418; 443-444; 460-468; 622-624.

Gore, A.V., Monzo, K., Cha, Y.R., Pan, W., and Weinstein, B.M. (2012). Vascular development in the zebrafish. Cold Spring Harb Perspect Med 5, a006684.

Grassi Milano, E., Basari, F., and Chimenti, C. (1997). Adrenocortical and adrenomedullary homologs in eight species of adult and developing teleosts: morphology, histology, and immunohistochemistry. Gen Comp Endocrinol *108*, 483-496.

Hanke, C.J., and Campbell, W.B. (2000). Endothelial cell nitric oxide inhibits aldosterone synthesis in zona glomerulosa cells: modulation by oxygen. Am J Physiol Endocrinol Metab *279*, E846-E854.

Hardy, S., Legagneux, V., Audic, Y., and Paillard, L. (2010). Reverse genetics in eukaryotes. Biol Cell *102*, 561-580.

Heck, D., Wortmann, S., Kraus, L., Ronchi, C.L., Sinnott, R.O., Fassnacht, M., and Sbiera, S. (2105). Role of endocrine gland-derived vascular endothelial growth factor (EG-VEGF) and its receptors in adrenocortical tumors. Horm Cancer *6*, 225-236.

Heikkila, P., Arola, J., Voutilainen, R., Salmenkivi, K., Kahri, A.I., and Liu, J. (2000). Expression of vascular endothelial growth factor in human adrenals. Endocr Res *26*, 867-871.

Helker, C.S., Schuermann, A., Karpanen, T., Zeuschner, D., Belting, H.G., Affolter, M., Schulte-Merker, S., and Herzog, W. (2013). The zebrafish common cardinal veins develop by a novel mechanism: lumen ensheathment. Development *140*, 2776-2786.

Herbert, S.P., Huisken, J., Kim, T.N., Feldman, M.E., Houseman, B.T., Wang, R.A., Shokat, K.M., and Stainier, D.Y. (2009). Arterial-venous segregation by selective cell sprouting: an alternative mode of blood vessel formation. Science *326*, 294-298.

Hogan, B.M., Herpers, R., Witte, M., Helotera, H., Alitalo, K., Duckers, H.J., and Schulte-Merker, S. (2009). Vegfc/Flt4 signalling is suppressed by Dll4 in developing zebrafish intersegmental arteries. Development *136*, 4001-4009.

Hoivik, E.A., Lewis, A.E., Aumo, L., and Bakke, M. (2010). Molecular aspects of steroidogenic factor 1 (SF-1). Mol Cell Endocrinol *315*,27-39.

Hsu, H.C. (2010). The role of endoderm for the interrenal tissue development in the zebrafish. Master Thesis. Tunghai University.

Hsu, H.J., Lin, G., and Chung, B.C. (2003). Parallel early development of zebrafish interrenal glands and pronephros: differential control by *wt1* and *ff1b*. Development *130*, 2107-2116.

Huber, K. (2006). The sympathoadrenal cell lineage: Specification, diversification, and new perspectives. Dev Biol *298*, 335-343.

Isogai, S., Horiguchi, M., and Weinstein, B.M. (2001). The vascular anatomy of the developing zebrafish: an atlas of embryonic and early larval development. Dev Biol *230*, 278-301.

Jin, S.W., Beis, D., Mitchell, T., Chen, J.N., and Stainier, D.Y. (2005). Cellular and molecular

analyses of vascular tube and lumen formation in zebrafish. Development *132*, 5199-5209.

Joukov, V., Kumar, V., Sorsa, T., Arighi, E., Weich, H., Saksela, O., and Alitalo, K. (1998). A recombinant mutant vascular endothelial growth factor-C that has lost vascular endothelial growth factor receptor-2 binding, activation, and vascular permeability activities. J Biol Chem *273*, 6599-6602.

Jülich, D., Geisler, R., Holley, S.A., and Tübingen 2000 Screen Consortium. (2005). Integrinalpha5 and delta/notch signaling have complementary spatiotemporal requirements during zebrafish somitogenesis. Dev Cell *8*, 575-586.

Kikuchi, Y., Agathon, A., Alexander, J., Thisse, C., Waldron, S., Yelon, D., Thisse, B., and Stainier, D.Y. (2001). *casanova* encodes a novel *Sox*-related protein necessary and sufficient for early endoderm formation in zebrafish. Genes Dev *15*, 1493-1505.

Kim, A.C., Barlaskar, F.M., Heaton, J.H., Else, T., Kelly, V.R., Krill, K.T., Scheys, J.O., Simon, D.P., Trovato, A., Yang, W.H, and Hammer, G.D. (2009). In search of adrenocortical stem and progenitor cells. Endocr Rev *30*, 241-263.

Koeppen, B.M., and Stanton, B.A. (2008). Physiology. Berne and Levy, Sixth Edition. Mosby.

Kool, M.M., Galac, S., Kooistra, H.S., and Mol, J.A. (2014). Expression of angiogenesis-related genes in canine cortisol-secreting adrenocortical tumors. Domest Anim Endocrinol *47*, 73-82.

Koshida, S., Kishimoto, Y., Ustumi, H., Shimizu, T., Furutani-Seiki, M., Kondoh, H., and Takada, S. (2005). Integrinalpha5-dependent fibronectin accumulation for maintenance of somite boundaries in zebrafish embryos. Dev Cell *8*, 587-598.

Kovacic, J.C., Mercader, N., Torre, M., Boehm, M., and Fuster, V. (2012). Epithelial-tomesenchymal and endothelial-to-mesenchymal transition: from cardiovascular development to disease. Circulation *125*, 1795-1808.

Kuchler, A.M., Gjini, E., Peterson-Maduro, J., Cancilla, B., Wolburg, H., and Schulte-Merker, S. (2006). Development of the zebrafish lymphatic system requires VEGFC signaling. Curr Biol *16*, 1244-1248.

Kühl, M. (2002). Non-canonical Wnt signaling in Xenopus: regulation of axis formation and gastrulation. Semin Cell Dev Biol *13*, 243-249.

Lawson, N.D., and Weinstein, B.M., (2002). Arteries and veins: making a difference with zebrafish. Nat Rev Genet *3*, 674-82.

LeCouter, J., Lin, R., and Ferrara, N. (2002). Endocrine gland-derived VEGF and the emerging hypothesis of organ-specific regulation of angiogenesis. Nat Med *8*, 913-917.

LeCouter, J., Kowalski, J., Foster, J., Hass, P., Zhang, Z., Dillard-Telm, L., Frantz, G., Rangell, L., DeGuzman, L., Keller, G.A., *et al.* (2001). Identification of an angiogenic mitogen selective for endocrine gland endothelium. Nature *412*, 877-884.

Lelievre, E., Mattot, V., Huber, P., Vandenbunder, B., and Soncin, F. (2000). ETS1 lowers capillary endothelial cell density at confluence and induces the expression of VE-cadherin. Oncogene *19*, 2438-2446.

Liang, D., Chang, J.R., Chin, A.J., Smith, A., Kelly, C., Weinberg, E.S., and Ge, R. (2001). The role of vascular endothelial growth factor (VEGF) in vasculogenesis, angiogenesis, and hematopoiesis in zebrafish development. Mech Dev *108*, 29-43.

Liao, E.C, Paw, B.H, Oates, A.C, Pratt, S.J, Postlethwait, J.H., and Zon, L.I. (1998). SCL/Tal-1 transcription factor acts downstream of cloche to specify hematopoietic and vascular progenitors in zebrafish. Genes Dev *12*, 621-626.

Lightman, S.L., and Conway-Campbell, B.L. (2010). The crucial role of pulsatile activity of the HPA axis for continuous dynamic equilibration. Nat Rev Neurosci *11*, 710-718.

Lin, R., LeCouter, J., Kowalski, J., and Ferrara, N. (2002). Characterization of endocrine gland-derived vascular endothelial growth factor signaling in adrenal cortex capillary endothelial cells. J Biol Chem *277*, 8724-8729.

Lindahl, P., Hellstrom, M., Kalen, M., Karlsson, L., Pekny, M., Pekna, M., Soriano, P., and Betsholtz, C. (1998). Paracrine PDGF-B/PDGF-Rbeta signaling controls mesangial cell development in kidney glomeruli. Development *125*, 3313-3322.

Liu, Y.W. (2007). Interrenal organogenesis in the zebrafish model. Organogenesis *3*, 44-48.

Liu, Y.W., and Guo, L. (2006). Endothelium is required for the promotion of interrenal morphogenetic movement during early zebrafish development. Dev Biol *297*, 44-58.

Luo, X., Ikeda, Y., and Parker, K.L. (1994). A cell-specific nuclear receptor is essential for adrenal and gonadal development and sexual differentiation. Cell *77*, 481-490.

Majumdar, A., and Drummond, I.A. (1999). Podocyte differentiation in the absence of endothelial cells as revealed in the zebrafish avascular mutant, *cloche*. Dev Genet *24*, 220-229.

Mallet, C., Feraud, O., Ouengue-Mbele, G., Gaillard, I., Sappay, N., Vittet, D., and Vilgrain, I. (2003). Differential expression of VEGF receptors in adrenal atrophy induced by dexamethasone: a protective role of ACTH. Am J Physiol Endocrinol Metab 284, E156-167.

Marlow, F., Topczewski, J., Sepich, D., and Solnica-Krezel, L. (2002). Zebrafish Rho kinase 2 acts downstream of Wnt11 to mediate cell polarity and effective convergence and extension movements. Curr Biol *4*, 876-884.

Matsui, T., Raya, A., Callol-Massot, C., Kawakami, Y., Oishi, I., Rodriguez-Esteban, C., and Belmonte, J.C. (2007). *miles-apart*-Mediated regulation of cell-fibronectin interaction and myocardial migration in zebrafish. Nat Clin Pract Cardiovasc Med *4* Suppl. *1*, S77-S82.

Matsui, T., Raya, A., Kawakami, Y., Callol-Massot, C., Capdevila, J., Rodriguez-Esteban, C., and Izpisúa Belmonte, J.C. (2005). Noncanonical Wnt signaling regulates midline convergence of organ primordia during zebrafish development. Genes Dev *19*, 164-175.

Mauch, T.J., Yang, G., Wright, M., Smith, D., and Schoenwolf, G.C. (2000). Signals from trunk paraxial mesoderm induce pronephros formation in chick intermediate mesoderm. Dev Biol *220*, 62-75.

McKinley, M., and O'Loughlin, V. (2008). Human Anatomy. McGraw-Hill, Second Edition, pp.820-821; 622-624.

Mesiano, S., and Jaffe, R.B. (1997). Developmental and functional biology of the primate fetal adrenal cortex. Endocr Rev *18*, 378-403.

Mizrachi, Y., Naranjo, J.R., Levi, B.Z., Pollard, H.B., and Lelkes, P.I. (1990). PC12 cells differentiate into chromaffin cell-like phenotype in coculture with adrenal medullary endothelial cells. Proc Natl Acad Sci U.S.A. *87*, 6161-6165.

Mudumana, S.P., Hentschel, D., Liu, Y., Vasilyev, A., and Drummond, I.A. (2008). *odd skipped related1* reveals a novel role for endoderm in regulating kidney versus vascular cell fate. Development *135*, 3355-3367.

Müller-Deile, J., Worthmann, K., Saleem, M., Tossidou, I., Haller, H., and Schiffer, M. (2009). The balance of autocrine VEGF-A and VEGF-C determines podocyte survival. Am J Physiol Renal Physiol *297*, F1656-1667.

Nicoli, S., Standley, C., Walker, P., Hurlstone, A., Fogarty, K.E., and Lawson, N.D. (2010). MicroRNA-mediated integration of haemodynamics and Vegf signalling during angiogenesis. Nature *464*, 1196-1200.

Ober, E.A., Olofsson, B., Makinen, T., Jin, S.W., Shoji, W., Koh, G.Y., Alitalo, K., and Stainier, D.Y. (2004). Vegfc is required for vascular development and endoderm morphogenesis in zebrafish. EMBO Rep *5*, 78-84.

Osborne, N.J., Begbie, J., Chilton, J.K., Schmidt, H., and Eickholt, B.J. (2005). Semaphorin/neuropilin signaling influences the positioning of migratory neural crest cells within the hindbrain region of the chick. Dev Dyn *232*, 939-949.

Parker, L.H., Schmidt, M., Jin, S.W., Gray, A.M., Beis, D., Pham, T., Frantz, G., Palmieri, S., Hillan, K., Stainier, D.Y., et al. (2004). The endothelial-cell-derived secreted factor Egfl7 regulates vascular tube formation. Nature *425*, 754-758.

Patterson, L.J., and Patient, R. (2006). The "Ets" factor: vessel formation in zebrafish--the missing link? PLoS Biol *4*, e24.

Perner, B., Englert, C., and Bollig, F. (2007). The Wilms tumor genes *wt1*a and *wt1b* control different steps during formation of the zebrafish pronephros. Dev Biol *309*, 87-96.

Quaggin, S.E., and Kreidberg, J.A. (2008). Development of the renal glomerulus: good neighbors and good fences. Development *135*, 609-620.

Quek, S.I. (2009). Molecular characterization of the zebrafish *ff1b* gene. Ph.D. thesis. National University of Singapore.

Quek, S.I., and Chan, W.K. (2009). Transcriptional activation of zebrafish *cyp11a1* promoter is dependent on the nuclear receptor Ff1b. J Mol Endocrinol *43*, 121-130.

Reissmann, E., Ernsberger, U., Francis-West, P.H., Rueger, D., Brickell, P.M., and Rohrer, H., (1996). Involvement of bone morphogenetic protein-4 and bone morphogenetic protein-7 in the differentiation of the adrenergic phenotype in developing sympathetic neurons. Development *122*, 2079-2088.

Roberts, W.G., and Palade, G.E. (1995). Increased microvascular permeability and endothelial fenestration induced by vascular endothelial growth factor. J Cell Sci *108*, 2369-

2379.

Saito, D., Takase, Y., Murai, H., and Takahashi, Y. (2012). The dorsal aorta initiates a molecular cascade that instructs sympatho-adrenal specification. Science *336*, 1578-1581.

Saito, D., and Takahashi, Y. (2015). Sympatho-adrenal morphogenesis regulated by the dorsal aorta. Mech Dev *138*, 2-7.

Sakaguchi, T., Kikuchi,Y., Kuroiwa, A., Takeda, H., and Stainier, D.Y. (2006). The yolk syncytial layer regulates myocardial migration by influencing extracellular matrix assembly in zebrafish. Development *133*, 4063-4072.

Satchell, S.C., Tasman, C.H., Singh, A., Ni, L., Geelen, J., von Ruhland, C.J., O'Hare, M.J., Saleem, M.A., van den Heuvel, L.P., and Mathieson, P.W. (2006). Conditionally immortalized human glomerular endothelial cells expressing fenestrations in response to VEGF. Kidney Int *69*, 1633-1640.

Savagner, P. (2001). Leaving the neighborhood: molecular mechanisms involved during epithelial-mesenchymal transition. Bioessays *23*, 912-923.

Schottenfeld, J., Sullivan-Brown, J., and Burdine, R.D. (2007). Zebrafish *curly up* encodes a Pkd2 ortholog that restricts left-side-specific expression of southpaw. Development *134*, 1605-1615.

Sehnert, A.J., Huq, A.,Weinstein, B.M.,Walker, C., Fishman, M., and Stainier, D.Y. (2002). Cardiac troponin T is essential in sarcomere assembly and cardiac contractility. Nat Genet *31*, 106-110.

Serluca, F.C., Drummond, I.A., and Fishman, M.C. (2002). Endothelial signaling in kidney morphogenesis. A role for hemodynamic forces. Curr Biol *12*, 492-497.

Shifren, J.L., Mesiano, S., Taylor, R.N., Ferrara, N., and Jaffe, R.B. (1998). Corticotropin regulates vascular endothelial growth factor expression in human fetal adrenal cortical cells. J Clin Endocrinol Metab *83*, 1342-1347.

Siekmann, A.F., Standley, C., Fogarty, K.E., Wolfe, S.A., and Lawson, N.D. (2009). Chemokine signaling guides regional patterning of the first embryonic artery. Genes Dev *23*, 2272-2277.

Steed, E., Faggianelli, N., Roth, S., Ramspacher, C., Concordet, J.P., and Vermot, J. (2016). klf2a couples mechanotransduction and zebrafish valve morphogenesis through fibronectin synthesis. Nat Commun *7*, 11646.

Sumanas, S., and Lin, S. (2006). Ets1-related protein is a key regulator of vasculogenesis in zebrafish. PLoS Biol *4*, e10.

Tada, M., Concha, M.L., and Heisenberg, C.P. (2002) Non-canonical Wnt signalling and regulation of gastrulation movements. Semin Cell Dev Biol *13*, 251-260.

To, T.T., Hahner, S., Nica, G., Rohr, K.B., Hammerschmidt, M., Winkler, C., and Allolio, B. (2007). Pituitary-interrenal interaction in zebrafish interrenal organ development. Mol Endocrinol *21*, 72-85.

Tufro, A., Norwood, V.F., Carey, R.M., and Gomez, R.A. (1999). Vascular endothelial growth factor induces nephrogenesis and vasculogenesis. J Am Soc Nephrol *10*, 2125-2134.

Trinh, L.A., and Stainier, D.Y. (2004). Fibronectin regulates epithelial organization during myocardial migration in zebrafish. Dev Cell *6*, 371-382.

Val, P., Martinez-Barbera, J.P., and Swain, A. (2007). Adrenal development is initiated by Cited2 and Wt1 through modulation of Sf-1 dosage. Development *134*, 2349-2358.

Vermot, J., Forouhar, A.S., Liebling, M., Wu, D., Plummer, D., Gharib, M., and Fraser, S.E. (2009). Reversing blood flows act through *klf2a* to ensure normal valvulogenesis in the developing heart. PLoS Biol *7*, e1000246.

Vervenne, H.B., Crombez, K.R., Lambaerts, K., Carvalho, L., Köppen. M., Heisenberg, C.P., Van de Ven, W.J., and Petit, M.M. (2008). Lpp is involved in Wnt/PCP signaling and acts together with Scrib to mediate convergence and extension movements during zebrafish gastrulation. Dev Biol *320*, 267-277.

Vittet, D., Ciais, D, Keramidas, M., De Fraipont, F., and Feige, J.J. (2000). Paracrine control of the adult adrenal cortex vasculature by vascular endothelial growth factor. Endocr Res *26*, 843-852.

Wakiya, K., Begue, A., Stehelin, D., and Shibuya, M. (1996). A cAMP response element and an Ets motif are involved in the transcriptional regulation of *flt-1* tyrosine kinase (vascular endothelial growth factor receptor 1) gene. J Biol Chem *271*, 30823-30828.

Wang, Y., Kaiser, M.S., Larson, J.D., Nasevicius, A., Clark, K.J., Wadman, S.A., Roberg-Perez, S.E., Ekker, S.C., Hackett, P.B., McGrail, M., and Essner, J.J. (2010). Moesin1 and Ve-cadherin are required in endothelial cells during in vivo tubulogenesis. Development *137*, 3119-3128.

Wang, L., Zhang, P., Wei, Y., Gao, Y., Patient, R., and Liu, F. (2011). A blood flow-dependent *klf2a*-NO signalling cascade is required for stabilization of hematopoietic stem cell programming in zebrafish embryos. Blood *118*, 4102-4110.

Wingert, R.A., and Davidson, A.J. (2008). The zebrafish pronephros: a model to study nephron segmentation. Kidney Int *73*, 1120-1127.

Wood, M.A., and Hammer, G.D. (2011). Adrenocortical stem and progenitor cells: unifying model of two proposed origins. Mol Cell Endocrinol *336*, 206-212.

Zhong, T.P., Childs, S., Leu, J.P. and Fishman, M.C. (2001). Gridlock signalling pathway fashions the first embryonic artery. Nature *414*, 216-220.

Zhou, W., Boucher, R.C., Bollig, F., Englert, C., and Hildebrandt, F. (2010). Characterization of mesonephric development and regeneration using transgenic zebrafish. Am J Physiol Renal Physiol *299*, F1040-F1047.

Zhu, S., Liu, L., Korzh, V., Gong, Z., and Low, B.C. (2006). RhoA acts downstream of Wnt5 and Wnt11 to regulate convergence and extension movements by involving effectors Rho kinase and Diaphanous: use of zebrafish as an *in vivo* model for GTPase signaling. Cell Signal *18*, 359-272.

List of tables and figures

Table 1. Sequence of MOs

Name	Sequence	Dosage (pmole)	Reference
*etv2*MO1	5'-TTGGTACATTTCCATATCTTAAAGT-3'	1.2 (MO1+MO2)	(Sumanas & Lin, 2006)
*etv2*MO2	5'-CACTGAGTCCTTATTTCACTATATC-3'		(Sumanas & Lin, 2006)
*flt4*MO	5'-TTAGGAAAATGCGTTCTCACCTGAG-3'	0.7	(Covassin et al., 2006)
*hey2*MO	5'-CGCGCAGGTACAGACACCAAAAACT-3'	1.2	(Zhong et al., 2001)
*klf2a*MO	5'-GGACCTGTCCAGTTCATCCTTCCAC-3'	1.2	(Nicoli et al., 2010)
*mmp2*MO	5'-GGGAGCTTAGTAAACACAAACCTGT-3'	1.2	(Detry et al., 2012)
*osr1*MO	5'-ATCTCATCCTTACCTGTGGTCTCTC-3'	0.9	(Mudumana et al., 2008)
*pkd2*MO	5'-AGGACGAACGCGACTGGAGCTCATC-3'	0.5	(Sun et al., 2004)
*tal1*MO1(*scl*)	5'-GCGGCGTTACCTGTTAATAGTGGCG-3'	1.2 (MO1+MO2)	(Dooley et al., 2005)
*tal1*MO2(*scl*)	5'-AATGCTCTTACCATCGTTGATTTC-3'		(Dooley et al., 2005)
*sox32*MO	5'-CAGGGAGCATCCGGTCGAGATACAT-3'	0.5	(Dickmeis et al., 2001)
STD-MO	5'-CCT CTTACCTCAGTTACAATTTATAA-3'	1.4	
*tnnt2a*MO	5'-CATGTTTGCTCTGATCTGACACGCA-3'	1	(Sehnert et al., 2002)
*vegfC*MO	5'-GAAAATCCAAATAAGTGCATTTTAG-3'	1	(Ober et al., 2004)

Table 2. Plasmids for making anti-sense riboprobes

Insert	Vector	Restriction enzyme for linearization/ Transcription enzyme	Labelling
dβh	pGEMT	NcoI/SP6	DIG
ephb2	pSPORT1	SalI/SP6	DIG
flt4	pBK-CMV	EcoRI/T7	DIG
ff1b	pGEMT-easy	SalI/T7	Flu
wt1a	pCRII-TOPO	BamHI/T7	DIG or Flu
wt1b	pCRII-TOPO	BamHI/T7	DIG or Flu

Table 3. Concentration of primary antibodies

Name	Concentration	Host	Brand
anti-βCatenin	1:50	Rabbit	Sigma
anti-Cdh1	1:200	Rabbit	GeneTex
anti-Fn	1:200	Rabbit	Sigma
anti-Laminin	1:200	Rabbit	Abcam
anti-pFAK	1:100	Rabbit	BD Transduction Laboratories
anti-Vimentin	1:200	Mouse	Abcam
anti-VegfC	1:50	Rabbit	Santa Cruz

Table 4. Phenotypic analysis of interrenal morphogenesis in *etv2* morphants

		Control		*etv2*MO	
	Morphology of the interrenal tissue	No.	(%)	No.	(%)
Normal	Single cluster to the right of the midline	112	(96.6)	12	(11.3)
Class(I)	Single cluster from the midline fusion of bilateral ones	0		36	(34.0)
Class(II)	Bilateral elongated clusters with caudal fusing at the midline	0		31	(29.2)
Class(II)	Bilateral clusters across the midline	4	(3.4)	27	(25.5)
Total		116		106	

Table 5. Phenotypic analysis of interrenal migration in *hey2* MO- or *hey2* mRNA-injected embryos

	Control		*hey2*MO		*hey2*mRNA	
Morphology of the interrenal tissue	No.	(%)	No.	(%)	No	(%)
Bilateral clusters widely across the midline	0		0		76	(30.1)
Bilateral clusters immediately across the midline	2	(1.4)	2	(3.2)	45	(17.9)
Single cluster at the central midline	0		60	(95.2)	74	(29.4)
Single cluster to the left of the midline	7	(5.0)	0		38	(15.1)
Single cluster to the right of the midline	131	(93.6)	1	(1.6)	19	(7.5)
Total	140	(100)	63	(100)	252	(100)

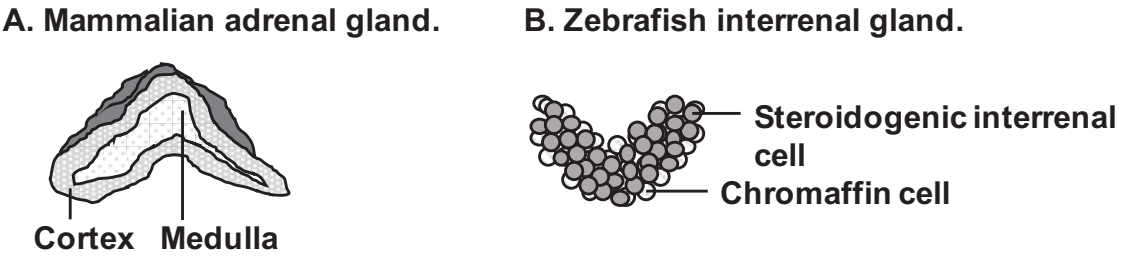

Fig. 1. Schematic diagram of the mammalian adrenal gland and the zebrafish interrenal gland.

(A). The mammalian adrenal gland contains the outer cortex and the inner medulla. (modified from McKinley and O'Loughlin, 2008) (B). The zebrafish interrenal gland contains the steroidogenic interrenal tissue which is counterpart of the adrenal cortex, and the chromaffin cell which is counterpart of the adrenal medulla.

CRH: corticotropin-releasing hormone
ACTH: adrenocorticotripic hormone

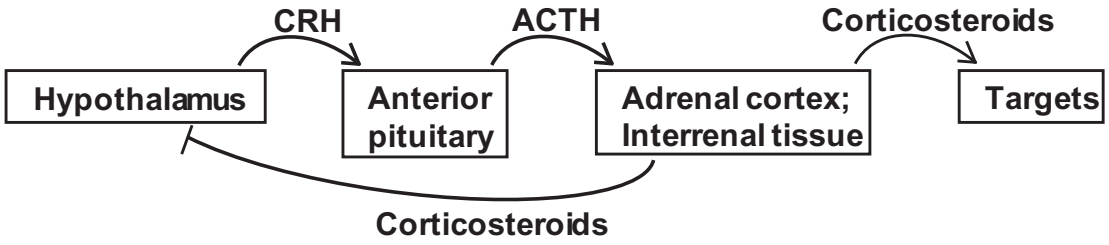

Fig 2. The HPA axis (HPI axis in fish).

The HPA/HPI axis is activated in response to the stress, the hormones are transported through the blood flow. The CRH is produced by the hypothalamus, which stimulates the anterior pituitary to release ACTH. ACTH stimulates the adrenal cortex (in mammalian) or the interrenal tissue (in teleosts) to release corticosteroids which are received by the targets such as the liver, the kidney and the muscle. (reviewed in Lightman and Conway-Campbell, 2010)

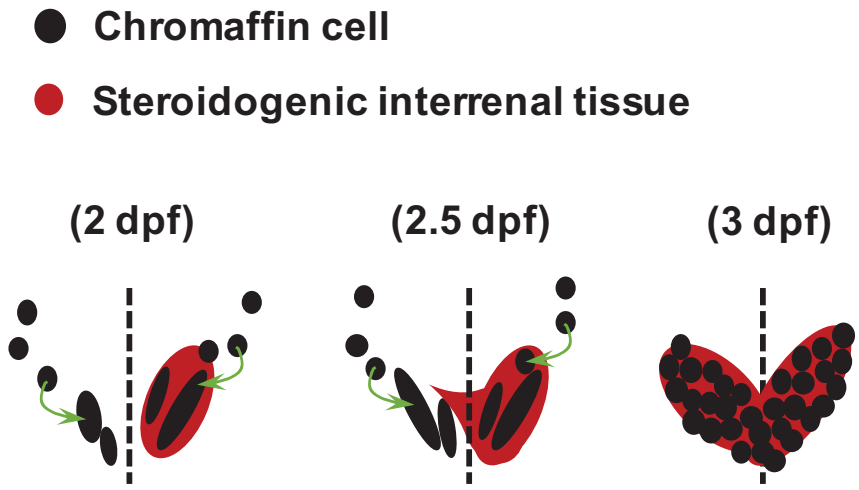

Fig. 3. Morphogenetic movements of the interrenal tissue and the chromaffin cell.

Schematic diagram of the functional assembly of the zebrafish interrenal gland, dorsal view. The interrenal tissue (red) extended to the midline during 2 to 3 dpf, at the meantime, the chromaffin cell (black) migrated bilaterally from the dorsal along the notochord to reach the interrenal tissue.

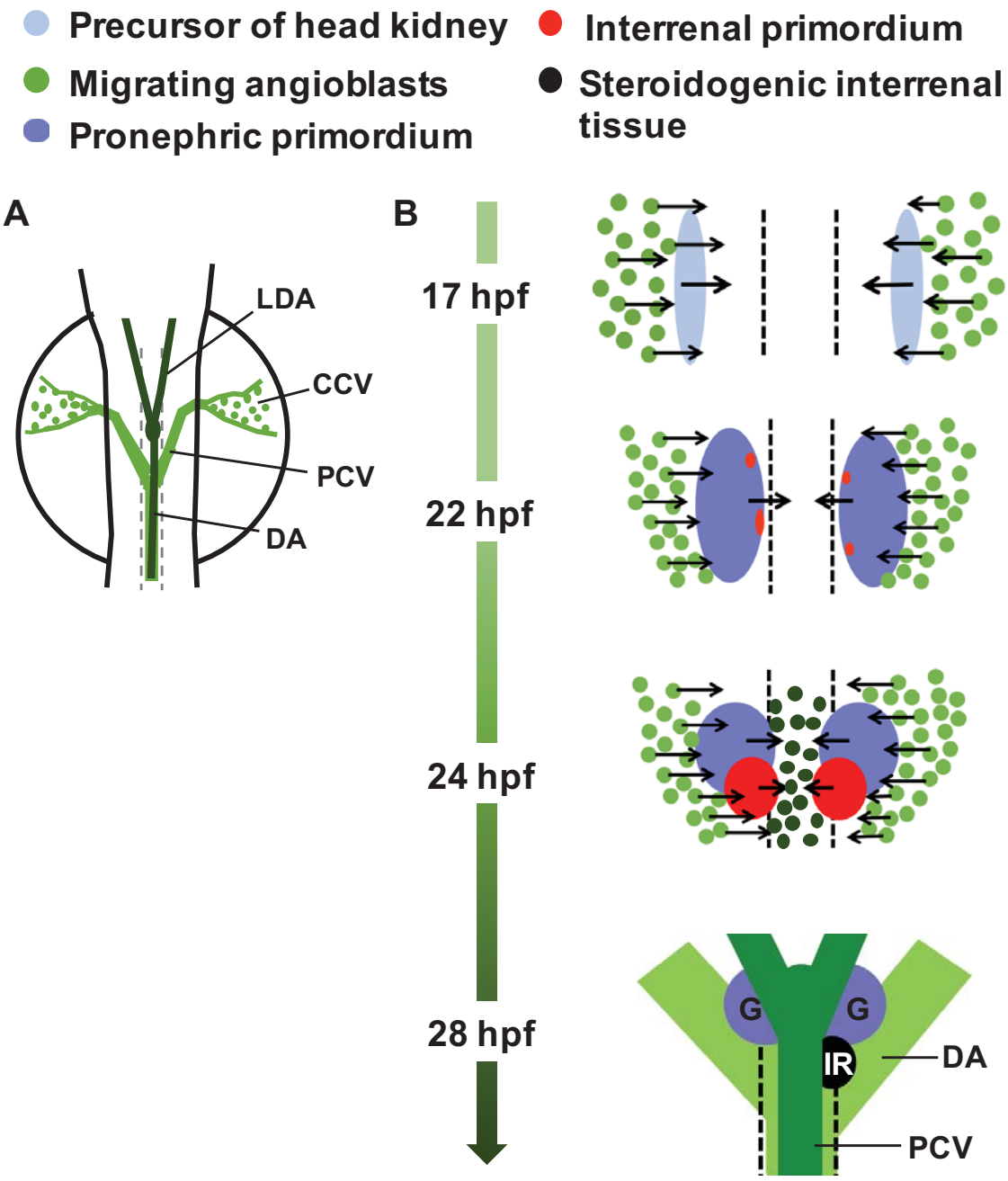

Fig. 4. Morphogenetic movements of the head kidney and the EC in the zebrafish.

(A). Schematic diagram of the zebrafish vasculature at the midtrunk at 24 hpf, dorsal view with anterior to the top (modified form Lawson and Weinstein, 2002). (B). Schematic diagram of midline convergences of the head kidney and the ECs (modified from Liu, 2007). Bilateral common precursors of the head kidney arise before 17 hpf and co-migrate toward the midline with the adjacent angioblasts. Precursors of the interrenal tissue (IR) are specified form the pronephric region around 22 hpf, fuse after 24 hpf, and differentiate around 28 hpf. The angioblasts assemble at the midline and formed the DA and the PCV. The bilateral pronephric glomeruli (G) later fuse at the midline around 2 dpf.

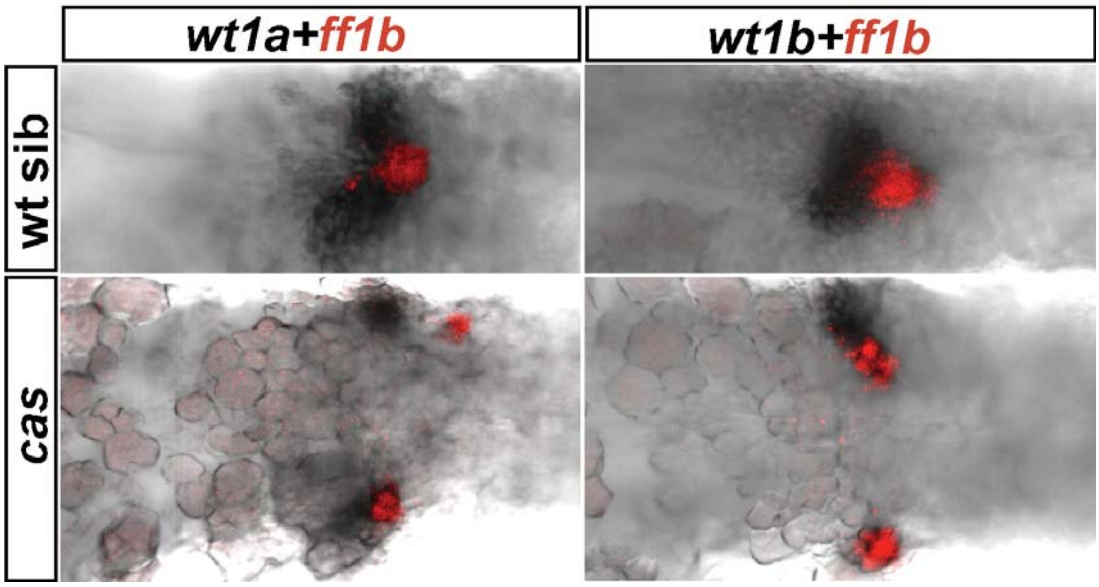

Fig. 5. The phenotype of the head kidney in the *cas* mutant.

Two color ISH of either *wt1a* (black) plus *ff1b* (red) or *wt1b* (black) plus *ff1b* (red) in the wildtype sibling and the *cas* mutant at 34 hpf. Both *wt1a* and *wt1b* represented the pronephric glomerulus while *ff1b* represented the interrenal tissue. In the wildtype sibling, two clusters of the glomeruli were immediately associated, while the fused interrenal tissue caudal to the glomeruli. In the *cas* mutant, midline convergence of both the pronephric glomerulus and the interrenal tissue was severely inhibited.

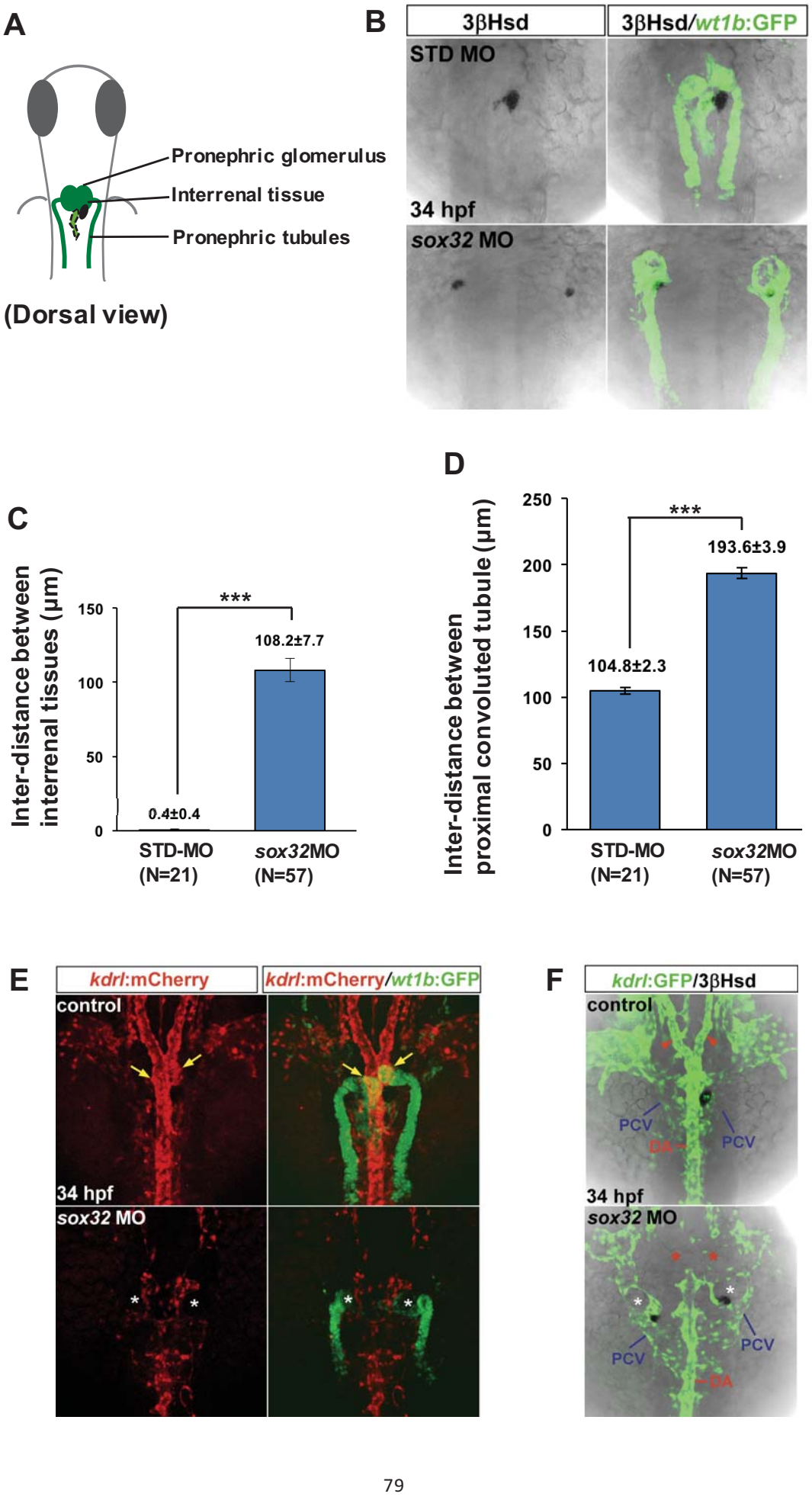
A
Pronephric glomerulus
Interrenal tissue
Pronephric tubules
(Dorsal view)
B
3βHsd
3βHsd/wt1b:GFP
STD MO
34 hpf
sox32 MO
C
Inter-distance between interrenal tissues (μm)
150
100
50
0
***
108.2±7.7
0.4±0.4
STD-MO (N=21)
sox32MO (N=57)
D
Inter-distance between proximal convoluted tubule (μm)
250
200
150
100
50
0
***
193.6±3.9
104.8±2.3
STD-MO (N=21)
sox32MO (N=57)
E
kdrl:mCherry
kdrl:mCherry/wt1b:GFP
control
34 hpf
sox32 MO
F
kdrl:GFP/3βHsd
control
PCV
DA
PCV
34 hpf
sox32 MO
PCV
PCV
DA

Fig. 6. Effects of *sox32*MO injection on the head kidney and the vasculature.

(A). Schematic diagram of a *Tg(wt1b:GFP)*^{li1} embryo assayed for 3βHsd enzymatic activity staining, dorsal view with anterior to the top. (B). *Tg(wt1b:GFP)*^{li1} embryos were injected with standard control morpholino (STD-MO) or *sox32*MO, and assayed for 3βHsd enzymatic activity staining. The pronephros was marked by GFP and the interrenal tissue was visualized by 3βHsd enzymatic activity assay. Midline convergence of the head kidney was severely inhibited in the *sox32* morphant, distance between the bilateral interrenal tissues and distance between the bilateral pronephric glomeruli were quantified in panel C and D, respectively. (E). Dorsal views of the *Tg(wt1b:GFP)*^{li1}x*Tg(kdrl:mCherry)*^{ci5} embryo with anterior to the top. The pronephros was marked by GFP; the EC was marked by red fluorescence; and the interrenal tissue was visualized by 3βHsd enzymatic activity assay. Angiogenesis of the pronephric glomerulus could be found in the control embryo (indicated by yellow arrows), but not in the *sox32* morphant (marked by white asterisks). (F). Dorsal view of *Tg(kdrl:GFP)*^{s843} embryos. In the control embryo, the interrenal tissue was sandwiched between the DA and the right branch of the PCV, but in the *sox32* morphant, the bilateral interrenal tissues were disassociated with the DA and still tight associated with the malformed PCV. The formation of LDA (red arrowhead) was inhibited in the *sox32* morphant (the absence of LDA was marked by red asterisks). (student's t-test, ***$p<0.001$; scale bar, 50 μm)

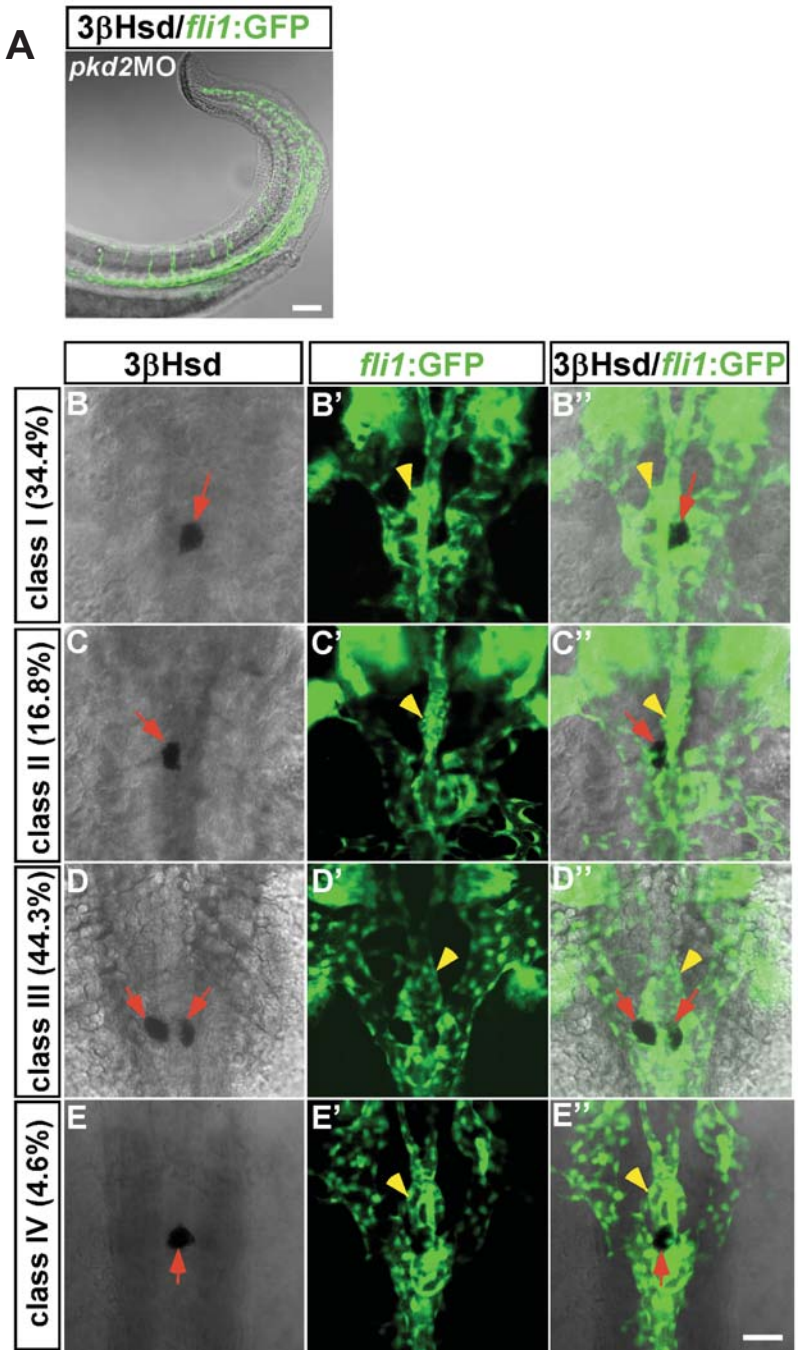

Fig. 7. Confocal images of the *pkd2*MO-injected *Tg(fli1:EGFP)^{y1}* embryos at 2 dpf.

(A). The *pkd2* morphant displayed the curly tail phenotype and phenocopied the *pkd2* mutant (lateral view). Scale bar, 100 μm. (B-E). The interrenal tissue was detected by 3βHsd enzymatic activity staining and its neighboring endothelium was labeled by GFP (dorsal view with anterior oriented to the top). Loss of *pkd2* resulted in disruption of the left-right asymmetry, the steroidogenic interrenal tissue displayed randomization of the laterality. Orange arrows indicated interrenal tissues and yellow arrowheads indicated the pronephric glomerulus. Scale bar, 50 μm.

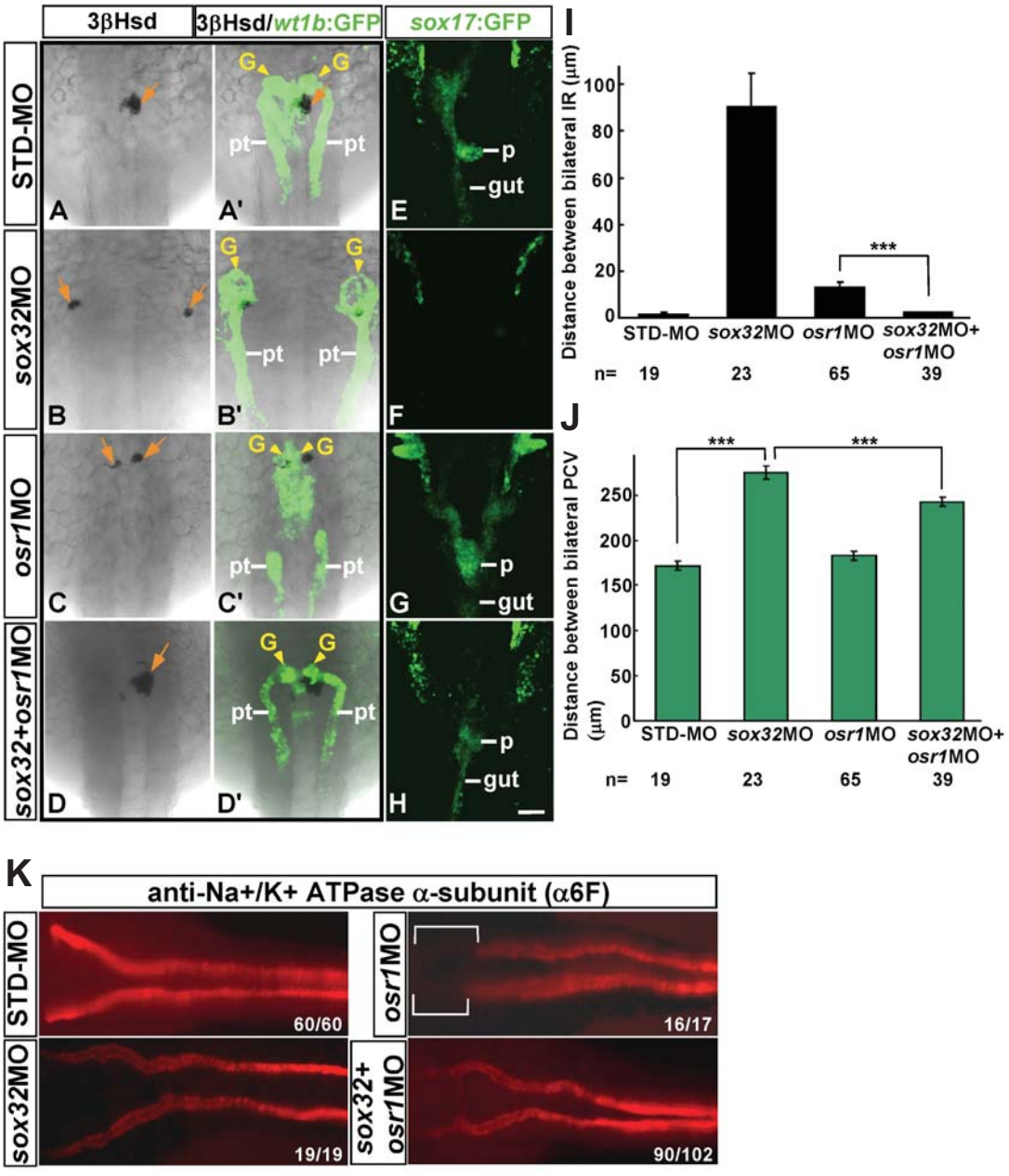
3βHsd
3βHsd/wt1b:GFP
sox17:GFP
STD-MO
sox32MO
osr1MO
sox32+osr1MO
A
A'
B
B'
C
C'
D
D'
E
F
G
H
G
pt
p
gut
I
Distance between bilateral IR (μm)
100
80
60
40
20
0
***
STD-MO
sox32MO
osr1MO
sox32MO+ osr1MO
n= 19 23 65 39
J
Distance between bilateral PCV (μm)
250
200
150
100
50
0
***
***
STD-MO
sox32MO
osr1MO
sox32MO+ osr1MO
n= 19 23 65 39

K
anti-Na+/K+ ATPase α-subunit (α6F)
STD-MO
60/60
osr1MO
16/17
sox32MO
19/19
sox32+ osr1MO
90/102

Fig. 8. *osr1*MO co-injection alleviated midline convergence defects of the head kidney in the endodermless embryo.

(A-D). Dorsal views of *Tg(wt1b:GFP)*^{li1} embryos at 34 hpf. The pronephric morphology was represented by GFP and the steroidogenic cell was marked by 3βHsd staining (orange arrow). The severe defective midline convergence of the head kidney in the *sox32* morphant (B) and the loss of proximal pronephric tubule in the *osr1* morphant (C) were rescued by double knockdown of *osr1* and *sox32* (D). Distance between the bilateral interrenal tissues and distance between the bilateral pronephric glomeruli were quantified in panel I and J, respectively. (E-H). Dorsal views of *Tg(sox17:GFP)*^{s870} embryos at 34 hpf. The GFP represented the endoderm tissues, such as pancreas (p) and gut, which were absent in the endodermless embryo (F). The endoderm loss in the *sox32* morphant was rescued by a simultaneous knockdown of *osr1* (H). (K). Staining of α6F showed that the anterior pronephric tubules was absent (white basket) in the *osr1* morphant, and that could be rescued by additional knockdown of *sox32*. (G, glomerulus; pt, pronephric tubule.)

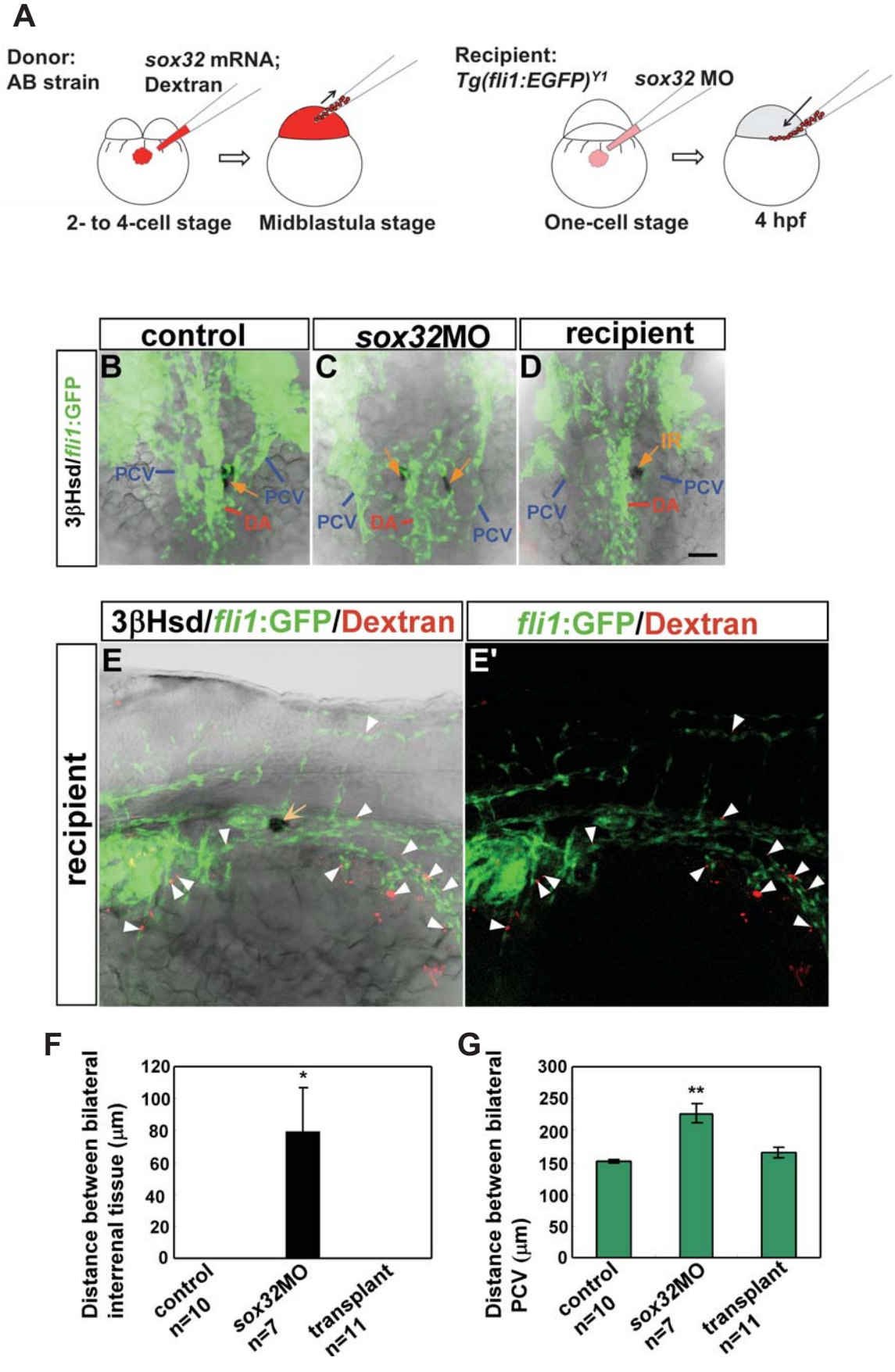
A
Donor:
AB strain
sox32 mRNA;
Dextran
2- to 4-cell stage
Midblastula stage
Recipient:
Tg(fli1:EGFP)Y1
sox32 MO
One-cell stage
4 hpf
control
sox32MO
recipient
3βHsd/fli1:GFP
B
C
D
PCV
DA
IR
3βHsd/fli1:GFP/Dextran
fli1:GFP/Dextran
recipient
E
E'
F
Distance between bilateral interrenal tissue (μm)
120
100
80
60
40
20
0
*
control n=10
sox32MO n=7
transplant n=11
G
Distance between bilateral PCV (μm)
300
250
200
150
100
50
0
**
control n=10
sox32MO n=7
transplant n=11

Fig. 9. Transplantation of *sox32*-overexpressed cells into the *sox32* morphant.

(A). Schematic diagram of the transplantation experiment. The donor embryo was injected with *sox32* mRNA and fluorescent dextran at 2- to 4-cell stage, and some cells were taken off from the animal pole at midblastula stage. The recipient was injected with *sox32*MO at one-cell stage, and the dextran-labelled cells form the donor embryo were transplanted into the margin of the blastoderm of the recipient. (B-D). The interrenal morphology in the control embryo, the *sox3*2 morphant, and the recipient. (Dorsal view, the interrenal tissue was indicated by orange arrows) (E). Lateral view with anterior to the left of the recipient at 48 hpf. The dextran-labelled *sox32*-overexpressing cells (white arrowheads) were associated with the venous endothelium (marked by GFP). (F,G). Quantifications of distance between the bilateral interrenal tissues and distance between the bilateral pronephric glomeruli. In the recipient, the distance between the bilateral interrenal tissue and the distance between the bilateral PCV were similar to that in the control embryo and were much lower than that in the *sox3*2 morphant.

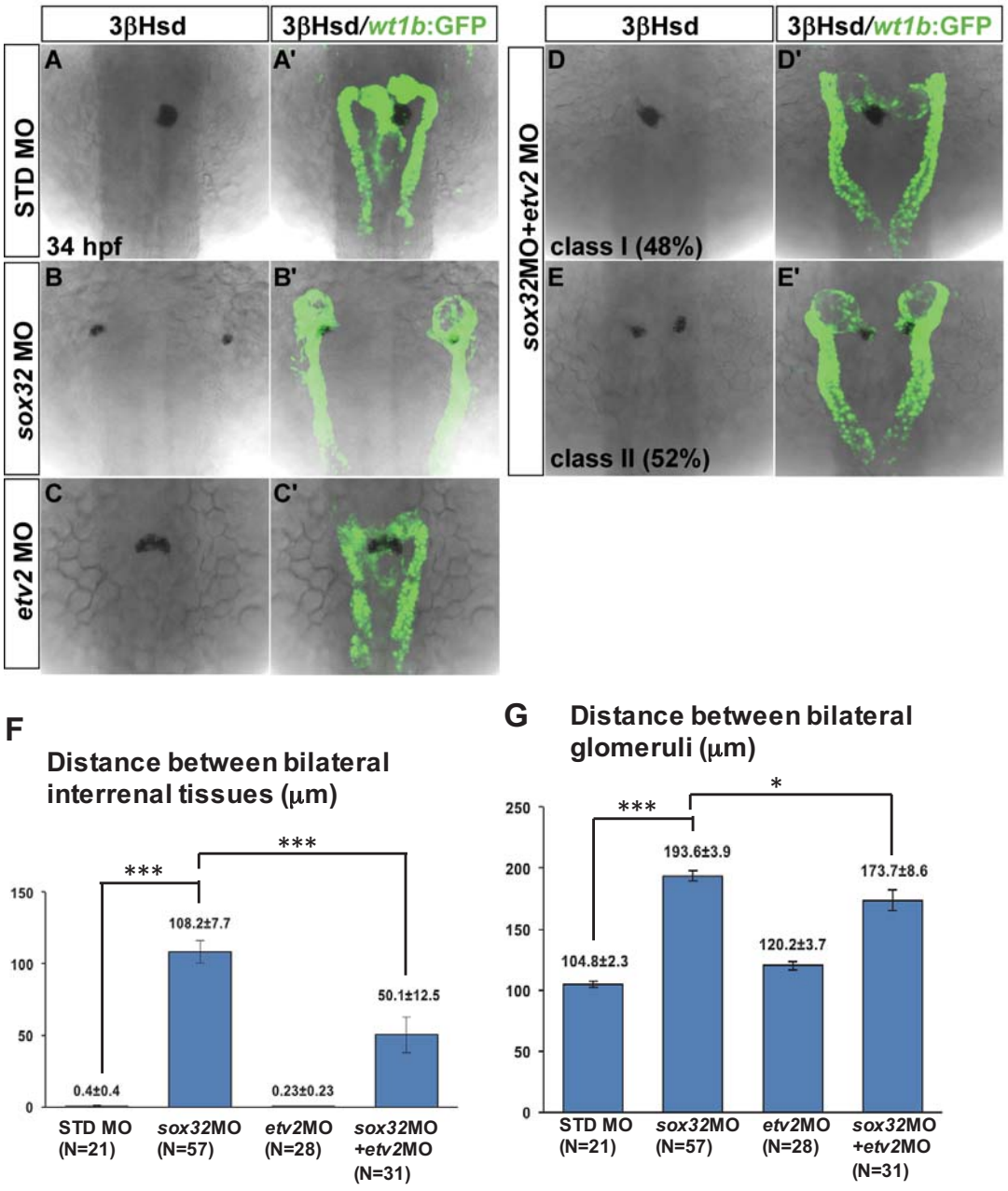

Fig. 10. The severe midline convergence phenotype of the head kidney in the *sox32* morphant was suppressed by a knockdown of *etv2*.

(A-E). Dorsal views of *Tg(wt1b:GFP)*^{li1} embryos at 34 hpf. Distance between the bilateral interrenal tissues and distance between the bilateral pronephric glomeruli were quantified in panel F and G, respectively. (student's t-test, *p<0.05, ***p<0.001)

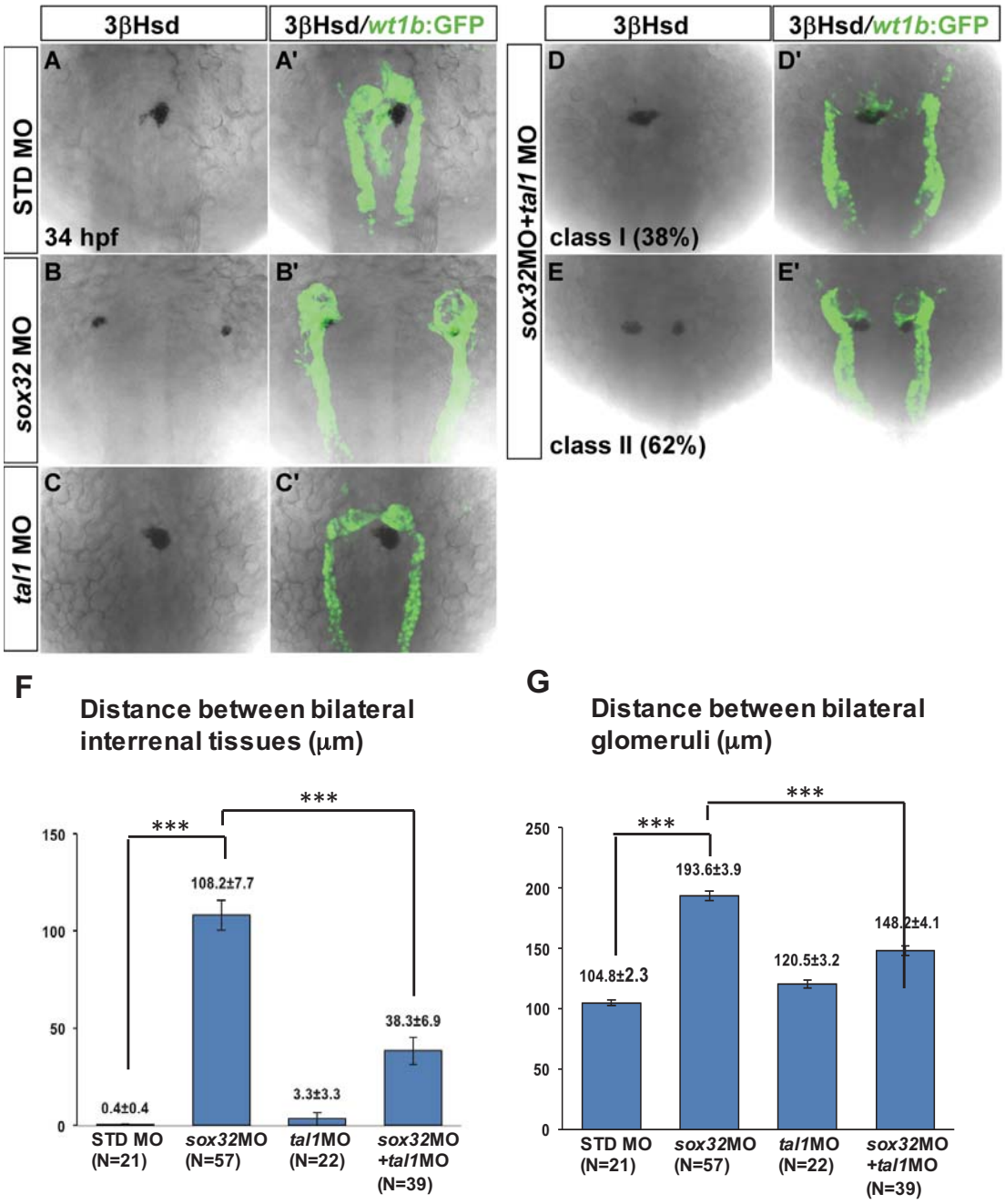

Fig. 11. The severe midline convergence phenotype of the head kidney in the *sox32* morphant was suppressed by a knockdown of *tal1*.

(A-E). Dorsal views of *Tg(wt1b:GFP)*^{li1} embryos at 34 hpf. Distance between the bilateral interrenal tissues and distance between the bilateral pronephric glomeruli were quantified in panel F and G, respectively. (student's t-test, ***p<0.001)

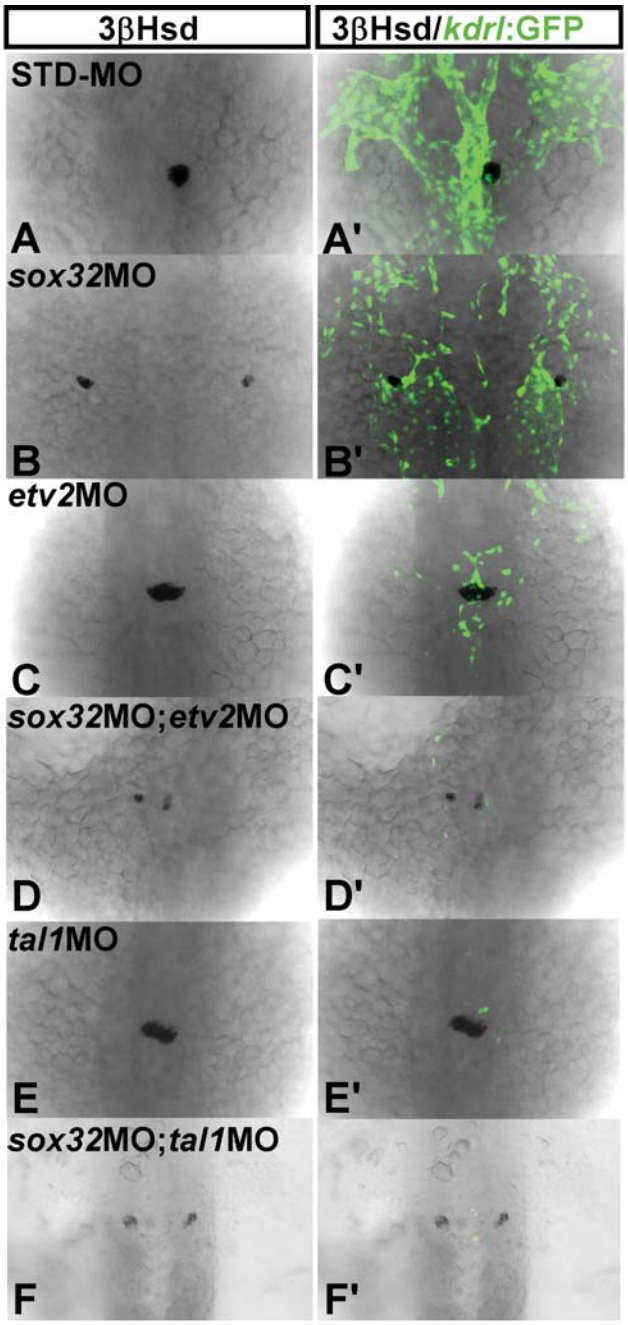

Fig. 12. Effects of *etv2*MO/*sox32*MO and *tal1*MO/*sox32*MO on developments of the EC and the head kidney.

Dorsal views of *Tg(kdrl:GFP)*^{s843} embryos at 34 hpf. The *kdrl*-driven GFP was reduced in the *etv2* morphant (C') and was nearly absent in the *sox32*MO/*etv2*MO double morphant (D'), the *tal1* morphant (E'), and the *sox32*MO/*tal1*MO double morphant (F'). Although the interrenal tissue displayed an unfused phenotype in either the *sox32*/*etv2* double morphant or the *sox32*MO/*tal1*MO double morphant, the distance between the bilateral interrenal tissues was shorter than that in the *sox32* morphant. It suggested that simultaneously disrupted the endothelium could rescue the severe midline convergence phenotype of the steroidogenic interrenal tissue in the endodermless embryo.

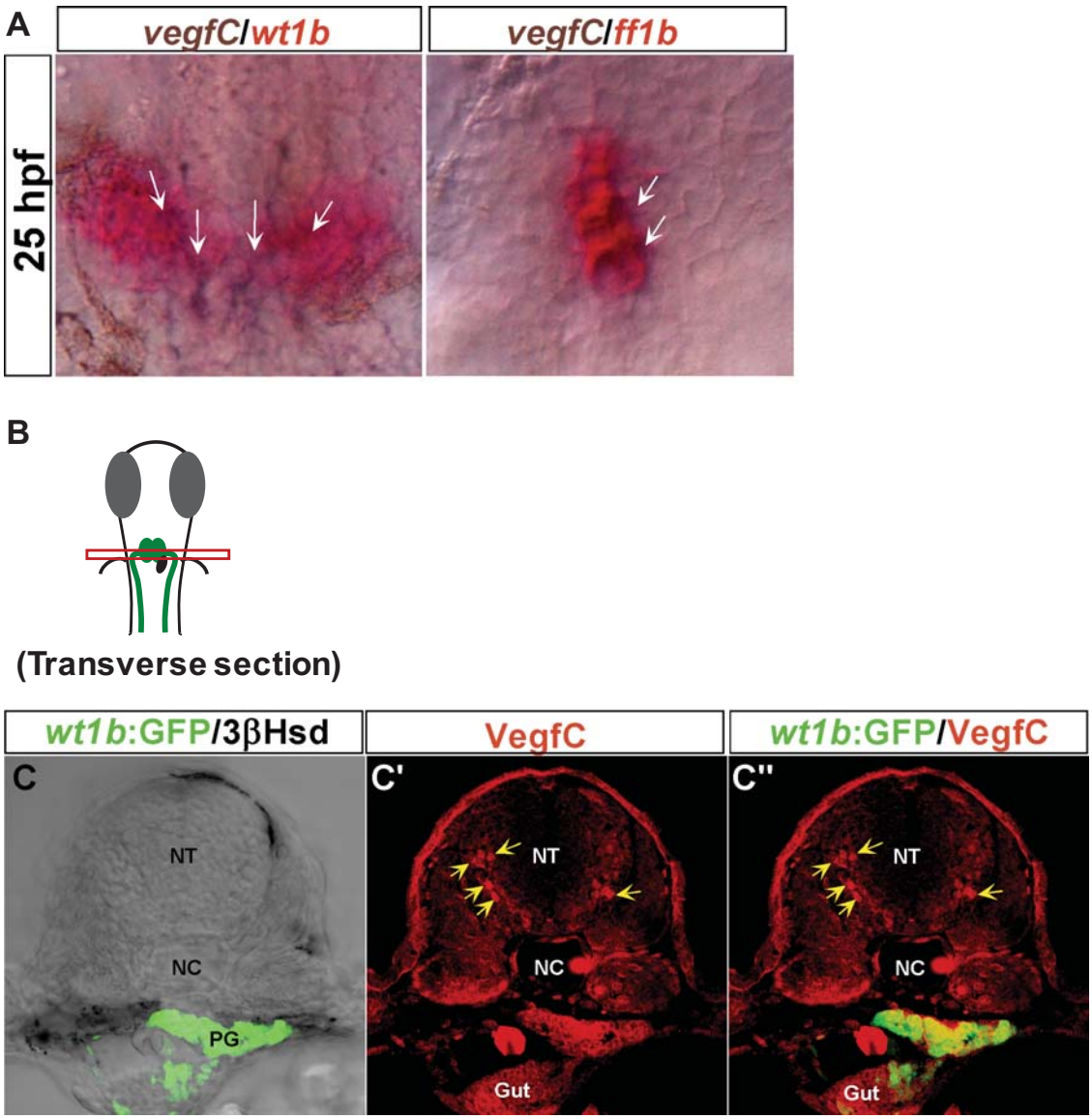

Fig. 13. Expression of VegfC of mRNA and protein levels.

(A). Two color ISH of *vegfC* plus *wt1b* and *vegfC* plus *ff1b* in the wildtype embryo at 25 hpf, ventral flat-mount view. The *vegfC* mRNA expression (indicated by white arrows) was colocalized with either the *wt1b*-expressing pronephros (left panel) or the *ff1*b-expressing interrenal tissue (right panel). (B). Schematic diagram of the section of the pronephric glomerulus. (C). Confocal image of the IHC staining in a wildtype *Tg(wt1b:GFP)*^{li1} embryo at 34 hpf. The VegfC protein could be detected at the pronephric glomerulus, neural cells (indicated by yellow arrows), and gut. (G, gut; PG, pronephric glomerulus; NT, neural tube; NC, notochord; vibratome section, 100 μm)

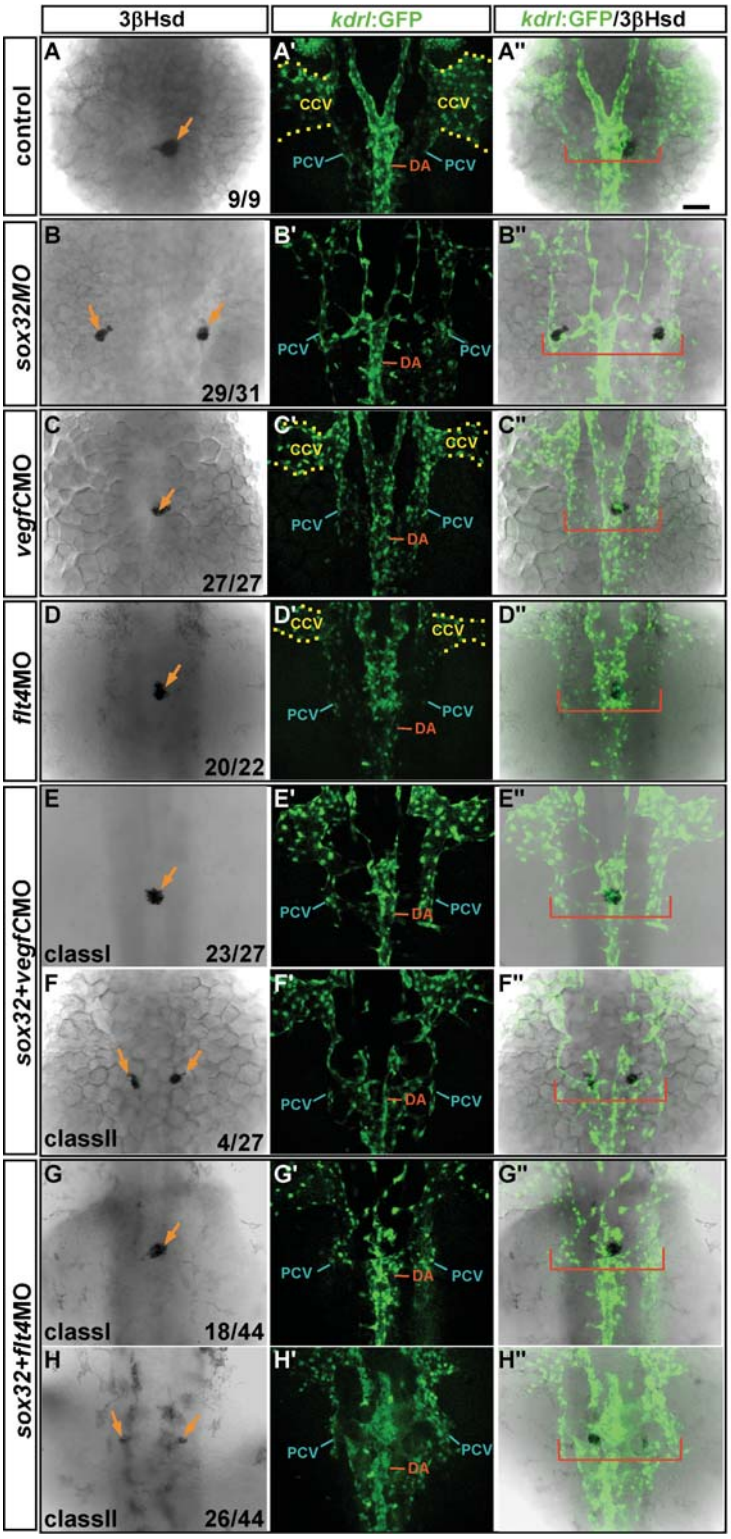

Fig. 14. Severe convergence defect of the interrenal tissue in the endodermless embryo was VegfC/Flt4-dependent.

Dorsal view of *Tg(kdrl:GFP)*^{s843} embryos at 34 hpf. Either the *sox32*MO/*vegfC*MO double morphant or the *sox32*MO/*vegfC*MO double morphant displayed a milder defect in midline convergence of the interrenal tissue than in the *sox32* morphant, suggesting that the VegfC/Flt4 signaling might be required for head kidney-venous EC interaction. (CCV, common cardinal vein)

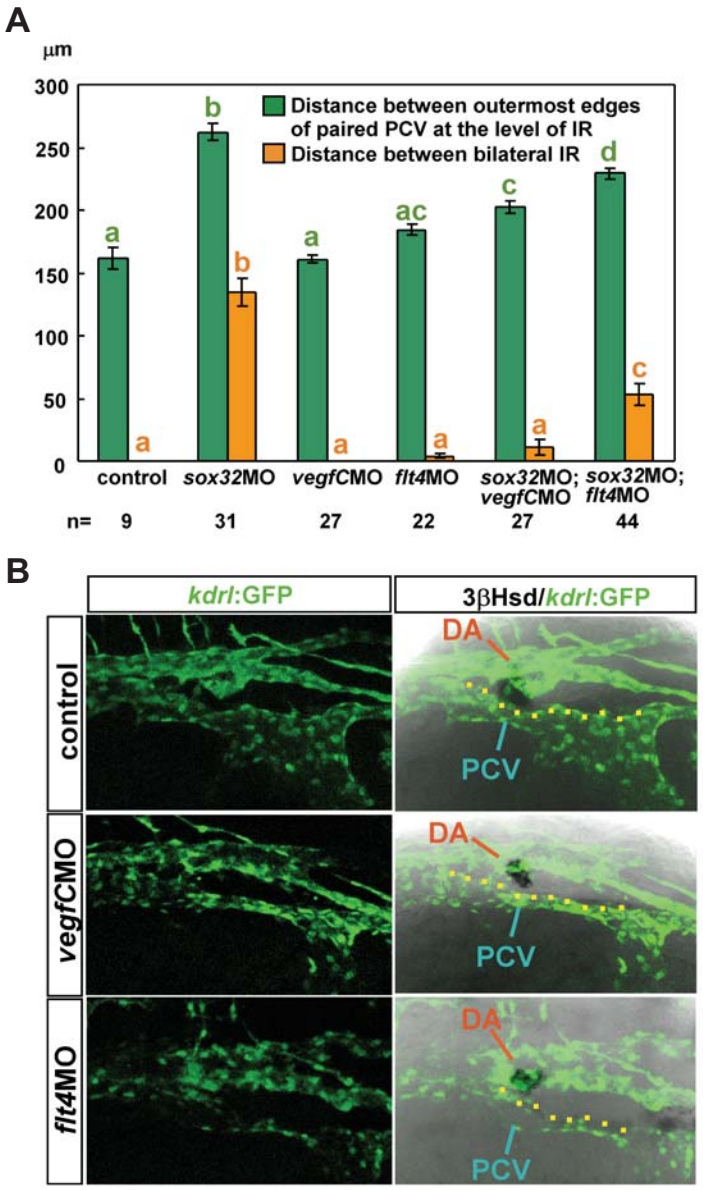

Fig. 15. VegfC/Flt4 signaling is required for head kidney-venous EC interaction.

(A). Distance between the bilateral interrenal tissues and between the bilateral edges of the PCV at the level of the interrenal tissue. (B). Dorsal-lateral view of *Tg(kdrl:GFP)*^{s843} embryos at 34 hpf. In either the *sox32*MO/*vegfC*MO double morphant or the *sox32*MO/*vegfC*MO double morphant, the interrenal tissue was disassociated with the PCV but re-associated with the DA.

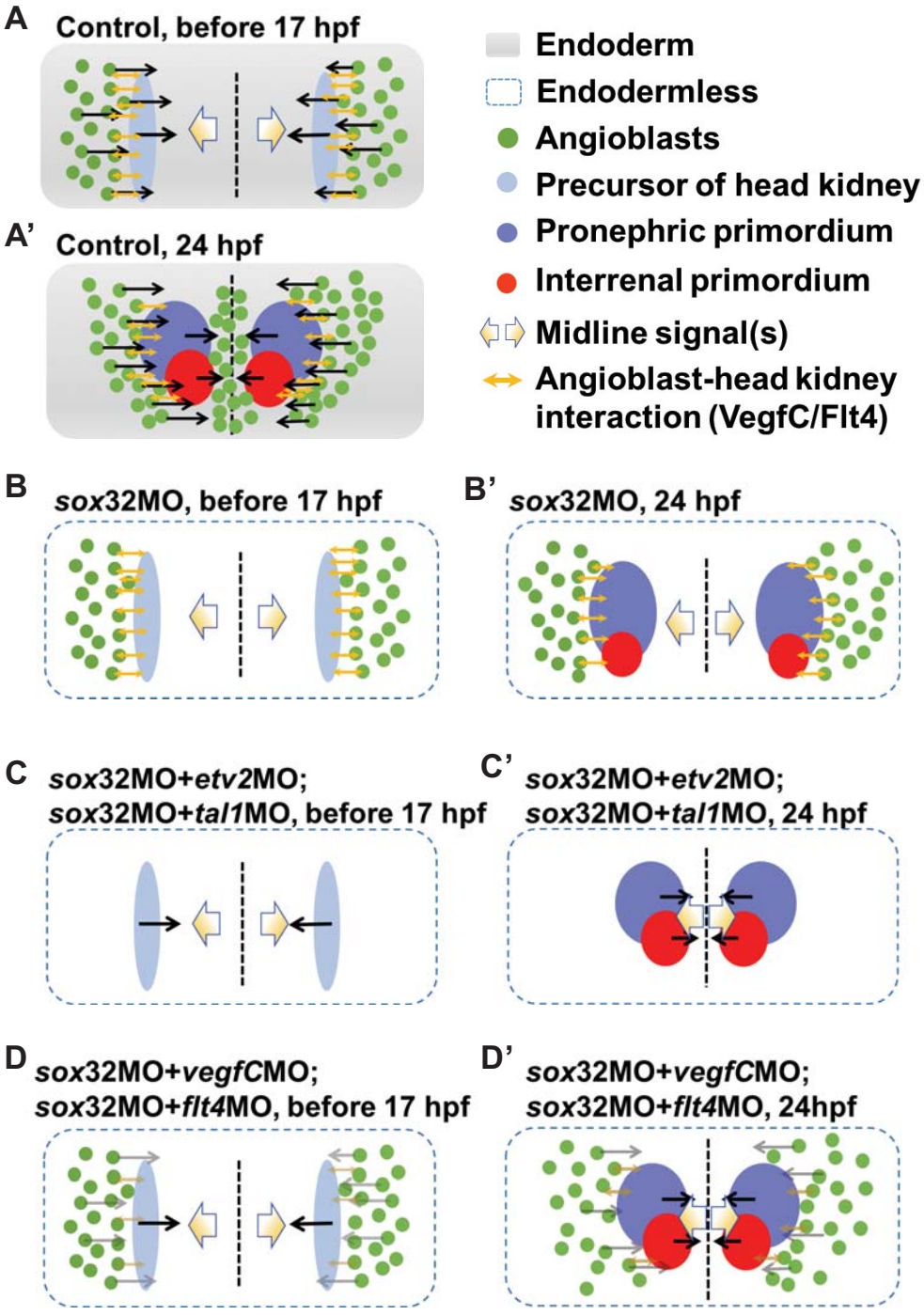

Fig. 16. Summary of the Part 1 study.

(A). The control embryo. The head kidney and the angioblast were attracted by the midline signal and migrated toward the midline. (B). The *sox32* morphant. Midline convergence of the head kidney was severely inhibited due to the defective migration of the venous angioblast. (C,D). The severely defective midline convergence of the head kidney in the *sox32* morphant was rescued by either simultaneous inhibition of the angioblast (C) or breakage the interaction between the angioblast and the head kidney (D).

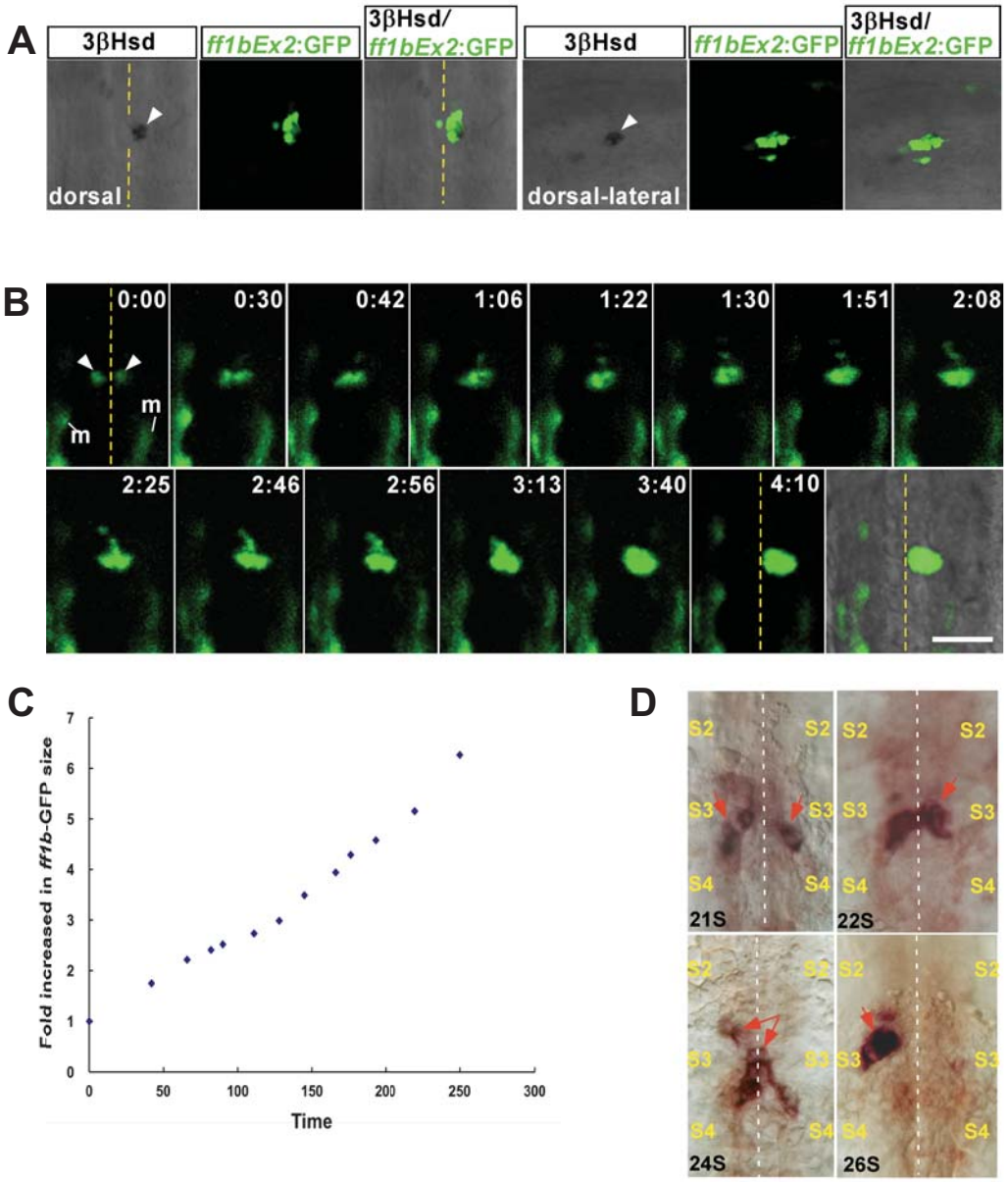

Fig. 17. Midline fusion and lateral relocalization of the interrenal tissue. (A). Confocal images of *Tg(ff1bEx2:GFP)* embryos. The *ff1b*-expressing cell was labeled by GFP and the steroidogenic cell was visualized by 3βHsd enzymatic activity staining. The colocalization of the GFP-expressing cell and the 3βHsd staining cell indicated that the GFP represented both the differentiated and undifferentiated interrenal tissue. (B). Confocal time-lapse images of a live *Tg(ff1bEx2:GFP)* embryo (dorsal view with anterior to the top, time is indicated by hours:minutes). (C). Relative increased size of interrenal fluorescence. (D). ISH of *ff1b* in wildtype embryos at 21-, 22-, 24-, and 26-somite stages (21- 26S; ventral flat mount views). Bilateral interrenal tissues migrated toward the midline and fused at the central midline during 22 to 24 somite stage, and laterally relocated to right of the midline before 26 somite stage. (S2, S3, and S4; the second, third and the forth somite; white arrowhead/red arrow, interrenal tissue; m, muscle cell. Scale bar, 50 μm)

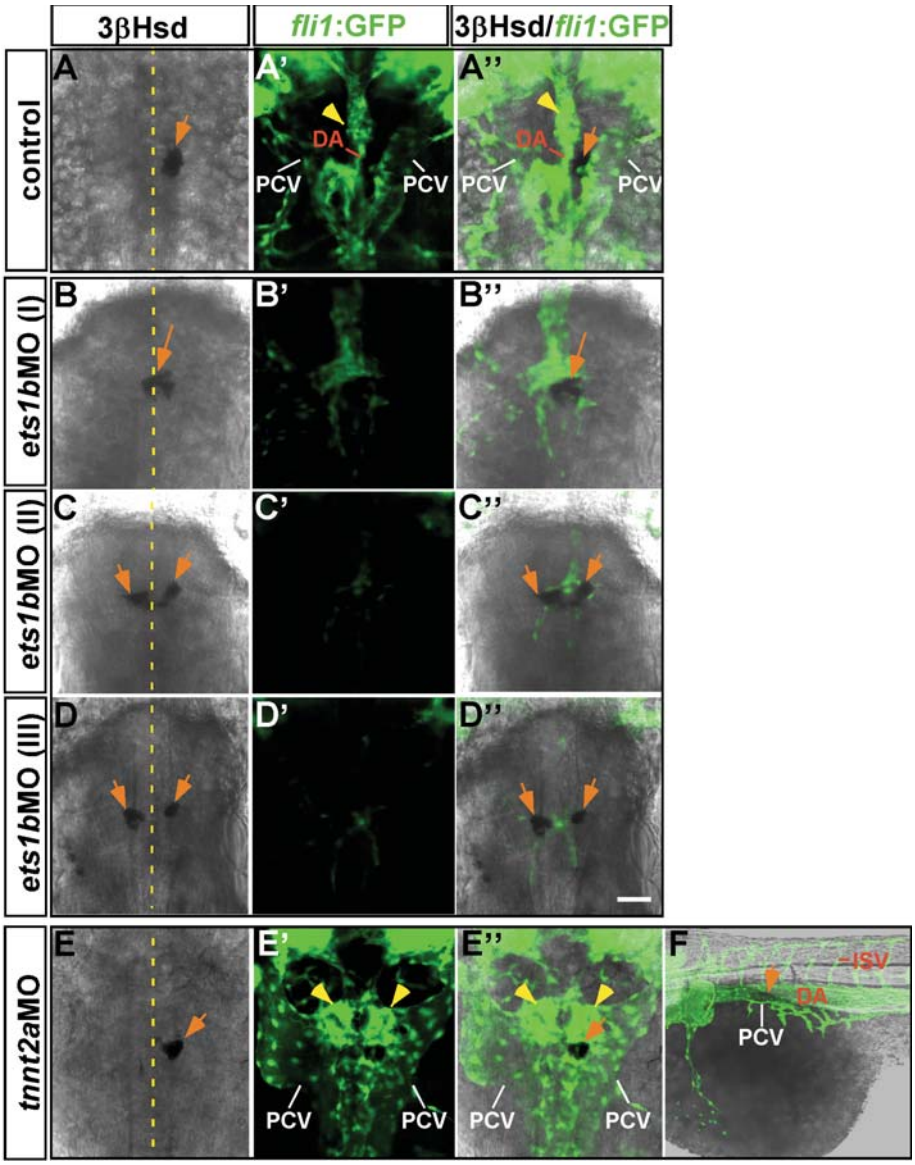

Fig. 18. Phenotypes of the steroidogenic interrenal tissue and the vasculature in the *etv2* morphant and *tnnt2a* morphant at 2 dpf.

Confocal images of *Tg(fli1:EGFP)*^{Y1} embryos injected with STD-MO (A) or *etv2*MO (B-D) or *tnnt2a*MO (E,F), and assayed for 3βHsd enzymatic activity staining. Formation of the axial vessel was severely reduced and central fusion of the interrenal tissue was inhibited in the *etv2* morphant. The phenotypic analysis of interrenal morphogenesis was shown in table 4. Knockdown of *tnnt2a* did not affect interrenal central fusion but inhibited interrenal lateral relocalization (E). Angiogenesis of both the glomerular capillary and the ISV was also unperturbed in the *tnnt2a* morphant. (A-E, Dorsal view with anterior to the top. F, Lateral view. Yellow arrowhead, pronpehric glomerulus; orange arrow, interrenal tissue. Scale bar, 50 μm)

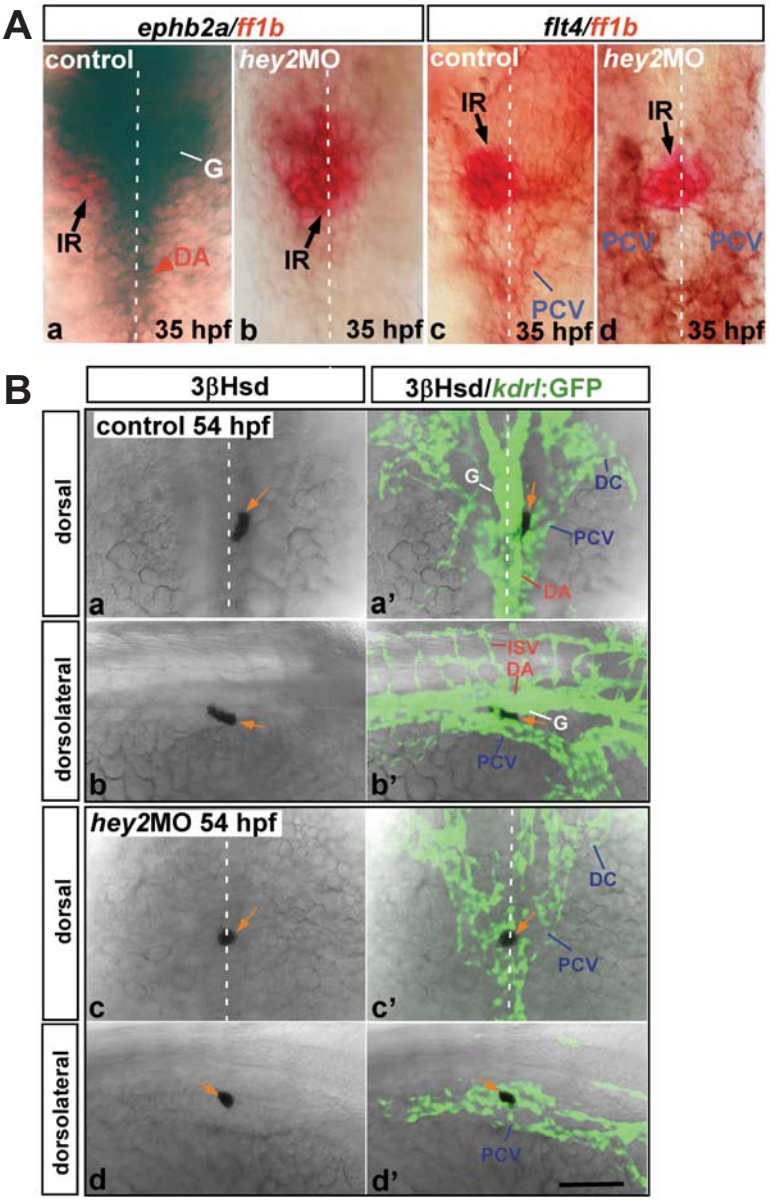

Fig. 19. Phenotypes of the interrenal tissue and the vasculature in the *hey2* morphant.

(A-D). Two-color ISH of either *ff1b* (red) plus *ephb2a* (black) or *ff1b* (red) plus *flt4* (black) in the control embryo (A,C) or in the *hey2* morphant (B,D) at 35 hpf, ventral flat mount views with anterior to the top. Inhibition of *hay2* reduced the expression of arterial marker *ephb2a*, while the expression of venous marker *flt4* seemed not be affected. (E-H). Confocal images of *Tg(kdr:EGFP)*^{s843} embryos uninjected or injected with *hey2*MO, and assayed for GFP and 3βHsd enzymatic activity staining at 54 hpf. In the control embryo, interrenal tissue was associated tightly with the DA and the right branch of the PCV (E,F). In the *hey2* morphant, formation of DA and ISV was inhibited, and the interrenal tissue was arrested at central midline (G,H). (G, glomerulus; DA, dorsal aorta; ISV, intersegmental vessel; PCV, posterior cardinal vein; DC, duct of Cuvier. Scale bar, 50 μm)

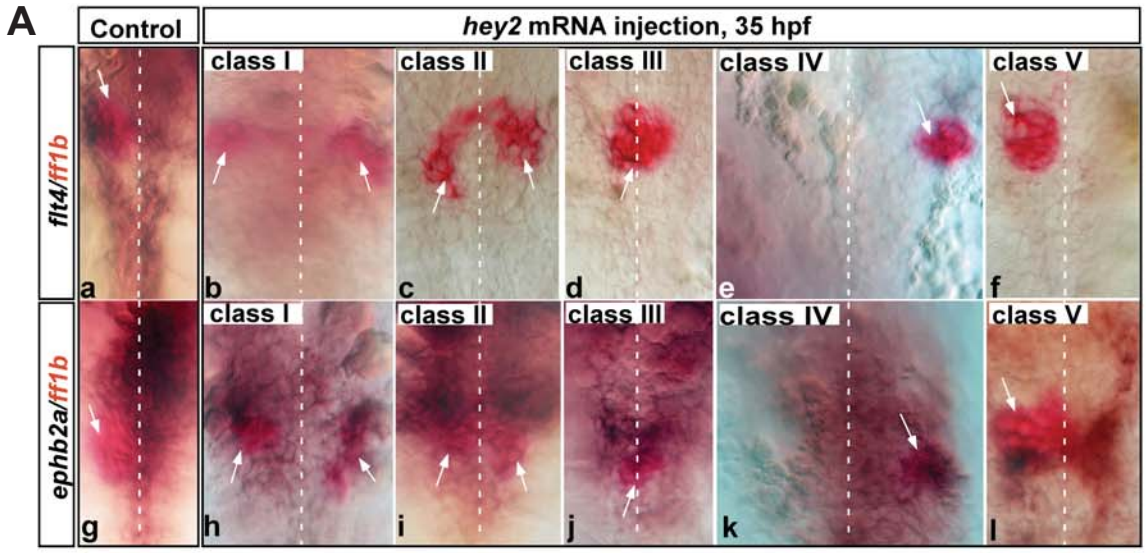
A
Control
hey2 mRNA injection, 35 hpf
flt4/flf1b
ephb2a/flf1b
class I
class II
class III
class IV
class V
a
b
c
d
e
f
g
h
i
j
k
l

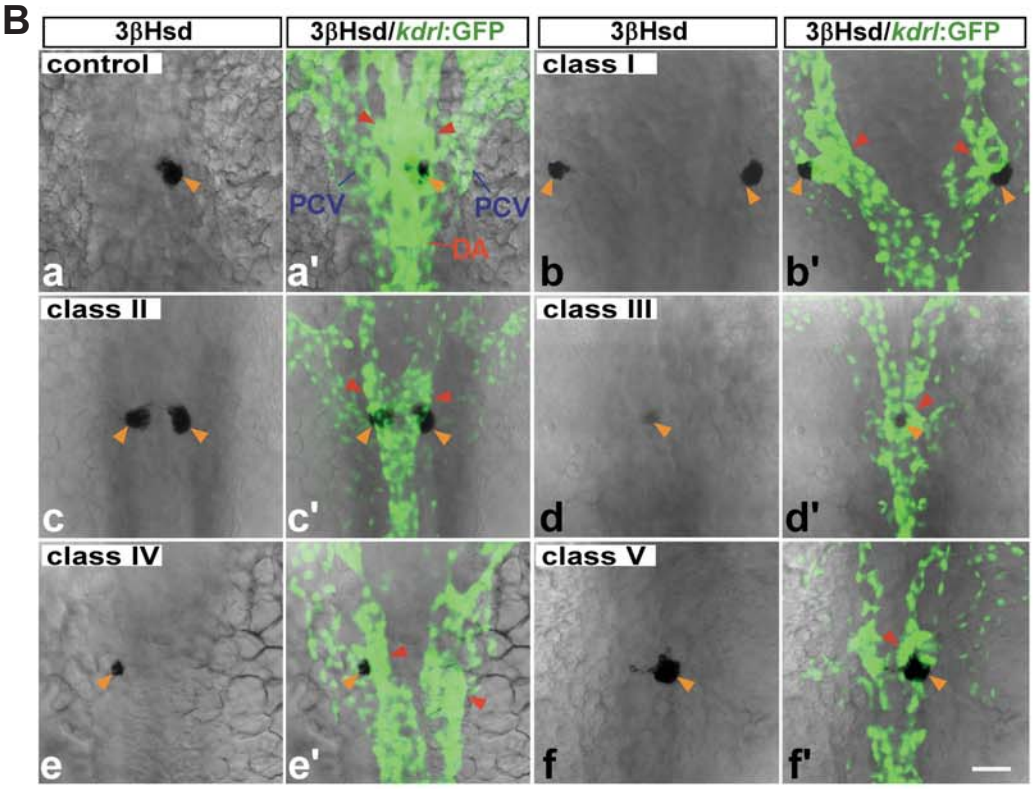
B
3βHsd
3βHsd/kdrl:GFP
control
class I
class II
class III
class IV
class V
PCV
PCV
DA
a
a'
b
b'
c
c'
d
d'
e
e'
f
f'

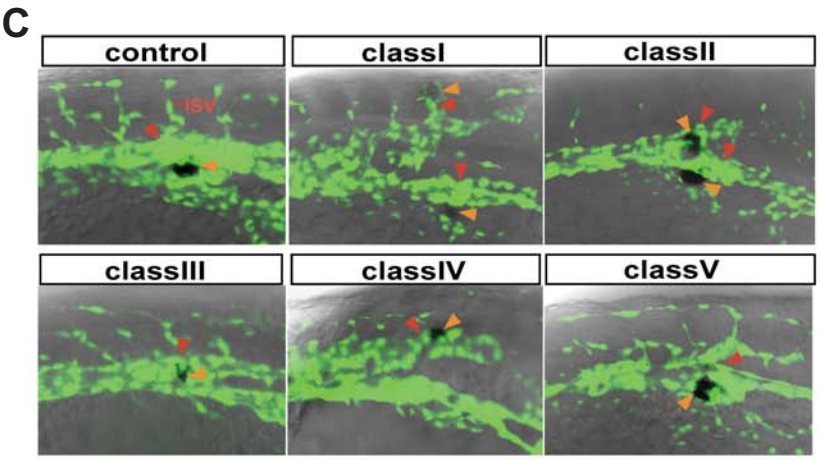
C
control
classI
classII
classIII
classIV
classV
ISV

Fig. 20. Effects of *hey2* mRNA injection on axial vessel formation and interrenal migration.

(A). Two-color ISH of either *ff1b* (red) plus *flt4* (black) or *ff1b* (red) plus *ephb2a* (black) in the control embryo (a, g) or in the *hey2*-overexpressed embryo (b-f, h-i) at 35 hpf. Overexpression of *hay2* reduced the expression of venous marker *flt4* and affected the expression of arterial marker *ephb2a*. (Ventral flat mount views with anterior to the top) (B,C). Confocal images of *Tg(kdr:EGFP)*^{s843} embryos uninjected (a) or injected with *hey2* mRNA (b-f), and assayed for GFP and 3βHsd activity staining at 34 hpf with dorsal views (B) or lateral views (C). In the *hey2*-overexpressed embryo, formation of the vein and the ISV was reduced and morphology of the DA was also abnormal. Migration phenotype of the interrenal tissue in the *hey2*-overexpressed embryo could be divided into five classes (Class I-V), and the phenotypic analysis was shown in table 5. (Scale bar, 50 μm)

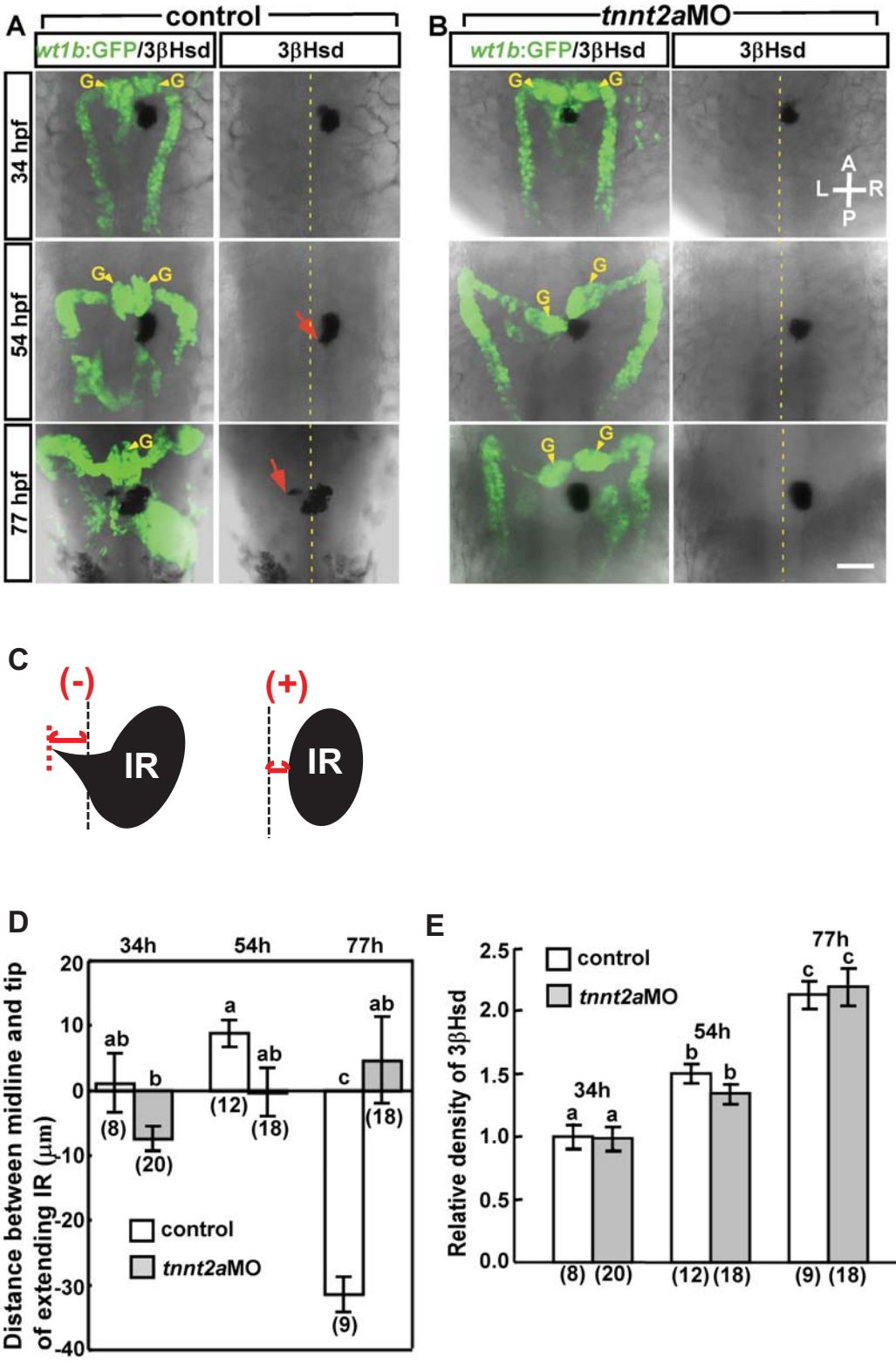
A
control
wt1b:GFP/3βHsd
3βHsd
34 hpf
54 hpf
77 hpf
G
B
tnnt2aMO
wt1b:GFP/3βHsd
3βHsd
A
L
R
P
C
(-)
IR
(+)
IR
D
34h
54h
77h
Distance between midline and tip of extending IR (μm)
20
10
0
-10
-20
-30
-40
ab
b
a
ab
c
ab
(8)
(20)
(12)
(18)
(9)
(18)
control
tnnt2aMO
E
Relative density of 3βHsd
2.5
2.0
1.5
1.0
0.5
0.0
control
tnnt2aMO
34h
54h
77h
a
a
b
b
c
c
(8) (20)
(12) (18)
(9) (18)

Fig. 21. Effects of the blood flow on interrenal and pronephric development.

(A,B). Confocal images of the *Tg(wt1b:GFP)*^{li1} uninjected (A) or injected with *tnnt2a*MO (B), and assayed for 3βHsd enzymatic activity staining at 34, 54, and 77 hpf. Morphogenetic movements of the pronephros and the interrenal tissue were defective in the absence of blood flow. In the control embryo, steroidogenic interrenal tissue formed a protruding extension (red arrow) across the midline by 54 hpf, while the pronephric glomerulus (G, yellow arrowheads) assembled at the midline by 77 hpf. Medial extension of the interrenal tissue and midline assembly of the pronephros were disrupted in the flowless *tnnt2a* morphant. (C). Schematic diagram displayed the measurement of the interrenal tissue medial extension. The negative value meant that the interrenal tissue across to the midline, and the positive value meant that the interrenal tissue did not reach to the midline. (D). Statistics of the distance between the tip of the interrenal tissue and the midline. In the control embryo, the value of the distance was negative at 77 hpf and was different to that at either 34 or 54 hpf, suggesting that the interrenal tissue extended across to the midline. However, in the *tnnt2a* morphant, the value of the distance did not show a significant difference among the different stages. It suggested that the inhibition of the blood flow inhibited medial extension of the interrenal tissue. (E). Statistics of the 3βHsd staining in the control embryo and the *tnnt2a* morphant at 34, 54, and 77 hpf. The relative density of 3βHsd was increased in the later stage, and there was no significant difference between the control embryo and the *tnnt2a* morphant when they at the same stage. (ANOVA and Duncan's multiple test, $P<0.05$; the different letters above the histograms meant the significant difference among each other)

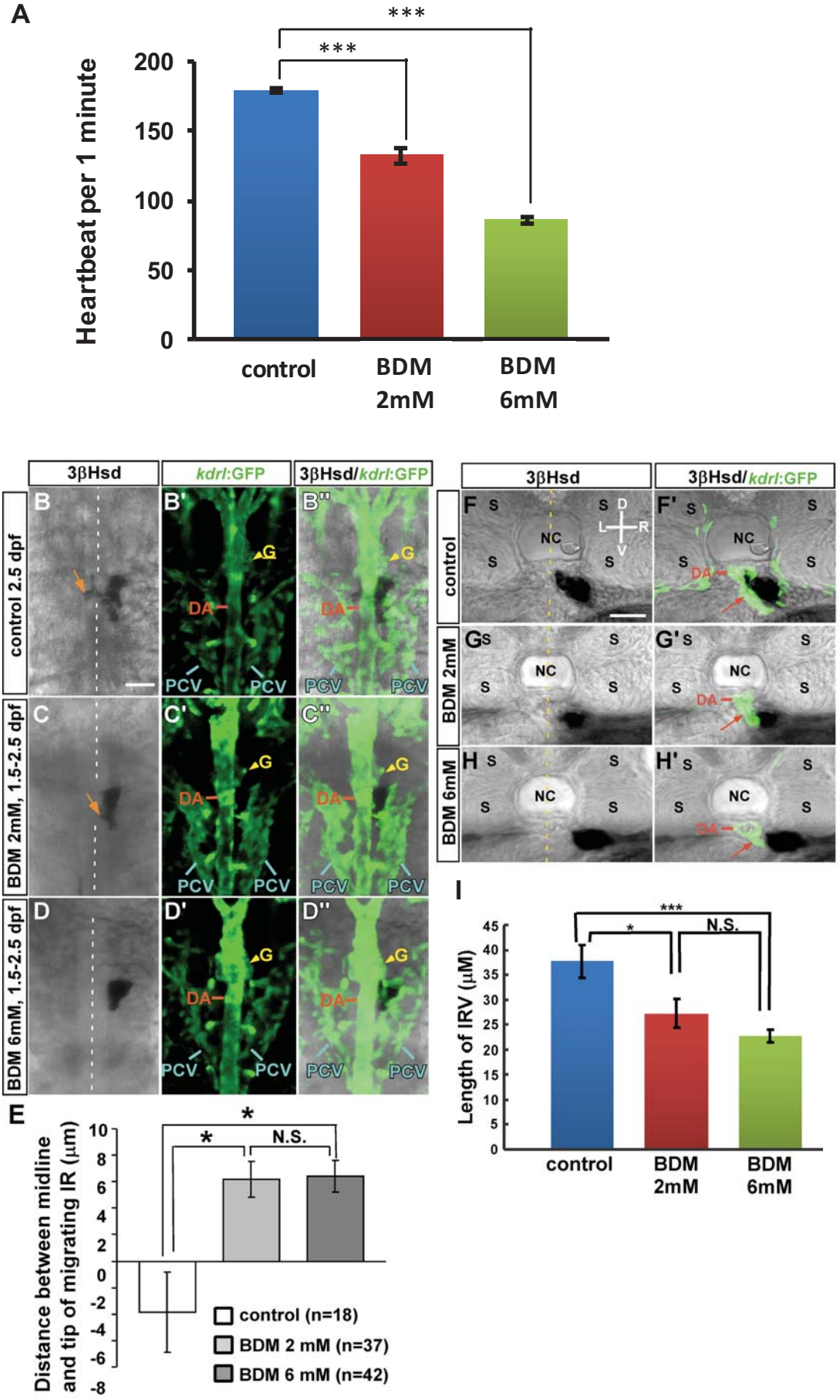
A
***
***
Heartbeat per 1 minute
200
150
100
50
0
control
BDM 2mM
BDM 6mM
3βHsd
kdrl:GFP
3βHsd/kdrl:GFP
control 2.5 dpf
BDM 2mM, 1.5-2.5 dpf
BDM 6mM, 1.5-2.5 dpf
B
B'
B''
C
C'
C''
D
D'
D''
G
DA
PCV
F
F'
G
G'
H
H'
NC
S
D
L
R
V
E
Distance between midline and tip of migrating IR (μm)
10
8
6
4
2
0
-2
-4
-6
-8
*
*
N.S.
control (n=18)
BDM 2 mM (n=37)
BDM 6 mM (n=42)
I
Length of IRV (μM)
45
40
35
30
25
20
15
10
5
0
***
*
N.S.
control
BDM 2mM
BDM 6mM

Fig. 22. Inhibition of the blood flow represses interrenal medial extension and IRV growth.

Tg(kdrl:GFP)^{s843} embryos were treated with 2,3-BDM from 1.5 dpf onwards to 2.5 dpf. (A). Heartbeat counting after 2,3-BDM treatment (1.5 dpf). Heartbeat of the 2,3-BDM-treated embryo was significantly reduced compared to the control embryo. (B-D). Dorsal views, the medial extension of the steroidogenic interrenal tissue (orange arrow) was inhibited by 2,3-BDM treatment, but the morphology of the axial vessels was unperturbed. (F-H). Transverse sections, angiogenesis of the IRV (red arrow) was reduced in 2,3-BDM-treated embryos. Medial extension of the interrenal tissue and length of the IRV were quantified in panel E and I, respectively. (student's t-test, *$p<0.05$, ***$p<0.001$, N.S, not significant; G, pronephric glomerulus; IR, interrenal tissue; NC, notochord; S, somite; vibratome section, 100 μm; scale bar, 50 μm.)

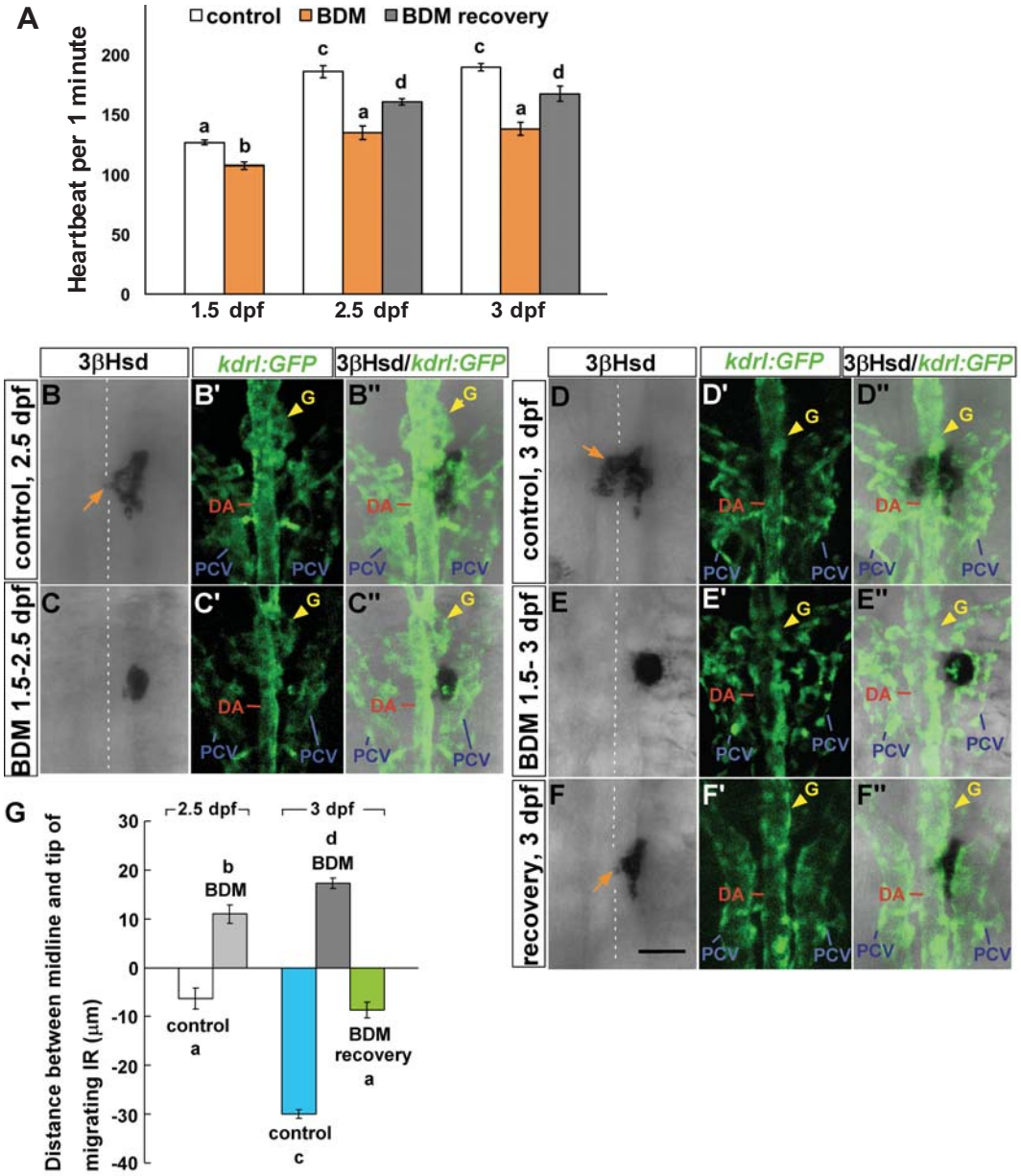

Fig. 23. Recovery of the blood flow rescued the defective medial extension of the interrenal tissue.

(A-E). Dorsal views of the *Tg(kdrl:GFP)*^{s843} embryos treated by 6 mM 2,3-BDM form 1.5 dpf to 2.5 dpf (B), or from 1.5 dpf to 3 dpf (D), or form 1.5 dpf, recovery at 2.5 dpf, and fixed at 3 hpf (E). (F). Heartbeat counting after 2,3-BDM treatment (1.5 dpf), or after 2,3-BDM washout (2.5 dpf), or before fixation (3 dpf). Compared to the control embryo, heartbeat of the 2,3-BDM-treated embryo was significantly reduced. In addition, the heartbeat was immediately recovered after washout of the 2,3-BDM. (G). Statistics of interrenal tissue medial extension. Inhibition of the blood flow by 2,3-BDM inhibited the medial extension of the interrenal tissue, and that could be rescued by washing out of the 2,3-BDM at 2.5 dpf. (ANOVA and Duncan's multiple test, $P<0.05$; the different letters above the histograms meant the significant difference among each other; scale bar, 50 μm)

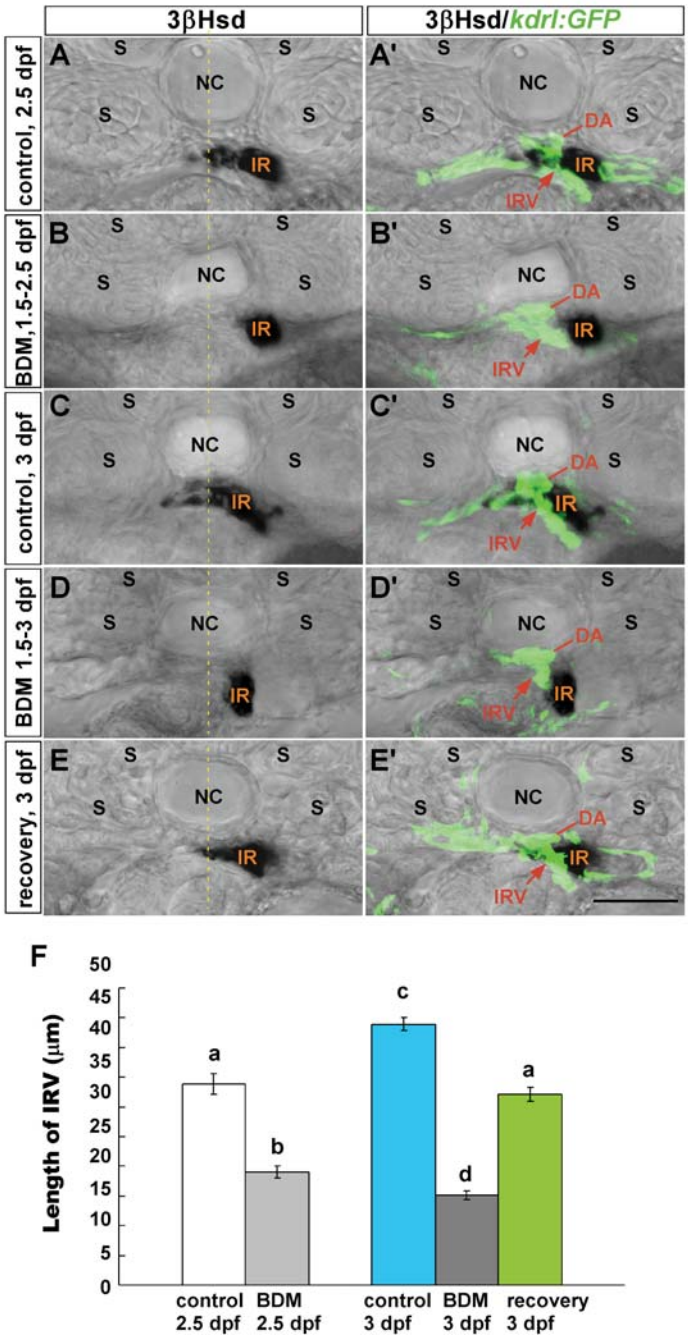

Fig. 24. Recovery of the blood flow rescued the growth of the IRV.

(A-E). Transverse section of the *Tg(kdrl:GFP)*^{s843} embryos treated by 6 mM of 2,3-BDM form 1.5 dpf to 2.5 dpf (B), or from 1.5 dpf to 3 dpf (D), or form 1.5 dpf, recovery at 2.5 dpf, and fixed at 3 hpf (E). (F). Statistics of the IRV length. Inhibition of the blood flow by 2,3-BDM inhibited the angiogenesis of the IRV, and that could be rescued by washing out of the 2,3-BDM at 2.5 dpf. (ANOVA and Duncan's multiple test, $P<0.05$; the different letters above the histograms meant the significant difference among each other; NC, notochord; IR, interrenal tissue; S, somite, vibratome section, 100 μm; scale bar, 50μm)

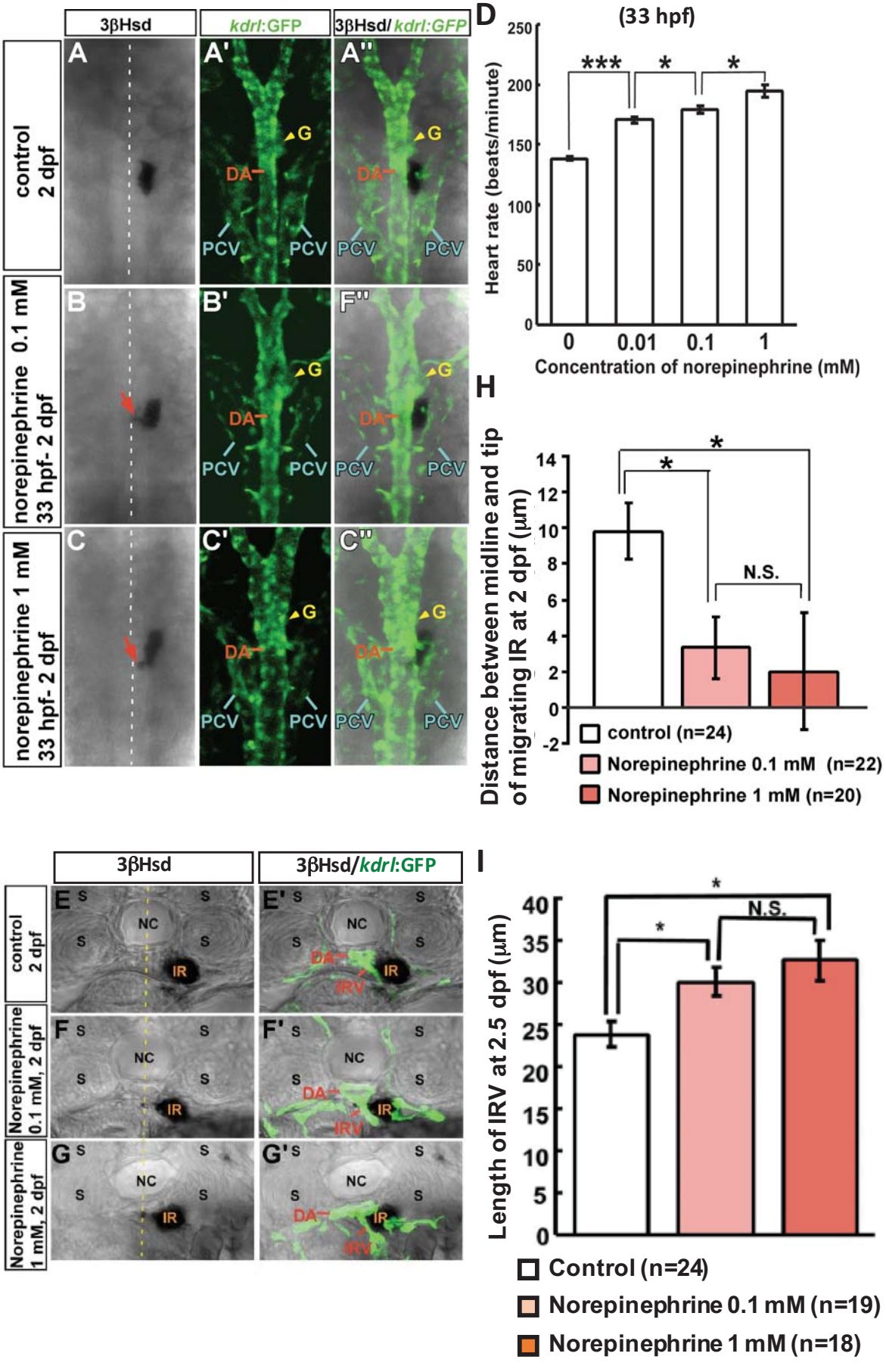
3βHsd
kdrl:GFP
3βHsd/ kdrl:GFP
control 2 dpf
norepinephrine 0.1 mM 33 hpf- 2 dpf
norepinephrine 1 mM 33 hpf- 2 dpf
A
A'
A''
B
B'
F''
C
C'
C''
G
DA
PCV
D
(33 hpf)
Heart rate (beats/minute)
Concentration of norepinephrine (mM)
***
*
H
Distance between midline and tip of migrating IR at 2 dpf (μm)
N.S.
control (n=24)
Norepinephrine 0.1 mM (n=22)
Norepinephrine 1 mM (n=20)
3βHsd
3βHsd/kdrl:GFP
E
E'
F
F'
G
G'
NC
IR
IRV
I
Length of IRV at 2.5 dpf (μm)
Control (n=24)
Norepinephrine 0.1 mM (n=19)
Norepinephrine 1 mM (n=18)

Fig. 25. Effects of norepinephrine on interrenal medial extension and IRV growth.

Tg(kdrl:GFP)^{s843} embryos were treated with norepinephrine from 33 hpf to 2 dpf. (A-C). Dorsal views, acceleration of the blood flow promoted interrenal tissue medial extension, there was a protrusion (red arrow) of the interrenal tissue in the norepinephrine-treated embryo at 2 dpf. (D). Heartbeat counting after norepinephrine treatment (at 33 hpf). The heart rate was increased and displayed a dose-dependent effect in norepinephrine-treated embryos. (E-G). Transverse sections, the length of IRV was elongated in the norepinephrine-treated embryo. Medial extension of the interrenal tissue and length of the IRV were quantified in panel D and H, respectively. (student's t-test, *$p<0.05$, N.S, not significant; NC, notochord; IR, interrenal tissue; S, somite; vibratome section, 100 μm)

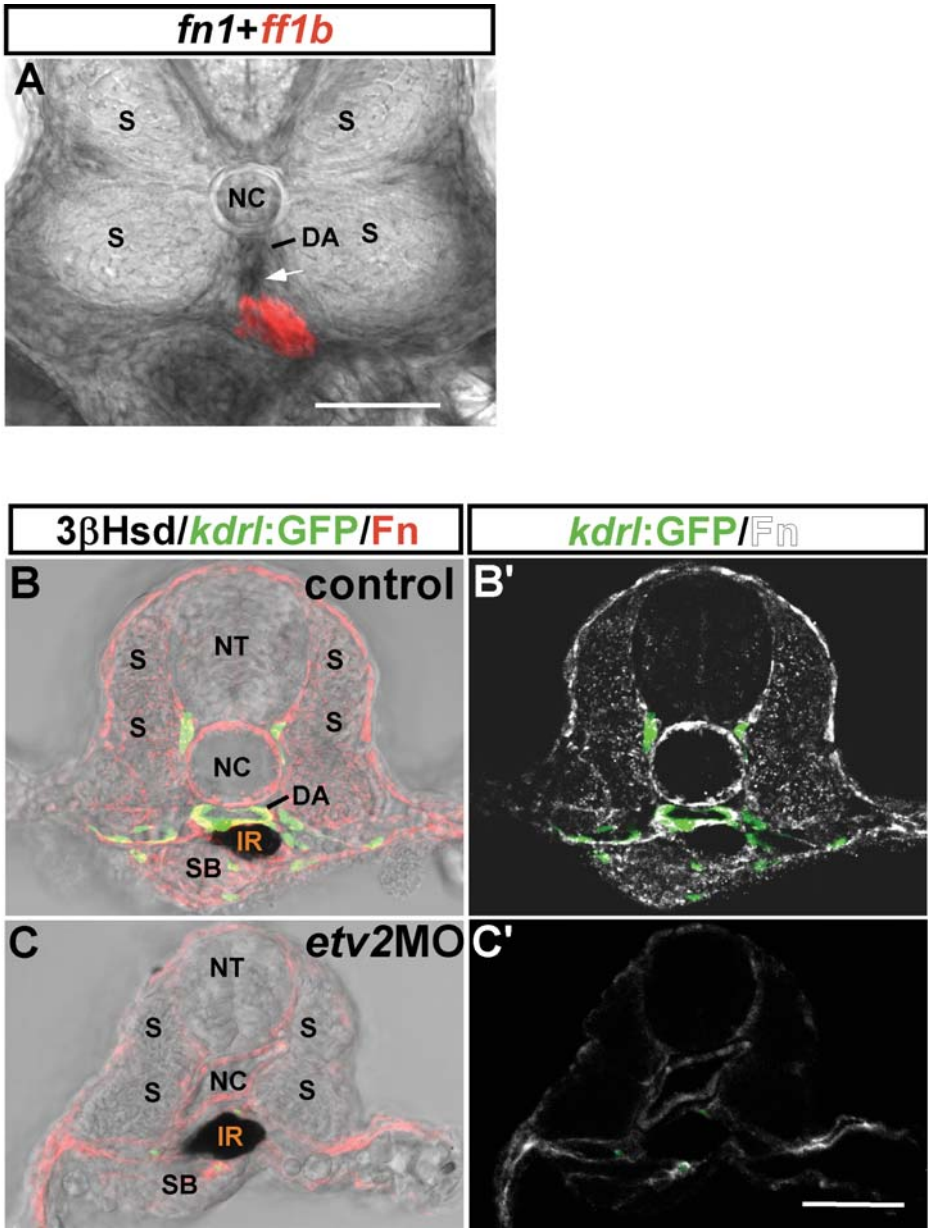

Fig. 26. Fn deposition at peri-interrenal region was contributed by the EC.

(A). Two color ISH of the *fn1*(black) and *ff1b* (red) at 2 dpf. The *fn1* was expressed around the the DA, and enriched in the ventral region of the DA (indicated by the white arrowhead). (B,C). *Tg(kdrl:GFP)*^{s843} embryos uninjected (B) or injected with *etv2*MO (C), assayed for 3βHsd enzymatic activity staining, and IHC of Fn in the transverse section at 34 hpf. Accumulation of the Fn in the DA and the peri-interrenal region was reduced in the *etv2* morphant. (NC, notochord; NT, neural tube; IR, interrenal tissue; SB, swim bladder; S, somite; vibratome section, 100 μm; scale bar, 50 μm.)

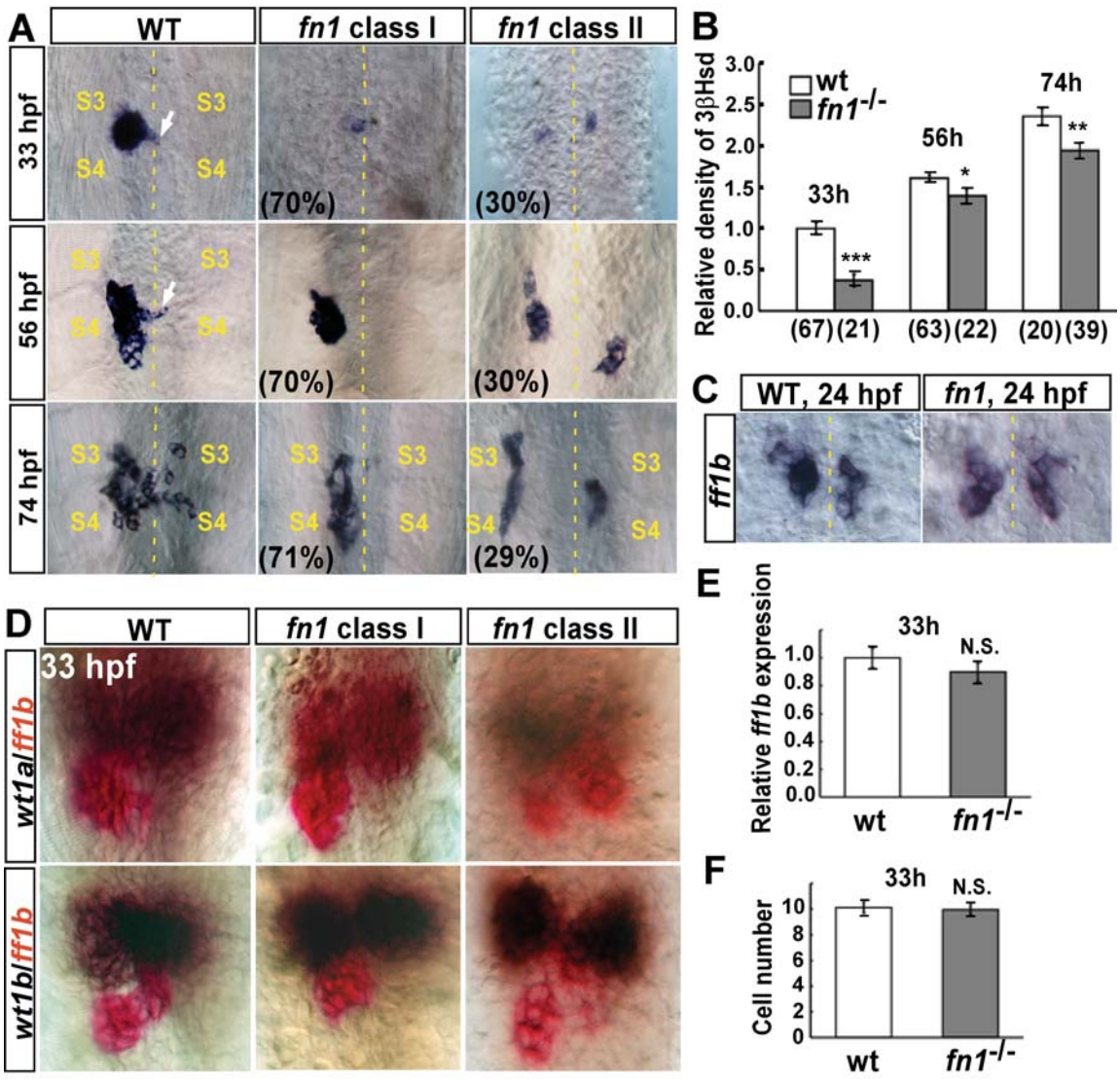

Fig. 27. Phenotypes of interrenal development in the *fn1* mutant.

(A). Ventral flat mount views with anterior to the top of the *fn1* mutant and its wildtype sibling. The interrenal tissue developed a protruding (white arrow) in the control embryo, but not in the *fn1* mutant. In *fn1* class (I) mutant, medial extension of the interrenal tissue was inhibited; the fused interrenal tissue failed to extend across the midline. In *fn1* class (II) mutant, midline convergence of the interrenal tissue was inhibited; the bilateral interrenal tissues could not fuse even at 74 hpf. The relative density of the 3βHsd was quantified in panel B. (C). ISH of *ff1b* in the *fn1* mutant and its wildtype sibling at 24 hpf, ventral flat-mount view. (D). Two color ISH of the *wt1a* (black) and *ff1b* (red) at 33hpf, ventral flat-mount view. The relative expression of *ff1b* and the number of *ff1b*-experssing cell were illustrated in panel E and F, respectively. Loss of *fn1* reduced interrenal differentiation, but not affect its specification. (student's t-test, ***$p<0.001$, *$p<0.05$, N.S, not significant; S3 and S4, the third and fourth somite)

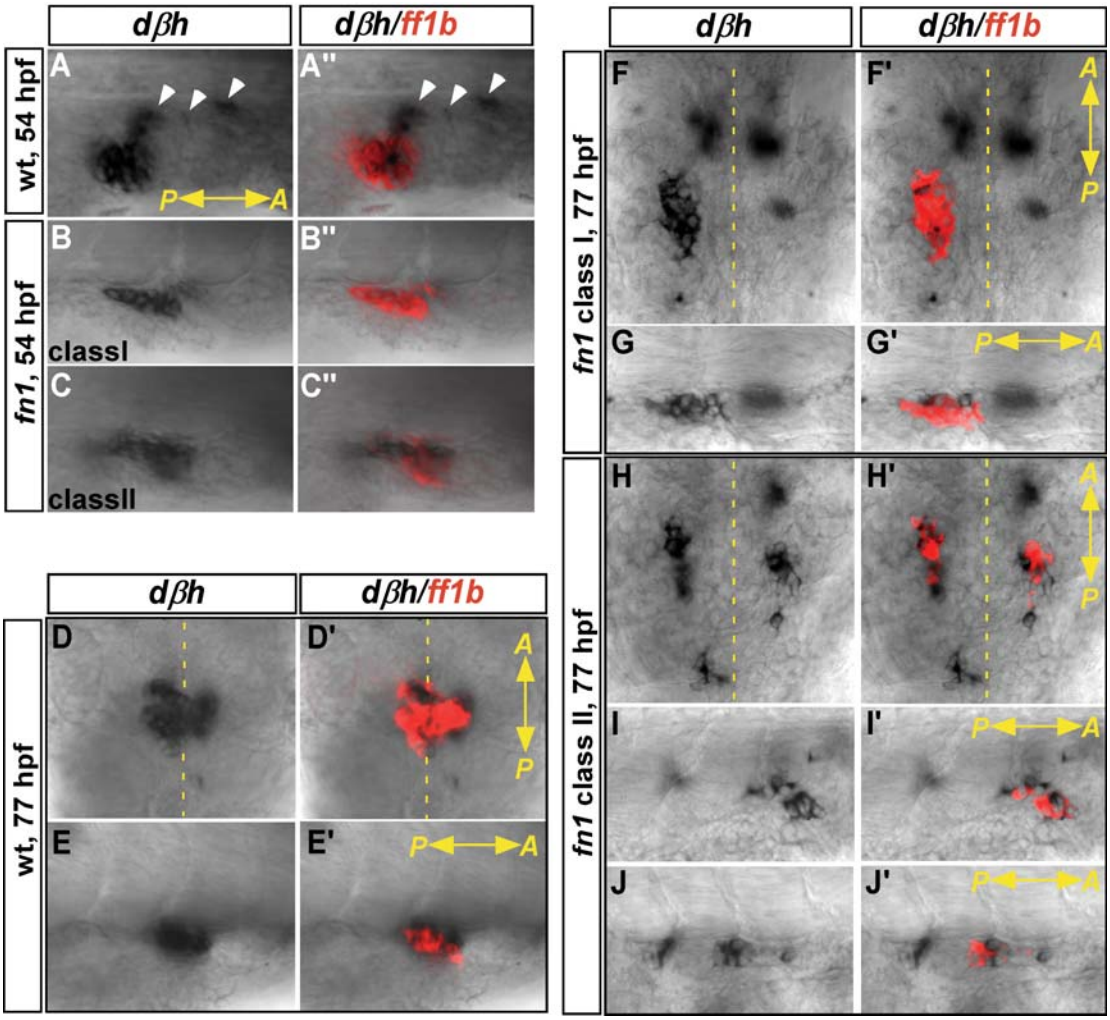

Fig. 28. Loss of *fn1* disrupted functional assembly of interrenal gland.

Two-color ISH of *dβh* (black) and *ff1b* (red) in the *fn1* mutant and its wildtype sibling at 54 (A-C) and 77 hpf (D-J), ventral flat mount views. (A-C). At 54 hpf, the *dβh*-expressing chromaffin cell migrated into the *ff1b*-expressing interrenal tissue in the wildtype sibling, but the migration of chromaffin cell was inhibited in the *fn1* mutant. (D,E). The interrenal tissue was intermingled with the chromaffin cell in the wildtype sibling at 77 hpf. (F-J). The defective morphogenetic movements of both interrenal tissue and chromaffin cells resulted in an incomplete assembly of the interrenal organ in the *fn1* mutant at 77 hpf.

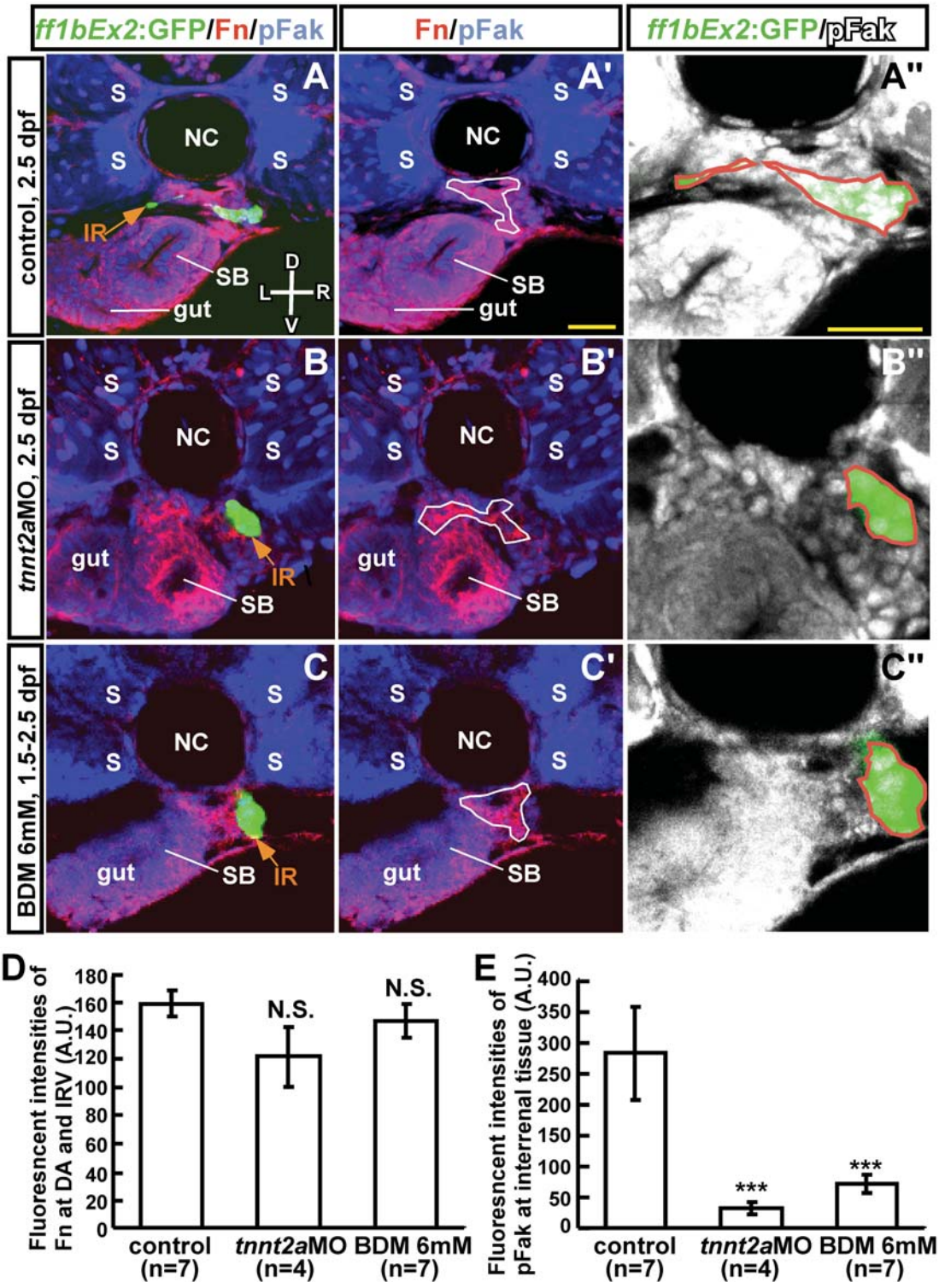
ff1bEx2:GFP/Fn/pFak
Fn/pFak
ff1bEx2:GFP/pFak
control, 2.5 dpf
tnnt2aMO, 2.5 dpf
BDM 6mM, 1.5-2.5 dpf
A
A'
A''
B
B'
B''
C
C'
C''
NC
S
IR
SB
gut
D
L
R
V
D
Fluoresncent intensities of Fn at DA and IRV (A.U.)
180
160
140
120
100
80
60
40
20
0
N.S.
N.S.
control (n=7)
tnnt2aMO (n=4)
BDM 6mM (n=7)
E
Fluoresncent intensities of pFak at interrenal tissue (A.U.)
400
350
300
250
200
150
100
50
0
***
***
control (n=7)
tnnt2aMO (n=4)
BDM 6mM (n=7)

Fig. 29. Inhibition of the blood flow affected Fn deposition and pFak expression at the interrenal tissue.

(A-C). *Tg(ff1bEx2:GFP)* embryos uninjected (A) or injected (B) with *tnnt2a*MO, or treated with 2,3-BDM from 1.5 dpf to 2.5 dpf (C), were analyzed for 3βHsd enzymatic activity assay, vibratome sections, and IHC of Fn. The Fn was accumulated at DA and IRV, and the pFAK was expressed in the interrenal tissue at control embryos (A). In blood flow-deficient embryos (B,C), the pattern of Fn deposition in the interrenal microenvironment was abnormal, and the activation of FAK in the interrenal tissue was inhibited. The fluorescent intensities of Fn at DA and IRV (ROI, marked by white lines), and the fluorescent intensities of pFAK at interrenal tissue (ROI, marked by orange lines) were quantified in panel D and E, respectively. The fluorescent intensities of Fn among the control embryo and the blood flow-defective embryos were not significantly different, but the fluorescent intensities of pFAK at the interrenal tissue was reduced in the blood flow-defective embryos compared to the control embryo. (student's t-test, ***$p<0.001$, N.S, not significant; NC, notochord; S, somite; IR, interrenal tissue; SB, swim bladder; vibratome section, 100 μm; scale bar, 50 μm.)

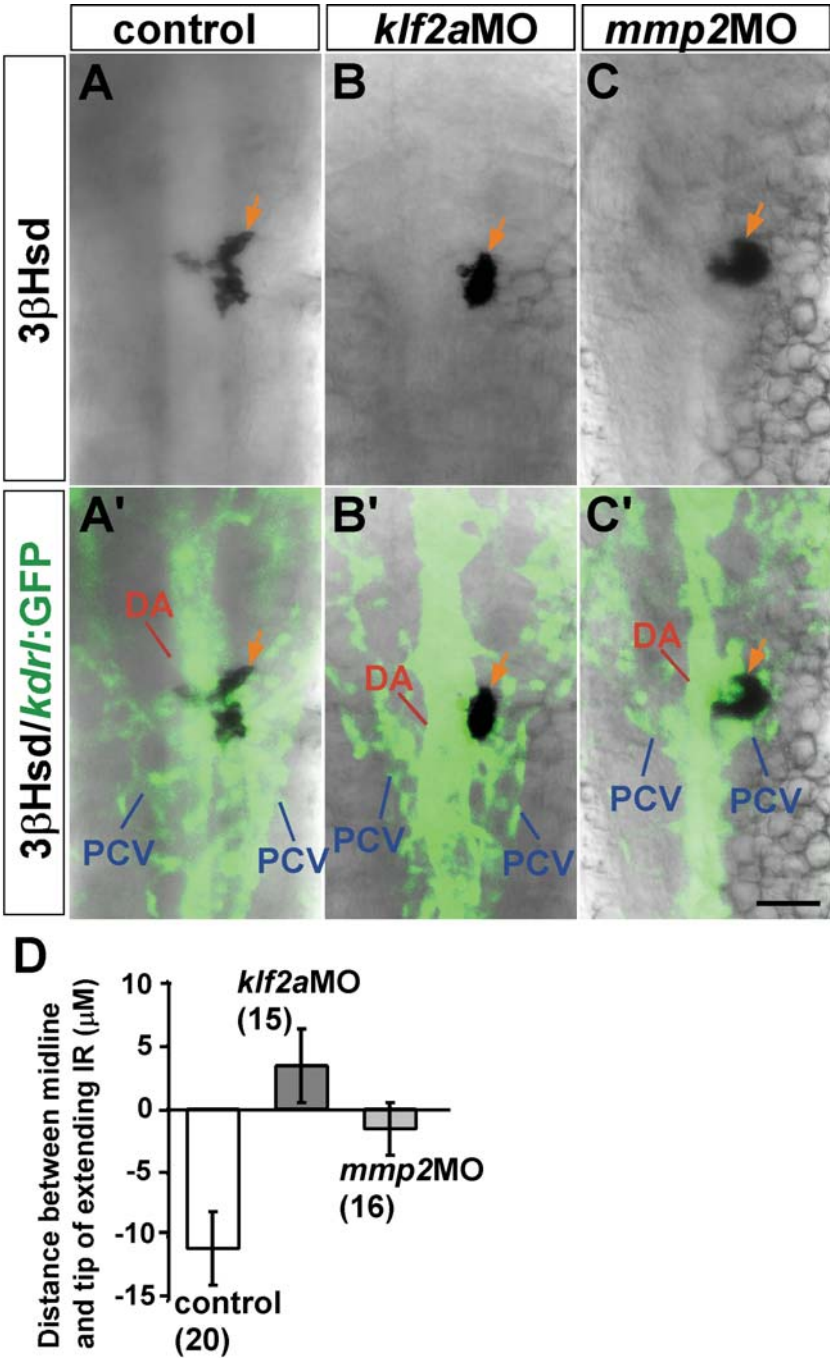

Fig. 30. Defective interrenal medial extension in either *klf2a* morphants or *mmp2* morphants.

(A-C). Confocal images of *Tg(kdrl:GFP)*^{s843} uninjected (A) or injected *klf2a*MO (B), or *mmp2*MO (C) and assayed for 3βHsd enzymatic activity staining at 34 hpf. Knockdown of either *klf2a* or *mmp2* did not affect the development of the vasculature, but inhibited the medial extension of the interrenal tissue. (D). Statistics of the interrenal tissue medial extension. Scale bar, 50 μm.

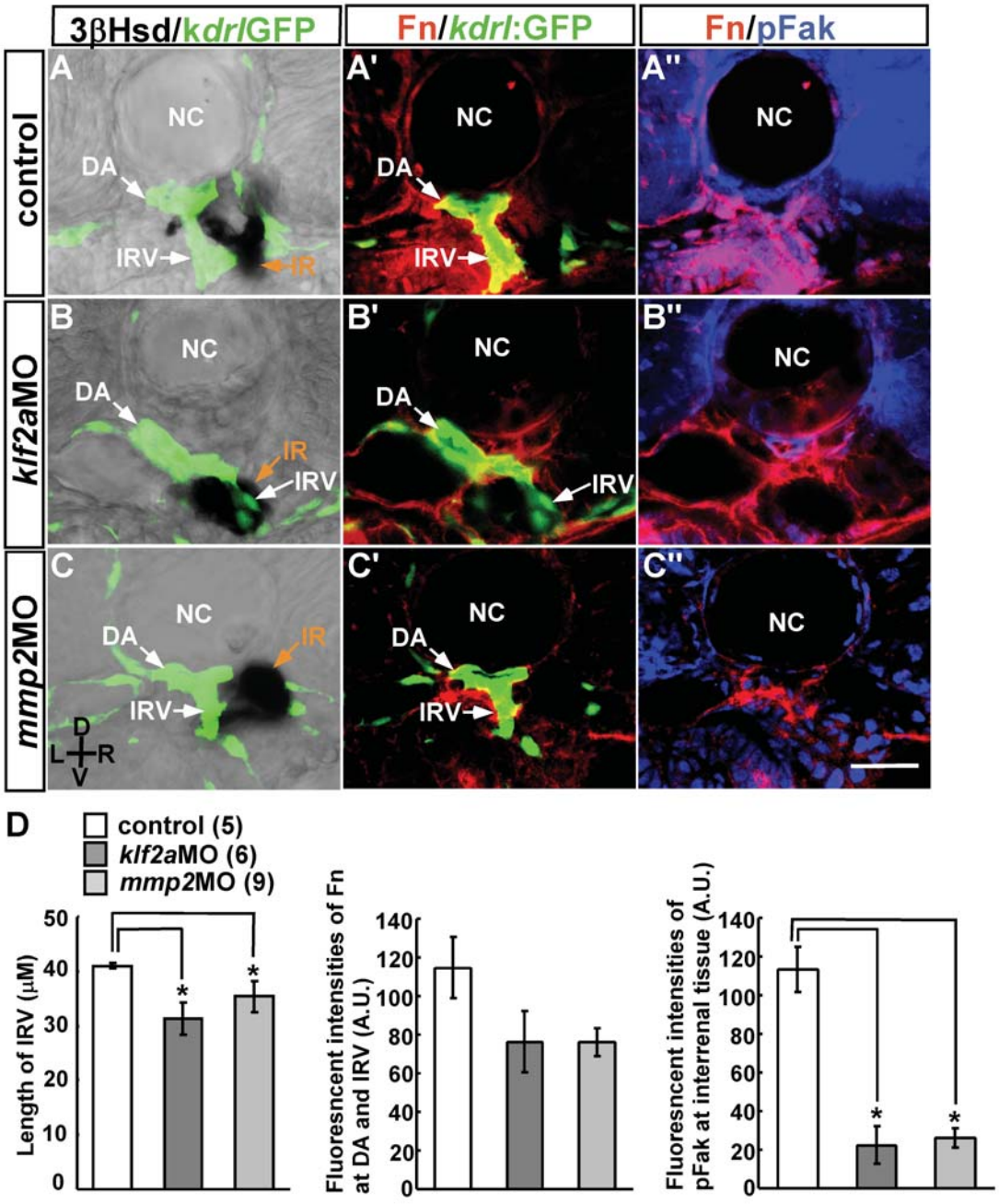

Fig. 31. IRV growth, Fn deposition, and pFAK expression in *klf2a* and *mmp2* morphants.

(A-C). Confocal images of *Tg(kdrl:GFP)*^{s843} uninjected (A) or injected *klf2a*MO (B), or *mmp2*MO (C) and assayed for 3βHsd enzymatic activity staining, vibratome sectioning, and IHC of Fn plus pFAK at 34 hpf. The length of IRV, fluorescent intensities of Fn at DA and IRV (ROI), and the fluorescent intensities of pFAK at interrenal tissue (ROI) were quantified in panel D. Compared to the control embryo, angiogenesis of IRV, accumulation of Fn in the DA as well as the IRV, and activation of FAK were reduced in either the *klf2a* morphant or the *mmp2* morphant. (student's t-test, ***p<0.001, *p<0.05, N.S, not significant; NC, notochord; vibratome section, 100 μm; scale bar, 50 μm.)

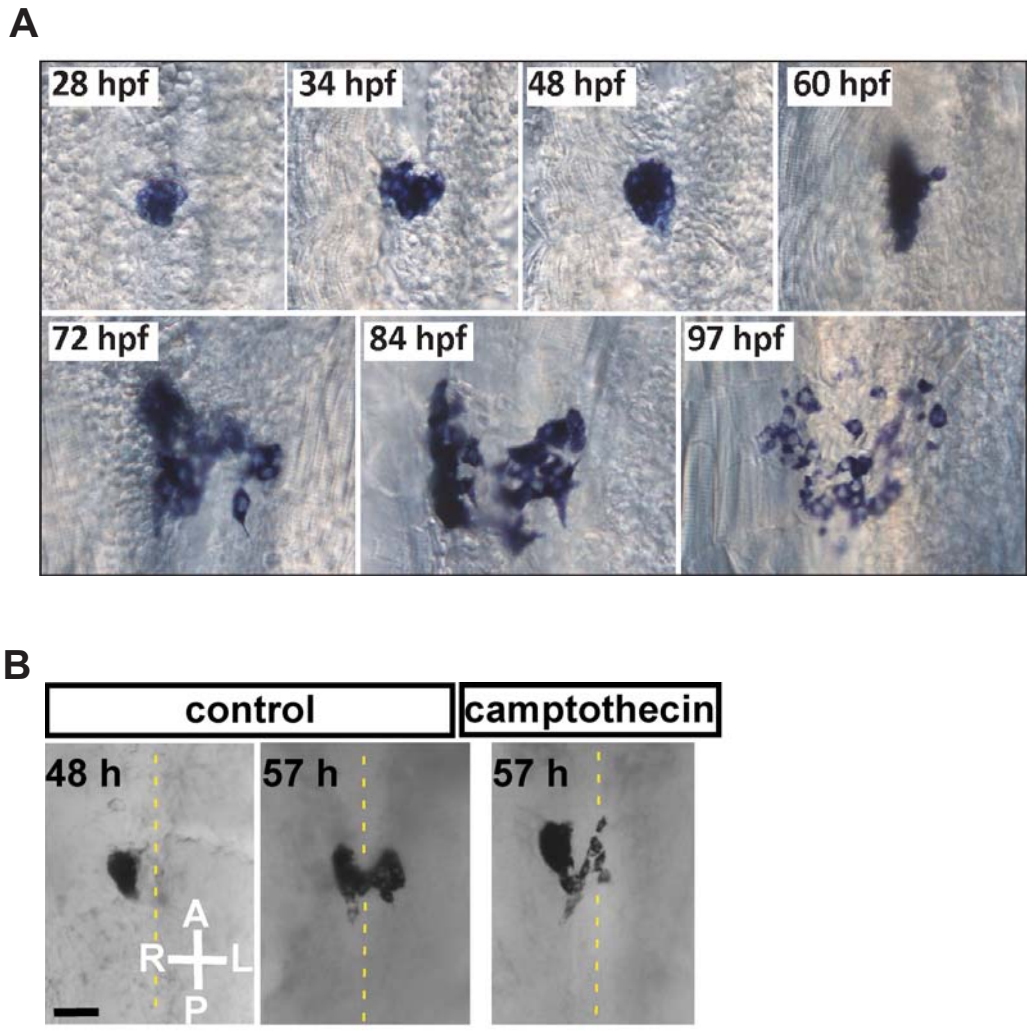

Fig. 32. Morphology change and migration of the steroidogenic interrenal cell during interrenal organ assembly.

(A). Ventral flat-mount views of wildtype embryos assayed for 3βHsd enzymatic activity staining at 28, 34, 48, 60, 72, 84, and 97 hpf. Before interrenal medial extension (28, 34, and 48 hpf), the interrenal cell associated tightly to each other. After interrenal medial extension (72, 84, and 97 hpf), the steroidogenic cell lose of cell-cell contact and with some protrusions on the cell surface. (B). Camptothecin treatment from 48 hpf to 57 hpf. Although the cell number was reduced by camptothecin treatment, the interrenal tissue still success extended across to the midline, suggesting that interrenal medial extension through cell-shape change and migration rather than cell proliferation.

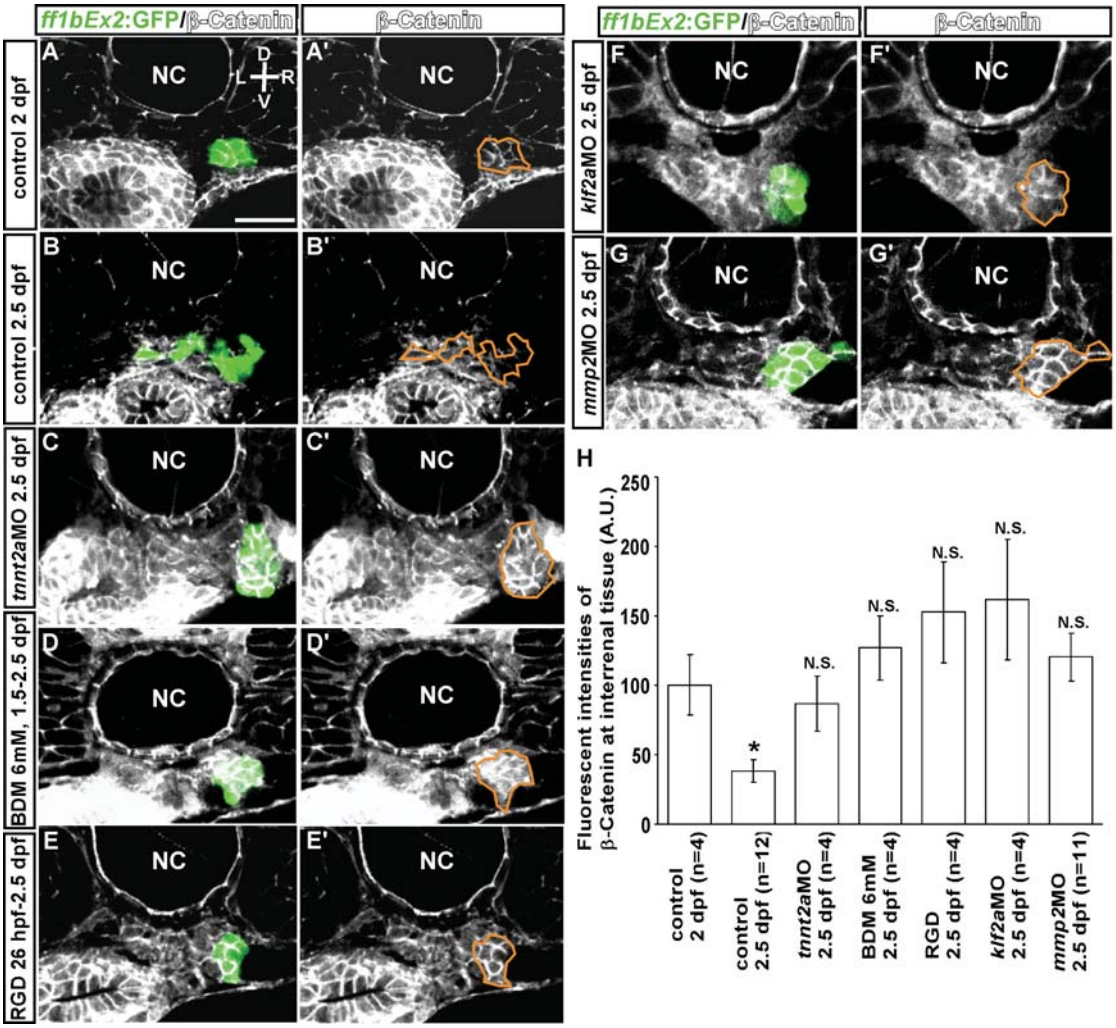

Fig. 33. Steroidogenic interrenal cells underwent an EMT-like change by the hemodynamic force and pFAK signaling.

(A-G). *Tg(ff1bEx2:GFP)* embryos were uninjected (A,B), injected with *tnnt2a*MO (C), *klf2*aMO (F) or *mmp2*MO (G), or treated with 2,3-BDM (D) or RGD (E), and analyzed for vibratome sections and IHC of β-Catenin. In the control embryo, β-Catenin was accumulated at the cell junction of the GFP-labelled interrenal tissue at 2 dpf (A), but that expression was decreased at 2.5 dpf (B), suggesting an EMT-like change in the interrenal cell during interrenal tissue medial extension. However, in blood flow-defective embryos (C,D), pFAK signaling inhibited embryos (E), *klf2a* morphants (F), or *mmp2* morphants (G), the interrenal tissue failed to extend across the midline and still maintained junctional β-Catenin at 2.5 dpf. The fluorescence intensity of β-Catenin in the interrenal tissue (ROI, marked by orange lines) was measured and was normalized to the size of the cluster. (The symbol above the histograms was the result of comparison with the 2 dpf control embryo by student's t-test, *$p<0.05$, N.S, not significant; NC, notochord; vibratome section, 100 μm; scale bar, 50 μm.)

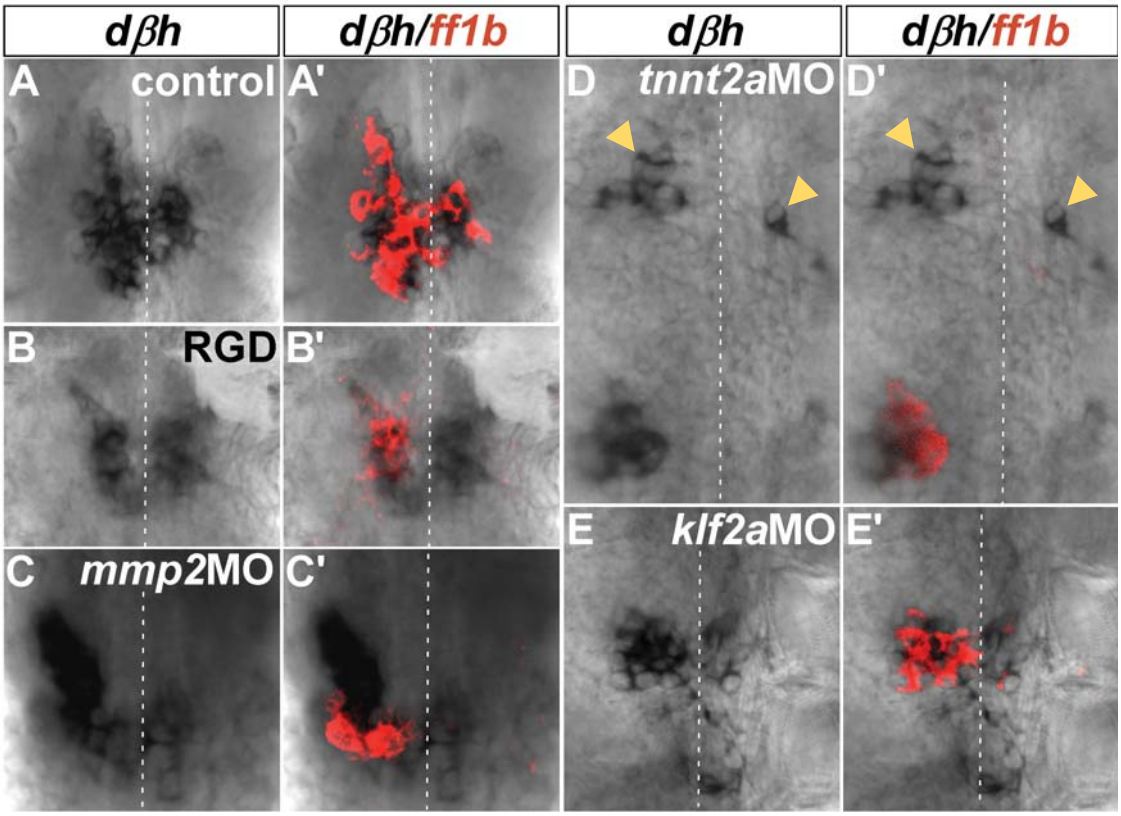

Fig. 34. Effects of *tnnt2a*MO, *klf2a*MO, *mmp2*MO, and RGD-treatment on the functional assembly of the interrenal gland.

(A-E). Double ISH of *ff1b* (red) and *dbh* (black) of the control embryo (A), the RGD-treated embryos (B), the *mmp2* morphant (C), the *tnnt2a* morphant (D), and the *klf2a* morphant (E); ventral flat mount views. The *dbh*-expressing chromaffin cell was fully colocalized with the *ff1b*-expressing interrenal tissue in control embryos. Migration of the chromaffin cell seemed not be affected in the RGD-treated embryo, the *mmp2* morphant, and the *klf2a* morphant, but medial extension of the interrenal tissue was failed in these embryos, resulted in an incomplete assembly of the interrenal organ. In the *tnnt2a* morphant, the functional assembly of the interrenal organ was severely inhibited. The chromaffin cell (yellow arrowheads) failed to converge at the interrenal area, and the medial extension of the interrenal tissue was also inhibited.

Abbreviation	Full name
2,3-BDM	2,3-Butanedione monoxime
3βHsd	3β-Hydroxysteroid dehydrogenase/Δ5-Δ4-isomerase
α6F	α-1 subunit of Na/K ATPase
ACTH	adrenocorticotropic hormone
AGP	adrenogonadal primordium
ANOVA	analysis of variance
BCIP	5-Bromo-4-chloro-3-indolyl phosphate
BMP	bone morphogenetic protein
cas	casanova
CCV	common cardinal vein
cited2	cAMP-response element binding protein binding protein/p300-interacting transactivator, with Glu/Asp-rich carboxy-terminal domain, 2
clo	cloche
CRF	corticotropin-releasing factor
cxcl12	chemokine (C-X-C motif) ligand 12
DA	dorsal aorta
dβh	dopamine beta-hydroxylase
DIG	Digoxigenin
DMSO	dimethyl sulfoxide
dpf	days post-fertilization
DZ	definitive zone
E	embryonic day
EC	endothelial cell
ECM	extracellular matrix
egfl7	EGF-like domain 7
eg-vegf	endocrine gland derived-vascular endothelial growth factor
EMT	epithelial-to-mesenchymal transition
EnMT	endothelial-to-mesenchymal transition
ephb2a	eph receptor B2a
erbbs	erb-b2 receptor tyrosine kinases
ETS	E26 transformation–specific sequence
etv2	ets variant 2

FCS	fetal calf serum
flk1	fetal liver kinase-1
flt4	Fms-related tyrosine kinase 4
Flu	Fluorescein
fn	fibronectin
FZ	fetal zone
GBM	glomerular basement membrane
GFP	green fluorescent protein
hey2	hes-related family bHLH transcription factor with YRPW motif 2
HPA	hypothalamic-pituitary-adrenal
hpf	hours post-fertilization
IHC	Immunohistochemistry
IRV	interrenal vessel
ISH	in situ hybridization
ISV	intersegmental vessel
kdrl	kinase insert domain receptor like
klf	Krüppel-like transcription factor
LDA	lateral dorsal aortae
MET	mesenchymal-to-epithelial transition
mmp2	matrix metalloproteinase-2
MO	anti-sense morpholino
NBT	nitroblue tetrazolium
NCC	neural crest cells
NO	nitric oxide
nrg1	neuregulin 1
osr1	odd-skipped related transcription factor 1
pax	paired-box transcription factor
PBDTx	1% BSA, 1% DMSO, 0.1% Triton X-100 in PBS
PBS	Phosphate-buffered saline
PBST	Phosphate-buffered saline containing 0.1% Tween 20
PBSTx	PBS containing 0.5% Triton X-100
PCT	proximal convoluted tubules
PCV	posterior cardinal vein

pFAK	phosphorylated focal adhesion kinase
pdgfB	platelet-derived growth factor-B
PFAT	paraformaldehyde containing 0.1% Tween 20
pSmad	phosphorylated SMAD family member
RGD	L-arginyl-L-glycyl-L-aspartic acid
ROI	region of interest
SA	sympatho-adrenal
sdf1	stromal derived factor 1
SEM	standard error of the mean
sf1	steroidogenic factor 1
SIV	subintestinal vessel
sox32	SRY (sex determining region Y)-box 32
tal1	T-cell acute lymphocytic leukemia 1
tnnt2a	cardiac troponin T2
vegf	vascular endothelial growth factor receptor
wt1	Wilm’s tumor suppressor
YSL	yolk syncytial layer

OPEN ACCESS Freely available online

PLOS ONE

The Hemodynamically-Regulated Vascular Microenvironment Promotes Migration of the Steroidogenic Tissue during Its Interaction with Chromaffin Cells in the Zebrafish Embryo

Chih-Wei Chou, You-Lin Zhuo, Zhe-Yu Jiang, Yi-Wen Liu*

Department of Life Science, Tunghai University, Taichung, Taiwan

Abstract

Background: While the endothelium-organ interaction is critical for regulating cellular behaviors during development and disease, the role of blood flow in these processes is only partially understood. The dorsal aorta performs paracrine functions for the timely migration and differentiation of the sympatho-adrenal system. However, it is unclear how the adrenal cortex and medulla achieve and maintain specific integration and whether hemodynamic forces play a role.

Methodology and Principal Findings: In this study, the possible modulation of steroidogenic and chromaffin cell integration by blood flow was investigated in the teleostean counterpart of the adrenal gland, the interrenal gland, in the zebrafish (*Danio rerio*). Steroidogenic tissue migration and angiogenesis were suppressed by genetic or pharmacologic inhibition of blood flow, and enhanced by acceleration of blood flow upon norepinephrine treatment. Repressed steroidogenic tissue migration and angiogenesis due to flow deficiency were recoverable following restoration of flow. The regulation of interrenal morphogenesis by blood flow was found to be mediated through the vascular microenvironment and the Fibronectin-phosphorylated Focal Adhesion Kinase (Fn-pFak) signaling. Moreover, the knockdown of *krüppel-like factor 2a* (*klf2a*) or *matrix metalloproteinase 2* (*mmp2*), two genes regulated by the hemodynamic force, phenocopied the defects in migration, angiogenesis, the vascular microenvironment, and pFak signaling of the steroidogenic tissue observed in flow-deficient embryos, indicating a direct requirement of mechanotransduction in these processes. Interestingly, epithelial-type steroidogenic cells assumed a mesenchymal-like character and downregulated β-Catenin at cell-cell junctions during interaction with chromaffin cells, which was reversed by inhibiting blood flow or Fn-pFak signaling. Blood flow obstruction also affected the migration of chromaffin cells, but not through mechanosensitive or Fn-pFak dependent mechanisms.

Conclusions and Significance: These results demonstrate that hemodynamically regulated Fn-pFak signaling promotes the migration of steroidogenic cells, ensuring their interaction with chromaffin cells along both sides of the midline during interrenal gland development.

Citation: Chou C-W, Zhuo Y-L, Jiang Z-Y, Liu Y-W (2014) The Hemodynamically-Regulated Vascular Microenvironment Promotes Migration of the Steroidogenic Tissue during Its Interaction with Chromaffin Cells in the Zebrafish Embryo. PLoS ONE 9(9): e107997. doi:10.1371/journal.pone.0107997

Editor: Sheng-Ping Lucinda Hwang, Institute of Cellular and Organismic Biology, Taiwan

Received April 10, 2014; **Accepted** August 24, 2014; **Published** September 23, 2014

Data Availability: The authors confirm that all data underlying the findings are fully available without restriction. All relevant data are within the paper and its Supporting Information files.

Funding: CWC, YLZ, ZYJ, and YWL were supported by Ministry of Science and Technology (http://web1.most.gov.tw/) grants (101-2313-B-029-001, 102-2628-B-029-002-MY3 and 102-2321-B-400-018). The funder had no role in study design, data collection and analysis, decision to publish, or preparation of the manuscript.

Competing Interests: The authors have declared that no competing interests exist.

* Email: dlslys@thu.edu.tw

Introduction

Although blood vessels have long been known to respond to hemodynamic forces through mechanotransduction, only recently have researchers begun to understand the influence of hemodynamics on organogenesis through modulation of cellular behaviors, the extracellular matrix (ECM) microenvironment, as well as cell signaling events [1]. The early zebrafish embryo does not rely on blood circulation to transport oxygen [2], making it an excellent *in vivo* model for studying the effect of blood flow on development. Various genetic and pharmacological approaches have been developed in the zebrafish model, which have revealed the crucial role of hemodynamics in the morphogenesis of heart, kidney, and brain vasculature [3,4,5,6]. Moreover, it is possible to study the role of hemodynamics in establishing the architecture of endocrine tissues in the zebrafish embryo, since the specification and differentiation of a variety of endocrine cells proceed even in the complete absence of vasculature [7,8,9,10,11].

How the adrenal cortex and medulla—arising because of distinct cell fate decisions in physically separated precursor cells—assemble to form the adrenal gland remains incompletely understood. The adrenal cortex is comprised of steroidogenic cells differentiated from the intermediate mesoderm, while the medulla contains chromaffin cells that originate from the neural

crest and are subsequently segregated from the sympatho-adrenal lineage [12]. Mice deficient in the transcription factor steroidogenic factor-1 (SF-1, NR5A1) lack an adrenal cortex, but exhibit normal differentiation of chromaffin cells, half of which are present in the suprarenal region, arguing against a role for the adrenal cortex in attracting chromaffin cells [13]. However, ectopic adrenocortical cells in the mouse thorax, induced through the transgenic overexpression of SF-1, are capable of recruiting sympatho-adrenal progenitors [14]. These findings suggestive of an undefined role of the adrenal cortex have been clarified by the recent demonstration of the dorsal aorta (DA) as a morphogenetic center that instructs the specification and segregation of the sympatho-adrenal lineage in the chick embryo [15]. The DA and the adrenal cortex both secrete Neuregulin 1, which attracts chromaffin cells to the suprarenal region. However, the existence of shared paracrine factors does not explain why chromaffin cells colonize the adrenal cortex rather than non-adrenal regions surrounding the DA, and additional molecular and cellular factors could participate in the integration of steroidogenic and chromaffin cells. It was hypothesized that in addition to instructing the migration and differentiation of chromaffin cells, the vasculature near the adrenal gland also specifies the behavior of adrenocortical cells, thereby promoting cortex-medulla amalgamation. This possibility was investigated in the present study in zebrafish, an established model for exploring the development and diseases of the cardiovascular and endocrine systems.

The teleostean interrenal gland is functionally equivalent to the adrenal gland in mammals, with steroidogenic and chromaffin cell populations arising from conserved molecular programs [16,17,18]. The integration of these two cell types occurs between 1.5 and 3 days post-fertilization (dpf), which is immediately followed by *de novo* cortisol synthesis in response to stress [18,19,20]. Within the same temporal window, the interrenal vessel (IRV) is patterned along with a vessel-derived, Fibronectin (Fn)-enriched microenvironment [21], which is essential for IRV growth, steroidogenic tissue morphogenesis, and positioning the interrenal organ. Nevertheless, little is known about how the Fn-enriched interrenal microenvironment is regulated and the cellular mechanisms governing morphogenetic movements during integration.

Previous studies have shown that Klf2a and MMP2 are hemodynamically regulated: KLF2 is a transcription factor activated in cultured endothelial cells by fluid shear stress from laminar flow [22,23], and the endothelial expression of mouse Klf2 and its ortholog *klf2a* in zebrafish reflects an increase in fluid-generated forces, while a loss of function leads to defective smooth muscle tone [24]. MMPs are known to mediate ECM remodeling and enable reshaping of tissues through peptidase activity [25]. In the zebrafish embryo, *mmp2* is expressed in the endothelium of developing axial vasculature in a flow-dependent manner [5]; and in rats and cultured cells, MMP2 activity in glomerular mesangial cells is induced by stretch [26,27] and regulated by cyclic strains in the endothelium resulting from turbulent flow, which modulates the migration of vascular smooth muscle cells [28,29]. Moreover, MMP2 cleaves a variety of ECM molecules, including type IV collagen, vitronectin, and fibronectin [30,31]. Abundant RNA transcripts of both *klf2a* and *mmp2* are restrictively localized at the axial vasculature at around Prim-25 stage (36 hpf) during zebrafish development [5,32], which is temporally correlated with the initiation of interrenal medial extension and angiogenesis. Furthermore, the nascent DA in the zebrafish does not recruit mural cells until 3 dpf [33], and differentiated vascular smooth muscle cells appear only after 7 dpf [34]; it was therefore hypothesized that hemodynamic forces could be transduced through the endothelium to influence closely associated interrenal cells.

In this study, the possible role of blood flow for the integration of steroidogenic and chromaffin cells was examined in the zebrafish interrenal gland, by using genetic and pharmacological approaches to abolish blood flow in the embryo. The vascular structure and associated ECM microenvironment in the interrenal region were examined for changes in the architecture of the developing interrenal tissue. The modulation of interrenal morphogenesis by blood flow through mechanotransduction was investigated by knocking down the mechanosensitive proteins Krüppel-like factor 2a (Klf2a) and Matrix metalloproteinase (Mmp)2. In addition, we demonstrated that steroidogenic cells undergo an epithelial-to-mesenchymal transition (EMT)-like change during organ assembly, which was correlated with a reduction in epithelial and a rise in mesenchymal markers. During EMT, which occurs at many critical steps during embryonic development, cell-cell contacts and polarity are lost and the cytoskeleton is extensively remodeled [35]. The present findings underscore the role of hemodynamics in regulating Fn-phosphorylated Focal adhesion kinase (pFak) signaling in the developing interrenal tissue, which in turn induces an EMT-like transformation in steroidogenic cells. Thus, in addition to the known chemoattractive function for chromaffin cells, the axial vasculature regulates the migration of steroidogenic cells through hemodynamically regulated signaling.

Methods

Ethics Statement

All of the zebrafish-use protocols in this research were reviewed and approved by the Institutional Animal Care and Use Committee of Tunghai University (IRB Approval NO. 101–12).

Zebrafish Husbandry

Zebrafish (*Danio rerio*) were reared according to standard protocols [36]. Embryos were obtained from natural crosses of wild-type or transgenic fish, and staged as previously described [37]. The following lines were used: *Tg(wt1b: GFP)(line 1)* [38] (a gift from Christoph Englert, Fritz-Lipmann Institute, Jena, Germany); *Tg(ff1bEx2: GFP)* [39] (a gift from Dr. Woon-Khiong Chan, National University of Singapore); and *Tg(kdrl: EGFP)*^{s843} [40] (a gift of Didier Stainier, University of California, San Francisco, CA, USA).

3β-Hydroxysteroid Dehydrogenase (3β-Hsd) Staining, In Situ Hybridization (ISH), Immunohistochemistry (IHC), Densitometry and Imaging

Embryos used for histological analysis were treated with 0.03% phenylthiourea (Sigma) from 12 h post-fertilization (hpf) onwards to inhibit pigmentation. The 3β-Hsd activity staining, ISH [9], and IHC [41] were performed with modifications according to previously published methods.

To delineate the morphology of steroidogenic interrenal tissue, histochemical staining for 3β-Hsd enzymatic activity was performed on whole embryos, and Nomarski images were captured using a BX51 microscope (Olympus).

For whole-mount ISH, digoxigenin (DIG)- and fluorescein-labeled antisense riboprobes were synthesized from linearized plasmids of *dopamine β hydroxylase* (*dβh*) and *ff1b* (*nr5a1a*) genes, respectively; the probes were detected with alkaline phosphatase-conjugated anti-DIG or -fluorescein antibody (Roche), and visualized with 5-bromo-4-chloro-3-indolyl-phosphate/nitro blue tetrazolium (Promega) or Fast Red (Roche). Stained embryos were

flat-mounted and photographed under an Axioplan II microscope (Zeiss).

For IHC experiments, *Tg(ff1bEx2: GFP)* and *Tg(kdrl: EGFP)*^{s843} embryos were fixed and embedded in 4% NuSieve GTG low-melting agarose (Lonza), cut into 100- μm sections with a VT1000M vibratome (Leica), and permeabilized with phosphate-buffered saline (PBS) containing 1% Triton X-100 before incubation with rabbit anti-human Fn (Sigma), mouse anti-human pFak (pY397) (BD Transduction Laboratories), mouse anti-chicken β-Catenin (Sigma), mouse anti-pig Vimentin (V9) (Abcam), and rabbit anti-zebrafish E-cadherin (Cdh1) (GeneTex) antibodies at 1:200, 1:100, 1:50, 1:200 and 1:200 dilutions, respectively. Dylight 594- and 650-conjugated anti-rabbit or anti-mouse IgG (abcam) were used as secondary antibodies at 1:200 dilution. Images were captured with an LSM510 confocal microscope with version 3.5 software (Zeiss).

For the quantification of 3β-Hsd activity, images of deyolked embryos in each group were taken with identical illumination and magnification using Axioskop 2 Plus microscope equipped with AxioVision 3.0 software (Carl Zeiss). Signal area and density were measured using Image Gauge Program, version 4.0 (Fuji Photo Film). Videos of embryos oriented with the anterior toward the left were taken by using an SMZ1500 microscope equipped with an AM4023X Dino-Eye eyepiece camera (Nikon).

Microinjection of Antisense Morpholino Oligonucleotides (MOs)

The MO for *cardiac troponin T2a* (*tnnt2a*MO) (5′-CAT GTT TGC TCT GAT CTG ACA CGC A-3′) [42], along with *klf2a*MO (5′-GGA CCT GTC CAG TTC ATC CTT CCA C-3′) [43], and *mmp2*MO (5′-GGG AGC TTA GTA AAC ACA AAC CTG T-3′) [44] were synthesized by Genetools LLC and diluted in 1 × Danieau solution, before injection into one- to two-cell stage embryos using a Nanoject (Drummond Scientific Company) at dosages of 1.0, 1.2, and 1.2 pmole per embryo, respectively.

Pharmacological Treatment

Camptothecin (Sigma # C9911) treatment was performed according to a previously described method [45] with modifications. The compound (60 μM in 0.1% dimethyl sulfoxide [DMSO]) was applied to 48 hpf embryos, which were harvested at 57 hpf for the 3β-Hsd activity assay. The treatment of embryos with 2,3-butanedione 2-monoxime (2,3-BDM; Sigma #B0753) was as described in an earlier report [46], except that dechorionated embryos were immersed in various concentrations of 2,3-BDM starting from 1.5 dpf. Norepinephrine treatment was performed by treating dechorionated embryos with 0.01, 0.1 or 1 mM norepinephrine (Sigma A7257) freshly prepared in egg water. L-NAME treatment was performed by treating dechorionated embryos with freshly prepared 100 μM Nω-nitro-L-arginine methyl ester (L-NAME) (#N5751, Sigma) in egg water with 0.1% DMSO at 36 hpf. For L-arginyl-L-glycyl-L-aspartic acid (RGD; #G1269, Sigma) treatment, the peptide was reconstituted to 1 mM in filter-sterilized egg water and applied to dechorionated embryos at a final concentration of 100 μM at 26 hpf; embryos were collected at 2.5 dpf and fixed for histological assays.

Statistical Analysis

All quantitative data are expressed as the mean ± standard error of the mean. Data were evaluated by analysis of variance (ANOVA), followed by Duncan's new multiple range test (Duncan's multiple test) or Student's t test. $P<0.05$ was considered statistically significant.

Results

Blood Flow is Required for the Morphogenesis of Kidney Glomerulus and Interrenal Tissue

The hemodynamic force drives the assembly of zebrafish kidney glomeruli at the midline [5]. Since the kidney and interrenal gland develop in parallel [16], with the DA acting as the source of angiogenesis in both organs [21,47], the role of blood flow in the morphogenesis of the interrenal gland was assessed. Kidney and interrenal tissue morphology was visualized by staining for 3β-Hsd enzymatic activity in *Tg(wt1b: GFP)* embryos, in which GFP is expressed in the glomerular podocytes, pronephric tubules, and proximal pronephric ducts [38,48], as well as in the exocrine pancreas due to a possible position effect of transgene insertion. The MO against *tnnt2a*, a gene essential for sarcomere assembly and heart contractility [42], was injected into *Tg(wt1b: GFP)* embryos, and 100% of the *tnnt2a* morphants (n = 56) displayed completely abolished heartbeat and blood flow. Consistent with the previous study [5], bilateral kidney glomeruli in control embryos assembled at the midline by 54 hpf, but failed to fuse in *tnnt2a* morphants (Figure 1A). The steroidogenic tissue in blood flow-deficient embryos grew as a round, tightly packed cell aggregate, without extending protrusions as in the case of controls. The extent of migration was quantified by measuring the distance between the tip of medially extending steroidogenic tissue and the midline, and although there was no difference at 54 hpf, the distance was decreased in morphants relative to control embryos at 77 hpf (Figure 1B). The inhibition of medial extension was not due to growth arrest of interrenal tissue, since organ size—as assessed by densitometric analysis of 3β-Hsd activity staining—was similar in *tnnt2a*MO-injected and control embryos at all stages examined (Figure 1C). To further evaluate the effect of tissue growth on interrenal morphogenetic movement, embryos were treated with camptothecin, which blocks cell proliferation in zebrafish embryos [45], from 48 to 57 hpf. Camptothecin-treated embryos showed an 18% reduction in interrenal tissue size compared to controls. Notably, the formation of protrusions was unaffected by camptothecin treatment (Figure 1D), suggesting that cell growth is not the major determinant for interrenal medial extension. Taken together, these results indicate that blood flow is required for the morphogenetic movement of both kidney and interrenal tissues. Based on the early defects in the ventral DA caused by *tnnt2a* knockdown [49,50], experiments were performed to establish whether interrenal morphogenetic movement during the temporal window of organ assembly is specifically subject to regulation by blood flow.

Medial Extension of Steroidogenic Tissue during Interrenal Organ Assembly is Regulated by Blood Flow

The pharmacological agent 2,3-BDM, which affects heart rate without affecting cell viability, has previously been used to evaluate the role of blood flow in zebrafish organogenesis [5,6,51]. To rule out the possibility that defective medial extension of the interrenal tissue in *tnnt2a* morphants was due to an early effect on blood vessel morphogenesis, blood flow was inhibited in embryos by application of 2,3-BDM from 1.5 dpf, by which interrenal medial extension and organ assembly are initiated (Figure 2). The 2,3-BDM treatment on zebrafish embryos leads to decreased myofibrillar ATPase and myocardial force in a dose-dependent manner, which affects heart rate at a concentration as low as 2 mM and is sufficient to eliminate blood flow at 6 mM [46]. Consistent with the previous study, a concentration of 6 mM produced a 53% reduction in heart rate and a cessation of blood flow (Video S1) compared to control embryos (Video S2). A lower

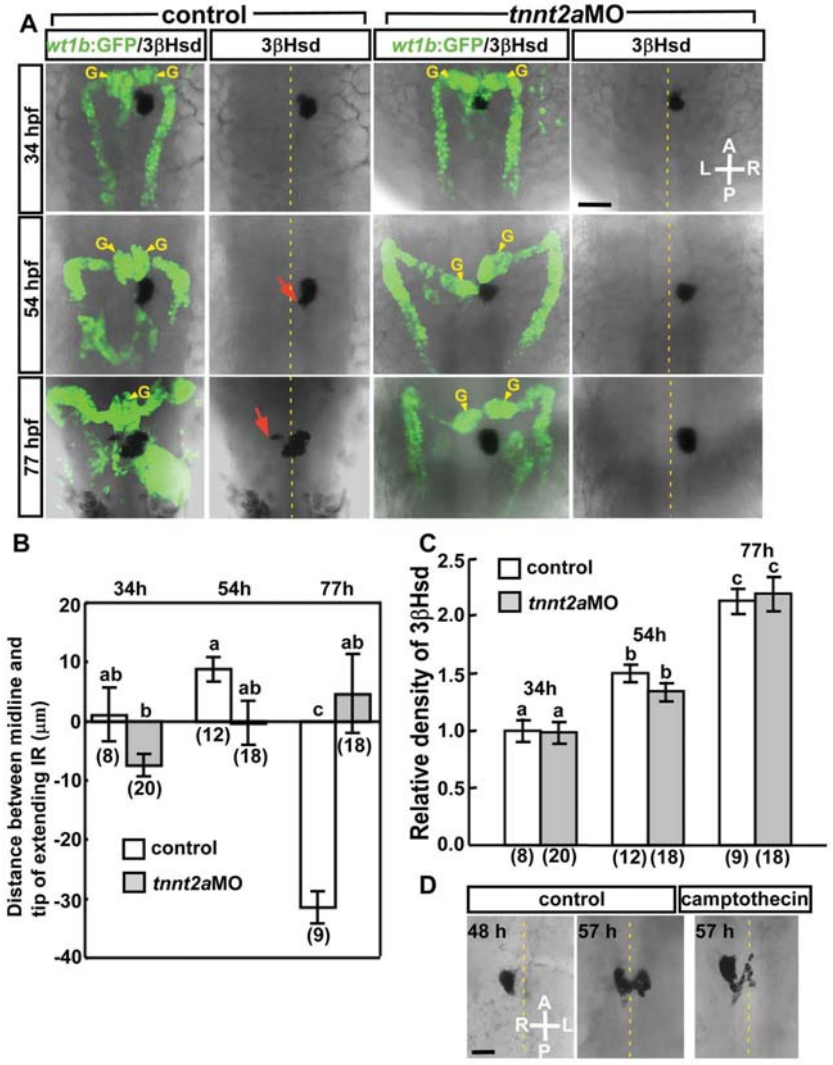

Figure 1. Morphology of pronephros and interrenal tissue in the absence of blood flow. (A) The interrenal steroidogenic tissue positive for 3β-Hsd activity forms an extension that protrudes toward the midline by 54 hpf (cell protrusions marked by red arrows), while kidney glomeruli delineated by *wt1b*: GFP expression (G, yellow arrowheads) assemble at the midline. Morphogenetic movements of kidney glomeruli and steroidogenic tissues are defective in the *tnnt2a* morphant. All panels show dorsal views of representative embryos. (B) Quantification of effects of *tnnt2a*MO injection on interrenal migration. The distance between the midline and the migrating tip of steroidogenic tissue was designated as positive if the migrating tip had not reached the midline, and negative if the tip had migrated across the midline. (C) Relative density of steroidogenic tissue, as assessed by 3β-Hsd activity staining in the ventral surface, in *tnnt2a* morphants compared to wild-type controls. The number of embryos in each group is indicated in parentheses in (B) and (C). Histograms with different letters above them are significantly different (ANOVA and Duncan's multiple test, $P<0.05$). (D) Effect of camptothecin treatment from 48 to 57 hpf on 3β-Hsd activity in steroidogenic cells. A, anterior; P, posterior; L, left; R, right. Broken yellow lines indicate position of the midline. Abbreviations: glomerulus (G). Scale bar, 50 μm.
doi:10.1371/journal.pone.0107997.g001

concentration of 2,3-BDM (2 mM) caused a 26% decrease in heart rate and a visibly weakened blood flow (Video S3). To examine the morphology of the DA adjacent to the kidney and interrenal regions, 2,3-BDM was applied to *Tg(kdrl: EGFP)*^{s843} embryos that express GFP in the developing blood vascular structure [40], which were then harvested at 2.5 dpf, when the migration of interrenal cells can be clearly observed [19]. Treatment with 2 or 6 mM 2,3-BDM suppressed interrenal medial extension across the midline (Figure 2B, B'', C, C''), with similar effects observed at both concentrations (Figure 2D). However, the interrenal tissue had more protrusions at 2 than at 6 mM 2,3-BDM (Figure 2B, C), suggesting that the effect of 2,3-BDM was dose-dependent. In contrast, the morphology of the DA and the pronephric glomerulus was unperturbed by 2,3-BDM treatment. Thus, the inhibition of medial extension of the interrenal tissue caused by loss of blood flow was not due to a general defect in the DA.

Conversely, as the heart rate was accelerated by norepinephrine treatment from 33 hpf, a significant enhancement of interrenal tissue extension was detected at 2 dpf (Figure 2E-E'', F-F'', G-G'', H). Norepinephrine accelerated the heart rate of developing embryos in a dose-dependent manner (Figure S1). 0.01, 0.1 and 1 mM of norepinephrine treatments on embryos at 33 hpf led to a 23%, 29% and 41% increase of heart rate, respectively. Compared to the control embryo (Figure 2E), both 0.1 and 1 mM of norepinephrine treatements led to a more evident migratory

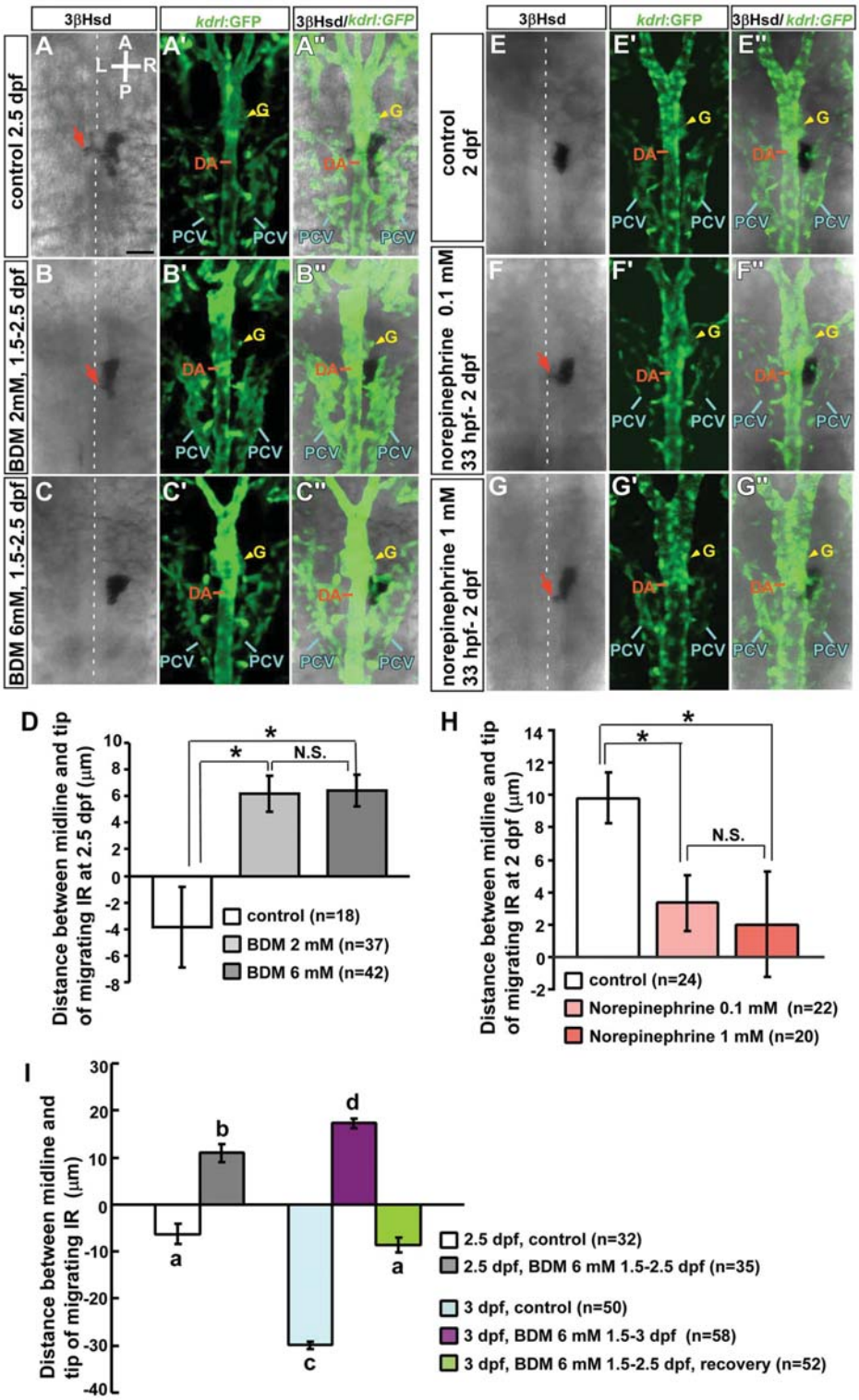

Figure 2. Effects of 2,3-BDM and norepinephrine on morphogenetic movements of interrenal tissue. For repression of blood flow, *Tg(kdrl: GFP)*^{s843} embryos were treated with (A–A'') vehicle (control), or 2,3-BDM at a concentration of (B–B'') 2 mM or (C–C'') 6 mM from 1.5 dpf. A suppression of the medial extension of steroidogenic cells was observed in 2,3-BDM-treated embryos at 2.5 dpf, while the morphology of the DA and the pronephric glomerulus (yellow arrowheads) appeared unperturbed. Protrusions (red arrow) formed at the lower concentration; the phenotype was more severe at the higher concentration. For acceleration of blood flow, *Tg(kdrl: GFP)*^{s843} embryos were treated with (E-E'') vehicle (control), or norepinephrine at a concentration of (F–F'') 0.1 mM or (G-G'') 1 mM from 33 hpf. An enhancement of interrenal medial extension, as evidenced by the formation of protrusions, was observed in norepinephrine-treated embryos at 2 dpf. The effects of 2,3-BDM and norepinephrine treatments on interrenal migration were quantified in (D) and (H), respectively. The distance between the midline and migrating tip of steroidogenic tissue was

designated as positive if the migrating tip had not reached the midline, and negative if the tip had migrated across the midline. *$P<0.05$; N.S., not significant (Student's t-test). (I) Suppressing effect of interrenal cell migration by 2,3-BDM at 6 mM from 1.5 dpf was reversible at 3 dpf, as the 2,3-BDM applied from 1.5 dpf was washed out at 2.5 dpf for restoring blood flow. The interrenal tissue in recovered embryos extended across the midline at 3 dpf and displayed a migration distance not significantly different from that in control embryos at 2.5 dpf. Histograms with different letters above them are significantly different (ANOVA and Duncan's multiple test, $P<0.05$). A, anterior; P, posterior; L, left; R, right. Broken white lines indicate position of the midline. Abbreviations: glomerulus (G), posterior cardinal vein (PCV). Scale bar, 50 μm.
doi:10.1371/journal.pone.0107997.g002

phenotype of interrenal tissue, as verified from the extending protrusions (red arrows in Figure 2F, G), which was consistent with the results of the quantification of interrenal tissue extension (Figure 2H). However, no significant difference in steroidogenic tissue extension could be detected between embryos treated with 0.1 or 1 mM of norepinephrine. Norepinephrine at 0.01 mM also enhanced steroidogenic tissue extension (4.3 ± 2.0 μm, $n=24$) compared to control embryos, while no significant statistical difference was found among norepinephrine treatments at 0.01, 0.1 and 1 mM. Our results thus indicated that a moderate elevation of heart rate by 23% was sufficient to promote migration of steroidogenic interrenal cells, although further increase of heart rate by treating with higher concentrations of norepinephrine did not lead to a dose-dependent enhancing effect on interrenal medial extension.

To confirm the relationship between blood flow and steroidogenic cell migration, we further tested whether interrenal medial extension repressed by 2,3-BDM treatment could be recovered by restoring the blood flow (Figure 2I, Figure S2). Steroidogenic tissue migrated across the midline by 2.5 dpf (Figure S2A, A'') and continued to extend and form a bilobed organ structure by 3 dpf (Figure S2C, C''). Extension of steroidogenic tissue was arrested as 2,3-BDM at 6 mM was applied to embryos from 1.5 dpf onwards (Figure S2B, B'', D, D''). The steroidogenic tissue extension in 2,3-BDM-treated embryos was recovered at 3 dpf as 2,3-BDM was washed out at 2.5 dpf (Figure S2E, E''). The interrenal tissue in 2,3-BDM-treated embryos appeared to be located further away from the midline at 3 dpf than at 2.5 dpf (Figure 2I), possibly due to continuous growth of peri-interrenal structures from 2.5 to 3 dpf. It is interesting to note that there was no significant difference of migration distance between control embryos at 2.5 dpf and recovered embryos at 3 dpf (Figure 2I), implying that the inhibited interrenal medial extension by 2,3-BDM treatment from 1.5 to 2.5 dpf could be rescued by resuming blood flow for 12 hours. Taken together, results in Figure 2 demonstrated that pharmacologic repression and acceleration of heart rates are well correlated with the extent of interrenal medial extension. Furthermore, the inhibited steroidogenic tissue extension caused by arrested blood flow was recoverable following restoration of blood flow, providing strong evidence that migratory activity of interrenal steroidogenic cells is indeed modulated by blood flow.

Blood Flow Regulates IRV Extension during Interrenal Organ Assembly

Interrenal medial extension temporally coincides with IRV angiogenesis, which is promoted by the IRV-associated vascular microenvironment [21], and therefore the effect of reduced blood flow on IRV angiogenesis was examined from 1.5 to 2.5 dpf (Figure 3). IRV growth was initiated normally when blood flow was inhibited starting at 1.5 dpf. However, in embryos treated with 2 or 6 mM 2,3-BDM, IRV lengths were reduced and the vessels reached but did not extend ventrally through the interrenal tissue, with a more severe phenotype observed at the higher concentration (Figure 3B'–C', D), indicating a dose-dependent effect of 2,3-BDM on IRV extension. Our previous study showed that IRV directionality, but not initiation of angiogenesis, is perturbed in the *tnnt2a* morphant [21]; accordingly, the present results indicated that the blood flow was not required for the sprouting of the IRV from the DA, but may play a role in its extension. Furthermore, the interrenal tissue in 2,3-BDM-treated embryos (Figure 3B–B', C–C') and *tnnt2a* morphants [21] only interacted with the tip of the IRV but not the DA, while the extending interrenal tissue in the control embryo remained closely associated with both the ventral DA and the IRV (Figure 3A–A').

To test whether accelerated blood flow could promote extension of the IRV, embryos were treated with norepinephrine at 0.1 or 1 mM at 33 hpf and harvested at 2 dpf for analysis (Figure 3E-G, E'-G'). It was found that norepinephrine at both concentrations significantly increased length of the IRV (Figure 3H), yet no difference in the IRV growth was observed between 0.1 and 1 mM of norepinephrine treatments. The promoting effects of norepinephrine treatments on extension of the IRV were therefore highly correlated with those on interrenal medial extension (Figure 2H). Similar to the case of interrenal medial extension in Figure 2I, restoring blood flow by 2,3-BDM washout after the treatment from 1.5 to 2.5 dpf led to a recovery of IRV growth at 3 dpf, with the IRV length in 3-dpf recovered embryos not significantly different from that in 2.5-dpf control embryos (Figure 3I, S3).

Our results from pharmacologic inhibition and acceleration of blood flow therefore strongly support that blood flow regulates both interrenal medial extension and IRV growth during interrenal organ assembly. While the processes of interrenal medial extension and IRV growth occur synchronously during development [21], they are both influenced by blood flow in a highly correlated manner. Therefore, it leads to the hypothesis that there might be a common flow-regulated molecular and cellular mechanism by which both interrenal medial extension and IRV angiogenesis are regulated. The initiation of IRV angiogenesis requires deposition of Fn at the ventral DA near the interrenal tissue, and the accumulation of this protein in the local microenvironment supports IRV extension [21]. While the interrenal tissue is closely associated with both the DA and the IRV, vessel-derived Fn functions at the tissue-vessel interface and thus modulates the migration of steroidogenic cells [19]. Therefore, it is possible that the vascular microenvironment established during IRV angiogenesis is regulated by blood flow, which in turn modulates the migration of steroidogenic cells.

Blood Flow is Required for Patterning the Fn-rich Microenvironment and pFak Distribution in the Interrenal Region

Possible perturbations in the interrenal microenvironment of blood flow-deficient embryos were assessed using the *Tg(ff1bEx2:GFP)* line, in which the GFP expression recapitulates the endogenous expression of *ff1b* [52]—the teleostean ortholog of mammalian SF-1—and marks the ontogeny of steroidogenic interrenal tissue [16,17]. Embryos were examined for expression of Fn and pFak (Figure 4). The elimination of blood flow by *tnnt2a*MO injection (Figure 4B–B'') or 6 mM 2,3-BDM treatment (Figure 4C–C'') did not diminish Fn accumulation in the interrenal microenvironment (Figure 4D). However, Fn was

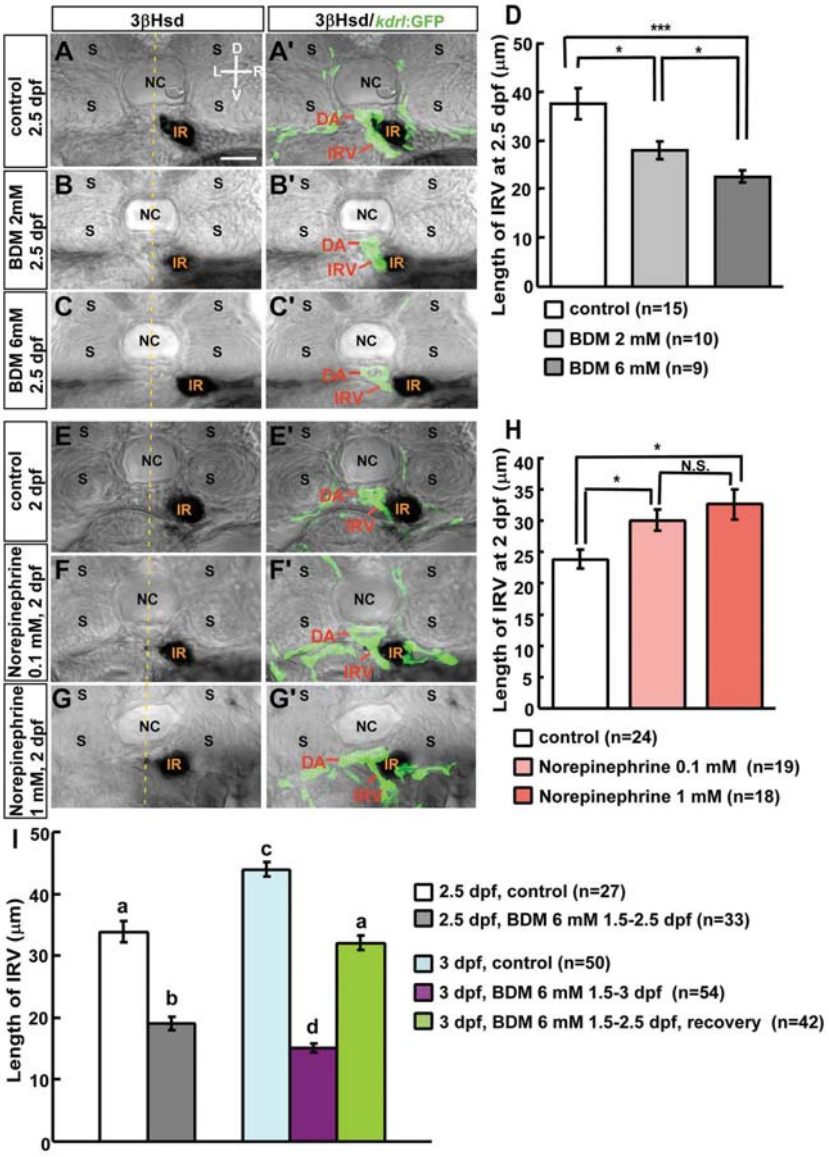

Figure 3. Effects of 2,3-BDM and norepinephrine on IRV formation. For repression of blood flow, *Tg(kdrl: GFP)*^{s843} embryos were treated with (A–A′) vehicle (control), or 2,3-BDM at a concentration of (B–B′) 2 mM or (C–C′) 6 mM from 1.5 dpf, and harvested at 2.5 dpf. For acceleration of blood flow, *Tg(kdrl: GFP)*^{s843} embryos were treated with (E-E′) vehicle (control), or norepinephrine at a concentration of (F–F′) 0.1 mM or (G-G′) 1 mM from 33 hpf, and harvested at 2 dpf. Transverse sections of harvested embryos were subject to analysis of 3β-Hsd activity (black) and GFP expression (green). IRV lengths of 2,3-BDM- or norepinephrine-treated embryos were quantified in (D) and (H), respectively; which were verified from confocal Z-stacks covering the full range of IRV growth, and measurements were made from single focal planes displaying the maximal range of ventrally extending IRV. *$P<0.05$, ***$P<0.0005$, N.S., not significant (Student's t-test). (I) Repressing effect of 2,3-BDM (6 mM) on IRV growth was reversible at 3 dpf, as the 2,3-BDM applied from 1.5 dpf was washed out at 2.5 dpf. The IRV length in recovered embryos at 3 dpf was not significantly different from that in control embryos at 2.5 dpf. Histograms with different letters above them are significantly different (ANOVA and Duncan's multiple test, $P<0.05$). D, dorsal; V, ventral; L, left; R, right. Abbreviations: interrenal tissue (IR), notochord (NC), somite (S). Scale bar, 25 μm.
doi:10.1371/journal.pone.0107997.g003

abnormally distributed, raising the possibility that in the absence of blood flow, the polymerization of Fn into fibrils was disrupted. To verify whether aberrant Fn deposition perturbed signaling events within the interrenal tissue, the localization of pFak—a downstream effector of Fn-Integrin signaling and an indicator of the dynamic reorganization of focal adhesions during cell migration—was examined (Figure 4A–C″). Indeed, pFak level within the interrenal tissue was significantly reduced compared to control embryos (Figure 4E), suggesting a disruption of Integrin-mediated signaling. In contrast, pFak distribution was readily detected at the somites, gut tube, and swim bladder in *tnnt2a* morphants (Figure 4B, B′) and 2,3-BDM-treated embryos (Figure 4C, C′). These results indicate that the interrenal microenvironment established during IRV angiogenesis is perturbed by reduced blood flow, resulting in the suppression of Fn-pFak signaling and steroidogenic cell migration.

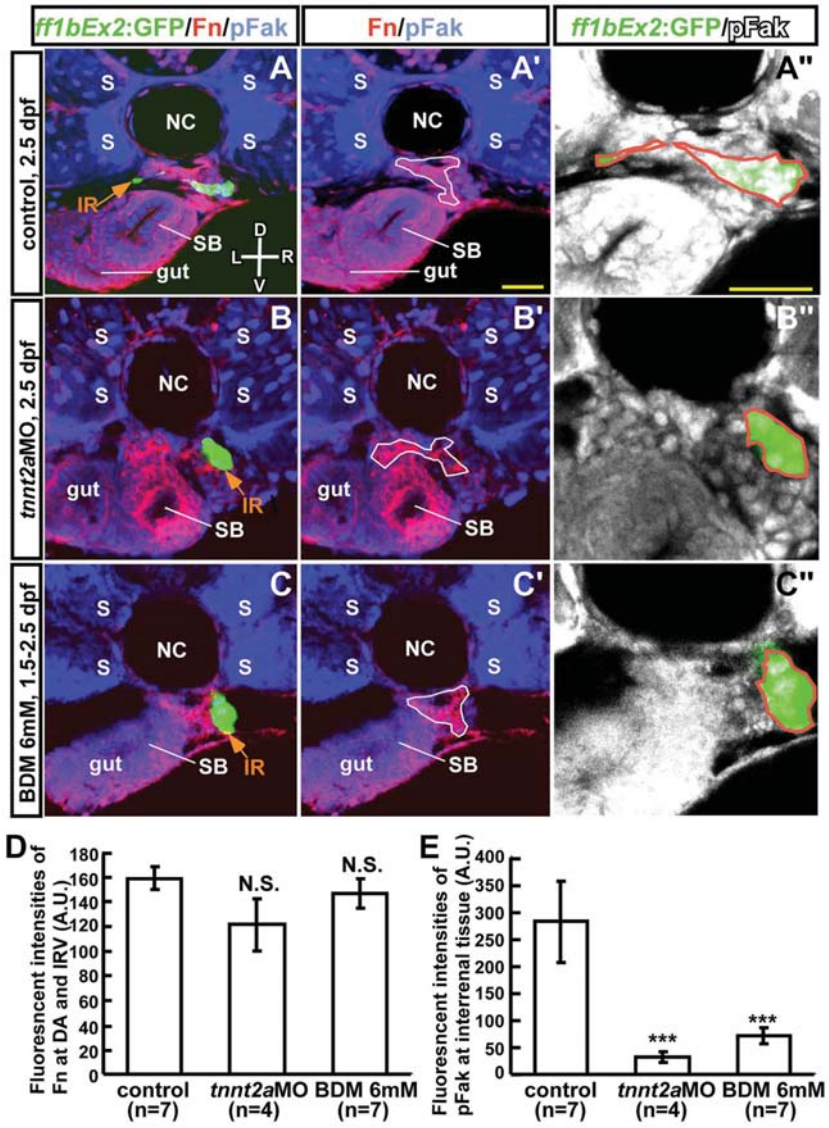

Figure 4. Effect of blood flow inhibition on the ECM microenvironment and pFak distribution in interrenal steroidogenic tissue. Transverse sections of *Tg(ff1bEx2: GFP)* embryos were (A–A″) uninjected (control), (B–B″) injected with *tnnt2a*MO, or (C–C″) treated with 6 mM 2,3-BDM from 1.5 dpf. Embryos were harvested at 2.5 dpf and assayed for expression of GFP (green), Fn (red), and pFak (blue in A–C and A′–C′; white in A″–C″). Images are single confocal planes showing the maximal transverse dimension of *ff1b*GFP-expressing steroidogenic tissue of a representative embryo, with magnified views shown in (A″–C″). (D) Fluorescence intensity of Fn in the DA and IRV selected as regions of interest (ROI; white lines in A′–C′) normalized to the size of the ROI. (E) Total fluorescence intensities of pFak within the steroidogenic tissue (ROI marked by orange lines in A″–C″) were normalized to the size of the cluster. The difference between the treatment and the control groups was analyzed by Student's t-test. ***$P<$ 0.001, N.S., not significant. D, dorsal; V, ventral; L, left; R, right. Abbreviations: arbitrary units (A.U.), interrenal tissue (IR), notochord (NC), somite (S), swim bladder (SB). Scale bar, 25 μm.
doi:10.1371/journal.pone.0107997.g004

Klf2a and MMP2 are Required for Migration, Angiogenesis, and Fn-pFak signaling in the interrenal tissue

To confirm whether hemodynamics, and not circulating factors, account for the effect of blood flow on steroidogenic tissue migration and angiogenesis, the role of Klf2a and MMP2 in interrenal morphogenesis was evaluated (Figure 5). While *Klf2a* deficiency leads to heart failure at 3 dpf [24], as evidenced by pericardial edema and venous pooling of blood around the yolk sac, a heart rate similar to that of control embryos is observed at 2 dpf [3]. In the present study, only mild cardiac edema was observed at 2.5 dpf, and circulation was unaffected, making it possible to evaluate the specific effect of hemodynamic forces on interrenal development at this stage. Consistent with the previous finding that primary vascular structures are not perturbed in the *klf2a* morphant [24], the axial vasculature was grossly normal in the peri-interrenal region at 2.5 dpf (Figure 5B'). However, the migration of steroidogenic cells was inhibited (Figure 5B, D), and IRV growth and directionality were perturbed (Figure 5F, H). In contrast to the *tnnt2a* morphant and 2,3-BDM-treated embryos in which the steroidogenic tissue and DA were not closely associated (Figure 3) [21], the interrenal tissue was proximal to the DA in the

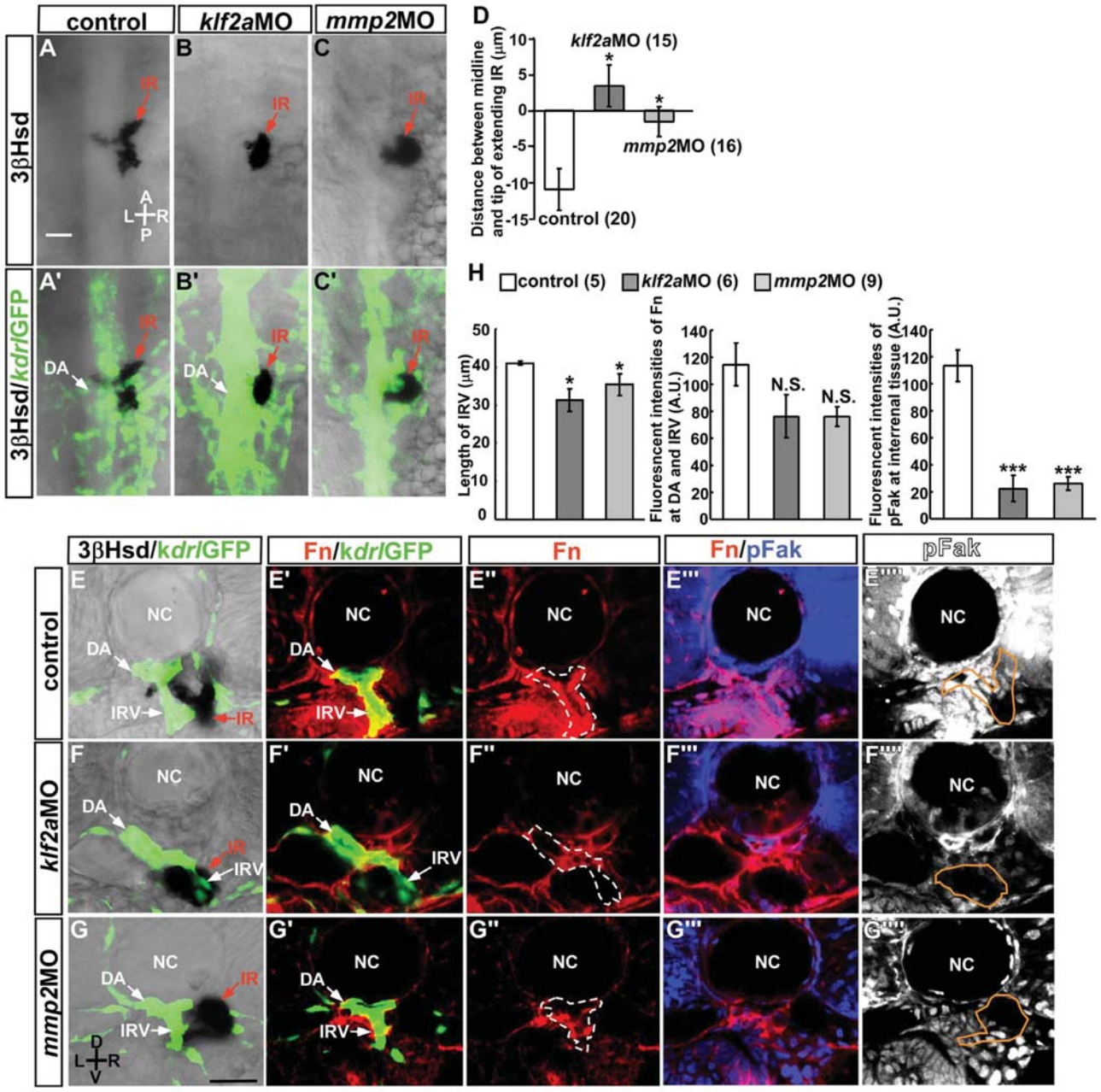

Figure 5. Suppression of interrenal tissue migration in *klf2a* and *mmp2* morphants. Dorsal view of interrenal steroidogenic tissue (IR, red arrows) as detected by 3β-Hsd activity staining, with adjacent vasculature marked by GFP expression. *Tg(kdrl: GFP)*^{s843} embryos were (A, A′) uninjected (control), or injected with (B, B′) *klf2a*MO or (C, C′) *mmp2*MO. (D) Quantification of the effects of MO-mediated gene knockdown on interrenal migration. The distance between the midline and the migrating tip of steroidogenic tissue was designated as positive if the migrating tip had not reached the midline and negative if it had crossed the midline. The number of embryos in each group is indicated in parentheses. The extent of interrenal medial extension of control 2.5-dpf embryos in panel 5D was not statistically different from those in Figure 2D and 2I. Fn and pFak expression in the interrenal region was examined in (E–E′′′′) uninjected (control), and (F–F′′′′) *klf2a*MO- and (G–G′′′′) *mmp2*MO-injected embryos by IHC. Images show transverse sections of a representative embryo from each treatment group. (H) Quantification of the effects of *klf2a*MO and *mmp2*MO on IRV growth, Fn level in the vicinity of the DA and IRV (ROI marked by broken lines in E′′–G′′), and pFak level in the steroidogenic tissue (ROI marked by orange lines in E′′′′–G′′′′). The number of embryos in each group is indicated in parentheses. Fluorescence intensities of Fn and pFak were normalized to their respective ROI sizes. The difference between the treatment and the control groups was analyzed by Student's t-test. $*P<0.05$, $***P<0.001$, N.S., not significant. A, anterior; P, posterior; L, left; R, right; D, dorsal; V, ventral. Abbreviations: notochord (NC). Scale bar, 25 μm.
doi:10.1371/journal.pone.0107997.g005

klf2a morphant. Despite these phenotypic differences between blood flow-deficient and *klf2a* morphant embryos, both types of embryos showed abnormal Fn distribution and reduced pFak level in the interrenal area (Figure 5F'–F'''', H).

Although blood flow regulates the generation of hematopoietic stem cells from the DA by a *klf2a-nitric oxide* (NO) pathway [49,50], steroidogenic interrenal tissue migration and angiogenesis were NO-independent (Figure S4). Treatment with the endothelial NO synthase inhibitor L-NAME from 1.5 to 2.5 dpf had no effect on interrenal tissue migration and angiogenesis, indicating that blood flow and Klf2a do not regulate interrenal morphogenesis through activation of NO signaling.

Embryos injected with 1.2 pmole *mmp2*MO had no major morphological abnormalities except for a kinked tail and mild (2%) reduction in heartbeat that did not cause any visible changes in blood flow. Nevertheless, morphants showed defects in migration, angiogenesis, and Fn-pFak signaling in the interrenal tissue (Figure 5C, D, G, H). This indicated that MMP2 activity may participate in the blood flow-regulated interrenal microenvironment. As observed upon *klf2a* knockdown, the steroidogenic tissue remained associated with both the DA and the IRV, suggesting that neither Klf2a nor MMP2 was essential for this association, which likely depends on other hemodynamically regulated molecules.

Medial Extension of the Interrenal Tissue Involves EMT-like Changes in Steroidogenic Cell Morphology that are Hemodynamically Regulated and pFak-Dependent

The interaction of cancerous epithelial cells with Fn *in vitro* promotes EMT [53,54]. The morphology of the interrenal steroidogenic tissue and the associated Fn-enriched microenvironment suggested that an EMT-like phenotypic change could occur during interrenal medial extension. An examination of interrenal tissue morphology by high resolution Nomarski microscopy revealed that while steroidogenic cells positive for 3β-Hsd activity formed a cluster to the right of the midline by 48 hpf (Figure 6A, B), protrusions were detected at 48 hpf that became more evident by 60 hpf (Figure 6C) and continuously spread across the midline until a bilobed structure was formed by 84 hpf (Figure 6E). During the morphogenetic movement, interrenal steroidogenic cells became more loosely associated with each other and demonstrated a mesenchymal-like phenotype with cell surface protrusions (Figure 6D, E). These morphological features likely reflected an EMT-like process during organ assembly.

To confirm whether interrenal steroidogenic cells undergo a transformation from epithelial to mesenchymal phenotypes, the expression of β-Catenin—a marker for adherent junctions in epithelial cells [55]—was examined. At 2 dpf, β-Catenin was clearly detected at cell-cell junctions of interrenal steroidogenic cells visible by GFP expression in *ff1bEx2: GFP* embryos (Figure 6F–F'), while at 2.5 dpf, β-Catenin was markedly reduced within the steroidogenic tissue cluster (Figure 6G–G'), reflecting the adoption of a mesenchymal-like character.

Since an EMT-like change occurred in steroidogenic cells during interrenal medial extension, the roles of hemodynamic forces and Fn-pFak signaling in this process was assessed. The accumulation of β-Catenin was observed in the interrenal tissue of blood flow-deficient embryos generated by *tnnt2a*MO microinjection (Figure 6H–H') or 6 mM 2,3-BDM treatment (Figure 6I–I'), providing evidence that blood flow induces an EMT-like change in steroidogenic cells. Since blood flow regulates interrenal medial migration via Fn-pFak signaling (Figure 4), Fn signaling was inhibited without perturbing blood flow to determine whether the EMT-like change in steroidogenic cells could be repressed. The RGD peptide, an antagonist of Fn, was applied to *Tg(ff1bEx2: GFP)* embryos at a concentration of 100 μM starting from 26 hpf, when circulation is initiated; in these embryos, junctional β-Catenin distribution was significantly higher than in controls at 2.5 dpf (Figure 6J–J', M). RGD effectively reduced pFak level in the interrenal area (Figure S5), thus suggesting that the inhibition of pFak signaling was responsible for the observed suppression of EMT-like changes in steroidogenic cells. Moreover, β-Catenin accumulation at cell-cell junctions was evident in both *klf2a* and *mmp2* morphants at 2.5 dpf (Figure 6K–K', L–L', M) as compared to the control embryo.

Consistent with the results of β-Catenin expression, immunohistochemial analysis of E-cadherin, a central component of cell-cell adhesion junction which is required for the formation of epithelia [56,57], detected a clear epithelial phenotype of the interrenal tissue at 2 dpf (Figure S6A, A'). At 2.5 dpf, the E-cadherin expression was reduced at the interrenal tissue where a migratory phenotype was manifested (Figure S6B, B'). In contrast, junctional E-cadherin distribution at the interrenal tissue was not reduced in 2.5 dpf embryos where interrenal medial migration was suppressed by a disruption of either circulation (Figure S6C, C') or pFak-mediated signaling (Figure S6D, D'), or hemodynamics-regulated molecules (Figure S6E, E', F, F'). It was noted that RGD-treated embryos and *mmp2* morphants at 2.5 dpf displayed a higher expression level of junctional E-cadherin than control embryos at 2 dpf did (Figure S6G), with the underlying mechanism remaining unclear. Nevertheless, the immunohistochemistry results of β-Catenin and E-cadherin both indicated a clear reduction of epithelial nature at the interrenal tissue from 2 to 2.5 dpf. Moreover, mesenchymal phenotype of the interrenal tissue at 2.5 dpf correlated well with a rise of Vimentin expression in the *ff1b*-expressing steroidogenic cells (Figure S7A, A', B, B'). Vimentin, a type III intermediate filament protein and a widely used mesenchymal marker, plays a predominant role for inducing changes in cell shape, adhesion and motility during the EMT [58,59]. In contrast to the reduction of β-Catenin and E-cadherin during interrenal medial extension, the Vimentin expresison is significantly increased from 2 to 2.5 dpf, and this accumulation of Vimentin was not detected in embryos deficient in either blood flow (Figure S7C, C') or pFak signaling (Figure S6D, D'), or hemodynamic transducers (Figure S7E, E', F, F'). Therefore, an inverse correlation between epithelial and mesenchymal markers was observed during interrenal medial expression. Taken together, these results indicate that blood flow, through mechanotransduction and Fn-pFak signaling, promotes EMT-like changes in steroidogenic cells during interrenal organ assembly.

Migration of Differentiated Chromaffin Cells Requires Blood Flow but is Independent of Mechanotransduction and Fn-Mediated Signaling

To determine whether blood flow also regulates the development of the chromaffin cell lineage, ISH was performed to detect transcript expression of *ff1b* and *dβh*, markers for steroidogenic and chromaffin cell lineages, respectively (Figure 7). Consistent with the findings of our earlier study [19], the integration of the two cell populations was detected as early as 36 hpf (Figure 7A–A'), and was not affected in *tnnt2a* morphants (Figure 7B–B'), while interrenal medial migration and organ assembly were observed at 56 hpf and 3 dpf (Figure 7C–C', E–E'), respectively. Since the medial extension of steroidogenic tissue was inhibited in *tnnt2a* morphants, chromaffin cells that reached the interrenal region remained closely associated with steroidogenic cells, and were located to the right of the midline (Figure 7D–D', F–F'). While the convergence of differentiated chromaffin cells colonizing

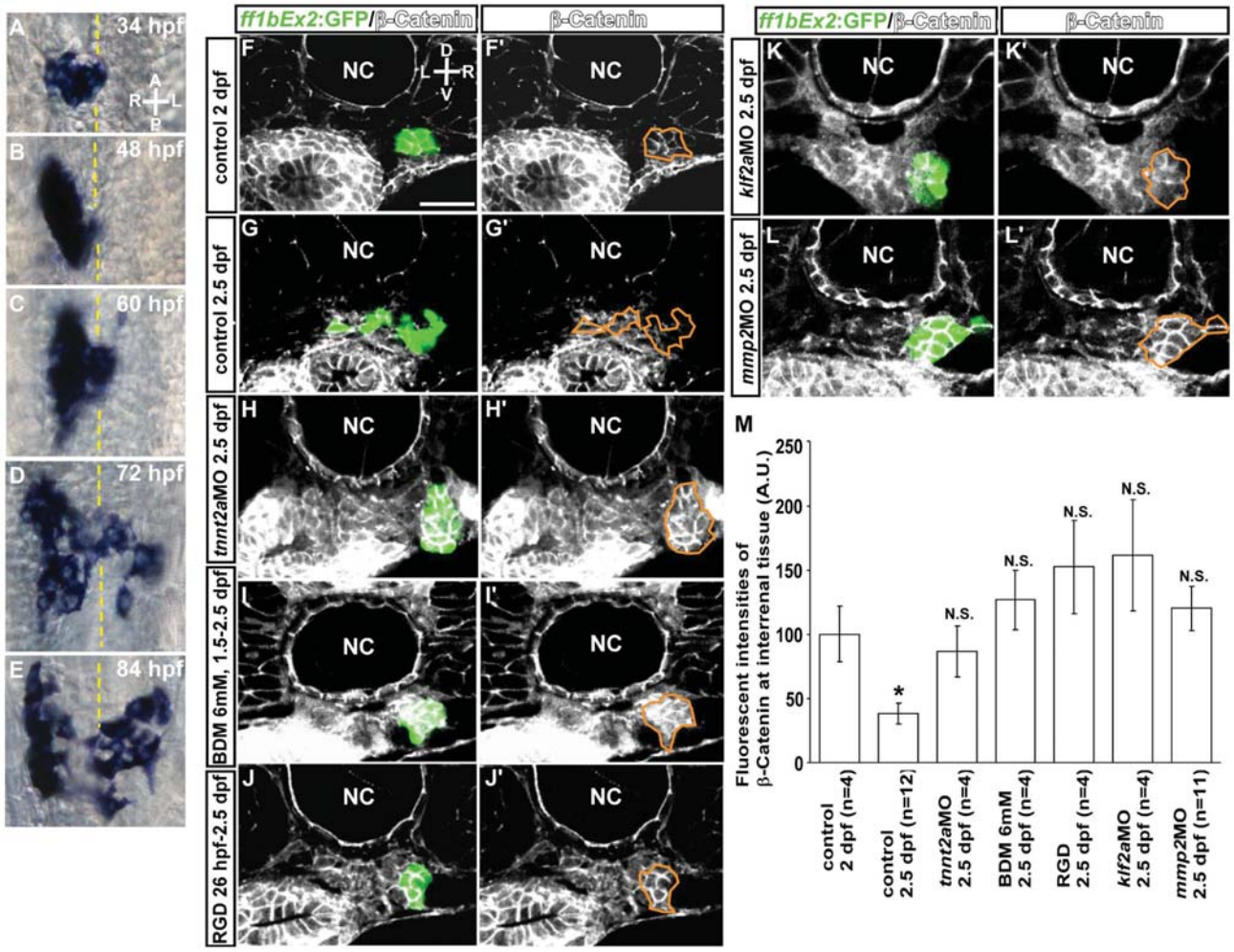

Figure 6. Steroidogenic cells are induced to undergo an EMT-like change by hemodynamic forces and pFak signaling. (A–E) Ventral view of the midtrunk from 34 to 84 hpf; steroidogenic cells become loosely associated and develop protrusions at the cell surface. The accumulation of β-Catenin at cell-cell junctions in the steroidogenic tissue can be seen in cross sections of *Tg(ff1bEx2: GFP)* embryos (F, F') 2 dpf, but not at (G, G') 2.5 dpf. The decrease in junctional β-Catenin was not observed in (H, H') *tnnt2a* morphants, (I, I') 2,3-BDM- or (J, J') RGD-treated embryos, or (K, K') *klf2a* or (L, L') *mmp2* morphants. Sections are shown of a representative embryo from each treatment group. (M) Fluorescence intensity of β-Catenin in *ff1b*GFP-expressing steroidogenic tissue (ROI marked by orange lines) is normalized to the size of the cluster, with the number of embryos indicated in parentheses. The difference between 2-dpf control group and any of the other groups was analyzed by Student's t-test. *$P<0.05$, N.S., not significant. A, anterior; P, posterior; L, left; R, right; D, dorsal; V, ventral. Broken yellow lines indicate position of the midline. Abbreviations: notochord (NC). Scale bar, 25 μm.
doi:10.1371/journal.pone.0107997.g006

the interrenal organ was completed by 3 dpf in wild-type embryos (Figure 7E'), clusters of differentiated chromaffin cells were located outside the interrenal region in *tnnt2a* morphants (Figure 7F–F'), apparently due to the unsuccessful migration of chromaffin cells, indicating that although they are still capable of interacting with steroidogenic cells, their migration is defective in blood flow-deficient embryos, leading to an incomplete assembly of the interrenal organ.

Interestingly, while blood flow was required, mechanotransduction and Fn-pFak signaling were dispensable for chromaffin cell migration. Embryos injected with *klf2a*MO or *mmp2*MO, or treated with 100 μM RGD starting from 26 hpf, had defective medial migration of *ff1b*-expressing cells but normal convergence of chromaffin cells at the midline (Figure 7G–I, G'–I'), resulting in only partial integration of the two cell lineages. This implies that the migration of steroidogenic and chromaffin cells are differentially modulated by blood flow.

Discussion

The results of this study indicate that in addition to supplying steroids and maintaining tissue homeostasis, blood flow ensures maximal interaction between steroidogenic and chromaffin cells in teleosts (Figure 8). During interrenal organ assembly, hemodynamic forces pattern the vascular microenvironment and regulate the morphology of steroidogenic cells and the associated angiogenic endothelium. The data presented here illustrate a mechanism by which an EMT-like process and tissue-tissue interactions can be modulated by blood flow. A disruption of the vascular microenvironment or mechanotransduction perturbs steroidogenic tissue morphogenesis but not chromaffin cell migration,

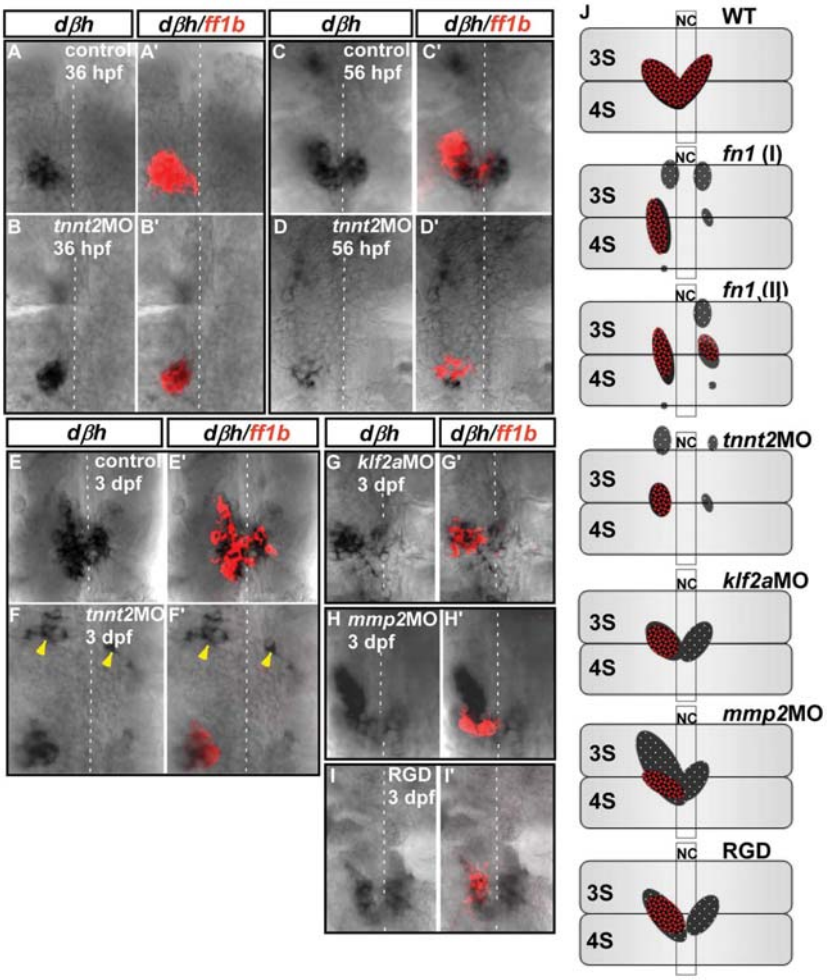

Figure 7. Interaction between interrenal steroidogenic and chromaffin cells in *tnnt2a*, *klf2a*, and *mmp2* morphants and RGD-treated embryos during interrenal gland assembly. Double ISH assays showing colocalization of *ff1b* (red) and *dbh* (black) transcripts in uninjected control embryos and *tnnt2a* morphants at (A, A'; B, B') 36 hpf (n = 3 and 6, respectively), (C, C'; D, D') 56 hpf (n = 3 and 5, respectively), and (E, E'; F, F') 3 dpf (n = 17 and 15, respectively), and in (G, G') *klf2a* (n = 9) and (H, H') *mmp2* (n = 8) morphants and (I, I') RGD-treated embryos (n = 18) at 3 dpf. Ventral flat mount views are shown for representative embryos in each group, oriented with anterior at the top. Yellow arrowheads indicate chromaffin cell clusters that failed to converge at the interrenal area in *tnnt2a* morphants. Broken white lines indicate position of the midline. (J) Schematic representation of various phenotypic defects associated with interrenal organ assembly. Panels show ventral views of wild-type, mutant, morphant, and drug-treated embryos at 3 dpf, oriented with anterior at the top. Phenotypes depicted for *cloche* (*clo*) and *fn1* mutants are based on previous reports [9,21]. Abbreviations: notochord (NC), the third somite (3S), the fourth somite (4S).
doi:10.1371/journal.pone.0107997.g007

indicating that blood flow regulates these processes through different pathways.

The obstruction of blood flow in the zebrafish embryo produced a phenotype similar to that of the *fn1* mutant [19] (Figure 7), providing evidence that the interrenal Fn-enriched microenvironment is regulated by hemodynamic forces (Figure 4). However, while blood flow-deficient embryos have similar defects in steroidogenic and chromaffin cell migration, 20%–30% of *fn1* mutants exhibit a more severe phenotype, where the bilateral fusion of early interrenal tissues is unsuccessful (Figure 7). The variable expressivity of this phenotype in *fn1* mutants could be due to a more profound effect of Fn deficiency on early development prior to the onset of blood flow [41,60]. Indeed, early bilateral interrenal tissues arise in close association with pre-vascular angioblasts, and their fusion occurs in parallel with the assembly of axial vasculature independently of the initiation of blood flow [9,52].

The phenotype of the RGD-treated embryo—that is, defective migration of steroidogenic but not chromaffin cells—was different from that of the *fn1* mutant, in which the migration of both cell types was compromised (Figs. 7 and 8). Fn regulates the fusion of bilateral cardiac primordia, and is therefore essential for the development of myocardial epithelia [41]; thus, *fn1* mutants have impaired cardiac function and consequently, reduced blood flow, which may cause the aberrant migration of chromaffin cells. Nevertheless, these cell clusters in *fn1* mutants were more dispersed than in *tnnt2a* morphants (Figure 7J), suggesting that the presence of Fn ensures that the microenvironment stimulates chromaffin cell migration prior to the onset of circulation. Trunk neural crest cells, from which the sympathochromaffin lineage is derived, migrate along the medial surface of each somite but not the somite boundary where Fn accumulates [60,61]. However, disrupted somite formation in the *fn1* mutant leads to the uncoupling of slow- and fast-twitch muscle fibers, and hence a

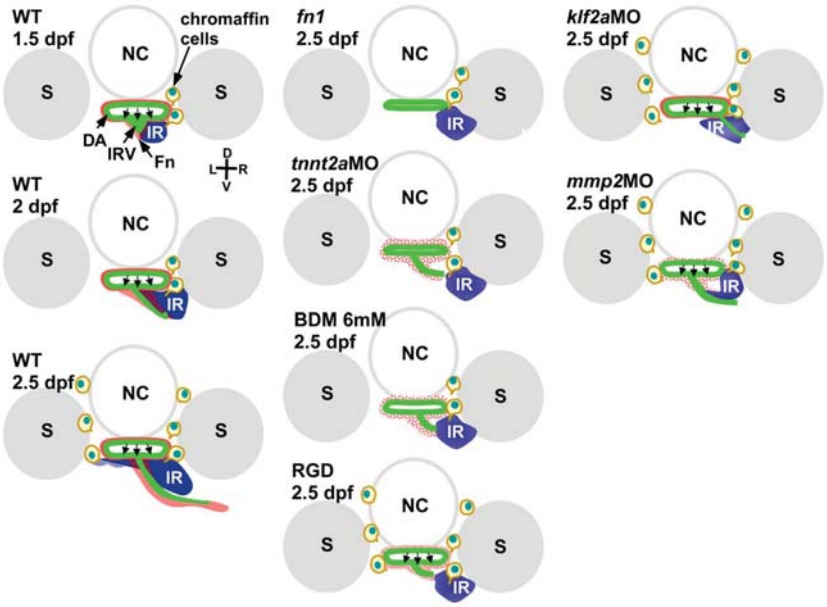

Figure 8. Schematic representation of interrenal steroidogenic tissue (IR) and chromaffin cell integration that takes place in the vicinity of the DA and extending IRV. An Fn-enriched microenvironment promotes medial extension of the steroidogenic tissue and culminates in steroidogenic-chromaffin interactions on both sides of the midline (left); various defects in extension lead to incomplete assembly of the interrenal organ (middle and right). D, dorsal; V, ventral; L, left; R, right. Abbreviations: notochord (NC). Somite (S).
doi:10.1371/journal.pone.0107997.g008

disorganized myofibril pattern [62], which is another factor that could compromise chromaffin cell migration. In contrast, the RGD-treatment in this study was initiated at 26 hpf without evident perturbation of cardiac flow and somite morphology, which might explain why chomaffin cells migrate normally in RGD-treated embryos.

EMT is initiated by transforming, fibroblast, epithelial, and hepatocyte growth factors as well as the oncogene Harvey rat sarcoma. During this process, there is a downregulation of epithelial and concomitant upregulation of mesenchymal markers, while cells assume a proliferative and migratory character [35]. EMT is similar to the endothelial-to-mesenchymal transition (EnMT), a critical step in vertebrate heart development in which endothelial endocardial cells give rise to heart cushion cells that form the mesenchymal portion of septa and valves [63]. In various vertebrate models including zebrafish, alterations in hemodynamic forces during cardiogenesis have profound effects on cardiac septation and valvulogenesis [3,4,46,64], suggesting that EnMT is regulated by hemodynamics. The present study underscores a novel role for hemodynamics in the EMT-like behavior of vessel-associated endocrine cells via modulation of the vascular microenvironment and Fn-pFak signaling.

In addition to being an epithelial cell marker, β-Catenin also transduces canonical Wnt signals and is implicated in cell proliferation [65]. Cytoplasmic β-Catenin is stabilized upon activation of Wnt signaling, leading to its translocation to the nucleus, where it interacts with T-cell factors (TCFs) to stimulate the transcription of target genes. There was no obvious enrichment of nuclear β-Catenin detected in steroidogenic cells during interrenal organ assembly (Figure 6), and it is possible that canonical Wnt signaling is not involved in zebrafish interrenal development. Nevertheless, Wnt4 can inhibit β-Catenin/TCF signaling by redirecting nuclear β-Catenin to the membrane [66]. During mammalian sex differentiation, Wnt4 inhibits the migration of endothelial and steroidogenic cells into the female gonad [67], and is also expressed in the outermost region of the adrenal cortex, where it may play a role in migration events that segregate adrenal and gonadal lineages during early development [68]. It therefore remains to be explored whether Wnt signals are directly or indirectly regulated by hemodynamic forces and thereby guide cell migration during interrenal organ assembly.

It will be of interest to explore whether other morphogens participate in the interrenal organogenesis. Pregnenolone, a steroid produced from cholesterol by the steroidogenic enzyme Cyp11a1, promotes cell migration by activating CLIP-170 and stabilizing microtubules [69,70]. The function of pregnenolone for cell movement has been well studied in the zebrafish gastrulation which is well before the onset of blood flow as well as interrenal organogenesis. While *cyp11a1* is expressed at the zebrafish interrenal tissue by 1 dpf [18], it remains unclear whether pregnelolone would also form a morphogen gradient during the interrenal morphogenetic movement. On the other hand, the molecular and cellular mechanisms by which blood flow regulates chromaffin cell migration remain to be explored. In the blood flow-deficient zebrafish embryo, the expression of endothelial CXCR4a is upregulated during collateral formation [71]. CXCR4a is the G protein-coupled receptor for the chemokine stromal cell-derived factor 1 (SDF-1). SDF-1, along with Bone Morphogenetic Proteins (BMPs) and Neuregulin 1 of the epidermal growth factor family, are the three groups of paracrine factors that participate in the generation of sympatho-adrenal progenitors from the neural crest [12,72,73,74]. BMPs are produced by the DA and are critical for the production of SDF-1 and Neuregulin 1 in the vicinity of the DA, while SDF-1 and Neuregulin 1 function as chemoattractants for the migration of neural crest cells [15]. It will therefore be intriguing to examine whether a loss of blood flow would influence the activity of SDF-1 through upregulating CXCR4a expression.

Supporting Information

Figure S1 Effect of norepinephrine on the heart beat of zebrafish. Norepinephrine treatments resulted in a dose-dependent increase of heart rate at 33 hpf. The difference between groups treated with various concentrations of norepinephrine was analyzed by Student's t-test. *$P<0.05$, ***$P<0.0005$.
(TIF)

Figure S2 Interrenal cell migration suppressed by 2,3-BDM was recovered following the removal of 2,3-BDM. The interrenl tissue stained by 3β-Hsd activity assay in the control *Tg(kdrl: GFP)*^{s843} embryo continued to extend across the midline from 2.5 dpf (A-A'') to 3 dpf (C-C''), while migration of interrenal cells was repressed by 2,3-BDM treatment at 6 mM from 1.5 to 2.5 dpf (B-B'') or 3 dpf (D-D''). Migration of interrenal cells was recovered at 3 dpf as 2,3-BDM was washed out at 2.5 dpf (E-E''). Protrusions of extending interrenal tissues (red arrows) were detected in control as well as recovered embryos. Broken white lines indicate position of the midline. Abbreviations: glomerulus (G), posterior cardinal vein (PCV). Scale bar, 50 μm.
(TIF)

Figure S3 Effects of blood flow inhibition on IRV growth was reversible following the removal of 2,3-BDM. The IRV in the control *Tg(kdrl: GFP)*^{s843} embryo continued to extend from 2.5 dpf (A, A') to 3 dpf (C, C'), while the IRV growth was repressed by 2,3-BDM treatment at 6 mM from 1.5 to 2.5 dpf (B, B') or 3 dpf (D, D'). Extension of IRV was recovered at 3 dpf as 2,3-BDM was washed out at 2.5 dpf (E, E'). The interrenal tissue (IR) was detected by 3β-Hsd acitivity assay. D, dorsal; V, ventral; L, left; R, right. Broken yellow lines indicate position of the midline. Abbreviations: notochord (NC), somite (S). Scale bar, 50 μm.
(TIF)

Figure S4 Effect of L-NAME on morphogenetic movements of interrenal steroidogenic tissue and IRV formation. (A–A'') *Tg(kdrl: GFP)*^{s843} embryos treated with 100 μM L-NAME from 1.5 dpf onwards had interrenal steroidogenic tissue (IR) morphology (orange arrows) and (B–B'') IRV length similar to control embryos (Figure 3A, A', D) at 2.5 dpf (n = 8). The activity of endothelial NO synthase was inhibited by L-NAME at concentrations higher than 10 μM [50]. D, dorsal; V, ventral; L, left; R, right. Abbreviations: posterior cardinal vein (PCV). Scale bar, 50 μm.
(TIF)

Figure S5 Effect of RGD treatment on pFAK distribution in the interrenal region. Transverse sections of *Tg(kdrl: GFP)*^{s843} embryos either untreated (control; n = 6) or treated with 100 μM RGD peptide (n = 10) from 26 hpf and harvested at 2.5 dpf for evaluation of 3β-Hsd activity and pFak level by IHC. Sections are shown of a representative embryo from each group, oriented with the dorsal side at the top. Abbreviations: interrenal tissue (IR), notochord (NC), somite (S).
(TIF)

Figure S6 Steroidogenic cells display a decrease of E-cadherin expression which is induced by hemodynamic forces and pFak signaling. E-cadherin in the fluorescent steroidogenic tissue of *Tg(ff1bEx2: GFP)* embryos was decreased from 2 dpf (A-A') to 2.5 dpf (B-B'). The decrease in E-cadherin was not observed in (C, C') *tnnt2a* morphants, (D, D') RGD-treated embryos, or (E, E') *klf2a* or (F, F') *mmp2* morphants. Sections are shown of a representative embryo from each treatment group. (F) Fluorescence intensity of E-cadherin in *ff1b*GFP-expressing steroidogenic tissue is normalized to the size of the cluster, with the number of embryos indicated in parentheses. The difference between 2-dpf control group and any of the other groups was analyzed by Student's t-test. *$P<0.05$, **$P<0.005$, N.S., not significant. D, dorsal; V, ventral; L, left; R, right. Abbreviations: notochord (NC). Scale bar, 25 μm.
(TIF)

Figure S7 Steroidogenic cells display a rise of Vimentin expression which is induced by hemodynamic forces and pFak signaling. Vimentin in the steroidogenic tissue (marked by green fluorescence) of *Tg(ff1bEx2: GFP)* embryos was increased from 2 dpf (A-A') to 2.5 dpf (B-B'). The increase in Vimentin was not observed in (C, C') *tnnt2a* morphants, (D, D') RGD-treated embryos, or (E, E') *klf2a* or (F, F') *mmp2* morphants. Sections are shown of a representative embryo from each treatment group. (G) Fluorescence intensity of Vimentin in *ff1b*GFP-expressing steroidogenic tissue (ROI marked by orange lines) is normalized to the size of the cluster, with the number of embryos indicated in parentheses. The difference between 2-dpf control group and any of the other groups was analyzed by Student's t-test. **$P<0.005$, N.S., not significant. D, dorsal; V, ventral; L, left; R, right. Abbreviations: notochord (NC). Scale bar, 25 μm.
(TIF)

Video S1 Complete blockage of blood flow in the posterior cardinal vein of a 36-hpf embryo treated with 6 mM 2,3-BDM.
(WMV)

Video S2 Normal blood flow in the posterior cardinal vein of a wild-type 36-hpf embryo.
(WMV)

Video S3 Partial reduction in blood flow in the posterior cardinal vein of a 36-hpf embryo treated with 2 mM 2,3-BDM.
(WMV)

Acknowledgments

The authors would like to thank Dr. Christoph Englert, Dr. Woon-Khiong Chan, and Prof. Didier Stainier for generously providing the zebrafish strains; Ru Shiangli, Jamie Lin, Yang Huang, Yusyuan Tian, Kuan-Chieh Wang and Hsin-Yu Hou for excellent technical assistance; Dr. Yi-Ching Lin for helpful advice on statistical analysis; and the Taiwan Zebrafish Core Facility, Zebrafish Core in Academia Sinica, and Zebrafish Core Facility at NTHU-NHRI (ZeTH) for assistance with fish culturing.

Author Contributions

Conceived and designed the experiments: YWL. Performed the experiments: CWC YLZ ZYJ YWL. Analyzed the data: CWC YLZ ZYJ YWL. Wrote the paper: YWL.

References

1. Culver JC, Dickinson ME (2010) The effects of hemodynamic force on embryonic development. Microcirculation 17: 164–178.
2. Pelster B, Burggren WW (1996) Disruption of hemoglobin oxygen transport does not impact oxygen-dependent physiological processes in developing embryos of zebra fish (Danio rerio). Circ Res 79: 358–362.
3. Vermot J, Forouhar AS, Liebling M, Wu D, Plummer D, et al. (2009) Reversing blood flows act through klf2a to ensure normal valvulogenesis in the developing heart. PLoS Biol 7: e1000246.

4. Hove JR, Koster RW, Forouhar AS, Acevedo-Bolton G, Fraser SE, et al. (2003) Intracardiac fluid forces are an essential epigenetic factor for embryonic cardiogenesis. Nature 421: 172–177.
5. Serluca FC, Drummond IA, Fishman MC (2002) Endothelial signaling in kidney morphogenesis: a role for hemodynamic forces. Curr Biol 12: 492–497.
6. Banjo T, Grajcarek J, Yoshino D, Osada H, Miyasaka KY, et al. (2013) Haemodynamically dependent valvulogenesis of zebrafish heart is mediated by flow-dependent expression of miR-21. Nat Commun 4: 1978.
7. Field HA, Dong PD, Beis D, Stainier DY (2003) Formation of the digestive system in zebrafish. II. Pancreas morphogenesis. Dev Biol 261: 197–208.
8. Field HA, Ober EA, Roeser T, Stainier DY (2003) Formation of the digestive system in zebrafish. I. Liver morphogenesis. Dev Biol 253: 279–290.
9. Liu YW, Guo L (2006) Endothelium is required for the promotion of interrenal morphogenetic movement during early zebrafish development. Dev Biol 297: 44–58.
10. Opitz R, Maquet E, Huisken J, Antonica F, Trubiroha A, et al. (2012) Transgenic zebrafish illuminate the dynamics of thyroid morphogenesis and its relationship to cardiovascular development. Dev Biol 372: 203–216.
11. Alt B, Elsalini OA, Schrumpf P, Haufs N, Lawson ND, et al. (2006) Arteries define the position of the thyroid gland during its developmental relocalisation. Development 133: 3797–3804.
12. Huber K (2006) The sympathoadrenal cell lineage: specification, diversification, and new perspectives. Dev Biol 298: 335–343.
13. Gut P, Huber K, Lohr J, Bruhl B, Oberle S, et al. (2005) Lack of an adrenal cortex in Sf1 mutant mice is compatible with the generation and differentiation of chromaffin cells. Development 132: 4611–4619.
14. Zubair M, Oka S, Parker KL, Morohashi K (2009) Transgenic expression of Ad4BP/SF-1 in fetal adrenal progenitor cells leads to ectopic adrenal formation. Mol Endocrinol 23: 1657–1667.
15. Saito D, Takase Y, Murai H, Takahashi Y (2012) The dorsal aorta initiates a molecular cascade that instructs sympatho-adrenal specification. Science 336: 1578–1581.
16. Hsu HJ, Lin G, Chung BC (2003) Parallel early development of zebrafish interrenal glands and pronephros: differential control by wt1 and ff1b. Development 130: 2107–2116.
17. Chai C, Liu YW, Chan WK (2003) Ff1b is required for the development of steroidogenic component of the zebrafish interrenal organ. Dev Biol 260: 226–244.
18. To TT, Hahner S, Nica G, Rohr KB, Hammerschmidt M, et al. (2007) Pituitary-interrenal interaction in zebrafish interrenal organ development. Mol Endocrinol 21: 472–485.
19. Chou CW, Chiu CH, Liu YW (2013) Fibronectin mediates correct positioning of the interrenal organ in zebrafish. Dev Dyn 242: 432–443.
20. Alsop D, Vijayan MM (2009) Molecular programming of the corticosteroid stress axis during zebrafish development. Comp Biochem Physiol A Mol Integr Physiol 153: 49–54.
21. Chiu CH, Chou CW, Takada S, Liu YW (2012) Development and fibronectin signaling requirements of the zebrafish interrenal vessel. PLoS One 7: e43040.
22. Parmar KM, Larman HB, Dai G, Zhang Y, Wang ET, et al. (2006) Integration of flow-dependent endothelial phenotypes by Kruppel-like factor 2. J Clin Invest 116: 49–58.
23. Dekker RJ, van Thienen JV, Rohlena J, de Jager SC, Elderkamp YW, et al. (2005) Endothelial KLF2 links local arterial shear stress levels to the expression of vascular tone-regulating genes. Am J Pathol 167: 609–618.
24. Lee JS, Yu Q, Shin JT, Sebzda E, Bertozzi C, et al. (2006) Klf2 is an essential regulator of vascular hemodynamic forces in vivo. Dev Cell 11: 845–857.
25. Page-McCaw A, Ewald AJ, Werb Z (2007) Matrix metalloproteinases and the regulation of tissue remodelling. Nat Rev Mol Cell Biol 8: 221–233.
26. Yasuda T, Kondo S, Homma T, Harris RC (1996) Regulation of extracellular matrix by mechanical stress in rat glomerular mesangial cells. J Clin Invest 98: 1991–2000.
27. Singhal PC, Sagar S, Garg P (1996) Simulated glomerular pressure modulates mesangial cell 72 kDa metalloproteinase activity. Connect Tissue Res 33: 257–263.
28. Cummins PM, von Offenberg Sweeney N, Killeen MT, Birney YA, Redmond EM, et al. (2007) Cyclic strain-mediated matrix metalloproteinase regulation within the vascular endothelium: a force to be reckoned with. Am J Physiol Heart Circ Physiol. pp. H28–42.
29. von Offenberg Sweeney N, Cummins PM, Birney YA, Cullen JP, Redmond EM, et al. (2004) Cyclic strain-mediated regulation of endothelial matrix metalloproteinase-2 expression and activity. Cardiovasc Res 63: 625–634.
30. Xu J, Rodriguez D, Petitclerc E, Kim JJ, Hangai M, et al. (2001) Proteolytic exposure of a cryptic site within collagen type IV is required for angiogenesis and tumor growth in vivo. J Cell Biol 154: 1069–1079.
31. Kenny HA, Kaur S, Coussens LM, Lengyel E (2008) The initial steps of ovarian cancer cell metastasis are mediated by MMP-2 cleavage of vitronectin and fibronectin. J Clin Invest 118: 1367–1379.
32. Corti P, Young S, Chen CY, Patrick MJ, Rochon ER, et al. (2011) Interaction between alk1 and blood flow in the development of arteriovenous malformations. Development 138: 1573–1582.
33. Santoro MM, Pesce G, Stainier DY (2009) Characterization of vascular mural cells during zebrafish development. Mech Dev 126: 638–649.
34. Miano JM, Georger MA, Rich A, De Mesy Bentley KL (2006) Ultrastructure of zebrafish dorsal aortic cells. Zebrafish 3: 455–463.
35. Acloque H, Adams MS, Fishwick K, Bronner-Fraser M, Nieto MA (2009) Epithelial-mesenchymal transitions: the importance of changing cell state in development and disease. J Clin Invest 119: 1438–1449.
36. Westerfield M (2000) The Zebrafish Book: Guide for the Laboratory Use of Zebrafish (Danio rerio). Eugene, OR.: Univ. of Oregon Press.
37. Kimmel CB, Ballard WW, Kimmel SR, Ullmann B, Schilling TF (1995) Stages of embryonic development of the zebrafish. Dev Dyn 203: 253–310.
38. Perner B, Englert C, Bollig F (2007) The Wilms tumor genes wt1a and wt1b control different steps during formation of the zebrafish pronephros. Dev Biol 309: 87–96.
39. Quek SI (2009) Molecular characterization of the zebrafish *ff1b* gene. Singapore: National University of Singapore.
40. Jin SW, Beis D, Mitchell T, Chen JN, Stainier DY (2005) Cellular and molecular analyses of vascular tube and lumen formation in zebrafish. Development 132: 5199–5209.
41. Trinh LA, Stainier DY (2004) Fibronectin regulates epithelial organization during myocardial migration in zebrafish. Dev Cell 6: 371–382.
42. Sehnert AJ, Huq A, Weinstein BM, Walker C, Fishman M, et al. (2002) Cardiac troponin T is essential in sarcomere assembly and cardiac contractility. Nat Genet 31: 106–110.
43. Nicoli S, Standley C, Walker P, Hurlstone A, Fogarty KE, et al. (2010) MicroRNA-mediated integration of haemodynamics and Vegf signalling during angiogenesis. Nature 464: 1196–1200.
44. Detry B, Erpicum C, Paupert J, Blacher S, Maillard C, et al. (2012) Matrix metalloproteinase-2 governs lymphatic vessel formation as an interstitial collagenase. Blood 119: 5048–5056.
45. Vasilyev A, Liu Y, Mudumana S, Mangos S, Lam PY, et al. (2009) Collective cell migration drives morphogenesis of the kidney nephron. PLoS Biol 7: e9.
46. Bartman T, Walsh EC, Wen KK, McKane M, Ren J, et al. (2004) Early myocardial function affects endocardial cushion development in zebrafish. PLoS Biol 2: E129.
47. Drummond IA, Majumdar A, Hentschel H, Elger M, Solnica-Krezel L, et al. (1998) Early development of the zebrafish pronephros and analysis of mutations affecting pronephric function. Development 125: 4655–4667.
48. Bollig F, Perner B, Besenbeck B, Kothe S, Ebert C, et al. (2009) A highly conserved retinoic acid responsive element controls wt1a expression in the zebrafish pronephros. Development 136: 2883–2892.
49. Wang L, Zhang P, Wei Y, Gao Y, Patient R, et al. (2011) A blood flow-dependent klf2a-NO signaling cascade is required for stabilization of hematopoietic stem cell programming in zebrafish embryos. Blood 118: 4102–4110.
50. North TE, Goessling W, Peeters M, Li P, Ceol C, et al. (2009) Hematopoietic stem cell development is dependent on blood flow. Cell 137: 736–748.
51. Watson O, Novodvorsky P, Gray C, Rothman AM, Lawrie A, et al. (2013) Blood flow suppresses vascular Notch signalling via dll4 and is required for angiogenesis in response to hypoxic signalling. Cardiovasc Res 100: 252–261.
52. Chou CW, Hsu HC, Quek SI, Chan WK, Liu YW (2010) Arterial and venous vessels are required for modulating developmental relocalization and laterality of the interrenal tissue in zebrafish. Dev Dyn 239: 1995–2004.
53. Park J, Schwarzbauer JE (2013) Mammary epithelial cell interactions with fibronectin stimulate epithelial-mesenchymal transition. Oncogene: doi: 10.1038/onc.2013.1118. [Epub ahead of print].
54. Sun XJ, Fa PP, Cui ZW, Xia Y, Sun L, et al. (2013) The EDA-containing cellular fibronectin induces epithelial mesenchymal transition in lung cancer cells through integrin alpha9beta1-mediated activation of PI3-K/Akt and Erk1/2. Carcinogenesis 35: 184–191.
55. Savagner P (2001) Leaving the neighborhood: molecular mechanisms involved during epithelial-mesenchymal transition. Bioessays 23: 912–923.
56. Cano A, Perez-Moreno MA, Rodrigo I, Locascio A, Blanco MJ, et al. (2000) The transcription factor snail controls epithelial-mesenchymal transitions by repressing E-cadherin expression. Nat Cell Biol 2: 76–83.
57. Moreno-Bueno G, Cubillo E, Sarrio D, Peinado H, Rodriguez-Pinilla SM, et al. (2006) Genetic profiling of epithelial cells expressing E-cadherin repressors reveals a distinct role for Snail, Slug, and E47 factors in epithelial-mesenchymal transition. Cancer Res 66: 9543–9556.
58. Mendez MG, Kojima S, Goldman RD (2010) Vimentin induces changes in cell shape, motility, and adhesion during the epithelial to mesenchymal transition. Faseb J 24: 1838–1851.
59. Vuoriluoto K, Haugen H, Kiviluoto S, Mpindi JP, Nevo J, et al. (2011) Vimentin regulates EMT induction by Slug and oncogenic H-Ras and migration by governing Axl expression in breast cancer. Oncogene 30: 1436–1448.
60. Koshida S, Kishimoto Y, Ustumi H, Shimizu T, Furutani-Seiki M, et al. (2005) Integrinalpha5-dependent fibronectin accumulation for maintenance of somite boundaries in zebrafish embryos. Dev Cell 8: 587–598.
61. Honjo Y, Eisen JS (2005) Slow muscle regulates the pattern of trunk neural crest migration in zebrafish. Development 132: 4461–4470.
62. Snow CJ, Peterson MT, Khalil A, Henry CA (2008) Muscle development is disrupted in zebrafish embryos deficient for fibronectin. Dev Dyn 237: 2542–2553.
63. Kovacic JC, Mercader N, Torres M, Boehm M, Fuster V (2012) Epithelial-to-mesenchymal and endothelial-to-mesenchymal transition: from cardiovascular development to disease. Circulation 125: 1795–1808.
64. Granados-Riveron JT, Brook JD (2012) The impact of mechanical forces in heart morphogenesis. Circ Cardiovasc Genet 5: 132–142.

65. Klaus A, Birchmeier W (2008) Wnt signalling and its impact on development and cancer. Nat Rev Cancer 8: 387–398.
66. Bernard P, Fleming A, Lacombe A, Harley VR, Vilain E (2008) Wnt4 inhibits beta-catenin/TCF signalling by redirecting beta-catenin to the cell membrane. Biol Cell 100: 167–177.
67. Jeays-Ward K, Hoyle C, Brennan J, Dandonneau M, Alldus G, et al. (2003) Endothelial and steroidogenic cell migration are regulated by WNT4 in the developing mammalian gonad. Development 130: 3663–3670.
68. Heikkila M, Peltoketo H, Leppaluoto J, Ilves M, Vuolteenaho O, et al. (2002) Wnt-4 deficiency alters mouse adrenal cortex function, reducing aldosterone production. Endocrinology 143: 4358–4365.
69. Weng JH, Liang MR, Chen CH, Tong SK, Huang TC, et al. (2013) Pregnenolone activates CLIP-170 to promote microtubule growth and cell migration. Nat Chem Biol 9: 636–642.
70. Hsu HJ, Liang MR, Chen CT, Chung BC (2006) Pregnenolone stabilizes microtubules and promotes zebrafish embryonic cell movement. Nature 439: 480–483.
71. Packham IM, Gray C, Heath PR, Hellewell PG, Ingham PW, et al. (2009) Microarray profiling reveals CXCR4a is downregulated by blood flow in vivo and mediates collateral formation in zebrafish embryos. Physiol Genomics 38: 319–327.
72. Kasemeier-Kulesa JC, McLennan R, Romine MH, Kulesa PM, Lefcort F (2010) CXCR4 controls ventral migration of sympathetic precursor cells. J Neurosci 30: 13078–13088.
73. Britsch S, Li L, Kirchhoff S, Theuring F, Brinkmann V, et al. (1998) The ErbB2 and ErbB3 receptors and their ligand, neuregulin-1, are essential for development of the sympathetic nervous system. Genes Dev 12: 1825–1836.
74. Shah NM, Groves AK, Anderson DJ (1996) Alternative neural crest cell fates are instructively promoted by TGFbeta superfamily members. Cell 85: 331–343.

RESEARCH ARTICLE

Fibronectin Mediates Correct Positioning of the Interrenal Organ in Zebrafish

Chih-Wei Chou, Chih-Hao Chiu, and Yi-Wen Liu*

ABSTRACT: Background: Fibronectin (Fn) forms a centripetal gradient during the fetal adrenal gland organogenesis, and modulates hormone responsiveness of adrenocortical cells in the primary culture. However, how Fn is involved in organ formation of the adrenal gland remains unclear. Results: In this study, we found that Fn accumulates around migrating *ff1b*-expressing interrenal cells, which were marked by the *ff1b* promoter-driven transgenic fluorescence, during the course of interrenal organ assembly. The interrenal cells displaying the migratory phenotype were absent in the *fn1* mutant, while specification and kidney association of the interrenal tissue remained normal. The Fn deposition in the interrenal microenvironment was severely reduced in the vessel-deficient *ets1b* morphant, implying its origin of synthesis from the peri-interrenal vasculature. In the *fn1* mutant, early-migrating chromaffin cells were capable of interacting with steroidogenic interrenal cells, yet continuous migration and midline convergence of chromaffin cells were disrupted. Migration defects of both interrenal and chromaffin lineages, in the absence of Fn, thus led to incomplete interrenal organ assembly in aberrant positions. Conclusions: Our results indicate that Fn is essential for patterning interrenal organ formation, by modulating the migratory behavior of both steroidogenic interrenal and chromaffin cells. *Developmental Dynamics 000:000–000, 2013.* © 2013 Wiley Periodicals, Inc.

Key words: zebrafish; adrenal; interrenal; steroidogenic; chromaffin; fibronectin

Key Findings:

- Fibronectin accumulates around migrating steroidogenic cells, which are detected by a steroidogenic cell-specific zebrafish transgenic line, during the course of interrenal organ assembly.
- Migration but not specification of steroidogenic interrenal cells is defective in the zebrafish *fibronectin* mutant.
- Fibronectin distribution in the zebrafish interrenal microenvironment is at least in part contributed by the neighboring vasculature.
- The assembly of zebrafish interrenal organ is aberrant in the absence of Fibronectin, due to migration defects of both steroidogenic and chromaffin cells.

Accepted 13 January 2013

INTRODUCTION

The teleostean interrenal gland is a functional counterpart of the mammalian adrenal gland, a crucial component of the hypothalamic-pituitary-adrenal axis. The adrenal gland is composed of the outer cortex, which produces steroid hormones in a zone-specific manner, and the inner medulla, which synthesizes catecholamines. Although lacking a highly organized zonal structure, the interrenal gland demonstrates conserved functional features as the major steroid-producing organ. Functional

Additional Supporting Information may be found in the online version of this article.

Department of Life Science, Tunghai University, Taichung, Taiwan, R.O.C

Contract grant sponsor: National Science Council (R.O.C.); Contract grant numbers: 96-2628-B-029-002-MY3; 99-2311-B-029-001; 99-2632-B-029-001-MY3; 100-2313-B-029-001; 100-2321-B-400-003; 101-2313-B-029-001.

***Correspondence to: Yi-Wen Liu, Department of Life Science, Tunghai University, No. 181, Sec. 3, Taichung-Port Road, Taichung, 40704, Taiwan R.O.C. E-mail: dlslys@thu.edu.tw**

DOI: 10.1002/dvdy.23932
Published online in Wiley Online Library (wileyonlinelibrary.com).

assembly of the interrenal gland is marked by the integration of steroidogenic interrenal tissue with chromaffin cells, the functional equivalent of adrenal medulla. In the zebrafish embryo, the integration between interrenal and chromaffin cells is evident by 3 days post-fertilization (dpf), when the fish embryo is able to physiologically respond to stress and secrete steroids (To et al., 2007; Alsop and Vijayan, 2009). It means that teleostean steroid function in the embryo is initiated concurrently with highly dynamic tissue–tissue interactions. Meanwhile, a hypothalamic-pituitary-interrenal axis develops and functions as early as assembly of the interrenal organ, which is essential for maintaining the growth and differentiation of interrenal steroidogenic cells. Hence, these temporally compressed events for zebrafish interrenal organogenesis might enable us to explore those molecular and cellular mechanisms that are conserved between mammals and teleosts.

In the zebrafish, the interrenal tissue is derived from the embryonic kidney (the pronephros) during the segmentation stage, and is segregated from the pronephric field by 30 hr post-fertilization (hpf). Both the kidney and the interrenal tissue arise as bilateral clusters across the midline, and converge at the midline in a coordinated fashion (Hsu et al., 2003; Liu, 2007). While central assembly of the pronephros requires the hemodynamic force (Serluca et al., 2002), medial fusion of bilateral primordial interrenal tissues is regulated by the interrenal-associated endothelium, possibly prior to vessel formation (Liu and Guo, 2006). Bilateral interrenal tissue clusters merged at the midline, and then relocalized to the right of the midline, with the relocalization event regulated by the adjacent axial artery and vein, which are under active assembly. As a result, the interrenal tissue from 28 hpf onwards is located to the right of the midline, and juxtaposed between the dorsal aorta (DA) and the right branch of the posterior cardinal vein. From about 2 dpf onwards, the interrenal cell cluster further extends medially across the midline, and becomes integrated with the chromaffin cells, which are derived from the trunk neural crest. The assembly of the interrenal organ is evident at 3 dpf by the intimate intermingling between interrenal and chromaffin cells. Intrinsic and extrinsic molecules that determine the interrenal cell migration during the process of interrenal organ assembly have remained unclear.

By using a fluorescent transgenic line driven by the promoter of nuclear receptor *ff1b*, the functional ortholog of adrenal 4 binding protein/steroidogenic factor 1 (Ad4BP/SF-1; officially designated NR5A1) as well as the key gene for specification and differentiation of the interrenal tissue (Chai et al., 2003; Hsu et al., 2003; Quek, 2009), we found in this study that interrenal cells appeared to display an active migratory phenotype during the stage of interrenal organ assembly. Interestingly, a rich enrichment of extracellular matrix protein Fn was deposited around migrating *ff1b*-expressing cells during the interrenal morphogenetic movement. Fn, a major adhesive molecule of the extracellular matrix, interacts with the Integrin receptor family to mediate a wide range of cellular processes including cytoskeletal organization, cell-substratum adhesion and spreading, and cell migration (Hynes, 1992; Astrof and Hynes, 2009). In the human fetal adrenal gland, Fn forms a centripetal gradient of accumulation, and is highly enriched at the fetal zone (Chamoux et al., 2001). Experiments on primary cultures derived from whole fetal adrenal glands have revealed that Fn orchestrates with other extracellular matrix components including Laminin and Collagen IV to modulate hormonal responsiveness, steroid secretion, and cell turnover (Chamoux et al., 2002a,b). On the other hand, the Fn distribution of the fetal adrenal gland appears highly parallel with the centripetal migration of fetal adrenocortical cells (Ishimoto and Jaffe, 2011). However, whether Fn participates in the fetal adrenal centripetal migration remains unknown. It is also unclear how the Fn accumulation in the fetal adrenal gland is regulated.

Studies performed on the zebrafish *fn1* mutant (*natter*) have revealed essential roles of Fn for the development of somites and the heart. Fn accumulates at the somite boundaries in an Integrinα5-dependent manner, and is required for maintenance but not specification of somite boundaries (Koshida et al., 2005). Fn is also detected around the myocardial precursors, and at the midline region between the endoderm and endocardial precursors (Trinh and Stainier, 2004). The peri-myocaridal Fn appears to be generated by the endothelium, and regulates epithelial organization for the migrating myocardial cells. We, therefore, hypothesized that the Fn deposition associated with steroidogenic interrenal cells might be essential for the interrenal morphogenetic movement, and hence implicating a role of Fn in the interrenal–chromaffin interaction. Therefore, we utilized the genetic *fn1* mutant to check whether the interrenal morphogenetic movements were perturbed in the absence of Fn. We found that the *fn1* mutant displayed a normal specification of the interrenal tissue, which was successfully segregated from and remained associated with the pronephros. However, defects of interrenal morphogenetic movements were exhibited in the *fn1* mutant. Furthermore, the Fn accumulation in the interrenal microenvironment was severely reduced in embryos deficient in Ets1b, which is essential for blood vessel formation, suggesting that the source of Fn in the interrenal microenvironment was at least in part contributed by the neighboring vasculature. Interestingly, the convergence of chromaffin cells at the midline was also perturbed in the *fn1* mutant, with initial but not continuous recruitment of chromaffin cells to the interrenal region being successful. Defective morphogenetic movements of both interrenal and chromaffin cells in the *fn1* mutant together led to incomplete assembly of the interrenal organ in aberrant locations. Our study thus supported a role for Fn to be essential for cell migratory events that ensure correct interrenal organ assembly in teleosts.

RESULTS AND DISCUSSION

The Fn Protein Accumulates Around Migrating *ff1b*-Expressing Interrenal Cells During the Stage of Interrenal Organ Assembly

Following the early midline fusion and lateral relocalization, the steroidogenic component of the interrenal organ develops into a bilobed organ lateral to the notochord from 3 dpf onwards, with the right lobe generally larger than the left lobe (Chai et al., 2003; To et al., 2007). It remains unclear whether the asymmetric bilobed organ structure is due to uneven expansion, or to the migratory behavior of steroidogenic cells during a general expansion of developing interrenal tissue. To check whether steroidogenic cells display migratory activity following the early morphogenetic movements, a transgenic line *Tg(ff1bEx2:GFP)* was used to mark both primordial and differentiated interrenal cells (Fig. 1). Our earlier study showed that the reporter gene expression driven by the *ff1b* promoter could recapitulate the expression of *ff1b* during zebrafish embryogenesis, and has been used to delineate morphogenetic movements of the developing interrenal tissue (Chou et al., 2010).

Vibratome sections of the *Tg(ff1bEx2:GFP)* embryos demonstrated that while *ff1b*-expressing cells formed a single cluster to the right of the midline by 1.5 dpf (Fig. 1A), a protruding extension toward the midline was detected at 2 dpf (Fig. 1B), which was possibly constituted by migrating interrenal cells. At 2.5 dpf, interrenal cell clusters showing migratory behavior were detected near the midline region (Fig. 1C), and some steroidogenic cells were situated at the left of the midline, obviously representing those cells that have migrated across the midline. The migration and extension of the interrenal tissue led to a dispersed distribution of interrenal morphology at 3 dpf (Fig. 3D), which was accompanied by a continuous size expansion of the *ff1b*-expressing domains. It thus suggested that the asymmetric bilobed structure of the interrenal organ from 3 dpf onwards was actually due to a continuous migratory behavior of interrenal cell clusters from 2 to 3 dpf.

Interestingly, the protruding extension of the interrenal tissue cluster at 2 dpf was directed toward an enriched deposition of Fn protein accumulated near the midline region and ventral to the notochord and the DA (Fig. 1B", white arrowheads), while the Fn protein was also deposited around the notochord as well as the DA. From 2.5 to 3 dpf, interrenal clusters migrating across the midline continued to associate with the Fn deposited along the course of interrenal medial extension (Fig. 1C",D"). It thus indicated that the Fn accumulation in the interrenal microenvironment displayed a temporal correlation with the interrenal cell migration from 2 to 3 dpf. Therefore, it is of interest to explore whether Fn could modulate morphogenesis of the interrenal tissue during the process of medial extension and functional assembly.

Although the fluorescent intensity of a 24-hpf *Tg(ff1bEx2:GFP)* embryo in whole-mount could be captured by confocal microscopy (Chou et al., 2010), it was too weak on vibratome sections for locating bilateral interrenal clusters. Nevertheless, indirect evidence has pointed out the possibility of Fn deposition in the microenvironment of bilateral interrenal tissues. At around 24 hpf, bilateral interrenal tissues are associated with those *flk1*-expressing angioblasts that could be involved in the assembly of axial vasculature (Liu and Guo, 2006). Fibronectin has been found to deposit around the *flk1*-expressing anigoblasts as early as 16 hpf (Jin et al., 2005), and hence would likely accumulate in the vicinity of the endothelium-associated interrenal clusters at 24 hpf.

Morphogenetic Movements of Steroidogenic Interrenal Cells Are Defective, Despite a Normal Interrenal Specification, in the *fn1* Mutant

To examine whether Fn plays a role in the morphogenesis of developing interrenal gland, we checked the morphology of steroidogenic interrenal tissue in the *fn1* mutant as well as its wild-type siblings (Fig. 2A, B, C, E). The ventral flat-mount view (Fig. 2A) of deyolked wild-type embryos demonstrated an onset of central migration for steroidogenic interrenal cells by 33 hpf. The migrating steroidogenic cells formed a coherent protruding extension from the aggregated interrenal tissue cluster, which became more evident by 56 hpf (Fig. 2A, white arrows). Along with an expansion of interrenal size, those interrenal cells displaced away from the main cluster appeared loosely-associated at 74 hpf, which was temporally correlated with an intermingling of steroidogenic interrenal and differentiated chromaffin cells at this stage (Chai et al., 2003; To et al., 2007). For all the stages assayed, most of the *fn1* mutants displayed an interrenal phenotype where no migrating cells were detected (*fn1* class I: 70% at 33 hpf, n = 22; 70% at 56 hpf, n = 53; 71% at 74 hpf, n = 45), whereas the rest showed a more severe morphological defect by the presence of bilateral interrenal tissue clusters (*fn1* class II). In contrast, the majority of wild type siblings displayed a migratory interrenal tissue phenotype (78% at 33 hpf, n = 67; 99% at 56 hpf, n = 145; 96% at 74 hpf, n = 125). Since interrenal progenitors appeared as bilateral clusters in either the *fn1* mutant (100%, n=25) or its wild-type siblings (100% in 31 randomly-selected samples) at 24 hpf (Fig. 2B), the phenotype of *fn1* class II was apparently due to an unsuccessful fusion of bilateral interrenal progenitors after their specification. Cross-sections of the *fn1* mutant and its wild type siblings at 3 dpf revealed that the Fn protein expression was severely reduced in both classes of *fn1* mutants (Fig. 2C). While interrenal cells migrated along the ventral side of the DA in the wild-type embryo, those in the *fn1* mutant did not migrate and remained as single (class I) or bilateral (class II) clusters associated with the lateral side(s) of the DA. Although Integrin-mediated signaling is involved in the interaction between mesoderm and endoderm during gastrula (Nair and Schilling, 2008), the migration phenotypes of the interrenal tissue in the *fn1* mutant were not due to an early effect, as the embryos treated with Fn

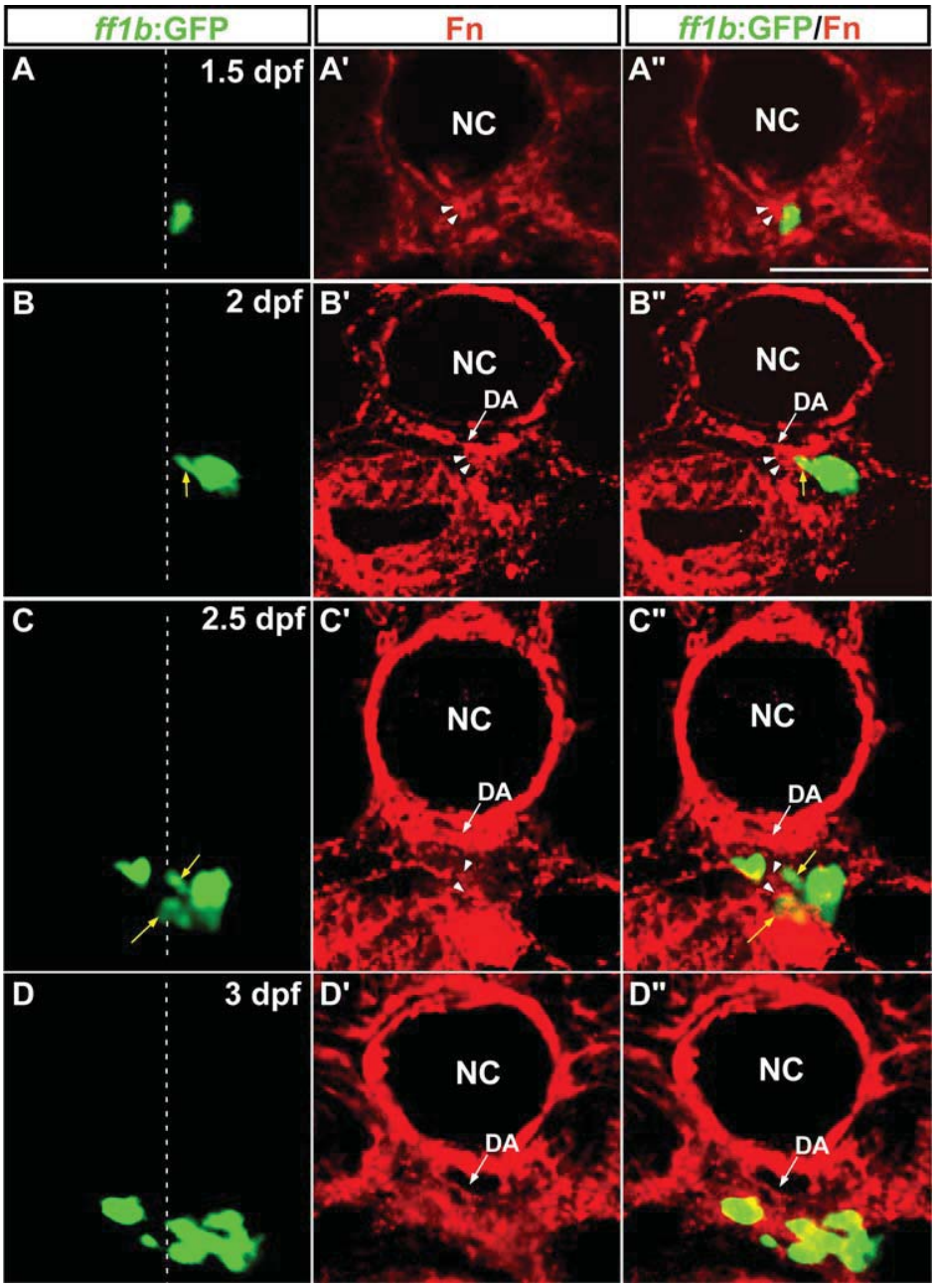

Fig. 1. The distribution of Fn around migrating interrenal cells. Interrenal cells (GFP as driven by *ff1b* promoter in **A–D** and **A"–D"**) formed a protruding extension at 2 dpf (**B, B"**) and dispersed clusters at 2.5 (**C, C"**) and 3 dpf (**D, D"**), on transverse sections of *Tg(ff1bEx2:GFP)* embryos. Migrating interrenal cell clusters (denoted by yellow arrows) were closely associated with the Fn protein (red fluorescence in **A'–D'** and **A"–D"**; Fn enrichment in the interrenal microenvironment highlighted by white arrowheads) throughout the medial extension process of the interrenal tissue. All sections are oriented with the dorsal side toward the top. White dotted lines indicate the position of the midline. NC, notochord; DA, dorsal aorta. Scale bar = 50 μM.

antagonist RGD peptide from 16 hpf (14-somite stage) onwards also led to migration defects of the interrenal tissue, albeit in a slightly more severe manner (see Supp. Fig. S1, which is available online). The migration of interrenal cells in the RGD-treated embryo (n=38) was arrested either at the stage of midline fusion (class II; 29%) or during the subsequent lateral relocalization event (class I; 71%).

Apart from the evident defect of interrenal morphogenetic movements, functional differentiation of the interrenal tissue demonstrated a mild yet significant reduction in the *fn1* mutant. Both density and area of 3βHsd activity, as estimated by densitometry analysis from the ventral surface of the stained interrenal tissue, showed a trend of constant increase from 33 to 74 hpf in either *fn1* mutant or its wild-type siblings (Fig. 2D). However, for all the stages assayed, the *fn1* mutant persistently demonstrated a slightly yet significantly lower level of 3βHsd activity than its wild-type sibling.

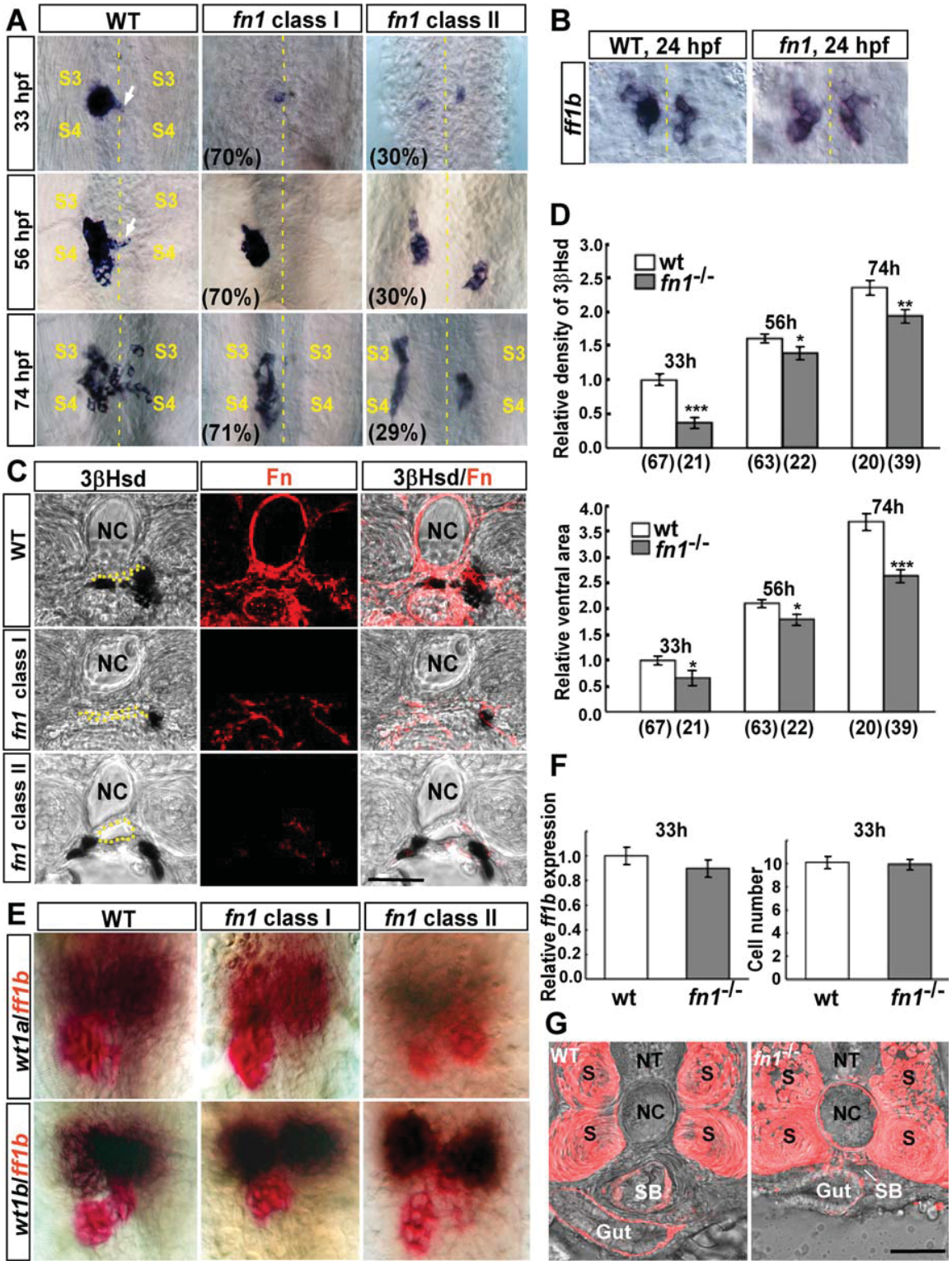

Fig. 2.

Despite a downregulation of interrenal steroidogenic activity in the *fn1* mutant as shown in Figure 2D, specification of the interrenal tissue from the pronephric field is neither perturbed nor delayed (Fig. 2E). Quantification of the *ff1b*-expressing domains in randomly selected *fn1* mutants (n = 25; 19 class I and 6 class II) and their wild-type siblings (n = 18) showed that there was no significant difference in the expression

levels of *ff1b* mRNA. Moreover, the number of *ff1b*-expressing cells showed no apparent difference between the *fn1* mutant and its wild-type sibling. Since the medial extension of interrenal cells was initiated by 33 hpf (Fig. 2A), of which in the *fn1* mutant could not be entitled to an insufficient cell number at this stage. In the situation where proliferative activity of interrenal cells is reduced due to a repressed hypothalamic-piuitary-interrenal axis (To et al., 2007), medial extension and organ assembly of the interrenal gland remain unperturbed, further supporting that the factors that determine migratory activity of interrenal cells might be decoupled from those promoting interrenal cell proliferation.

On the other hand, the simultaneous detection of either *wt1a* or *wt1b* transcripts with those of *ff1b* revealed that the unperturbed interrenal specification in the *fn1* mutant was followed by proper segregation from, and association with, the *wt1*-expressing pronephric glomerulus (Fig. 2E). It further supports that the function of Fn for the interrenal morphogenesis is mainly on the cell migration and independent of either organ specification or even functional differentiation.

The interrenal phenotype in the *fn1* mutant is reminiscent of the previous finding regarding how Fn regulates the cardiomyocyte migration during the process of heart formation (Trinh and Stainier, 2004). It thus raises the question as to whether Fn is commonly involved in migratory events during the process of organ formation. While Fn is also expressed by and deposited at the early endoderm of the zebrafish embryo (Jin et al., 2005), the Fn deficiency did not seem to affect either endodermal migration or gut tube formation, although differentiation and gross morphology of the gut tube were obviously defective (Fig. 2G). On the other hand, the swim bladder as another endoderm-derived organ is surrounded by abundant Fn deposition and appeared severely disrupted in the absence of Fn. We thus speculate that while Fn participates in the microenvironment of many organ or cell types, it might play differential roles for each specific type during development.

The Fn Distribution in the Interrenal Microenvironment Is at Least in Part Contributed by the Neighboring Endothelial Structure

The interrenal tissue is tightly associated with angioblasts and the vascular endothelium since the onset of organ formation and throughout its development (Liu and Guo, 2006). It is thus of interest to explore whether the Fn deposition in the interrenal microenvironment was synthesized by the adjacent vasculature. Consistent with the previous study by Jin et al. (2005), Fn was found to deposit around the DA segment associated with the steroidogenic interrenal tissue, as well as at somites and the swim bladder, at 34 hpf (Fig. 3A, A'). Later at 60 hpf, Fn appeared more highly enriched around the DA and the swim bladder, in the vicinity of the interrenal tissue, which was marked by *ff1b* promoter-driven fluorescence, and also accumulated at the ventral side of the gut tube (Fig. 3C, C'). We then examined the Fn distribution in the embryo injected with the antisense morpholino nucleotides (MO) against the *ets1b* gene (Fig. 3B, B'; D, D'). The *ets1b* gene is required for vasculogenesis in the zebrafish embryo (Sumanas and Lin, 2006), a knockdown of which leads to defects in either midline fusion or lateral relocalization of the developing interrenal tissue (Chou et al., 2010). In this work, all the *ets1b* morphants injected at a dosage of 1.2 pmol per embryo displayed severely disrupted vasculogenesis at the midtrunk at 34 hpf (n=28). The vibratome sections at the level of the midtrunk showed that Fn was severely reduced in the *ets1b* morphant, where the peri-interrenal vasculature was largely deficient (Fig. 3 B, B'). In the *ets1b* morphant, a significant reduction of Fn deposition in the interrenal microenvironment was evident at 60 hpf (Fig. 3D, D'). In contrast, Fn could still be detected around the swim bladder and ventral to the gut tube. Consistently, the phosphorylated Focal Adhesion Kinase (pFAK), an activated downstream component of Integrin signaling (Crawford et al., 2003), also

Fig. 2. The analysis of interrenal morphogenesis in the *fn1* mutant. **A:** Morphogenetic movements of the steroidogenic interrenal tissue in the *fn1* mutant (*fn1*) and its wild type siblings (WT) at 33, 56, and 74 hpf were detected by whole-mount 3β-Hsd staining. Ventral flat-mount views of deyolked samples showed that the steroidogenic interrenal tissue appeared as a single aggregated cell cluster in the wild-type embryo, with the medially-migrating cells forming a protruding extension (white arrows) evident as early as 33 hpf, at the level between the third (S3) and fourth (S4) somites, which was extended across the midline (yellow dotted lines) by 56 hpf and became more loosely associated at 74 hpf. The medial extension and dispersion of single interrenal cell cluster was defective in the class I *fn1* mutant, while the class II mutant displayed a more severe phenotype where bilateral interrenal primordia did not converge. **B:** Bilateral interrenal clusters expressing *ff1b* transcripts were detected in both the *fn1* mutant and its wild-type sibling at the stage of 24 hpf, as assayed by an ISH analysis. **C:** The interrenal migration phenotype of the *fn1* mutant at 72 hpf, which displayed disrupted Fn expression (red), was further demonstrated by vibratome sections with the dorsal side oriented toward the top. The lumen of the DA is marked by yellow dots. **D:** Relative density (top chart) and area (bottom chart) of steroidogenic interrenal tissues as assessed by 3βHsd activity staining from the ventral surface, in the *fn1* mutant compared with its wild-type sibling control. The number of embryos for each population is indicated in parentheses. Both density and area of 3βHsd activity-positive interrenal cells were mildly yet significantly reduced in the *fn1* mutant. $^{*}P < 0.05$; $^{**}P < 0.005$; $^{***}P < 10^{-5}$. **E:** Double ISH assays showing the colocalization of *ff1b* (red) with *wt1a* and *wt1b* (dark brown), respectively, at 33 hpf in the *fn1* mutant as well as its wild-type sibling. **F:** The Fast Red fluorescent intensity of *ff1b* ISH signals, and the number of *ff1b*-expressing interrenal cells as measured from the ventral surface, are quantified in left and right charts, respectively. Expression levels of *ff1b* transcripts, as well as the number of *ff1b*-expressing interrenal cells, are essentially invariable between the *fn1* mutant (n = 25) and its wildtype siblings (n = 18) at the early stage of interrenal differentiation. **G:** The morphology of the developing gut tube in the *fn1* mutant. Vibratome sections at the level of anterior gut region in the *fn1* mutant ($fn1^{-/-}$) as well as its wild-type sibling (WT) were stained with the antibody against Acta2 for demarcating smooth muscle cells located at the outer layers of gut tube (Gut) and swim bladder (SB), while the antibody also detected myofibrils at the somites (S). Morphology but not laterality of the gut tube is affected in the absence of Fn. NT, neural tube. NC, notochord. Scale bar = 50 μM.

appeared greatly reduced in the interrenal area but not in the swim bladder or the gut tube structures. Nevertheless, it is to be noted that the swim bladder and the gut tube were hypomorphic in the *ets1b* morphant, implying that the deletion of vasculature from the embryo might affect organogenesis at multiple levels, however not necessarily through the down-regulation of Fn. Our result is in agreement with the previous report that the RNA expression of *fn1* is absent at the anterior trunk region of the endothelium-free *cloche* (*clo*) mutant (Trinh and Stainier, 2004). It also suggests that Fn might participate in the vessel-derived extracellular matrix microenvironment, which shapes the developing interrenal gland in the fish embryo.

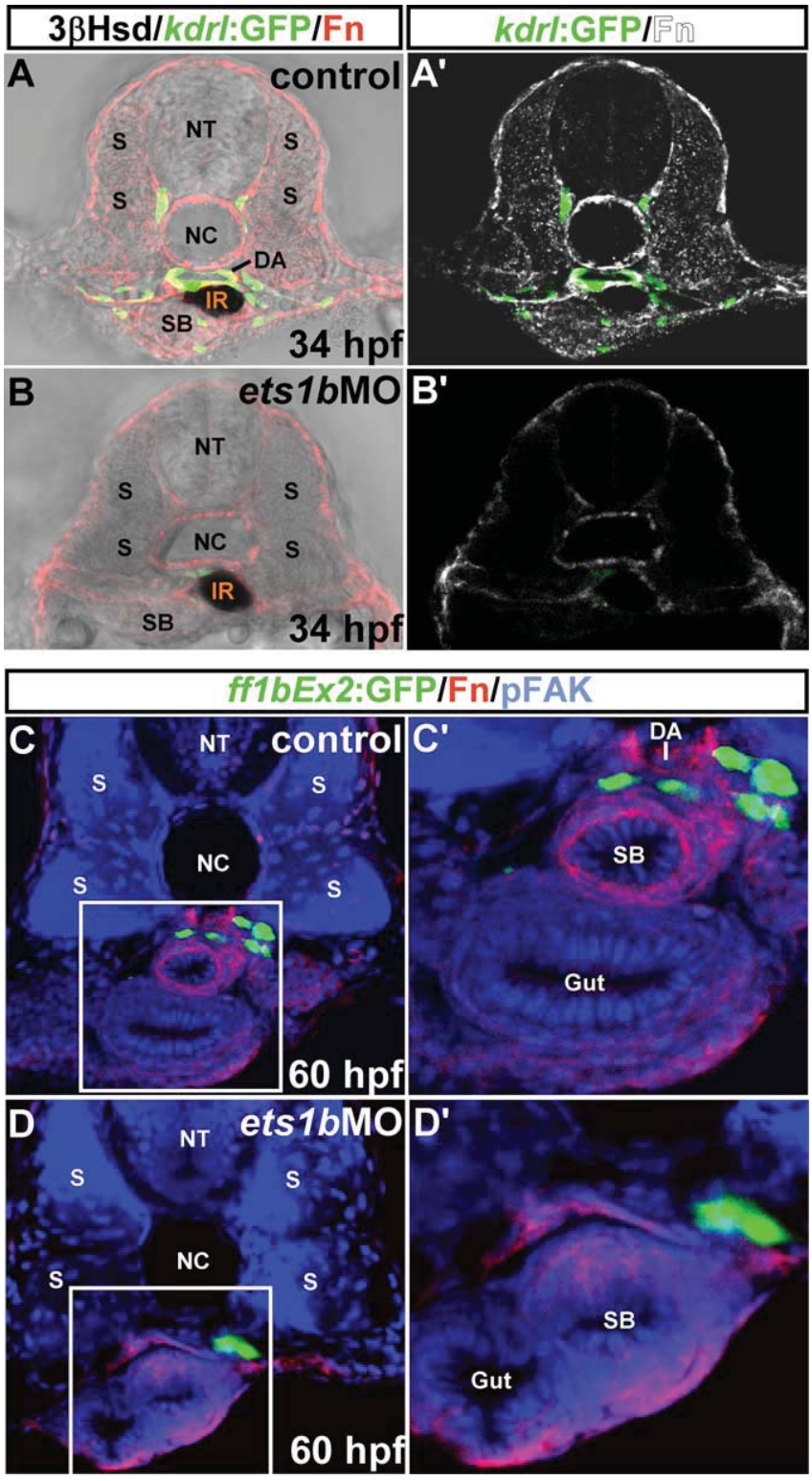

Fig. 3.

Defective Migration Defects of Both Interrenal and Chromaffin Cells in the *fn1* Mutant Lead to Incomplete Interrenal Gland Assembly in Aberrant Locations

The central migration of steroidogenic interrenal cells from 1.5 dpf onwards is temporally correlated with the functional integration between interrenal and chromaffin cells. While the steroidogenic interrenal and chromaffin cells are originated from the intermediate mesoderm and the neural crest, respectively, co-development of these two interrenal organ components starts before 2 dpf, and the resulting interrenal gland assembly is evident at around 3 dpf (Chai et al., 2003; To et al., 2007). To examine whether the interrenal gland assembly was disrupted in the *fn1* mutant where the interrenal morphogenesis was defective, the morphology of differentiated chromaffin cells was delineated by the RNA expression of *dopamine β-hydroxylase* (*dbh*) gene, which functions to convert dopamine to noradrenaline.

Co-localization of *dbh* and *ff1b* transcripts by double in situ hybridization (ISH) at 34 and 54 hpf showed that the initial integration between interrenal and chromaffin cells was not disrupted in the *fn1* mutant (Fig. 4). We found that interrenal and chromaffin cells were closely associated as early as 34 hpf (Fig. 4A–A", B–B"), a stage shortly after the onset of steroidogenesis; and the association was not affected in the *fn1* class I (Fig. 4C–C", D–D") and II (Fig. 4E–E", F–F") mutants where morphogenetic movements of the interrenal tissues was defective. More *dβh*-expressing

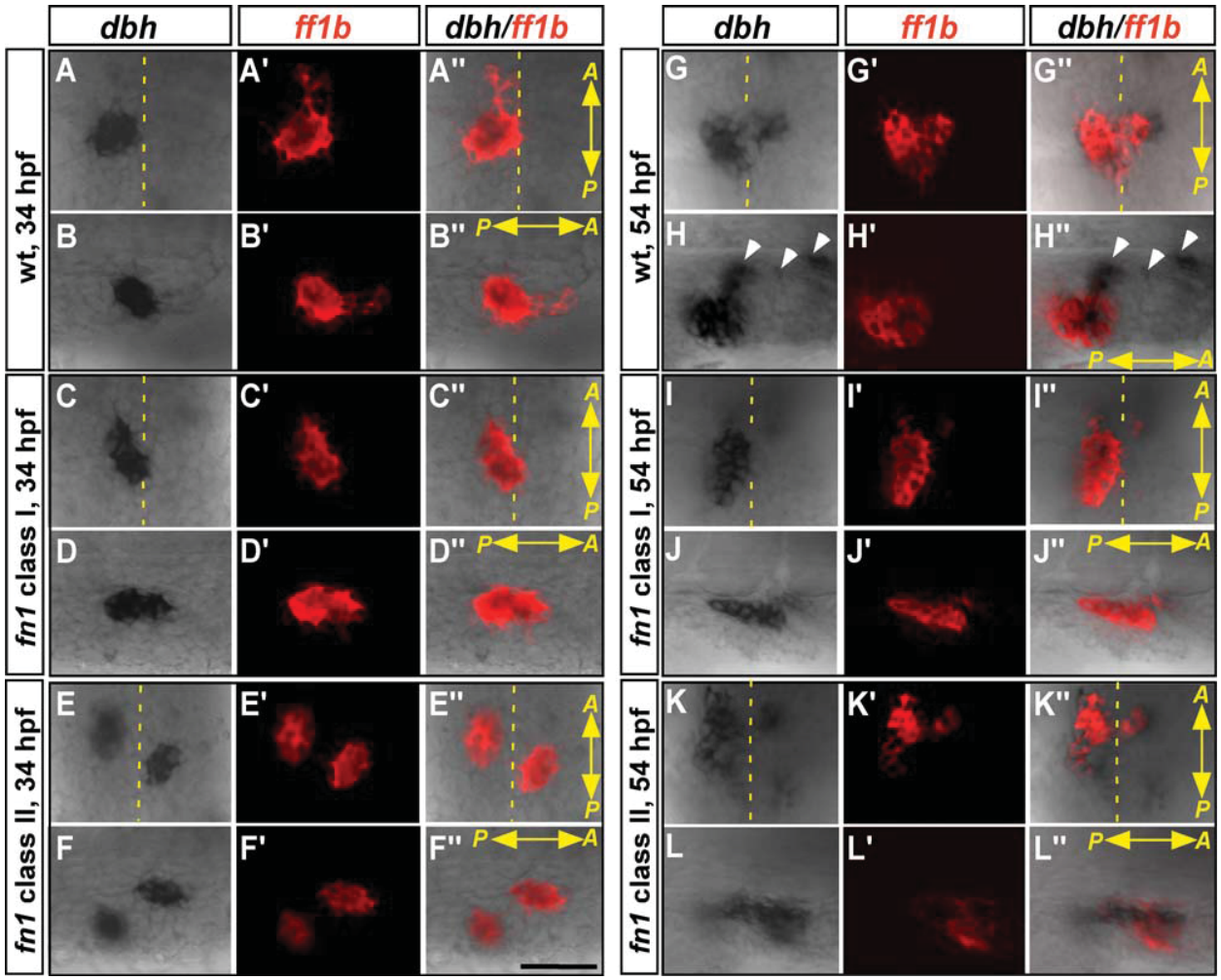

Fig. 4. The interaction between interrenal and chromaffin cells in the *fn1* mutant at 34 and 54 hpf. Double ISH assays showing the colocalization of *ff1b* (red) with *dbh* (black) in the class I and II *fn1* mutants, as well as their wild-type siblings. Ventral flat mount (**A–A", C–C", E–E", G–G", I–I", K–K"**) and lateral (**B–B", D–D", F–F", H–H", J–J", L–L"**) views are shown for the representative embryo of each phenotypic type (n =17, 10, and 24 for the 34-hpf *fn1* mutant class I, class II, and their wild-type siblings, respectively; n = 6, 3, and 18 for the 54-hpf *fn1* mutant class I, class II, and their wild-type siblings, respectively). The anterior (*A*) versus posterior (*P*) orientation of each sample is indicated, and the midline is marked by yellow dotted lines. The embryos in the lateral view panels are oriented with the dorsal side to the top, and migrating chromaffin cell clusters are highlighted by white arrowheads. The initial interaction between interrenal and chromaffin cell populations appears normal; while the continuous recruitment of chromaffin cells to the interrenal region is defective in the *fn1* mutant. Scale bar = 50 μM.

chromaffin cells were detected at the dorsal side of the *ff1b*-expressing interrenal tissue cluster in the wild-type embryo at 54 hpf, apparently representing those chromaffin cells that are migrating to colonize the interrenal organ (Fig. 4H–H"). In contrast, this continuous recruitment of chromaffin cells from the dorsal side into the interrenal area could barely be detected in either class I (Fig. 4J–J") or class II (Fig. 4L–L") of the *fn1* mutant.

Co-localization of *dbh* and *ff1b* transcripts at 77 hpf further displayed that the continuous integration between interrenal and chromaffin cells was severely disrupted in the absence of Fn (Fig. 5). At this stage, continuously-migrating chromaffin cells have reached and assembled in the interrenal region, forming a bilobed structure of chromaffin cell cluster immediately dorsal to the *ff1b*-expressing interrenal tissue (Fig. 5A", B"). In contrast, the *dbh*-expressing cells in the *fn1* mutant failed to

Fig. 3. The effect of *ets1b*MO on the Fn distribution in the interrenal region. Top: Transverse sections of *Tg(kdrl:GFP)*^{s843} embryos either uninjected (**A, A'**) or injected with *ets1b*MO (**B, B'**) were harvested at 34 hpf and assayed for 3β-Hsd activity (black), GFP (green), and Fn expression (red in A, B; white in A', B'). The result of *ets1b* morphant in B, B' is a representative of 9 sectioned samples, which all showed disrupted vasculature at the level of the midtrunk. Bottom: Transverse sections of *Tg(ff1bEx2:GFP)* embryos either uninjected (**C, C'**) or injected with *ets1b*MO (**D, D'**) were harvested at 60 hpf and assayed for GFP (green), Fn expression (red), and pFAK (blue). C', D' are magnified views of the outlined areas in C, D. The result of *ets1b* morphant in D, D' is a representative of 20 sectioned samples. The accumulation of Fn in the interrenal microenvironment is severely reduced in the *ets1b* morphant. All sections are oriented with the dorsal side toward the top. DA, dorsal aorta; IR, interrenal tissue; NC, notochord; NT, neural tube; S, somite; SB, swim bladder.

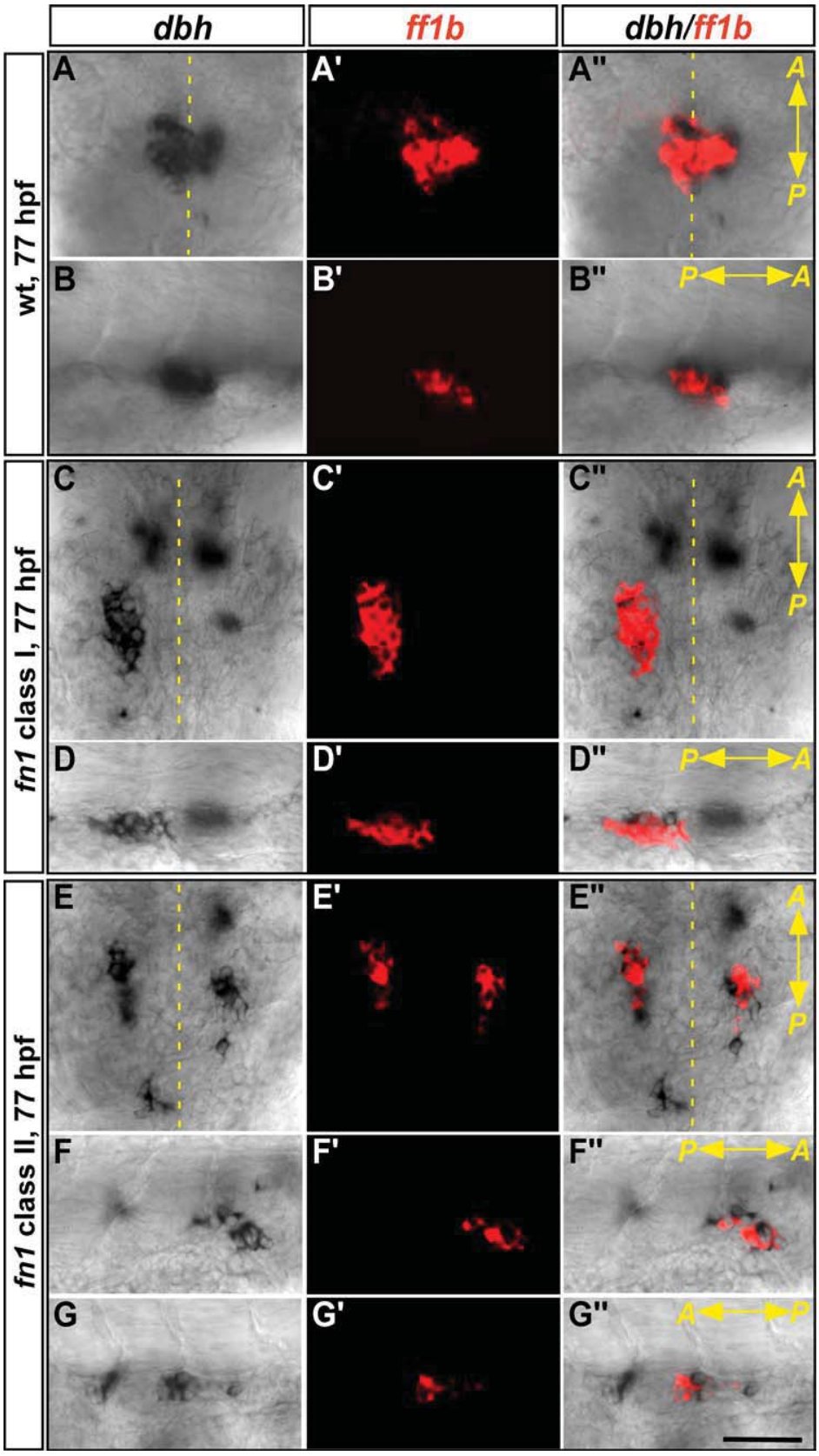

Fig. 5. The interaction between interrenal and chromaffin cells in the *fn1* mutant at 77 hpf. Double ISH assays showing the colocalization of *ff1b* (red) with *dbh* (black) at 77 hpf in the class I and II *fn1* mutants, as well as their wild-type sibling. Ventral flat mount (**A–A", C–C", E–E"**) and lateral (**B–B", D–D", F–F", G–G"**) views are shown for the representative embryo of each phenotypic type (n = 14, 7, and 58 for the *fn1* mutant class I, class II, and their wild-type siblings respectively). The anterior (*A*) versus posterior (*P*) orientation of each sample is indicated. The embryos in the lateral view panels are oriented with the dorsal side to the top. Defective migration and convergence of chromaffin cells in the *fn1* mutant result in incomplete interrenal organ assembly. Scale bar = 50 μM.

converge at the midline, and distributed as discrete clusters in two rows bilaterally along the midline (Fig. 5C"–G"). It implied that the continuous migration of chromaffin progenitor cells was defective in the absence of Fn. Nevertheless, those *dbh*-expressing cell clusters situated in close proximity to interrenal tissues in the *fn1* mutant demonstrated intimate interactions with the *ff1b*-expressing cells, implicating that the Fn deficiency did not disrupt the interaction between interrenal cells and those chromaffin cells that have colonized the interrenal area at the early stage. Our results thus suggested that Fn is required for correct positioning of interrenal organ assembly, by ensuring normal morphogenetic movements for both steroidogenic interrenal and chromaffin cells.

It remains to be explored why the convergence of differentiated chromaffin cells was defective in the *fn1* mutant. As trunk neural crest cells in the zebrafish migrate along the middle of the medial surface of each somite (Honjo and Eisen, 2005), rather than along the somite boundary where Fn accumulates (Koshida et al., 2005), the migration defect of chromaffin cells in the *fn1* mutant might not be due to a loss of Fn along the migration course of trunk neural crest cells. However, the early defect of somite boundary formation in the *fn1* mutant leads to a disorganized myofibril pattern, where fast- and slow-twitch muscle lengths are uncoupled (Snow et al., 2008). It is, therefore, possible that the disorganized muscle fiber organization in the *fn1* mutant might result in defective migration of trunk neural crest cells, and so their derived chromaffin cells.

Our results support that the Fn-containing microenvironment in the interrenal region contributes to promote morphogenetic movements of both steroidogneic interrenal and chromaffin lineages, yet might not play an essential role for reciprocal interactions between these two cell types. It is interesting to note that the location of interrenal–chromaffin integrations seemed to be defined by the aberrantly positioned interrenal tissues, arguing for a role of interrenal-derived factors for recruiting chromaffin cells.

Do Interrenal-Derived Factors Play a Role in the Interrenal–Chromaffin Interaction?

Previous studies in mice have implicated a role of developing adrenocortical cells for the migration of chromaffin cells. Ectopic adrenocortical cells that resulted from transgenic expression of *Ad4BP/SF-1* are capable of recruiting sympathoadrenal progenitor cells, albeit in a relatively inefficient manner (Zubair et al., 2009). In the adult mice, the transgenic Ad4BP/SF-1 expression leads to eccentric chromaffin cell location and thus a disorganized adrenal organ architecture. Similarly, reduced size of the adrenal cortical anlagen in *Ad4BP/SF-1* heterozygous mice leads to unsuccessful immigration of chromaffin progenitors into the cortical anlagen (Lohr et al., 2006). On the other hand, differentiation of the chromaffin cell lineage was not affected upon a lack of the adrenal cortex in *Ad4BP/SF-1* homozygous mice (Gut et al., 2005). Our results in the zebrafish model are consistent with those in mice in that the presence of steroidogenic cells is essential for recruiting chromaffin cells during the organ assembly, yet not required for the generation and differentiation of chromaffin cells. This implicates that steroidogenic tissue-derived factor(s) might play a role in the guidance of chromaffin cell migration. A disruption of pituitary–interrenal interactions in zebrafish, whether by genetic mutation, dexamethasone treatment, or morpholino knockdown, does not affect the migration of, as well as integration between, interrenal and chromaffin cells (To et al., 2007). It thus ruled out the possibility of interrenal-derived steroids playing any role in regulating the interrenal–chromaffin interaction.

The endothelium-free zebrafish *clo* mutant has been found defective in both the migration of steroidogenic cells, and the interrenal–chromaffin interactions (Liu and Guo, 2006). While the interrenal specification and differentiation are not perturbed in the *clo* mutant, bilateral interrenal primordia fail to fuse at the midline in the absence of peri-interrenal vasculature, and the differentiated chromaffin cells converge at an extra-interrenal location, which is well separated from the interrenal region. Although the interrenal tissue phenotype of class II *fn1* mutants highly resembles that of the *clo* mutant, steroidogenic interrenal cells in the class II *fn1* mutant, however, are able to recruit chromaffin cells (Figs. 4E", F", K", L", 5E"–G"; for a comparison between the *clo* and *fn1* mutants see Fig. 6). Since the vessel–interrenal association was not disrupted in the *fn1* mutant (Chiu et al., 2012) as well as in embryos treated with the Fn antagonist RGD peptide (Supp. Fig. S1), it indicates that the adrenal/interrenal-derived guidance cue for chemoattracting chromaffin cells might be generated during the process of interrenal–vessel interaction. Much similar to the adrenal cortex, the adrenal medulla is a highly vascularized endocrine organ that provides a well-developed network of capillaries, venules, and large veins for chromaffin cells to release their product (Kikuta and Murakami, 1984). For the teleostean interrenal organ where steroidogenic and chromaffin cells intermingle instead of forming discrete compartments, both cell types might be exposed to the same set of endothelium-derived signals, and a dissection of such would help us to understand the mechanism that governs assembly of the adrenal/interrenal organ.

EXPERIMENTAL PROCEDURES

Ethics Statement

All of the zebrafish-use protocols in this research were reviewed and approved by the Institutional Animal Care and Use Committee of Tunghai University (IRB Approval NO. 96–05).

Zebrafish Husbandry

Zebrafish (*Danio rerio*) were raised according to standard protocols (Westerfield, 2000). Embryos were obtained from natural crosses of wild-type, transgenic, or heterozygous mutant fish, and staged as previously described (Kimmel et al., 1995). The following lines were used in this study: $fn1^{kt259}$ (Koshida et al., 2005) (gift of Prof. Shinji Takada, National

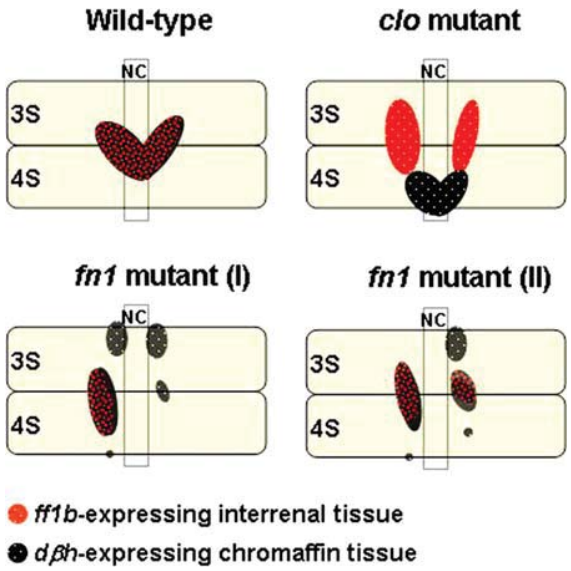

Fig. 6. The *clo* and *fn1* mutants display various types of phenotypic defects in the interrenal organ assembly. The panels represent ventral views of wild-type or mutant embryos at 3 dpf, oriented with anterior to the top. The phenotype of the *clo* mutant is depicted based on the result of Liu and Guo (2006). NC, notochord. 3S and 4S, the third and fourth somite respectively.

Institutes of Natural Sciences, Okazaki, Japan); *Tg(ff1bEx2:GFP)* (Quek, 2009) (gift of Dr. Woon-Khiong Chan, NUS, Singapore); *Tg(kdrl:EGFP)*^{s843} (gift of Didier Stainier, University of California, San Francisco, CA); and *Tg(fli1:EGFP)*^{y1} (Zebrafish International Resource Center, Eugene, OR).

3β-Hydroxysteroid Dehydrogenase (3β-Hsd) Staining, ISH, Densitometry and Immunohistochemistry (IHC)

Embryos to be subject to histological analysis were treated with 0.03% phenylthiourea (Sigma, St. Louis, MO) from 12 hpf onwards to inhibit pigment formation. 3β-Hsd activity staining, ISH, and IHC were performed essentially according to Grassi Milano et al. (1997) Liu and Guo (2006), and Trinh and Stainier (2004), respectively, with modifications.

To delineate the morphology of steroidogenic interrenal tissue, histochemical staining for 3β-Hsd enzymatic activity was performed on whole embryos, and Nomaski images were captured using an Olympus BX51 microscope system.

For whole-mount ISH assays, digoxigenin-labeled antisense riboprobes were synthesized from linearized plasmids of *wt1a, wt1b*, and *dβh* respectively. Fluorescein-labeled antisense riboprobes were synthesized from linearized *ff1b* plasmids. DIG-labeled riboprobes were detected with alkaline phosphatase conjugated anti-DIG antibody (Roche, Indianapolis, IN) while fluorescein-labeled probes were detected by alkaline phosphatase conjugated anti-fluorescein antibody (Roche). Visualization was performed either with BCIP/TNBT (Millipore, Billerica, MA), or with Fast Red (Roche). Stained embryos were post-fixed in 4% paraformaldehyde in PBS and washed in PBS supplemented with 0.1% of Tween 20. Stained embryos were subject to yolk-sac removal and flat-mount analysis. The specimens were cleared in 50% glycerol in PBS, mounted on glass slides, and photographed under Nomaski optics on an Olympus (Center Valley, PA) BX51 microscope system or a Zeiss (Thornwood, NY) Axioplan II microscope equipped with LSM510.

For the quantification of 3β-Hsd activity, photos of embryos from each respective group were taken with identical illumination and magnification, by using Axioskop 2 plus microscope equipped with AxioVision 3.0 (Carl Zeiss) software. Areas and density of the respective signal were measured by the Image Gauge Program, Version 4.0 (Fuji Photo Film).

For the quantification of *ff1b* expression levels, the Fast Red fluorescence signals of the *ff1b* transcripts were assessed from image stacks acquired at a 8-μM z-steps, by using a Zeiss Axioplan II microscope equipped with LSM510. Intensity values from the consecutive stacks encompassing the interrenal region were summated to obtain the relative *ff1b* expression level for each sample.

For IHC experiments performed on *Tg(ff1bEx2:GFP)* and *Tg(kdrl:EGFP)*^{s843} embryos, fixed embryos were embedded in 4% NuSieve GTG low-melting agarose, cut into 100-μM sections with a Leica VT1000M vibratome, and permeabilized with PBS containing 1% Triton X-100, before antibody staining in PBDT (1% BSA, 1% DMSO, 0.1% Triton X-100 in PBS). Rabbit polyclonal anti-human Fibronectin (Sigma), mouse monoclonal anti-human FAK [pY397] (BD Transduction Laboratories, San Diego, CA), and rabbit polyclonal anti-zebrafish Acta2 (GeneTex, San Antonio, TX) were used at 1:200, 1:100, and 1:100 dilutions; respectively. Dylight^{TM}594-conjugated or Dylight^{TM}650-conjugated goat anti-rabbit IgG was used as the secondary antibody at a 1:200 dilution. Images of vibratome-sectioned embryos were captured with the confocal microscopy.

Microinjection of Antisense Morpholino Oligonucleotides (MOs)

MOs targeting the *ets1b* gene, *ets1b*MO1, and *ets1b*MO2, were synthesized at Genetools LLC (Philomath, OR), diluted in 1× Danieau solution, and co-injected in equimolar amounts for a total of 1.2 pmol per embryo, into one- to two-cell stage embryos by using a Nanoject (Drummond, Broomall, PA). The nucleotide sequences of the *ets1b*MO1 and *ets1b*MO2 are 5′ – TTG GTA CAT TTC CAT ATC TTA AAG T - 3′ (Sumanas and Lin, 2006) and 5′ – CAC TGA GTC CTT ATT TCA CTA TAT C - 3′

(Sumanas and Lin, 2006), respectively.

Statistical Analysis

All quantitative data are expressed as the mean±SE of the mean (SEM). Statistical analysis of the data was performed using analysis of variance, followed by Student's *t*-test. A probability of $P < 0.05$ was considered statistically significant.

ACKNOWLEDGMENTS

We thank Dr. Woon-Khiong Chan, Prof. Shinji Takada, and Prof. Didier Steinier for the kind gifts of *Tg(ff1bEx2:GFP)*, *fn1*^{kt259}, and *Tg(kdrl:EGFP)*^{s843} strains, respectively; You-Lin Zhuo and Zhe-Yu Jiang for excellent technical assistance; and the Taiwan Zebrafish Core Facility (TZCF), the Zebrafish Core in Academia Sinica (TZCAS), and the Zebrafish Core Facility at NTHU and NHRI (TZeTH) for assistances on fish culture.

REFERENCES

Alsop D, Vijayan M. 2009. The zebrafish stress axis: molecular fallout from the teleost-specific genome duplication event. Gen Comp Endocrinol 161:62–66.

Astrof S, Hynes RO. 2009. Fibronectins in vascular morphogenesis. Angiogenesis 12:165–175.

Chai C, Liu YW, Chan WK. 2003. Ff1b is required for the development of steroidogenic component of the zebrafish interrenal organ. Dev. Biol. 260:226–244.

Chamoux E, Bolduc L, Lehoux JG, Gallo-Payet N. 2001. Identification of extracellular matrix components and their integrin receptors in the human fetal adrenal gland. J Clin Endocrinol Metab 86:2090–−2098.

Chamoux E, Narcy A, Lehoux JG, Gallo-Payet N. 2002a. Fibronectin, laminin, and collagen IV as modulators of cell behavior during adrenal gland development in the human fetus. J Clin Endocrinol Metab 87:1819–1828.

Chamoux E, Narcy A, Lehoux JG, Gallo-Payet N. 2002b. Fibronectin, laminin, and collagen IV interact with ACTH and angiotensin II to dictate specific cell behavior and secretion in human fetal adrenal cells in culture. Endocr Res 28:637–640.

Chiu CH, Chou CW, Takada S, Liu YW. 2012. Development and fibronectin signaling requirements of the zebrafish interrenal vessel. PLoS One 7:e43040.

Chou CW, Hsu HC, Quek SI, Chan WK, Liu YW. 2010. Arterial and venous vessels are required for modulating developmental relocalization and laterality of the interrenal tissue in zebrafish. Dev Dyn 239:1995–2004.

Crawford BD, Henry CA, Clason TA, Becker AL, Hille MB. 2003. Activity and distribution of paxillin, focal adhesion kinase, and cadherin indicate cooperative roles during zebrafish morphogenesis. Mol Biol Cell 14:3065–3081.

Grassi Milano E, Basari F, Chimenti C. 1997. Adrenocortical and adrenomedullary homologs in eight species of adult and developing teleosts: morphology, histology, and immunohistochemistry. Gen Comp Endocrinol 108:483–496.

Gut P, Huber K, Lohr J, Bruhl B, Oberle S, Treier M, Ernsberger U, Kalcheim C, Unsicker K. 2005. Lack of an adrenal cortex in Sf1 mutant mice is compatible with the generation and differentiation of chromaffin cells. Development 132:4611–4619.

Honjo Y, Eisen JS. 2005. Slow muscle regulates the pattern of trunk neural crest migration in zebrafish. Development 132:4461–4470.

Hsu HJ, Lin G, Chung BC. 2003. Parallel early development of zebrafish interrenal glands and pronephros: differential control by wt1 and ff1b. Development 130:2107–2116.

Hynes RO. 1992. Integrins: versatility, modulation, and signaling in cell adhesion. Cell 69:11–25.

Ishimoto H, Jaffe RB. 2011. Development and function of the human fetal adrenal cortex: a key component in the feto-placental unit. Endocr Rev 32:317–355.

Jin SW, Beis D, Mitchell T, Chen JN, Stainier DY. 2005. Cellular and molecular analyses of vascular tube and lumen formation in zebrafish. Development 132:5199–5209.

Kikuta A, Murakami T. 1984. Relationship between chromaffin cells and blood vessels in the rat adrenal medulla: a transmission electron microscopic study combined with blood vessel reconstructions. Am J Anat 170:73–81.

Kimmel CB, Ballard WW, Kimmel SR, Ullmann B, Schilling TF. 1995. Stages of embryonic development of the zebrafish. Dev Dyn 203:253–310.

Koshida S, Kishimoto Y, Ustumi H, Shimizu T, Furutani-Seiki M, Kondoh H, Takada S. 2005. Integrinalpha5-dependent fibronectin accumulation for maintenance of somite boundaries in zebrafish embryos. Dev Cell 8:587–598.

Liu YW. 2007. Interrenal organogenesis in the zebrafish model. Organogenesis 3:44–48.

Liu YW, Guo L. 2006. Endothelium is required for the promotion of interrenal morphogenetic movement during early zebrafish development. Dev Biol 297:44–58.

Lohr J, Gut P, Karch N, Unsicker K, Huber K. 2006. Development of adrenal chromaffin cells in Sf1 heterozygous mice. Cell Tissue Res 325:437–444.

Nair S, Schilling TF. 2008. Chemokine signaling controls endodermal migration during zebrafish gastrulation. Science 322:89–92.

Quek SI. 2009. Molecular characterization of the zebrafish ff1b gene. In: Biological Sciences. Singapore: National University of Singapore.

Serluca FC, Drummond IA, Fishman MC. 2002. Endothelial signaling in kidney morphogenesis: a role for hemodynamic forces. Curr Biol 12:492–497.

Snow CJ, Peterson MT, Khalil A, Henry CA. 2008. Muscle development is disrupted in zebrafish embryos deficient for fibronectin. Dev Dyn 237:2542–2553.

Sumanas S, Lin S. 2006. Ets1-related protein is a key regulator of vasculogenesis in zebrafish. PLoS Biol 4:e10.

To TT, Hahner S, Nica G, Rohr KB, Hammerschmidt M, Winkler C, Allolio B. 2007. Pituitary-interrenal interaction in zebrafish interrenal organ development. Mol Endocrinol 21:472–485.

Trinh LA, Stainier DY. 2004. Fibronectin regulates epithelial organization during myocardial migration in zebrafish. Dev Cell 6:371–382.

Westerfield M. 2000. The zebrafish book: guide for the laboratory use of zebrafish (Danio rerio). Eugene, OR: Univ. of Oregon Press.

Zubair M, Oka S, Parker KL, Morohashi K. 2009. Transgenic expression of Ad4BP/SF-1 in fetal adrenal progenitor cells leads to ectopic adrenal formation. Mol Endocrinol 23:1657–1667.

DEVELOPMENTAL DYNAMICS 239:1995–2004, 2010

RESEARCH ARTICLE

Arterial and Venous Vessels Are Required for Modulating Developmental Relocalization and Laterality of the Interrenal Tissue in Zebrafish

Chih-Wei Chou,[1] Hsiao-Chu Hsu,[1] Sue-Ing Quek,[2] Woon-Khiong Chan,[2] and Yi-Wen Liu[1]*

During zebrafish embryogenesis, the endothelium signals to emergent bilateral interrenal primordia to converge toward the midline, yet the merged interrenal tissue has been found to be situated lateral to the midline. We show in this study that bilateral interrenal tissue clusters fused at the central midline, before relocating laterally to be juxtaposed between the dorsal aorta and the posterior cardinal vein. In *ets1b* morphants where the midtrunk vasculature failed to assemble, various degrees of interrenal fusion defects were displayed, and the interrenal laterality was lost. As either arterial or venous endothelium was specifically reduced, the interrenal tissue was defective in its relocalization and laterality, yet remained closely associated with the malformed vasculature. Our results showed evidence to support that assembly of the axial artery and vein, and its resulting vascular topology at the midtrunk, is required for patterning relocalization and laterality of the interrenal tissue after the initial medial fusion. *Developmental Dynamics 239:1995–2004, 2010.* © 2010 Wiley-Liss, Inc.

Key words: zebrafish; adrenal; interrenal; steroidogenic; endothelium; artery; vein; laterality; *ets1b*; *gridlock/hey2*

Accepted 4 May 2010

INTRODUCTION

Interactions between endothelial cells (EC) and the microenvironment are known to regulate organogenesis and pattern formation in the embryo (for a review see Cleaver and Melton, 2003; Nikolova et al., 2007; Red-Horse et al., 2007). The zebrafish, due to its optical clarity, has been shown to be a good model for observing the interplay between organs and vasculature during early development. Also, a vast array of mutants and morphants manifesting various types of vascular disorders has allowed a detailed genetic dissection of endothelial signals that modulate organogenesis. For example, in the developing zebrafish embryo, endothelium has been found to regulate cardiomyocyte movement during heart tube assembly (Holtzman et al., 2007), to provide guidance cues for defining the position of the thyroid gland (Alt et al., 2006), and to regulate the apicobasal polarization of hepatocytes (Sakaguchi et al., 2008). Furthermore, endothelium-derived signals play morphogenetic roles for the embryonic renal and interrenal organs (Serluca et al., 2002; Liu and Guo, 2006), while these two organs develop in a highly parallel manner.

The interrenal tissue, the teleostean counterpart of mammalian adrenal cortex, is derived from the embryonic kidney, or pronephros (Hsu et al., 2003; Chai et al., 2003). Although tissue organization and morphology of the interrenal tissue in zebrafish demonstrates species-specific differences from its mammalian counterpart, key mechanisms that control the interrenal organogenesis and steroidogenesis highly resemble those in mammals (for a review see Liu, 2007). In the zebrafish embryo, both kidney and interrenal tissue arise as bilateral clusters across the midline, and migrate centrally in a coordinated

Additional Supporting Information may be found in the online version of this article.

[1]Department of Life Science, Tunghai University, Taichung, Taiwan, R.O.C
[2]Department of Biological Sciences, National University of Singapore, Singapore

Grant sponsor: National Science Council (R.O.C.); Grant sponsor: NSC; Grant number: 96-2628-B-029-002-MY3; Grant sponsor: A*STAR-BMRC (Singapore); Grant number: BMRC07/1/21/19/527.

***Correspondence to: Yi-Wen Liu, Department of Life Science, Tunghai University, No. 181, Sec. 3, Taichung-Port Road, Taichung, 40704, Taiwan R.O.C. E-mail: dlslys@thu.edu.tw**

DOI 10.1002/dvdy.22335
Published online 28 May 2010 in Wiley InterScience (www.interscience.wiley.com).

fashion (Hsu et al., 2003). While central assembly of the pronephros requires the hemodynamic force (Serluca et al., 2002), medial migration of primordial interrenal cells toward the midline is regulated by the interrenal-associated endothelium, possibly prior to vessel formation (Liu and Guo, 2006). The converged interrenal tissue is located to the right of the midline, and juxtaposed between the dorsal aorta (DA) and the right branch of the posterior cardinal vein (PCV) (Liu and Guo, 2006). However, it remains unclear whether the initial merging point of bilateral interrenal clusters is at or to the right of the midline. Also, it could not be ruled out that the left interrenal cell cluster might disappear before reaching the midline, leaving the right cluster for subsequent morphogenesis. We hypothesized that in parallel with assembly of the DA and the PCV at the midtrunk area, the centrally-migrating primordial interrenal cells first fuse at the central midline, before a lateral relocalization to the right of the midline, resulting in a single interrenal tissue cluster "sandwiched" between the DA and the PCV. Also, developmental relocalization of the interrenal tissue after the convergence event could be modulated by its adjacent vessels. The functional differentiation of interrenal cells, detected by 3βHsd activity staining as early as 28 hpf, takes place approximately concurrent with the morphogenetic phase of interrenal relocalization, which implied that the endocrine function of steroid secretion might be ready right after the onset of blood circulation.

In order to validate the putative morphogenetic steps in our proposed model, we performed in situ hybridization (ISH) and transgenic reporter analyses to capture the morphology of bilateral interrenal tissues that were undergoing midline fusion. We also examined the interrenal phenotype in *ets1b* morphants where the trunk vasculature was severely disrupted, as well as in embryos with specific reduction in either arterial or venous cells. The results of our phenotypic analyses suggest that midline fusion and lateral relocalization take place in the process of embryonic interrenal morphogenesis, and these movements are dynamically regulated by the peri-interrenal endothelium, which participates in assembly of the DA and the PCV.

RESULTS AND DISCUSSION

The Midline Fusion of Primordial Interrenal Cells as Detected by Both ISH and Transgenic Reporter Analyses

The fusion and relocalizing processes of bilateral interrenal primordia were delineated through analyzing the expression of *ff1b* mRNA as well as the green fluorescence driven by *ff1b* promoter, immediately after the interrenal specification. *ff1b* (NR5A4) has been discovered to be the earliest gene expressed at the developing interrenal tissue (Chai et al., 2003; Hsu et al., 2003). *ff1b* is the orthologue of mammalian steroidogenic factor 1 (SF-1/Ad4BP; NR5A1), and the disruption of its expression leads to a complete ablation of the embryonic interrenal tissue. Earlier ISH results of detecting *ff1b* mRNA transcripts by using Fast Red chromogenic staining imply that bilateral interrenal cell clusters emerge at about 21-somite stage, and the convergence toward the midline is completed by 23-somite stage (Hsu et al., 2003; Liu et al., 2003). Those results, however, did not explicitly demonstrate the primary mechanism of interrenal asymmetry, and it could not be ruled out that the interrenal laterality could be due to asymmetric degeneration, apoptosis, or disassociation of one primordia. In order to address this issue, firstly we utilized NBT/BCIP staining to obtain better resolution of ISH in detecting the *ff1b* mRNA expression in embryos at the 21- to 26-somite stages. Consistent with the former studies, bilateral interrenal tissues were detectable in embryos as early as the 21-somite stage (Figs. 1A, 21S). In contrast, a single interrenal cell cluster of the shape as shown in Figure 1A, 22S, apparently formed by the fusion of bilateral clusters migrating toward the midline, was detected in embryos at the 22-somite stage. Subsequently, at approximately the 24-somite stage, some interrenal cells started to be displaced away from the midline (Fig. 1A, 24S), culminating in a single leaf-shaped interrenal tissue cluster localized to the right of the midline as viewed dorsally (ventral view shown in Fig. 1A, 26S).

To further validate the process of interrenal fusion and repositioning in the developing embryo, we performed a time-lapse confocal analysis on the embryo where the interrenal cells were traced by utilizing a *ff1b* promoter-driven green fluorescent line, *Tg(ff1bEx2:GFP)*. The interrenal identity of GFP-expressing cells in the *Tg(ff1bEx2:GFP)* embryo was verified by colocalization of the GFP expression with the 3βHsd enzymatic activity staining (Fig. 1B). At 32 hpf, most of the GFP-expressing cells near the third somite appeared as a leaf-shape cluster to the right of the midline as viewed dorsally, and the 3βHsd activity was detected in part of the GFP-expressing cells. This was consistent with our former results that 3βHsd activity is detected in some but not all of the *ff1b* -expressing interrenal cells during development (Chai et al., 2003; Liu et al., 2003). In some samples, a tiny cluster of GFP-expressing cells appeared to be dispersed from the main interrenal tissue and was localized at the left of the midline. This might be due to the differential rate of cell migration within the interrenal cell population. The *ff1b* promoter-driven fluorescence could be detected as early as the 21-somite stage, and a time-lapse confocal analysis was performed on the *Tg(ff1bEx2:GFP)* embryo starting from this stage (Fig. 1C). Bilateral rows of GFP-positive cells were also detected throughout the scanning period, which represented ectopic GFP expression at muscle pioneer cells, possibly due to the presence of an enhancer element near the site of transgene integration (Quek, 2009), and this domain of fluorescence weakened later at about 32 hpf. The live *Tg(ff1bEx2:GFP)* embryo was incubated at 23°C in order to slow down the developmental process for the purpose of clear observation. The bilateral interrenal clusters, as detected by *ff1b* promoter-driven GFP expression, started to fuse medially by 42 min after the onset of scanning. The interrenal morphology at the time of fusing was consistent with the

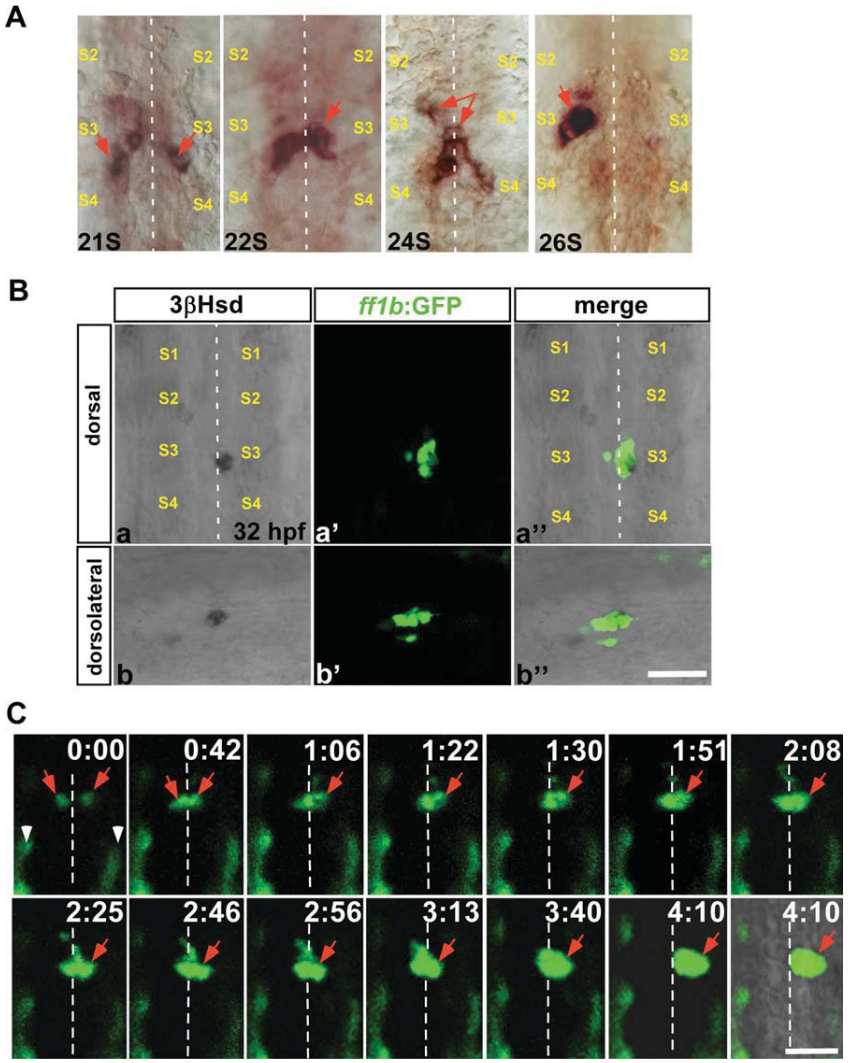

Fig. 1. The *ff1b*-expressing interrenal primordia during midline fusion and lateral repositioning. **A**: Ventral flat mount views of 21-somite (21S), 22-somite (22S), 24-somite (24S), and 26-somite (26S) stage embryos, which were subject to ISH for detecting *ff1b* mRNA, with anterior oriented to the top. **B**: The colocalization of steroidogenic activity and *ff1b*:GFP transgene expression at the interrenal tissue, in the *Tg(ff1bEx2:GFP)* embryo. Confocal images display the steroidogenic cells as detected by 3βHsd activity staining (a,b), and the green fluorescence driven by *ff1b* promoter (a′,b′), in a *Tg(ff1bEx2:GFP)* embryo at 32 hpf. The merged images of 3 μ-Hsd activity staining and GFP are shown in a″,b′. **a–a**″: Dorsal views with anterior to the top; (**b–b**″) dorsolateral views with anterior to the right. **C**: Confocal time-lapse imaging of the interrenal tissue in a live *Tg(ff1bEx2:GFP)* embryo. A dechorionated embryo at around 21-somite stages was mounted with the dorsal side up in 3% methyl cellulose. The fluorescent images were collected at 1-min intervals, and representative frames are shown. The last frame of the time series is a merge of fluorescent and bright-field images. Time is indicated by hours:minutes. Since the sample was kept at 23°C during observation, developmental stages cannot be accurately addressed. Each fluorescent image in B and C represents a projection of a consecutive z-stack encompassing the depth of the interrenal tissue. Both ISH and time-lapse *ff1b*:GFP analyses show that the interrenal primordia fuse at the midline prior to the lateral relocalization. Red arrows indicate *ff1b*-expressing interrenal primordia in A, and the *ff1b* promoter-driven interrenal-specific fluorescence in C. S2, S3, and S4, the second, third, and fourth somite, respectively. White arrowheads in C indicate ectopic GFP expression in muscle pioneer cells. White dotted lines indicate the position of the midline. Scale bar = 50 μM.

ff1b mRNA expression pattern as detected by ISH at the 22-somite stage in Figure 1A. By 1 hr, a fused interrenal tissue was found to be relocalized toward the right of the midline, with a tiny rostral cluster appearing to be dispersed from the main cluster. At this time, the fused interrenal tissue showed a 2.2-fold increase in size as compared to that which is summed from the bilateral clusters at time point 0:00 (Fig. 1C; see Supp. Fig. S1, which is available online), implying that *ff1b*-expressing cells from each of the bilateral interrenal tissue combined to result in a single interrenal tissue during the process of medial fusion. By 250 min after scanning, when the fused interrenal tissue was fully relocated to the right of the midline, the interrenal size expanded to about 2.8-fold of that right after the interrenal fusion, indicating active interrenal cell proliferation following the medial fusion event.

Altogether, both ISH and time-lapse transgenic reporter results support our hypothesis that medially migrating bilateral interrenal primordia first fuse at the central midline, and the merged interrenal tissue is subsequently relocalized to the right of the midline. It is then of interest to check how these morphogenetic movements could be modulated by the peri-interrenal vasculature.

Disrupted Formation of Trunk Vasculature Led to Defective Midline Fusion and Relocalization of the Interrenal Tissue

Subsequent to the medial migration and midline fusion, the interrenal tissue was laterally relocalized and juxtaposed between the DA and the right branch of the PCV (Fig. 2A–A″). Previously, it has been shown that central convergence as well as laterality of the interrenal tissue was normal in embryos injected with the antisense morpholino oligo against *cardiac troponin T2* (*tnnt2*) gene (Liu and Guo, 2006), where the blood flow is absent (Sehnert et al., 2002), suggesting that hemodynamic force might not be essential for the early interrenal morphogenetic movement. Instead, we propose here that right-sided laterality of the interrenal tissue might be correlated with patterning of the DA and the PCV at the mid-trunk. To test this hypothesis, we checked the embryonic interrenal morphology in *ets1b*-deficient embryos where the formation of trunk vasculature was

disrupted. Ets1-related protein (Etsrp; or Ets1b) has been identified to regulate endothelial but not hematopoietic development (Sumanas and Lin, 2006). Ets1b appears to function straight downstream of *clo* (Sumanas and Lin, 2006). Consistent with the former study, a mixed injection of two morpholino oligos against *ets1b* at a high dosage (15 ng) resulted in a complete loss of circulation, and severe elimination of endothelium (Fig. 2B′–D′) as verified by *fli1* promoter-driven vascular-specific GFP fluorescence in *Tg(fli1:EGFP)*^{Y1} embryos (Lawson and Weinstein, 2002). The remaining *fli1*-expressing cells in *ets1b* morphants were speculated to be aggregated angioblasts as a consequence of disrupted vasculogenesis, and appeared to display high affinity to the interrenal tissue (Fig. 2B′–D′,B″–D″). While the trunk vasculature was compromised, *ets1b* morphants displayed variable expressivity of interrenal convergence phenotype, which was accompanied by a loss of laterality (Fig. 2B–D). In contrast with the uniform interrenal convergence phenotype seen in angioblast-deficient *clo* mutant, that bilateral interrenal primordia fail to fuse and were separately located at two sides of the midline (Liu and Guo, 2006), we saw intermediate phenotypes shown as

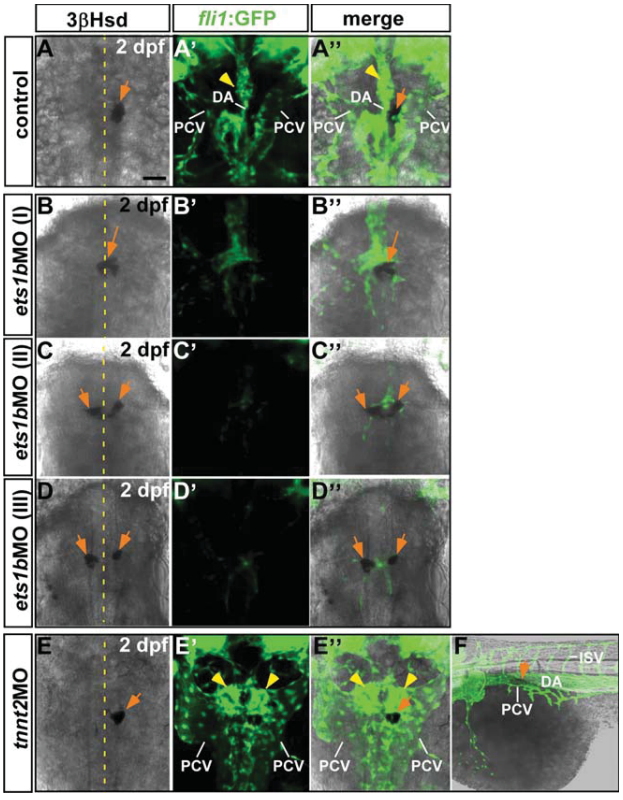

Fig. 2.

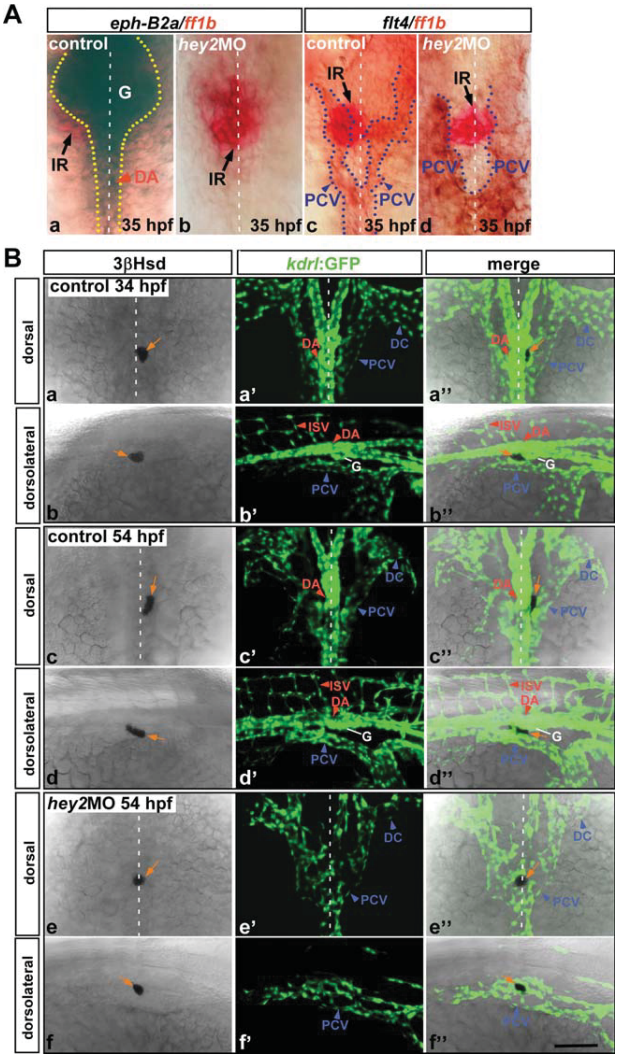

Fig. 3.

TABLE 1. Analysis of *ets1b* Morphant Phenotypes in 2-dpf *Tg(fli1:EGFP)*^{Y1} Embryos as Viewed From the Dorsal Side

		*ets1b*MO		Control	
Phenotype	Morphology of the interrenal tissue	No.	(%)	No.	(%)
Normal	Single cluster to the right of the midline	12	(11.3)	112	(96.6)
Class (I)	Single cluster from the midline fusion of bilateral ones	36	(34.0)	0	
Class (II)	Bilateral elongated clusters with caudal ends fusing at the midline	31	(29.2)	0	
Class (III)	Bilateral clusters across the midline	27	(25.5)	4	(3.4)
	Total	106		116	

reverse U-shape (class I in Fig. 2B) or V-shape (class II in Fig. 2C) interrenal clusters across the midline, which appeared to result from incomplete fusion. The most severe phenotype in class III (Fig. 2D) of *ets1b* morphants well resembled the interrenal morphology in the *clo* mutant. The severity of the interrenal fusion phenotype seemed to be correlated with that of the vascular disruption. While about 97% of uninjected control embryos displayed normal interrenal laterality (n = 116), 89% of *ets1b* morphants lost interrenal laterality (n = 106), ranging from defective relocalization after the convergence to unsuccessful medial migration (Table 1). The aberrant interrenal morphology in the vasculature-deficient embryo was not similar to the interrenal phenotype in the *tnnt2* morphant (a representative sample shown in Fig. 2E–E″,F). It is to be noted that in the absence of blood flow, the interrenal tissue remained juxtaposed between the DA and the PCV. Hence, we conclude that the formation of trunk vasculature near the interrenal region, but not vascular flow, might play a role in the laterality, or right-sidedness, of the fused interrenal tissue. Furthermore, phenotypic differences among the *clo* mutant, the *ets1b* morphant, and their wild type controls implied that the interrenal fusion at the midline and the later interrenal relocalization might occur as two distinct yet consecutive phases, differentially regulated by pre-vascular angioblasts and vascular ECs, respectively. To further examine whether arterial or venous vasculature plays a specific role in relocalization and laterality of the interrenal tissue, in the following experiments we checked the interrenal morphology in embryos deficient in either arterial or venous cells.

Inhibition of Artery Formation Led to Defective Relocalization and Laterality of the Interrenal Tissue

To manipulate arterial- versus venous-differentiation, the expression of *grl*/*hey2* was altered following what was reported by Zhong at al. (2001). Our earlier study showed that in *fli1* promoter-driven fluorescent embryos injected with the antisense morpholino oligo against *hey2*, medial migration and midline fusion of bilateral interrenal primordia were not affected, arguing against a specific role for arterial ECs to regulate the early interrenal convergence. It, however, remains unclear whether artery would pattern developmental relocalization and right-sided laterality of the interrenal tissue. To examine how the peri-interrenal vasculature reacts to the inhibition of *hey2* expression, we injected *hey2* morpholino at the dosage of about 1.2 pmol per embryo into wild type embryos, and the morphants manifesting notable vascular defects by a complete loss of circulation (53.1%; n = 143) were selected for the subsequent examination of either arterial- or venous-specific markers by ISH. Ventral flat-mount views showed that while the arterial-specific gene *eph-B2a* was abundantly expressed at the glomeruous and the DA in the control embryo at 35 hpf (Fig. 3Aa), it was absent at the DA and poorly expressed in the glomerular region of all the *hey2* morphants checked (n = 45; Fig. 3Ab). Conversely, the venous-specific gene *flt4* was excessively expressed at the PCV and its two bilateral branches in the *hey2* morphant, thus showing a malformed venous structure at the midtrunk (n = 31; Fig. 3Ad). The effects of *hey2* morpholino on the artery and vein were consistent with the data reported by Zhong et al. (2001). It is shown in Figure 3Aa that the laterally-positioned interrenal tissue was intimately associated with the arterial ECs that constitute the pronephric glomerulous and the DA. It is interesting to note that, albeit evident in its laterality, the *ff1b*-expressing interrenal tissue was in contact with both right and left branches of the PCV, implying a possible asymmetry of PCV structure at the midtrunk area. The *ff1b*-expressing interrenal tissue in 95% of the *hey2* morphants, which showed absence of circulation, was shown as a single cluster lying across the midline, with the centrally-positioned interrenal tissue juxtaposed between two branches of PCV (Fig. 3Ab,d). The intensity of *ff1b* expression did not appear to be reduced upon the disruption of its adjacent arterial vasculature. Our

Fig. 2. Effects of the *ets1b* antisense morpholino injection on the interrenal tissue and its neighboring vasculature. Confocal sections showing the interrenal tissue as detected by 3 β-Hsd activity staining (**A–E**), and the neighboring endothelium as labeled by green fluorescence (**A′–E′**), of 2-dpf *Tg(fli1:EGFP)*^{Y1} embryos uninjected (A), injected with *ets1b*MO (B–D), or with *tnnt2*MO (E), respectively. **A″–E″**: The merged images of 3 β-Hsd activity staining and GFP. A–E are dorsal views with anterior oriented to the top. **F**: The merged image of 3 β-Hsd staining and GFP of the same embryo as in E–E″, a lateral view with anterior to the left. B–B″, C–C″, D–D″: Classes I to III of interrenal phenotypes in the *ets1b* morphant, where the trunk endothelium was reduced and the axial vascular formation inhibited. Vascular ECs, but not the blood flow, are required for the convergence and laterality of the interrenal tissue. Yellow dotted lines indicate the position of the midline. Orange arrows, interrenal tissues; yellow arrowheads, angiogenic glomerulus; DA, dorsal aorta; PCV, posterior cardinal vein; ISV, intersegmental vessel. Scale bar = 50 μM.

Fig. 3. Effects of the *hey2* antisense morpholino injection on the interrenal tissue and its neighboring vasculature. **A**: Ventral flat-mount views showing the effects of *hey2*MO on the expressions of *eph-B2a* and *flt4* in the peri-interrenal region. Uninjected control (**a,c**) and injected embryos (**b,d**) were fixed at 35 hpf, and two-color ISH were carried out to detect the expression of *ff1b* together with either *eph-B2a* (a,b) or *flt4* (c,d). a–d: Oriented with anterior to the top. **B**: Confocal images display the interrenal tissue as detected by 3 β-Hsd activity staining (left panels, **a–f**), and the neighboring endothelium as labeled by green fluorescence (middle panels, **a′–f′**), of 34-hpf (a,b) and 54-hpf (c–f) *Tg(kdrl:EGFP)*^{s843} embryos uninjected (a–d) or injected with *hey2* antisense morpholino (e,f). The merged images of 3 β-Hsd activity staining and GFP are shown in the right panels (**a″–f″**). Each fluorescent image depicting the vascular morphology represents a projection of a consecutive z-stack encompassing the depth of the interrenal tissue. a–a″, c–c″, e–e″ are dorsal views with anterior oriented to the top, while b–b″, d–d″, f–f″ are dorsolateral views with anterior to the right. Relocalization and right-sided laterality of the interrenal tissue is perturbed upon the disruption of axial artery in the *hey2* morphant. Black and orange arrows indicate the *ff1b*-expressing and steroidogenic interrenal tissues, respectively. Red and blue arrowheads denote the arterial and venous vasculature, respectively. Yellow and blue dotted lines, boundaries of arterial and venous structures, respectively; white dotted lines, position of the midline; DA, dorsal aorta; ISV, intersegmental vessel; PCV, posterior cardinal vein; DC, duct of Cuvier; G, glomerulus; IR, interrenal tissue. Scale bar = 50 μM.

TABLE 2. Phenotypic Statistics of 34-hpf *Tg(kdrl:EGFP)*^{s843} Embryos Injected by Either *hey2* Antisense Morpholino Oligonucleotide or *hey2* mRNA

	Control		*hey2*MO		*hey2* mRNA	
Phenotype	No.	(%)	No.	(%)	No.	(%)
Bilateral clusters widely across the midline	0		0		76	(30.2)
Bilateral clusters immediately across the midline	2	(1.4)	2	(3.2)	45	(17.9)
Single cluster at the central midline	0		60	(95.2)	74	(29.4)
Single cluster to the left of the midline	7	(5.0)	0		38	(15.1)
Single cluster to the right of the midline	131	(93.6)	1	(1.6)	19	(7.5)
Total	140		63		252	

ISH results thus revealed that while the artery formation was inhibited in the *hey2* morphant, lateral relocalization of the *ff1b*-expressing interrenal cells was perturbed, culminating in a single interrenal tissue positioned at the central midline.

To examine how the inhibition of arterial fate decision would affect morphology of the functionally-differentiated steroidogenic interrenal tissue, as well as the three-dimensional vascular pattern in the peri-interrenal area, *hey2* morpholino was injected into *Tg(kdrl:EGFP)*^{s843} where the EGFP fluorescence is driven by the zebrafish *kinase insert domain receptor like* (*kdrl*) promoter (Jin et al., 2005). In the control embryo at 34 hr post-fertilization (hpf), part of the fused and lateralized interrenal tissue lies immediately ventral to the DA and caudal to the pronephric glomerulus (Fig. 3Ba–a″, b–b″). At 54 hpf, the entire interrenal tissue relocated slightly rightwards as viewed dorsally, and was positioned immediately lateral to the DA and tightly associated with the right branch of the PCV (Fig. 3Bc–c″, d–d″). In the dorsolateral view of wild-type embryos at 34 and 54 hpf, the interrenal tissue was situated ventral to the DA and dorsal to the PCV (Fig. 3Bb″,d″). Consistent with the ISH results in Figure 3A, assembly of the DA was disrupted in the *hey2* morphant, which lacks circulation, and the ISV was absent (Fig. 3Be′,f′). As compared with the control embryo, the DA structure dorsal to the interrenal tissue was severely disrupted (Fig. 3Bf″). In contrast with the severe disruption of the DA, the presence of the PCV and the duct of Cuvier was still evident in the *hey2* morphant (Fig. 3Be″). The interrenal tissue in the *hey2* morphant remained tightly associated with the PCV (Fig. 3Be″,f″), and was shown as a single cluster lying at the central midline (Fig. 3Be″) in more than 95% of the *hey2* morphants which displayed disrupted vasculature and loss of blood flow (n = 63; Table 2). The interrenal morphology of the *hey2* morphant suggested that formation of the DA might be essential for lateral relocalization of the interrenal tissue after the medial fusion.

Inhibition of Vein Formation Led to Defective Interrenal Morphogenetic Movements With a Range of Expressivities

In order to examine the role of venous vessels for morphogenetic movements of the interrenal tissue, the overexpression of *hey2* mRNA was utilized to inhibit venous vessel formation (Zhong et al., 2001). At the dosage of approximately 200 pg per embryo, the injection of *hey2*-capped mRNA into the wild type embryo led to a complete absence of blood circulation (43.3%, n = 157). To assess whether the *hey2* mRNA injection could efficiently and specifically inhibit the formation of venous vasculature in the peri-interrenal region, we examined the expression pattern of *eph-B2a* (Fig. 4Aa–f) and *flt4* (Fig. 4Ag–l) genes, respectively, with ISH. Each was assayed simultaneously with that of *ff1b* to mark the location of interrenal cells. Ventral flat-mount views showed that while the *flt4* expression was absent in the *hey2*-injected embryo at 35 hpf (n = 29; phenotypic classes shown in Fig. 4Ab–f), the *eph-B2a* expression could be clearly detected in the peri-interrenal region (n = 39; phenotypic classes shown in Fig. 4Ah–l). The *eph-B2a* expression in the *hey2*-injected embryo suggested a malformed arterial structure with variable expressivities, which, however, remained tightly associated with the *ff1b*-expressing interrenal cells (Fig. 4Ah–l). We classified *hey2* dominant-positive phenotypes into classes I to V, based on different locations of the interrenal tissue with respect to the midline. In classes I and II of the injected embryos, various degrees of interrenal migration defects were shown (Fig. 4Ab,c,h,i), while interrenal phenotypes in classes III and IV might have resulted from a disrupted laterality (Fig. 4Ad,e,j,k). Although the interrenal tissue in class-V embryos displayed normal laterality, its adjacent arterial vasculature was malformed (Fig. 4Al).

To evaluate the penetrance and expressivity of the interrenal phenotype upon the inhibition of venous formation, in the context of three-dimensional vascular architecture surrounding the interrenal tissue, the *hey2* mRNA was injected into *Tg(kdrl:EGFP)*^{s843} embryos for the subsequent 3βHsd activity staining. Consistent with the ISH results in Figure 4A, specific inhibition of venous formation was observed in all the injected embryos where the blood flow was absent (Fig. 4Bc′–l′). Concomitant with a severe disruption of the PCV structure at the peri-interrenal area, unsuccessful central assembly of the DA structure was detected in classes I, II, IV, and V (Fig. 4Bc′–f′,i′–l′). It was speculated that assembly defects of the DA in

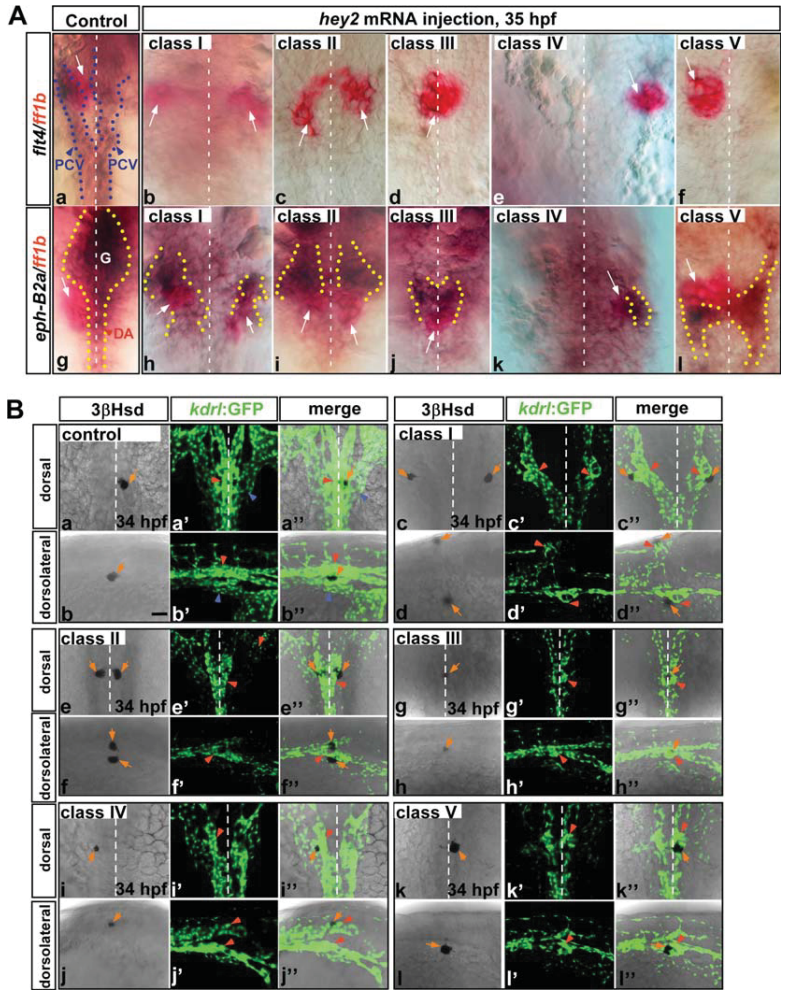

Fig. 4. Effects of *hey2* mRNA injections on the interrenal tissue and its neighboring artery and vein. **A**: Effects of *hey2* mRNA on the expressions of *flt4* and *eph-B2a* in the peri-interrenal region. Uninjected control (a, g) and injected embryos (b–f, h–l) were fixed at 35 hpf and subject to two-color ISH for detecting the expression of *ff1b* together with that of either *flt4* (**a–f**) or *eph-B2a* (**g–l**). All panels in A are ventral views with anterior oriented to the top. The *flt4* expression at the peri-interrenal area is absent in all phenotypic classes of injected embryos (classes I–V). **B**: Sets of confocal images display the interrenal tissues as detected by 3 β-Hsd activity staining (left panels of each set, a–l), and the neighboring endothelium as labeled by green fluorescence (middle panels of each set, **a′–l′**), of 34-hpf *Tg(kdrl:EGFP)*^{s843} embryos uninjected (a, b) or injected with *hey2* mRNA (c–l, classes I–V). The merged images of 3 β-Hsd activity staining and GFP are shown in the right panels of each set (**a″–l″**). Each fluorescent image depicting the vascular morphology represents a projection of a consecutive z-stack encompassing the depth of the interrenal tissue. a, c, e, g, i, k are dorsal views with anterior oriented to the top, while b, d, f, h, j, l are dorsolateral views with anterior to the right. The venous endothelium at the peri-interrenal area is severely reduced in all classes of *hey2* mRNA-injected embryos, which is accompanied by various expressivities of the interrenal morphogenetic defect. White and orange arrows, *ff1b*-expressing and steroidogenic interrenal tissues; red and blue arrowheads, artery and vein, respectively; blue and yellow dotted lines, boundaries of venous and arterial structures, respectively; white dotted lines, position of the midline; DA, dorsal aorta; PCV, posterior cardinal vein; G, glomerulus. Scale bar = 50 μM.

classes I, II, IV, and V could be due to an ectopic early effect of the *hey2* mRNA overexpression on the general convergence movement, which did not affect functional differentiation of the steroidogenic interrenal cells. Although assembly of the DA appeared to be normal in the class-III embryo (Fig. 4Bg′,h′), the amount of the arterial endothelium seemed to be less than that in the control embryo (Fig. 4Ba′,b′). In classes I and II, the severity of the DA assembly defect was correlated with that of the interrenal medial migration (Fig. 4Bc″,e″). In classes IV and V, a single interrenal tissue was associated with either the left (class IV) or the right (class V) of bilateral DA structures that failed to assemble centrally (Fig. 4Bi″,j″,k″,l″). It remains unclear whether the left-sided interrenal laterality in class IV was due to a defective fusion position of bilateral interrenal primordia, or to a randomized relocalization after midline fusion, or to a defective differentiation of the right interrenal cluster that did not migrate centrally. In class III, assembly of the DA as well as midline fusion of bilateral interrenal tissues were both successful, while lateral relocalization of the converged interrenal tissue was defective, culminating in a single interrenal tissue embedded within the DA at a level slightly posterior to the bifurcation point (Fig. 4Bg–g″,h–h″). The statistics for class I to V interrenal phenotypes in the experiment described above is summarized in Table 2. Our results thus suggest that the simultaneous presence of the DA and PCV branches is essential for developmental relocalization and laterality of the interrenal tissue.

Examination of the interrenal morphology, in a scenario where arterial versus venous formation was manipulated, led us to conclude that the existence of both the DA and the PCV was required for defining laterality of the interrenal tissue after the initial interrenal convergence and fusion. While the interrenal tissue in the artery-deficient embryo failed to relocate laterally, that in the vein-deficient embryo demonstrated a wide range of expressivities in terms of morphogenetic movements. It is interesting to note that the location of the interrenal tissue relative to the midline appeared to be correlated with the severity of arterial assembly defects, in all phenotypic classes of vein-deficient embryos (Fig. 4B). Phenotypic differences of the interrenal phenotype between artery-deficient and vein-deficient embryos might be in part explained by the fact that although the axial venous vasculature in the *hey2* morphant was hypomorphic, central assembly of the PCV was less perturbed (Fig. 3Ad, Be′,f′). As interrenal cells demonstrated affinities for both

arterial and venous ECs, in wild-type as well as manipulated embryos, it remains unclear whether relocalization and laterality of the interrenal tissue requires a simultaneous close association with both arterial and venous ECs. It is tempting to speculate that the presence of the DA and the PCV near the interrenal tissue might serve as vessel coordinates to define interrenal laterality. In this regard, the arterial versus venous fate specification might not be essential for guiding the interrenal morhogenetic movement. However, the results of our study could not explicitly address this question, as manipulation of the arterial versus venous fate by altering expression levels of *hey2* also led to a disruption of the vascular architecture at the midtrunk. Specifically for the midtrunk area, it remains to be explored whether and how the arterial versus venous fate decision could be manipulated without altering the vascular architecture.

In summary, we dissected in this study early morphogenetic steps of the interrenal primordial cells. Histological analysis upon various fashions of vascular disruption revealed an intimate interaction between interrenal cells and its adjacent endothelium, at each step of the interrenal morphogenetic movements. Furthermore, shaping of the embryonic interrenal morphology was secondary to and directed by ECs during the process of vascular assembly, while the architecture of both arterial and venous vessels at the midtrunk was essential for defining laterality of the interrenal tissue.

The Relationship Between Blood Vessels and a General Asymmetry Program in Patterning Laterality of the Interrenal Tissue

While our results indicate the importance of vascular topology at the midtrunk to pattern the interrenal laterality, our experiments did not answer the question of why the interrenal tissue was relocalized toward the right, rather than the left, of the midline. It remains to be explored whether the intimate interaction between the interrenal tissue and its adjacent artery and vein has to function, in conjunction with a general asymmetry molecular program, to determine the interrenal laterality. In our previous studies, it was found that central migration of bilateral interrenal tissues was defective in Nodal mutants *one-eyed pinhead* (*oep*) and *squint* (*sqt*) (Chai et al., 2003; Liu et al., 2003). However, multiple levels of developmental defects other than a loss of asymmetry are caused by the mutation of either *oep* or *sqt*, which include disruption of the endoderm and the axial vasculature (Alexander and Stainier, 1999; Brown et al., 2000). Therefore, a more comprehensive study of those gene that govern the general asymmetry program should be performed, in order to understand the specific influence of left-right axis formation on the interrenal tissue and its nascent vasculature. Our preliminary results showed that a randomization of interrenal laterality was observed in *polycystin-2* (*pkd2*) morphants, where the specification of left-right asymmetry was perturbed without obviously disrupting the midtrunk vasculature (data not shown). *pkd2* is expressed at the zebrafish brain, pronephros, and Kupffer's vesicle to regulate cilia-driven fluid flow, and whose function in the Kupffer's vesicle is required for establishing the organ situs (Kramer-Zucker et al., 2005). While *pkd2* is also important for the pronephric fluid flow, it awaits further clarification as to whether its specific function at Kupffer's vesicle regulates the interrenal laterality. Furthermore, it is to be examined how other members of the asymmetry program, such as *nodal*-related gene *southpaw* (Long et al., 2003), *lefty*-related genes *lefty1* and *lefty2* (Bisgrove et al., 1999; Wang and Yost, 2008), would function in patterning laterality of the interrenal tissue, and whether the interrenal laterality could be due to a possible asymmetry of the midtrunk vasculature.

As our results indicate that embryonic vessels might be involved in patterning interrenal laterality, it would be interesting to explore whether the same mechanism might participate in other aspects of organogenesis. While the budding of embryonic liver and pancreas from the developing gut occurs at the level posterior to the interrenal tissue at the midtrunk, the direction of outgrowth as well as laterality for these two digestive organs are unaffected in the endothelium-free *clo* mutant (Field et al., 2003a,b). The initial medial movement of cardiomyocytes was not affected in *clo*, yet the absence of endocardium leads to a later defect in the assembly and elongation of the heart tube (Holtzman et al., 2007). Nevertheless, laterality of the heart tube during its assembly is not aberrant in *clo*. Therefore, it remains unclear why laterality of the interrenal tissue, among other organs, could be particularly influenced by the vascular morphology. Unlike its mammalian counterpart, the interrenal tissue is formed not as a discrete organ in teleosts, with no formation of distinct steroidogenic zones during its development (Grassi Milano et al., 1997). While the outer cortex and inner medulla of the mammalian adrenal gland are well separated with clear boundaries formed in between, interrenal and chromaffin cells integrate to form the interrenal organ through intermingling of two cell populations (Grassi Milano et al., 1997; Chai et al., 2003; To et al., 2006). Extracellular matrix proteins Laminin, Collagen IV, and Fibronectin, as well as their Integrin receptors, are differentially expressed in various domains within the human fetal adrenal gland to coordinate specific steroidogenic pathways and cell turnover during development (Chamoux et al., 2001, 2002). The formation of basement membrane is evident, along with the distribution of laminin isoforms, in the fetal as well as the adult human adrenal gland (Virtanen et al., 2003). In contrast, the interrenal tissue in teleosts demonstrated high morphological plasticity during development, which might be correlated with a lack of stabilized basement membrane on its own. Hypothetically, peri-interrenal vessels might modulate the interrenal morphology through providing the basement membrane. Therefore, it remains to be investigated whether the basement membrane with its extracellular matrix (ECM) components is formed within the interrenal organ, or at the junction between the interrenal cell and its adjacent endothelium. Prospectively, elucidation of the pattern of ECM deposition at the interrenal and peri-interrenal

regions might shed some light on how vessels shape the interrenal tissue in the early zebrafish embryo.

EXPERIMENTAL PROCEDURES

Zebrafish Strains and Growth Conditions

Zebrafish (*Danio rerio*) were raised according to standard protocols (Westerfield, 2000). Embryos were obtained by natural spawning and cultured in embryo medium at 28.5°C. Staging of the embryos was carried out as previously described (Kimmel et al., 1995). Embryos to be subject to histological analysis were treated with 0.03% phenylthiourea (Sigma, St. Louis, MO) from 12 hpf onwards to inhibit pigment formation. *Tg(ff1bEx2:GFP)*, where a GFP cassette was inserted into exon2 of the *ff1b* locus, was developed through a BAC transgenesis strategy (Quek, 2009). A study describing the technical details and characterization of this line is currently underway. The *Tg(fli1:EGFP)*^{Y1} line was from the Zebrafish International Resource Center (Eugene, OR). The *Tg(kdrl:EGFP)*^{s843} line was a kind gift from Didier Stainier (San Francisco, CA).

Whole-Mount In-Situ Hybridization

Whole-mount in situ hybridization (ISH) was performed as described with minor modifications (Liu et al., 2003). Digoxigenin-labeled riboprobes were synthesized from plasmids containing cDNAs for *eph-B2a* and *flt4*. *eph-B2a* plasmid was linearized with *Sal*I and transcribed with *SP6* RNA polymerase. *flt4* plasmid was linearized with *Eco*RI and transcribed with *T7* RNA polymerase. Fluorescein-labeled riboprobes were synthesized from *Sal*I linearized *ff1b* plasmids and transcribed with *T7* RNA polymerase. DIG-labeled riboprobes were detected with alkaline phosphatase conjugated anti-DIG antibody (Roche, Nutley, NJ) while Fluorescein-labeled probes were detected by alkaline phosphatase conjugated anti-Fluorescein antibody (Roche). For one-color ISH, visualization of *ff1b* expression was performed with BCIP/TNBT (Chemicon, Temecula, CA). For two-color ISH, visualization of either *eph-B2a* or *flt4* expression was performed with BCIP/TNBT (Chemicon), and *ff1b* expression was stained with Fast Red (Roche) subsequently. The inactivation of the first antibody in two-color ISH was performed by heating the stained embryos at 65°C for 30 min. Stained embryos were post-fixed in 4% paraformaldehyde (PFA) in PBS and washed in PBS supplemented with 1% of Tween20 (PBST). This was followed by tissue clarification in 50% glycerol in PBS. Specimens were mounted on glass slides and photographed under Nomaski optics on an Olympus BX51 microscope system.

Microinjection of Morpholino Oligonucleotide and mRNA

To analyze how various types of endothelial defects affect the interrenal morphology, morpholino oligonucleotides (MO) were synthesized at Genetools LLC and diluted in 1 × Danieau solution before microinjections. The nucleotide sequences of the *ets1b*MO1, *ets1b*MO2, *tnnt2*MO, and *hey2*MO are 5′ – TTG GTA CAT TTC CAT ATC TTA AAG T - 3′ (Sumanas and Lin, 2006), 5′ – CAC TGA GTC CTT ATT TCA CTA TAT C - 3′ (Sumanas and Lin, 2006), 5′-CAT GTT TGC TCT GAT CTG ACA CGC A-3′ (Sehnert et al., 2002), and 5′-CGC GCA GGT ACA GAC ACC AAA AAC T-3′ (Zhong et al., 2001), respectively. Zebrafish *hey2* full-length cDNA clone (MGC:136746) was obtained from Open Biosystems and the ORF was subcloned into pCS2+. Capped mRNA of *hey2* was in vitro transcribed from the linearized plasmid by using Message Machine (Ambion, Austin, TX). MO- or mRNA-containing solutions (~2.3 nL) were injected into one- to two-cell-stage embryos by using a Nanoject (Drummond, Broomall, PA).

Histology and Microscopy

For monitoring dynamic morphogenetic movements of the interrenal tissue in the live embryo, time-lapse confocal imaging was performed to collect fluorescent images from *Tg(ff1bEx2:GFP)* embryos anesthetized by tricane, using a Zeiss Axioplan II microscope equipped with LSM 510 META and an objective lens (×10 N.A. 0.3) (Carl Zeiss Inc., Thornwood, NY). Images were acquired as a z stack (8-μM slices) and assembled as a 3D projection. To delineate the morphology of the steroidogenic interrenal tissue, histochemical staining for 3β-Hydroxysteroid dehydrogenase/Δ5-Δ4-isomerase (3β-Hsd) was performed on whole embryos as previously described (Grassi Milano et al., 1997). For simultaneous analysis of interrenal steroidogenic activity and endothelial GFP fluorescence, 3β-Hsd staining signals were captured using transmitted light, while the fluorescent signals were captured with an Argon 488-nm laser connected to the confocal microscope. Image processing and analysis were performed using the LSM 510 version 3.5 software.

ACKNOWLEDGMENTS

We thank Prof. Didier Stainier for the kind gift of *Tg(kdrl:EGFP)*^{s843} strain; Dr. Sheng-Ping Huang, Dr. Cheng-Chen Huang, Dr. Yung-Jen Chuang, Ms Lisa Chen, Dr. Maysu You, Dr. Yun-Jin Jiang, and Prof. Bon-chu Chung for generous support in aquaculture; Dr. Seng-Sheen Fan and his team for expert assistance on confocal microscopy. Sue-Ing Quek was supported by a NUS Postgraduate Research Scholarship.

REFERENCES

Alexander J, Stainier DY. 1999. A molecular pathway leading to endoderm formation in zebrafish. Curr Biol 9:1147–1157.

Alt B, Elsalini OA, Schrumpf P, Haufs N, Lawson ND, Schwabe GC, Mundlos S, Grüters A, Krude H, Rohr KB. 2006. Arteries define the position of the thyroid gland during its developmental relocalisation. Development 133:3797–3804.

Bisgrove BW, Essner JJ, Yost HJ. 1999. Regulation of midline development by antagonism of lefty and nodal signaling. Development 126:3253–3262.

Brown LA, Rodaway AR, Schilling TF, Jowett T, Ingham PW, Patient RK, Sharrocks AD. 2000. Insights into early vasculogenesis revealed by expression of the ETS-domain transcription factor Fli-1 in wild-type and mutant zebrafish embryos. Mech Dev 90:237–252.

Chai C, Liu YW, Chan WK. 2003. ff1b is required for the development of steroidogenic component of the zebrafish interrenal organ. Dev Biol 260:226–244.

Chamoux E, Bolduc L, Lehoux JG, Gallo-Payet N. 2001. Identification of extracellular matrix components and their integrin receptors in the human fetal adrenal gland. J Clin Endocrinol Metab 86:2090–2098.

Chamoux E, Narcy A, Lehoux JG, Gallo-Payet N. 2002. Fibronectin, laminin, and collagen IV as modulators of cell behavior during adrenal gland development in the human fetus. J Clin Endocrinol Metab 87:1819–1828.

Cleaver O, Melton DA. 2003. Endothelial signaling during development. Nat Med 9:661–668.

Field HA, Dong PD, Beis D, Stainier DY. 2003a. Formation of the digestive system in zebrafish. II. Pancreas morphogenesis. Dev Biol 261:197–208.

Field HA, Ober EA, Roeser T, Stainier DY. 2003b. Formation of the digestive system in zebrafish. I. Liver morphogenesis. Dev Biol 253:279–290.

Grassi Milano E, Basari F, Chimenti C. 1997. Adrenocortical and adrenomedullary homologs in eight Species of adult and developing teleosts: morphology, histology, and immunohistochemistry. Gen Com Endocrinol 108: 483–496.

Holtzman NG, Schoenebeck JJ, Tsai HJ, Yelon D. 2007. Endocardium is necessary for cardiomyocyte movement during heart tube assembly. Development 134:2379–2386.

Hsu HJ, Lin G, Chung BC. 2003. Parallel early development of zebrafish interrenal glands and pronephros: differential control by wt1 and ff1b. Development 130:2107–2116.

Jin SW, Beis D, Mitchell T, Chen JN, Stainier DY. 2005. Cellular and molecular analyses of vascular tube and lumen formation in zebrafish. Development 132:5199–5209.

Kimmel CB, Ballard WW, Kimmer SR, Ullmann B, Schilling TF. 1995. Stages of embryonic development of the zebrafish. Dev Dyn 203:253–310.

Kramer-Zucker AG, Olale F, Haycraft CJ, Yoder BK, Schier AF, Drummond IA. 2005. Cilia-driven fluid flow in the zebrafish pronephros, brain and Kupffer's vesicle is required for normal organogenesis. Development 132:1907–1921.

Lawson ND, Weinstein BM. 2002. In vivo imaging of embryonic vascular development using transgenic zebrafish. Dev Biol 248:307–318.

Liu YW. 2007. Interrenal organogenesis in the zebrafish model. Organogenesis. 3:44–48.

Liu YW, Guo L. 2006. Endothelium is required for the promotion of interrenal morphogenetic movement during early zebrafish development. Dev Biol 297: 44–58.

Liu YW, Gao W, The HL, Tan JH, Chan WK. 2003. Prox1 is a novel coregulator of Ff1b and is involved in the embryonic development of the zebra fish interrenal primordium. Mol Cell Biol 23:7243–7255.

Long S, Ahmad N, Rebagliati M. 2003. The zebrafish nodal-related gene southpaw is required for visceral and diencephalic left-right asymmetry. Development 130:2303–2316.

Nikolova G, Strilic B, Lammert E. 2007. The vascular niche and its basement membrane. Trends Cell Biol 17: 19–25.

Quek SI. 2009. Molecular characterization of the zebrafish *ff1b* gene. Ph.D. thesis. National University of Singapore.

Red-Horse K, Crawford Y, Shojaei F, Ferrara N. 2007. Endothelium-microenvironment Interactions in the developing embryo and in the adult. Dev Cell 12:181–194.

Sakaguchi TF, Sadler KC, Crosnier C, Stainier DY. 2008. Endothelial signals modulate hepatocyte apicobasal polarization in zebrafish. Curr Biol 18:1565–1571.

Sehnert AJ, Huq A, Weinstein BM, Walker C, Fishman M, Stainier DY. 2002. Cardiac troponin T is essential in sarcomere assembly and cardiac contractility. Nat Genet 31:106–110.

Serluca FC, Drummond IA, Fishman MC. 2002. Endothelial signaling in kidney morphogenesis: a role for hemodynamic forces. Curr Biol 12:492–497.

Sumanas S, Lin S. 2006. Ets1-related protein is a key regulator of vasculogenesis in zebrafish. PLoS Biol 4:e10.

To TT, Hahner S, Nica G, Rohr KB, Hammerschmidt M, Winkler C, Allolio B. 2007. Pituitary-interrenal interaction in zebrafish interrenal organ development. Mol Endocrinol 21:472–485.

Virtanen I, Korhonen M, Petäjäniemi N, Karhunen T, Thornell LE, Sorokin LM, Konttinen YT. 2003. Laminin isoforms in fetal and adult human adrenal cortex. J Clin Endocrinol Metab 88: 4960–4966.

Wang X, Yost HJ. 2008. Initiation and propagation of posterior to anterior (PA) waves in zebrafish left-right development. Dev Dyn 237:3640–3647.

Westerfield M. 2000. The zebrafish book: guide for the laboratory use of zebrafish (*Danio rerio*), 4th ed. Eugene, OR: University of Oregon Press.

Zhong TP, Childs S, Leu JP, Fishman MC. 2001. Gridlock signalling pathway fashions the first embryonic artery. Nature 414:216–220.